



Norwegian University of  
Science and Technology

# Efficiency- and Pressure pulsation measurements at a low head hydro power plant

**Stian Grunde Solvik**

Mechanical Engineering

Submission date: June 2016

Supervisor: Ole Gunnar Dahlhaug, EPT

Co-supervisor: K. Nielsen Torbjørn, EPT  
Gogstad Peter Joachim, EPT

Norwegian University of Science and Technology  
Department of Energy and Process Engineering



EPT-M-2016- 127

**MASTEROPPGAVE**

for

Stian Grunde Solvik  
Våren 2016

Virkningsgrad- og trykkpulsasjons-målinger ved et lavtrykks vannkraftverk  
*Efficiency- and pressure pulsation measurements at a low head hydropower plant*

**Bakgrunn og målsetting**

Trykkpulsasjoner er et velkjent fenomen som forekommer i Francis turbiner. Impulser av høy frekvens oppstår på grunn av interaksjonen mellom løpehjulet og ledeskovelene, og lavfrekvente svingninger i sugerøret. Disse trykkpulsasjonene forårsaker materialtretthet og reduserer løpehjulets levetid.

Ved Leirfossene Kraftverk i Trondheim har Statkraft problemer med at trykkpulsasjonene forplanter seg i berget og dette forstyrrer de som bor i området ved vibrasjoner kan føles inne i husene. Statkraft har utfordret NTNU til å finne en løsning som demper trykkpulsasjonene i turbinen. Ved Vannkraftlaboratoriet på NTNU er det utviklet en såkalt "stulke" som Peter Joachim Gogstad har tilpasset til Leirfossene Kraftverk. Denne skal redusere amplituden på trykkpulsasjonen, og arbeidet som skal gjennomføres vil evaluere om "stulken" vil gi den effekten som er beregnet. Det skal også gjennomføres virkningsgradsmålinger samtidig med trykkpulsasjonsmålingene for å avsløre om "stulken" har innflytelse på virkningsgraden.

**Mål**

Gjennomføre virkningsgrad- og trykkpulsasjonsmåling ved Leirfossene kraftverk.

**Oppgaven bearbeides ut fra følgende punkter**

1. Det skal gjennomføres et litteratursøk som finner status på FoU-aktivitet for trykkpulsasjoner på lavtrykks Francis turbiner.
2. Studenten skal sette seg inn i det teoretiske grunnlag for:
  - a. Hvordan trykkpulsasjoner oppstår i Francis turbiner og hvilke konsekvenser dette har på levetiden til turbinen.
  - b. Den termodynamiske metoden for virkningsgradsmålinger
3. Det skal gjennomføres virkningsgrad- og trykkpulsasjonsmålinger. Disse målingen skal gjennomføres i samarbeide med PhD-student Joachim Gogstad.
4. Resultatene fra forsøkene skal evalueres og sammenlignes med tilsvarende målinger fra andre kraftverk dersom dette er tilgjengelig data.

Senest 14 dager etter utlevering av oppgaven skal kandidaten levere/sende instituttet en detaljert fremdrift- og eventuelt forsøksplan for oppgaven til evaluering og eventuelt diskusjon med faglig ansvarlig/veiledere. Detaljer ved eventuell utførelse av dataprogrammer skal avtales nærmere i samråd med faglig ansvarlig.

Besvarelsen redigeres mest mulig som en forskningsrapport med et sammendrag både på norsk og engelsk, konklusjon, litteraturliste, innholdsfortegnelse etc. Ved utarbeidelsen av teksten skal kandidaten legge vekt på å gjøre teksten oversiktlig og velkrevet. Med henblikk på lesning av besvarelsen er det viktig at de nødvendige henvisninger for korresponderende steder i tekst, tabeller og figurer anføres på begge steder. Ved bedømmelsen legges det stor vekt på at resultatene er grundig bearbeidet, at de oppstilles tabellarisk og/eller grafisk på en oversiktlig måte, og at de er diskutert utførlig.

Alle benyttede kilder, også muntlige opplysninger, skal oppgis på fullstendig måte. For tidsskrifter og bøker oppgis forfatter, tittel, årgang, sidetall og eventuelt figurnummer.

Det forutsettes at kandidaten tar initiativ til og holder nødvendig kontakt med faglærer og veileder(e). Kandidaten skal rette seg etter de reglementer og retningslinjer som gjelder ved alle (andre) fagmiljøer som kandidaten har kontakt med gjennom sin utførelse av oppgaven, samt etter eventuelle pålegg fra Institutt for energi- og prosesssteknikk.

Risikovurdering av kandidatens arbeid skal gjennomføres i henhold til instituttets prosedyrer. Risikovurderingen skal dokumenteres og inngå som del av besvarelsen. Hendelser relatert til kandidatens arbeid med uheldig innvirkning på helse, miljø eller sikkerhet, skal dokumenteres og inngå som en del av besvarelsen. Hvis dokumentasjonen på risikovurderingen utgjør veldig mange sider, leveres den fulle versjonen elektronisk til veileder og et utdrag inkluderes i besvarelsen.

I henhold til ”Utfyllende regler til studieforskriften for teknologistudiet/sivilingeniørstudiet” ved NTNU § 20, forbeholder instituttet seg retten til å benytte alle resultater og data til undervisnings- og forskningsformål, samt til fremtidige publikasjoner.

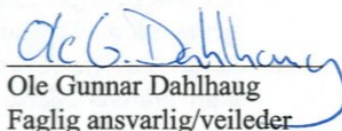
Besvarelsen leveres digitalt i DAIM. Et faglig sammendrag med oppgavens tittel, kandidatens navn, veileders navn, årstall, instituttnavn, og NTNUs logo og navn, leveres til instituttet som en separat pdf-fil. Etter avtale leveres besvarelse og evt. annet materiale til veileder i digitalt format.

- Arbeid i laboratorium (vannkraftlaboratoriet, strømningsteknisk, varmeteknisk)
- Feltarbeid

NTNU, Institutt for energi- og prosesssteknikk, 11. januar 2016



Olav Bolland  
Instituttleder



Ole Gunnar Dahlhaug  
Faglig ansvarlig/veileder

Medveileder(e):

- Torbjørn K. Nielsen      torbjorn.nielsen@ntnu.no
- Peter Joachim Gogstad      peter.j.gogstad@ntnu.no



# Preface

This Master Thesis is written by Master Student Stian Grunde Solvik. The thesis has been carried out through the department of Energy and Process Engineering at the Waterpower Laboratory at the Norwegian University of Science and Technology during the spring semester of 2016. The work presented covers the theoretical background of both pressure pulsation and thermodynamic efficiency analysis. The thesis will present the results of pressure pulsation and efficiency measurements performed at Leirfossene hydropower plant.

I would like to thank my supervisor Professor Ole Gunnar Dahlhaug, PhD. -Candidates Peter Joachim Gogstad and Carl Werdelin Bergan for their valuable guidance and for asking the right questions throughout the project. Fellow Master Student Magomed Selmurzaev for our collaboration in the semester project and all the good conversations throughout the last five years.

I would also like to thank the technical staff in the lab, especially Joar Grillstad. The staff has been supportive throughout the project, allowing me to make my own mistakes and develop my skill-set in a laboratory environment. The learning curve has been very steep. I have however enjoyed every part of it.

Last but not least, I would like to thank my family and friends who have supported me and helped me get to where I am today.

Without your help, this thesis would have been a difficult one.



## Abstract

Stian Solvik and Peter Joachim Gogstad completed efficiency Measurement for turbine 2 at Leirfossene power plant on 26 May 2016. The measurements were carried out as part of an ongoing research collaboration between NTNU and Statkraft. The thermodynamic method is used to measure the turbine efficiency. The measurements have been carried out in accordance with the International Standard IEC 60041, 3.ed 19991-11 [1]. One temperature sensor was installed at the inlet to the turbine and three temperature sensors with manifolds were installed in the outlet. Atmospheric pressure and pressure at the inlet of the turbine was measured with suitable pressure sensors, while pressure at the outlet has been numerically calculated. The relative efficiencies, net head and water flow at the nominal head of 58m is given in Table 17 and Table 18. The maximum uncertainty in efficiency is calculated to be 1.4%.

Pressure measurements has been performed in the draft tube on turbine 2. Eight pressure sensors have been used. Respectively four sensors are placed in the same vertical axis, on each side of the draft tube by a vertical distance of 860mm downstream of each other. The measurements were performed under steady state conditions, with a constant generator power and discharge. All operating point are related to the nominal discharge  $Q_n$ .

The pressure pulsation measurements show that the Rheingans frequency, runner frequency and runner vane frequency are present in the draft tube. The Rheingans frequency is the dominant frequency while operating at part load. The runner frequency displays a high intensity at both part- and high- load The runner vane frequency shows a high intensity at the outlet of the turbine. The analysis of the pressure intensity shows the highest pressure pulsations measured for BEP, part load and high load are respectively  $45kPa$ ,  $250kPa$ ,  $55kPa$ .

The sensors located closest to the inner radius of the draft tube bend experience a lower intensity than the sensors at the outer radius of the bend. This is probably a flow-specific phenomenon that occurs in the draft tube bend. Air injection into the draft tube is installed to reduce the intensity of pressure pulsations that occur during part load. Data with and without air injection from two operating point at  $0.46 \cdot Q_n$  and  $0.58 \cdot Q_n$ , have been compared. The analysis shows that the air injection reduces the overall intensity by 22% at  $0.46 \cdot Q_n$  and 10% at  $0.58 \cdot Q_n$ . The most powerful pulsations are reduced by 20% to 60%, while the remaining pulsations experienced a change from -14% to 17%. Frequency analysis at part load,  $0.46 \cdot Q_n$ , show two distinct frequencies at 4.64Hz and 5.06Hz when the turbine runs without air injection. When air is injected into the draft tube, these frequencies disappear altogether. The frequencies are probably related to elastic fluctuations in the system, which are damped by the injected air.





## Sammendrag

Virkningsgradsmåling for turbin 2 ved Leirfossene kraftverk ble gjennomført 26. mai 2016 av Stian Solvik og Peter Joachim Gogstad. Målingene ble gjennomført i anledning et pågående forsknings samarbeid mellom NTNU og Statkraft. Den termodynamiske metode ble benyttet for å måle virkningsgraden. Målingene har blitt gjennomført etter den internasjonale standarden IEC 60041, 3.ed 1991-11 [1]. En temperatursensor ble montert ved innløpet til turbinen og tre temperatursensorer med samlestokk ble montert i utløpet. Atmosfærisk trykk, samt trykk ved innløp ble målt med egnede trykksensorer. Trykk ved utløp er blitt numerisk beregnet. De relative virkningsgradene, netto fallhøyde og vannføring ved nominell fallhøyde på 58m er gitt i Table 17 og Table 18. Maksimale usikkerheten i virkningsgraden er beregnet til  $\pm 1.4\%$ .

Det er blitt gjennomført trykkpulsasjonsmålinger i sugerøret på turbin 2. Totalt åtte trykksensorer er benyttet til formålet. Henholdsvis fire sensorer er plassert i samme vertikale akse, på hver side av sugerøret med en vertikal avstand nedstrøms på ca.  $860\text{mm}$  fra hverandre. Målingene ble gjennomført under stabile forhold, med konstant generatoreffekt og volumstrøm. Alle driftspunkt er relatert til nominell volumstrøm  $Q_n$ .

Resultat av trykkpulsasjonsmålingene viser at Rheingans frekvensen (sugerørsvirvel), løpehjulsfrekvensen og løpeskovlsfrekvensen er påvist i sugerøret. Som forventet er Rheingans frekvensen den dominante frekvensen under kjøring på lavlast. Løpehjulsfrekvensen har høy intensitet på lav- og høy-last. Ved utløpet til turbinene måles det høye amplituder som følge av løpeskovlsfrekvensen, trenden viser en økende intensitet når lasten på turbinen øker. Analysen av trykk-intensiteten viser at den høyeste trykkpulsasjonen, uavhengig av sensor, målt for bestpunkt, lavlast og overlast er på henholdsvis  $45\text{kPa}$ ,  $250\text{kPa}$ ,  $55\text{kPa}$ .

Sensorene som ligger nærmest innersvingen til sugerørsbendet opplever en lavere intensitet enn de sensorene som ligger nærmest yttersvingen til sugerørsbendet. Forskjellen i intensitet opp til 4 ganger større under lavlast. Dette skyldes trolig et strømnings-spesifikt fenomenet som oppstår i bendet til sugerøret. Luftinjeksjon er installert for å redusere intensiteten av trykkpulsasjoner som oppstår på lavlast. Måledata med og uten luftinjeksjon fra to driftspunkt på  $0.46 \cdot Q_n$  og  $0.58 \cdot Q_n$ , har blitt sammenlignet. Analysen viser at luftinjeksjon reduserer den totale intensiteten med 22% ved  $0.46 \cdot Q_n$  og 10% ved  $0.58 \cdot Q_n$ . De kraftigste intensitetene blir redusert med 20% til 60%, mens de resterende pulsasjonene opplevde en endring fra  $\div 14\%$  til 17%. Analysen av lavlastpunktet  $0.46 \cdot Q_n$ , viser to frekvenser på  $4.64\text{Hz}$  og  $5.06\text{Hz}$  når turbinen kjøres uten luftinjeksjon. Når luft blir injisert i sugerøret kan en observere at frekvensen forsvinner helt. Trolig er denne frekvensen relatert til elastiske svingninger som blir dempet av luften.



# Contents

Preface .....	i
Abstract.....	iii
Sammendrag.....	v
Contents.....	vii
List of figures.....	xiii
List of tables .....	xv
Nomenclature .....	xvii
1 Introduction.....	1
1.1 Leirfossene power plant.....	1
1.2 Previous work.....	2
1.2.1 Pressure pulsation .....	2
1.2.2 The thermodynamic method .....	3
2 Theory.....	5
2.1 Pressure Pulsations .....	5
2.1.1 Runner frequency .....	6
2.1.2 Runner vane frequency.....	6
2.1.3 Guide vane frequency.....	6
2.1.4 Rheingans frequency .....	7
2.1.5 Elastic fluctuations .....	9
2.1.6 Cavitation .....	10
2.1.7 Von Karman Vortex shedding .....	10
2.2 Vibration.....	11
2.2.1 Mounting of accelerometers .....	11
2.2.2 Resonance.....	12
2.3 Methods of reducing pressure pulsations .....	13
2.4 Data acquisition.....	15
2.4.1 Sampling rate theorem .....	15
2.4.2 A/D converter .....	16

2.4.3	Aliasing .....	17
2.5	Post processing.....	18
2.5.1	Fast Fourier Transform .....	18
2.5.2	Window function .....	19
2.5.2.1	Flat top window.....	21
2.5.2.2	Hann window.....	21
2.5.2.3	Hamming Window.....	21
2.5.2.4	Kaiser window .....	22
2.5.3	Harmonies.....	23
2.5.4	Peak-to-peak analysis .....	23
2.6	Efficiency measurements .....	24
2.6.1	Methods of flow measurements .....	25
2.7	Thermodynamic method.....	29
2.8	Efficiency calculation.....	30
2.8.1	Flow.....	32
2.8.2	Mechanical energy.....	33
2.8.2.1	Mechanical Pressure energy .....	34
2.8.2.2	Mechanical Potential energy.....	34
2.8.2.3	Mechanical Kinetic energy.....	34
2.8.2.4	Mechanical Thermal energy .....	34
2.8.3	Hydraulic energy .....	35
2.8.3.1	Hydraulic Pressure energy.....	36
2.8.3.2	Hydraulic Potential energy .....	36
2.8.3.3	Hydraulic Kinetic energy.....	36
2.9	Uncertainties .....	37
2.9.1	Systematic error.....	37
2.9.2	Random error.....	38
2.9.3	Environmental influences .....	38
3	Preparation and execution of measurement .....	39
3.1	Leirfossene hydro power plant .....	39
3.1.1	Time- and running- schedule .....	41
3.2	Measurement setup.....	42



3.2.1	LabVIEW .....	42
3.2.2	Sampling Rate .....	42
3.3	Equipment .....	44
3.3.1	Temperature sensors .....	44
3.3.2	Pressure Transducers.....	45
3.3.3	Equipment Vibration sensors.....	47
3.4	Location of sensors .....	49
3.4.1	Efficiency measurement .....	49
3.4.2	Pressure measurements .....	51
3.4.3	Vibration Sensors .....	52
3.5	Analysis of measurements .....	53
3.5.1	Efficiency measurements.....	53
3.5.2	Pressure and vibration measurements.....	55
3.5.3	Uncertainty .....	56
3.5.4	Calibration.....	56
4	Experimental results and discussion .....	57
4.1	Efficiency measurements .....	58
4.1.1	Uncertainty .....	59
4.1.2	Head loss .....	59
4.2	Pressure pulsation measurement .....	60
4.2.1	Pressure intensity .....	64
4.2.2	Effects of air injection .....	68
4.2.2.1	Part load $-0.46 \cdot Q_n$ .....	68
4.2.2.2	Part load $-0.58 \cdot Q_n$ .....	72
4.2.3	Comment on the total pressure intensity .....	75
4.2.4	Vibration measurement.....	76
4.2.5	Comparing pressure and vibration measurements .....	77
5	Conclusion .....	79
6	Further work.....	80
7	Bibliography.....	81

Appendix A	Calculations of expected frequencies .....	85
Appendix B	Calculation example Efficiency.....	86
Appendix C	Example of Head loss and Friction coefficient .....	91
Appendix D	Uncertainty Efficiency calculation.....	92
Appendix E	Random uncertainty efficiency calculation .....	100
Appendix F	Pressure pulsations plots .....	103
Appendix G	LabVIEW Program .....	107
Appendix H	MATLAB script Efficiency.....	112
Appendix I	MATLAB script for 3D plots.....	126
Appendix J	MATLAB script Peak analysis .....	131
Appendix K	MATLAB script for Heat plot .....	136
Appendix L	Technical information Pressure Sensor .....	142
Appendix M	Calibration -Pressure sensors.....	146
I.	Draft tube sensor 1 .....	147
II.	Draft tube sensor 2 .....	149
III.	Draft tube sensor 3.....	151
IV.	Draft tube sensor 4.....	153
V.	Draft tube sensor 5 .....	155
VI.	Draft tube sensor 6.....	157
VII.	Draft tube sensor 7.....	159
VIII.	Draft tube sensor 8.....	161
IX.	Inlet Pressure sensor .....	163
X.	Pressure sensor at temperature inlet sensor .....	165
XI.	Atmospheric pressure sensor .....	167
Appendix N	Data sheet -Accelerometers.....	169
I.	Accelerometer 1 .....	169
II.	Accelerometer 2 .....	170
III.	Accelerometer 3, 4 and 5.....	171
Appendix O	Data sheet-Temperature Sensors .....	172
Appendix P	Calibration Temperature Sensor .....	174

I. Temperature sensor nr.01 .....	174
II. Temperature sensor nr-02 .....	176
III. Temperature sensor nr.03.....	178
IV. Temperature sensor nr.04.....	181
V. Temperature sensor nr.05 .....	183
Appendix Q Risk Assessment .....	185





# List of figures

FIGURE 1 - MACHINE HALL LEIRFOSSENE .....	1
FIGURE 2 - FRANCIS TURBINE VELOCITY PROFILE AT OUTLET - [23] .....	8
FIGURE 3 - VORTEX ROPE AT HIGH LOAD[24] .....	8
FIGURE 4 - VORTEX ROPE AT PART LOAD [24] .....	8
FIGURE 5 - RESONANCE [44] .....	12
FIGURE 6 - RUNNER .....	13
FIGURE 7 - RUNNER WITH RUNNER CONE EXTENSION.....	13
FIGURE 8 - ANALOG TO DIGITAL SIGNAL .....	15
FIGURE 9 - 1.5 SAMPLES PER CYCLE.....	16
FIGURE 10 - 2 SAMPLES PER CYCLE.....	16
FIGURE 11 - BIT RESOLUTION ON A SINUSOID [45].....	16
FIGURE 12 - ALIASING EXAMPLE .....	17
FIGURE 13 - WINDOW FUNCTIONS-FLAT TOP, HANN, HAMMING AND KAISER.....	19
FIGURE 14 - SPECTRAL LEAKAGE [43].....	20
FIGURE 15 - HARMONIES.....	23
FIGURE 16 - HISTOGRAM- PEAK TO PEAK.....	23
FIGURE 17 - ENTHALPY-ENTROPY DIAGRAM .....	30
FIGURE 18 - LEIRFOSSENE TURBINE 2 OVERVIEW .....	39
FIGURE 19 - MEASUREMENTS SETUP.....	42
FIGURE 20 - LOCATION OF INLET TEMPERATURE SENSOR, PRESSURE INLET-, PRESSURE TEMPERATURE INLET SENSORS.....	49
FIGURE 21 - HIGH PRESSURE PROBE [49] .....	49
FIGURE 22 - LOCATION OF OUTLET TEMPERATURE SENSOR .....	50
FIGURE 23 - TEMPERATURE SENOR AT INLET .....	50
FIGURE 24 - LOCATION OF PRESSURE SENSORS IN DRAFT TUBE.....	51
FIGURE 25 - LOCATION OF VIBRATION SENSORS.....	52
FIGURE 26 - LOCATION VIBRATION SENSOR V3 & V4.....	52
FIGURE 27 - RAW TEMPERATURE OUTPUT .....	53
FIGURE 28 - EFFICIENCY MEASUREMENT LEIRFOSSENE TURBINE 2.....	58
FIGURE 29 - EFFICIENCY MEASUREMENT - TOTAL UNCERTAINTY.....	59
FIGURE 30 - HEAD LOSS CURVE LEIRFOSSENE TURBINE 2 .....	59
FIGURE 31 - FFT FOR ALL MEASURED OPERATIONAL POINTS - DT1 [0Hz-800Hz] .....	60
FIGURE 32 - FFT FOR ALL MEASURED OPERATIONAL POINTS - DT1 [0Hz-70Hz] .....	61
FIGURE 33 - RHEINGANS FREQUENCY INTENSITY DT1 .....	61
FIGURE 34 - RUNNER FREQUENCY INTENSITY DT2 .....	61
FIGURE 35 - RUNNER VANE FREQUENCY INTENSITY DT1 .....	62
FIGURE 36 - RUNNER VANE INTENSITY AT $0.83 \cdot Q_n$ .....	62
FIGURE 37 - RHEINGANS FREQUENCY INTENSITY DEVELOPMENT.....	62
FIGURE 38 - PEAK PRESSURE COMPARISON SENSOR DT1 AND DT2 .....	64
FIGURE 39 - PEAK PRESSURE COMPARISON SENSOR DT3 AND DT4 .....	64
FIGURE 40 - PEAK PRESSURE COMPARISON SENSOR DT5 AND DT6 .....	65
FIGURE 41 - PEAK PRESSURE COMPARISON SENSOR DT7 AND DT8 .....	65
FIGURE 42 - INLET VELOCITY CONDITION BEFORE BEND .....	65
FIGURE 43 - PRESSURE PEAK VALUES W/WITHOUT AIR INJECTION – $0.46 \cdot Q_n$ .....	68

FIGURE 44 - SPECTROGRAM WITHOUT AIR INJECTION.....	70
FIGURE 45 - SPECTROGRAM WITH AIR INJECTION .....	70
FIGURE 46 - PRESSURE PEAK VALUES W/WITHOUT AIR INJECTION – $0.58 \cdot Q_n$ .....	72
FIGURE 47 - SPECTROGRAM WITHOUT AIR INJECTION.....	73
FIGURE 48 - SPECTROGRAM WITH AIR INJECTION .....	73
FIGURE 49 - FFT WITH AND WITHOUT AIR INJECTION-SENSOR DT4.....	75
FIGURE 50 - VIBRATION AT TURBINE COVER FOR ALL LOADS .....	76
FIGURE 51 - VIBRATION INTENSITY OF RUNNER FREQUENCY.....	77
FIGURE 52 - PRESSURE INTENSITY OF RUNNER FREQUENCY-DT2 .....	77
FIGURE 53 - VIBRATION INTENSITY OF RUNNER VANE FREQUENCY.....	77
FIGURE 54 - PRESSURE INTENSITY OF RUNNER VANE FREQUENCY DT2 .....	77
FIGURE 55 - AXIAL VIBRATION ON TURBINE COVER AT $0.46 \cdot Q_n$ .....	78
FIGURE 56 - PRESSURE PULSATION DT1 AT $0.46 \cdot Q_n$ .....	78
FIGURE 57 - WATERFALL PLOT -PRESSURE SENSOR DT1 .....	103
FIGURE 58 - WATERFALL PLOT -PRESSURE SENSOR DT2 .....	103
FIGURE 59 - WATERFALL PLOT -PRESSURE SENSOR DT3 .....	104
FIGURE 60 - WATERFALL PLOT -PRESSURE SENSOR DT4 .....	104
FIGURE 61 - WATERFALL PLOT -PRESSURE SENSOR DT5 .....	105
FIGURE 62 - WATERFALL PLOT -PRESSURE SENSOR DT6 .....	105
FIGURE 63 - WATERFALL PLOT -PRESSURE SENSOR DT7 .....	106
FIGURE 64 - WATERFALL PLOT -PRESSURE SENSOR DT8 .....	106
FIGURE 65 - LABVIEW FRONT PANEL PRESSURE .....	107
FIGURE 66 - LABVIEW FRONT PANEL TEMPERATURE.....	108
FIGURE 67 - LABVIEW FRONT PANEL EFFICIENCY.....	109
FIGURE 68 - LABVIEW SIGNAL INPUT.....	110
FIGURE 69 - LABVIEW BLOCKDIAGRAM - WRITE TO TDMS -TIMER.....	111
FIGURE 70 - LABVIEW CODE TO CALCULATE THE EFFICIENCY.....	112

# List of tables

TABLE 1 - TURBINE AND GENERATOR SPECIFICATIONS.....	1
TABLE 2 - BIT RESOLUTION .....	16
TABLE 3 - FLOW MEASUREMENTS METHODS .....	28
TABLE 4 - REFERENCE HEIGHTS AT LEIRFOSSENE.....	39
TABLE 5 - OVERVIEW OF TEMPERATURES, VIBRATION AND PRESSURES.....	40
TABLE 6 - TIME SCHEDULE .....	41
TABLE 7 - RUNNING SCHEDULE.....	41
TABLE 8 - CALCULATED EXPECTED FREQUENCIES .....	42
TABLE 9 - TEMPERATURE SENSOR OVERVIEW .....	44
TABLE 10 - PRESSURE-AREA OF INTERESTS .....	45
TABLE 11 - PRESSURE TRANSDUCER OVERVIEW .....	46
TABLE 12 - PRESSURE MEASUREMENTS HARDWARE OVERVIEW.....	46
TABLE 13 - ACCELEROMETER INFORMATION .....	47
TABLE 14 - VIBRATION MEASUREMENTS HARDWARE OVERVIEW .....	48
TABLE 15 - VIBRATION SENSOR MOUNTING INFORMATION .....	52
TABLE 16 - NOMINAL PARAMETERS TURBINE 2 LEIRFOSSENE .....	57
TABLE 17 - THE PERFORMED MEASUREMENT POINTS.....	57
TABLE 18 - NORMALIZED EFFICIENCY VALUES .....	58
TABLE 19 - PEAK PRESSURES ALL SENSORS FOR $0.46 \cdot Q_n$ .....	64
TABLE 20 - PEAK PRESSURE AT BEP ALL SENSORS .....	66
TABLE 21 - PEAK PRESSURE VALUES $0.46 \cdot Q_n$ .....	69
TABLE 22 - PEAK PRESSURE VALUES $0.58 \cdot Q_n$ .....	72
TABLE 23 - RANDOM UNCERTAINTY ACCORDING TO IEC60041.....	100
TABLE 24 - RANDOM UNCERTAINTY OF MEASURED QUANTITIES .....	100
TABLE 25 - DEADWEIGHT CALIBRATION TESTER .....	146



## Nomenclature

Symbol	Description	Unit
A	Area	$m^2$
$a$	Isothermal factor	$m^3/kg$
n	Rotational speed	rpm
c	velocity	$m/s$
$c_p$	Specific heat capacity	$J/kg \cdot K$
D	Diameter	$m$
E	Energy	J/kg
e	Absolute uncertainty	Depends on the input
f	Frequency	Hz
$f$	Relative uncertainty	- or %
g	Gravitational acceleration constant	$m/s^2$
H	Head	$m$
h	Enthalpy	$J/kg$
n	number of samples	-
p	Pressure	$kPa$
Q	Flow	$m^3/s$
S	Standard deviation	Depends on the input
s	Entropy	$J/(kg \cdot K)$
t	Time	s
t	student t factor	-
T	Temperature	$K$ or $^{\circ}C$
Z	Height	$m$
$Z_{rv}$	Number of runner vanes	-
$Z_{gv}$	Number of Guide Vanes	-
$\Delta$	Used to expressing a difference	Depends on the input
$\rho$	Density	$kg/m^3$
$\eta$	Efficiency	- or %

## Subscripts and Abbreviations

<b>Symbol</b>	<b>Description</b>
BEP	Best Efficiency Point
CFD	Computational Fluid Dynamics
FFT	Fast Fourier transform
gv	Guide vane
h	Hydraulic
HL	High load
k	Kinetic
i	Matrix denotation
m	Mechanical
NTNU	Norwegian University of Science and Technology
PL	Part Load
pot	Potential
RSI	Rotor Stator Interaction
rv	Runner vane
th	Theoretical
t	Thermal
1	Hydraulic Inlet
11	Mechanical inlet
2	Hydraulic outlet
21	Mechanical outlet

# 1 Introduction

In the early 1990s, a new law was implemented in the Norwegian energy market. The law opened a free market for sale and purchase of electricity both within Norway and Europe. [2] By exposing the market to competition, supply and demand became the method of controlling the price. This has directly affected the way power plant owners have run their turbines ever since. Before the 1990s, the turbines were typically run at their Best Efficiency Point (BEP), only stopping for annual maintenance. Since 1990 the situation is quite different. Some turbines are being stopped and started several times a day as well as being run outside of their BEP.

Turbines are designed to run at BEP, this ensures a steady and continuous operation with an ideal flow through the turbine, resulting in a high efficiency. By running turbines outside of their BEP, the ideal flow is disrupted, introducing pressure pulsations and flow patterns that can create serious operating challenges. Challenges concerning fatigue, cavitation, vibration and noise can occur and can be devastating for the operation of the power plant. In recent years, this has resulted in failures on both old and new runners, causing costly maintenance and downtime of the power plants.

Leirfossene is a new hydropower plant located in Trondheim, Norway. However, since the start one has experienced issues with powerful vibration during part load operation. The vibration are so strong that it travels through the bedrock and disturbed those who live in the area. Statkraft, the owner of the power plant, has challenged NTNU to come up with a solution to the vibration and noise issue at Leirfossene hydropower plant.

The objective of the thesis is to perform efficiency and pressure pulsation measurements at Leirfossene power plant.

This master thesis was originally supposed to evaluate the effect of a freely rotating runner cone extension, designed by PhD candidate Peter Joachim Gogstad, on the pressure pulsation and efficiency of the turbine. However, the measurements with the freely rotating runner cone extension could not be conducted due to unexpected challenges and the delay that followed because of it. Instead, Efficiency, pressure and vibration measurements were performed without the runner cone extension. The measurements are focused on steady state operating conditions and will evaluate the effect of air injection as a mean of reducing pressure pulsations in the system. The efficiency measurement is based on the thermodynamic method and follows the international IEC 60041 standard [1]. Only the relative efficiency is presented due to confidentiality.

## 1. Introduction

Pressure and vibration measurements are used to determine the source of pressure pulsation and vibrations in the system. Through analysis of the measurements one is able to investigate the intensity of the pulsations. When these measurements are performed regularly it can be useful in estimating the turbines maintenance interval and its lifetime. In this thesis the measurements will be used to determine the effect of air injection on the system as well to track frequencies and its intensity at different operating conditions.

Efficiency measurements are performed as part of the commissioning process of new turbines to ensure that the manufacturers design guarantees are met. In the course of the turbines lifetime it is common to repeat efficiency measurements with regular intervals to ensure the turbines condition and to have an accurate efficiency in order to accurately predict the potential financial gain. When experimenting with equipment to reduce pressure pulsation it is important to monitor the effect on the turbines efficiency. The higher the efficiency, the higher the potential financial gain for the power plant operator. However, if the means of reducing pulsation reduces the efficiency significantly, one might be better off using another method that still maintains a higher efficiency. The life cost analysis involved is an important part in considering which solution is best suited for each power plant, while still earning the operators most money.



### 1.1 Leirfossene power plant

Leirfossene power plant, built in 2008, is located close to the city of Trondheim, Norway, and is part of a network of three hydro power plants taking advantage of the flow in the river Nidelva. The river is placed under strong regulatory laws controlling the minimum flow of the river. Of the three power plants, Leirfossene is considered the main one. The two other plants are considered to be small hydro power plants, only taking advantage of the minimum flow of the river. The plants are operated by Statkraft and have a combined power capacity of 45 MW annually producing 195 GWh. Leirfossene on its own has a power capacity of 45MW divided over two Francis turbines with a power of 29MW (Turbine 1) and 16MW (Turbine 2). Annually the plant produces 150 GWh, enough to supply 10 000 households with electricity. [3] Figure 1 shows the machine hall with the generator top for both turbines.



Figure 1 - Machine hall Leirfossene

#### Turbine 2

Producer	Andino
Type	Vertical Francis
Rated head	58m
Rated speed	333.3 rpm
Runaway speed	640 rpm
Rated Power	16MW
Runner blade	11
Rotational direction	Clockwise

#### Generator 2

Producer	VG Power
Rated Power	18 500kVA
Rated Voltage/Current	7000V / 1526 A
Rated power factor	0.89

Table 1 - Turbine and Generator Specifications

Shortly after the turbines were put into operation, it was discovered that the power plant is the source of vibrations that propagate through the bedrock, disturbing the residences in the surrounding area. The following investigation determined that the turbine was not optimally designed for its operating conditions. Especially under part load conditions, vibrations and noise caused by low frequency pressure pulsations in the draft tube can be noticed. Table 1 displays the technical information about the investigated turbine 2 and the corresponding generator.

## 1.2 Previous work

The following paragraphs will highlight some of the previous work published on both pressure pulsations and efficiency measurements.

### 1.2.1 Pressure pulsation

Pressure pulsation in reaction turbines is a well-documented field of study, and has been observed in turbines build as far back as 1912. One of the first to supply technical data on the subject was W. J. Rheingans back in 1940 [4]. The work presented the phenomena of power swings in hydroelectric plants, caused mainly by the occurrence of pulsations due to draft tube surges. One important subject of the publication is the relationship between the magnitude of the pulsations and the natural frequency of the operating components, and the consequence of these two reaching the same value.

Oftebro and Lønning publication in 1967 discussing pressure pulsations in Francis turbines [5]. This paper focuses mainly on pulsations caused by the interference between guide vanes and runner vanes in a Francis Turbine, commonly known as the Rotor Stator Interaction (RSI). At this point, the pressure pulsation itself were not considered to be damaging to the machinery. The focus was rather on the sound and vibrations caused by the interference, and the harmful frequencies associated with it.

PhD student Einar Korbo studied pressure pulsations in Francis turbines, [6]. A significant part of his research was to establish the connection between the pressure pulsations in Francis model and prototype runners, with main focus on steady state operations. Master students Anders Tørklep [7] and Sigurd Haga [8] have studied effects of dynamic load variation during start-stop procedures.

Vibrations are believed to be directly related to the pressure pulsations in the turbines. However, not much research has been published on vibrations in Francis runners. Previous work by Master student Frode Kjørnes at the waterpower laboratory focused on the measurement the natural frequencies of a circular disc in air and water [9]. Kjørnes tried to determine how the natural frequencies of a circular disc are influenced by nearby rigid surfaces when it is submerged in water.

In 2007, a research team from China an experimental investigation of pressure fluctuation and vibration in a large Francis turbine [10]. They performed measurements at the Three-gorges hydropower Plant in China, investigating vibrations at unsteady flows. This research concluded that reducing the pressure pulsation intensity would also reduce the vibrations in the system.

“Flow induced pulsation and Vibration in Hydroelectric Machinery” by Dörfler, Sick and Coutu (2006) [11], as well as the IEC 60994 [12] standard has been used extensively in addition to the publications.

### 1.2.2 The thermodynamic method

Efficiency measurements have been researched extensively over the last century. Today, several different methods exist and are acknowledged by both the research community and the industry. Among others, the pressure time method, current meters and the thermodynamic method. There are multiple reasons for performing efficiency measurements.

- I. It is important for the production companies to predict their production in order to meet the demand in the market. Based on that knowledge, the plants profitability can be estimated. [13]
- II. It has become more and more common to state an efficiency guarantee in the contract when new turbines are commissioned. An important part of the contract is the specification of the accepted uncertainty in the measurement of the promised efficiency of the turbine. It usually also states which method of efficiency measurement is to be used. [13] If it is determined that the efficiency of a new turbine is too low according to its specifications, the operator might be entitled to financial benefits from the manufacturer.
- III. Efficiency measurements are used to monitor the condition of the turbine. If an unnatural drop in efficiency or a decreasing trend is observed, one can assume that there is an issue in the plant that has to be taken care of.

Campas and Willim developed the thermodynamic method for measurement of efficiency in turbines and pumps in the 1950s. The work they presented laid the foundation for the thermodynamic method used in the standard IEC 60041. [1] A key component in the thermodynamic method is the accurate measurement of temperature. IEC 60041 states that the temperature has to be measured with an accuracy of at least 0.001K. The accurate computation of the flows heat capacity, absolute volume and isothermal factor are essential for obtaining accurate efficiency measurements [14] [15]. Herbst and Rögener together with research institutions, [1] determined the computed parameters used in the standard today.

The IEC 60041 standard was published in 1991 and has since not been updated. Hulaas and Vinnogg discussed in their paper presentation in 2010 during IGHEM [28] that it is time to revise the standard. They pointed out that it has been in use for a while and that the experience from users should be taken into account more. They also presented specific suggestions to be specified in the standard. This included the use of collecting vessels to avoid kinetic friction from the water to the sensor and that one should use the absolute temperature rather than a constant relative value when discussing the relative uncertainty in the draft tube.[16]

Research in Norway has traditionally focused on the thermodynamic method because the conditions at most of the power plants are favorable for these measurements. In recent years it has become more common to explore other methods like the Pressure-Time method and the current meters method. These methods are used especially on low head power plants where the uncertainty of the thermodynamic method increases with the reduction of head. The IEC 60041 recommends a minimum head of 100m, unless the conditions are highly favorable. One of the requirements of the thermodynamic methods is that the temperature is not allowed to have an temperature increase of more than 0.005K per minute. [1]

The publication “Uncertainty analysis of Pressure-Time measurements”, 2006 by H. Hulaas and O.G. Dahlhaug [17] highlights the lack of research on the Pressure-Times method and especially the uncertainty around the measurements compared the Thermodynamic method. Ph.D Candidate Jørgen Ramdal published his doctoral thesis in 2011 about “Efficiency measurements in low head hydro power plants” [18] where efficiency measurements using both the pressure time and the thermodynamic methods are compared and evaluated. Ramdal also did experiments where he challenged the norm of the geometrical properties the IEC standard had set for the pressure time method. His findings support O.G Dahlhaug and T. K. Nielsen publication from 2006 [19] that the thermodynamic method for measuring efficiency is reliable for low head power plants down to 50m head as long as the conditions are favorable. The ongoing research by Ph.D. Candidate Peter Joachim Gogstad at NTNU has focused on the effect of installations that reduce pressure pulsation has on the efficiency of the turbine.

For the execution and setup of the efficiency measurements the Standard IEC 60041:1991 Field acceptance test to determine the hydraulic performance of hydraulic turbines, storage pumps and pump turbines [1] has been used extensively, as well as “introduction to engineering experimentation” (2004) by Wheeler, A.J. and A.R. Ganji [20].

## 2 Theory

The theory regarding pressure pulsation and vibration, is taken directly from the earlier published Semester Project with the title “Pressure oscillations and Vibration in Francis Turbines”, in agreement with co-author Magomed Selmurzaev [21]. Some of the theory has been processed, rewritten and/or extended to suit the purpose of this master thesis.

Pressure oscillation in combination with mechanical imbalance is the main source of vibrations in hydropower systems. Pressure pulsations always exists in a turbine system. The efficiency of a turbine is mainly affected by three phenomena: pressure pulsations, sand erosion and cavitation erosion. In addition to reducing the efficiency of the system, pressure pulsations expose the system to vibrations and large mass movements. The consequence of the loads acting on the turbine will eventually lead to damage and fatigue.

It is therefore important to perform pressure and vibration measurements to in order to compute which frequencies are present in the system. This makes it possible to track the frequencies over time. If the frequency changes or the frequency intensity increase, it may imply that something is damaged and precautions can be taken before fatal system failure occurs.

### 2.1 Pressure Pulsations

A turbine is originally designed to run at its best efficiency point (BEP). Per definition this is the point at which the turbine, for a given flow and head, operates at maximum efficiency. At this point, the only pressure pulsation present is caused by guide vane and stay vane interaction in the vanless space. Running outside BEP, however, introduces several other phenomena in the system, such as vortex shredding and separation of the flow at the inlet and outlet of the runner. Operation at overload has shown to give fluctuations of periodical nature, while low load fluctuations occur stochastically. Running the turbine at part load is more damaging as the fluctuations are of significantly higher intensity.

Several things determine the extent of the pulsations; the operational state of the turbine, the design of the machinery and the dynamic response of the system. During start and stop operation the turbine is exposed to pressure pulsations of low frequency.

In this chapter, the two main sources of pressure pulsations and vibrations will be presented. These are rotational dependent pulsations, related to the rotational speed of the runner, and elastic pulsations, caused by hydraulic instabilities often related to system inequality. When analysis pressure data, the result is often presented in the form of frequencies diagrams. The different frequencies can usually be related to a specific source in the system. The different causes with their related frequencies as well as the area of occurrence are described below.[31]

### 2.1.1 Runner frequency

This is the frequency caused by the rotation of the runner. Each element is exposed to constant pressure variation, switching from pressure side to suction side of the blade. This creates a pressure field rotating periodically with the speed of the runner. The runner frequency (Eq. 2-1) is considered to have a low amplitude and can be considered constant due to the uniform shape of the runner and normally operating at the same rotational speed. However, if the runner is damaged, e.g. erosion, cavitation, breaks or the generator/shaft is poorly installed or damaged, the frequency amplitude will increase. [31][33]

$$f_n = \frac{n}{60} [Hz] \quad (\text{Eq. 2-1})$$

### 2.1.2 Runner vane frequency

A pressure pulse is created every time a point on the impeller vane passes the same guide vane. The amplitude of this frequency is dependent on the distance between guide vanes and runner vanes, and thus the guide vane opening is of great influence. During steady state conditions, this is the dominating pressure oscillation in the system (Eq. 2-2). [31][32]

$$f_{rv} = f_n * z_{rv} [Hz] \quad (\text{Eq. 2-2})$$

Due to the constant presence, these forces will inflict abrasion on the runner even at low frequency.

### 2.1.3 Guide vane frequency

Every time an impeller vane passes a guide vane it will undergo a pressure pulsation. This is due to the pressure difference between the two sides of the guide vane, which is exposed to suction on the inside (flow inlet area), and pressure on the outside. The effect can be reduced by increasing the distance of the vanless space, as the amplitude is predominant at high guide vane angles. The magnitude of the frequency is dependent on number of guide vanes (Eq. 2-3). [31]

$$f_{gv} = f_n * z_{gv} [Hz] \quad (\text{Eq. 2-3})$$

It is important to avoid Rotor-Stator-Interaction (RSI) at several locations of the runner at the same time. This will lead to amplification of the pulsations, since several shock propagation waves occur at the same moment. The phenomena is well described in *Symposium on Hydraulic Machinery and Systems* [22].

### 2.1.4 Rheingans frequency

Described by Rheingans in 1940 [4], surge is one of the earliest researched pulsations problems in the Francis turbine. Surge describes the pressure pulsation that exists in the draft tube because of the flow exiting the runner with a tangential velocity. When the flow exits the runner at BEP, it does not have a tangential velocity (no swirl), meaning the flow is parallel to the shaft axis. At operation outside BEP, the direction of the outlet flow changes and creates a tangential velocity component. Figure 2 shows the outlet velocity triangle at three different operating conditions:

- I. Best Efficiency Point (BEP)     $(Q = Q^*)$
- II. Part Load (PL)                     $(Q < Q^*)$
- III. High Load (HL)                     $(Q > Q^*)$

The consequence of this is the occurrence of a vortex in the draft tube. Which way the vortex is rotating is dependent on the operating conditions. At part load, the direction of the flow is the same as the direction of the rotating runner, and opposite of the direction of the runner rotation at full load. The pressure inside the vortex is lower than the pressure in the surroundings, with creates pulsations every time the vortex passes a certain point on the wall. The amplitude becomes dominant at part load, as the rope swings closer to the draft tube wall, amplifying the oscillations. Equation 2-4 shows the expression used to determine the Rheingans frequency at part load.

$$f_R \cong \frac{f_n}{3.6} [Hz] \quad (\text{Eq. 2-4})$$

At certain conditions, a rotating cavitated vortex rope can occur in the draft tube. This vortex rope can become so strong that they cause radial force fluctuation so great that they propagate upstream through the runner. Worst-case scenario, the fluctuation coincides with the resonance frequencies of the system causing even greater fluctuation. The fluctuation present under these conditions are putting a lot of stress on the mechanical components in the system. Over time, this will lead to failure.

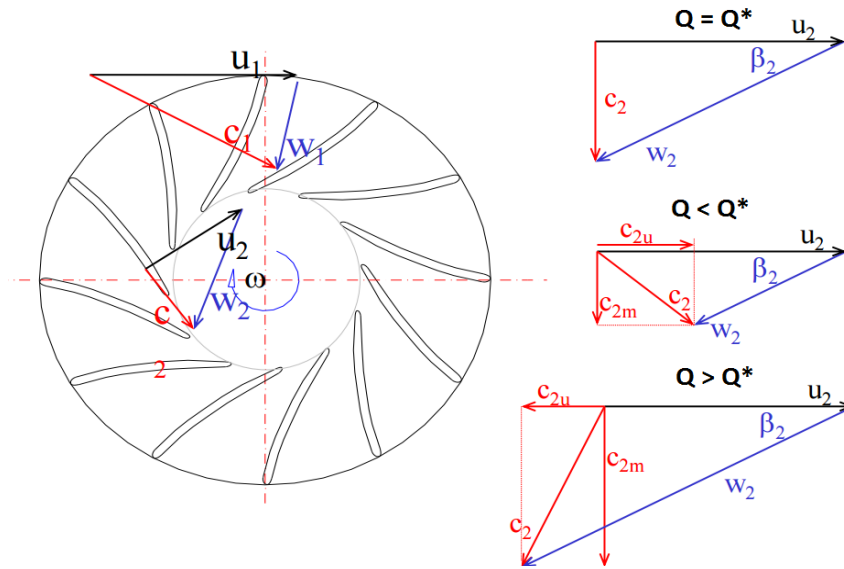


Figure 2 - Francis Turbine velocity profile at outlet - [23]

At high-load, a pulsating cavitated vortex core in the middle of the draft tube can occur. During these pulsations the system is affected by pressure oscillation that in line with the part load can propagate upstream of the runner as well. This might also surge the existing elastic fluctuations in the water. It is important to be aware that surge will still be present even when the cavitated vortex rope is not present. The effect on the system will however be less. [31][34]



Figure 4 - Vortex rope at part load [24]



Figure 3 - Vortex rope at high load[24]



### 2.1.5 Elastic fluctuations

An elastic fluctuation is a pressure oscillation that is not depended on the rotational speed of the runner. In a hydro power plant, these oscillations are categorized as mass oscillation or water hammer oscillations because of the moving masses of water oscillating in the waterway. These fluctuations are caused by system inequality and mechanical errors. These elastic fluctuations are always present in rotating hydro-machinery. The magnitude of the fluctuation is not directly affected by the rotational speed of the runner, but amplifies significantly if the water masses in the pipe are exposed to sudden pressure change. The most common source of sudden pressure change is the adjustment of the guide vane opening. Altering the guide vane opening will produces a change in internal pressure. These fluctuations in pressure propagate through the water at the speed of sound. This will either accelerate or break the flow both downstream and upstream of the runner, causing pressure oscillations in the system. [31] [36]

As the oscillations are closely related to the propagation of sound in water, the speed of sound must be closely considered. Sound is a vibration that propagates through a medium in form of mechanical wave of pressure, displacement or stress. The speed of the wave is therefore very dependent on the internal forces of the medium it is travelling through, such as geometric shape, elasticity and viscosity. The speed of sound is given by equation 2-5,  $\rho$  is the density of water and  $K$  is the coefficient of stiffness/bulk modulus:

$$a = \sqrt{K/\rho} \quad (\text{Eq. 2-5})$$

The bulk modulus is defined as the ratio of infinitesimal pressure increase to the resulting relative decrease of the volume. This indicates that the speed of sound can vary significantly for the same medium. In still standing water the speed can be approximated to 1500 m/s. However, a closed pipe, with bends, valves and varying diameters will drop the velocity considerably. Equation 2-6 and equation 2-7 can be used to estimate the water hammer frequency. Flow passing obstacles in the waterway will produce a pressure pulse, which is known to propagate to a free water surface [22]. The distance  $L$  describes the distance from any rigid object, like the turbine, to the free water surface.

$$t = \frac{2L}{a} \quad (\text{Eq. 2-6})$$

$$f = \frac{1}{t} = \frac{a}{2L} \quad (\text{Eq. 2-7})$$

The phenomenon, known as water hammer oscillations, is an important subject when considering high frequency pulsation. U-tube fluctuation have be considered when dealing with water hammer oscillations. U-tube fluctuation occurs do to large water hammer oscillations, travelling between the turbine and the surge chamber in a resonating manner. The initial u-tube oscillations has the greatest amplitude, but will decrease over time due to the internal friction of the system.

### 2.1.6 Cavitation

Cavitation is a phenomenon that occurs in fast moving fluid. When the static pressure decreases under the vapor pressure of the fluid, small vapor bubbles are created, that condensate and implode with immense force when the pressure increases. This will usually happen at the outlet of the turbine, typically at trailing edge of a runner vane. This force created from the cavitation bobble imploding, is big enough to create visible damage to the runner. Eventually the turbine has to be maintained to avoid erosive damage on the runner. [23]

Nowadays, it is common to design the turbines in a way that the cavitation happens in the draft tube instead of on the runner. In Francis turbines, cavitation is known to be present especially under part- and high- load operation. Cavitation is a leading factor in the formation of the vortex rope. [25]

### 2.1.7 Von Karman Vortex shedding

Von Karman vortex shedding is a flow that starts oscillating when it interacts with a solid surface at certain velocities. Vortex shedding is a known phenomenon in hydro power plants utilizing Francis runners. Usually one will be able to observe vortex shedding at the trailing edge of the stay vanes, guide vanes and runner vanes. This phenomenon will cause vibration and noise that can govern the operation of the runner. Based on the work on the von Karman vortex, it has become standard to design the trailing edges on the vanes in such a way that it reduces the vortex shedding in the unit. (Eq. 2-8) [25]

$$f_{\text{vortex}} = 190 \frac{B}{100t + 0.56} \frac{C}{\quad} \quad (\text{Eq. 2-8})$$

The von Karman vortex shedding is one of the hardest frequencies to accurately detect, because its amplitude usually is relative low and is highly dependent on the operating condition causing the frequencies to drift when the velocity changes. [36]

## 2.2 Vibration

Vibration is the periodic or random oscillations of physical back and forth movement and fluctuations around a reference position. A frequency, measured in Hertz (Hz) describes the number of times these motions complete a cycle within one second. Using the tuning fork as an example, it produces one continuous steady frequency component even as time passes. This makes it ideal to tune instruments, because it always recreates the same frequency. However, in most mechanical components, especially in rotating and moving equipment, there will be multiple frequency components in a vibration signal. An analysis has to be performed in order to determine which frequencies are present. Most commonly, a frequency spectrogram is used to plot vibration intensity against frequency.

As with pressure oscillations measurements, one looks for already known frequencies in the system. This enables an operator to track vibrations and its source in the machine. Frequencies with high amplitudes and the frequencies that can not be explained by already known frequencies are usually the ones that should be further investigated [26]. Typically, accelerometers will be used to measure vibrations. By integrating the accelerometers values, one can determine both the displacement and the velocity of the vibration.

Consequences of not analyzing or investigating vibrations in a mechanical system can be severe and can ultimately lead to system failure. During the last century, it has therefore become more and more common for companies to invest large sums in the study of vibrations. Annual measurements are performed and compared to previous sets of data in order to track the frequencies in the system. This helps companies to better predict maintenance downtime and avoid critical failures [10]. In a Francis turbine, system vibrations are most often caused by unsteady flow, e.g. pressure oscillation, or mechanical imbalances.

### 2.2.1 Mounting of accelerometers

Choosing the accelerometer mounting position depends on the machinery, the axis of the accelerator and the area to investigate. The sensitive axis of the accelerometer should be mounted in the direction of the motion one wants to investigate. The sensor should be positioned as close to the targeted area as possible in order to avoid other frequency components to influence the measurements. For example, you would not place a sensor on the outside of the car when you are investigating vibration from the bearing. [26]

The most common methods to mount accelerometers are: threaded stud, beeswax and cement. Each method has their own advantages and limitations. Threaded stud requires the stud to physically be drilled into the machinery. This method does not influence the resonant frequency in any significant amount. This method is used when accelerometers have to be permanently mounted to the machinery.

Under certain circumstances one wishes to have a permanently mounted accelerometer without drilling holes in the structure. The best option then is to fasten the sensor with glue, known as cementing. It is important to use a hard glue, to avoid the glue acting as a mechanical filter by lowering the resonance frequency.

Beeswax is a non-destructive mounting method where a thin layer of beeswax used to fasten the sensor to the machinery. This method causes a slight reduction in the resonant frequency of the accelerometer. The use of beeswax is limited by the surface temperature of the machinery because wax will melt at around 40 degrees Celsius. This method is used when a non-destructive method is preferred or when a quick setup is preferred. With the use of hard glue, resonant frequency is lowered about the same amount as the beeswax.

### 2.2.2 Resonance

Resonance is a phenomenon where an object or system gets in contact with another vibrating system that will force the original system to oscillate and amplify its frequency. [Figure 5] The cause of the amplification of the oscillations is that the original system has the ability to store the vibration energy [35]. Over time, these oscillations will lead to damage and fatigue on the machinery, ultimately causing total system failure. A well-known example is the Tacoma bridge collapse in Washington. The bridge experienced forced resonance due to high wind velocity that matched the natural frequency of the bridge, causing the amplification of the oscillations that led to the collapse.

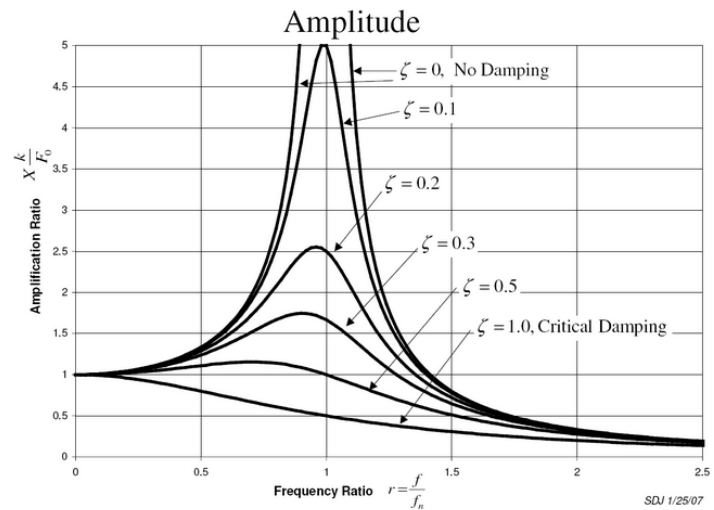


Figure 5 - Resonance [44]

### 2.3 Methods of reducing pressure pulsations

Current research focuses on finding methods of reducing and mitigating the effect of pressure pulsations. It is common to distinguish between active and passive installations. Active installations distinguishes themselves from passives installations because they requires something to be continuously added to the system. Typical active installations use water and air injections. These are often injected either through the hub of the turbine or through the wall of the draft tube. Air injection will change the viscosity of the water in the draft tube.

Passive installations have the advantage that when they first have been installed, they are considered permanent and do not need any additional control system to alter them. Traditionally the development has focused on fins in the draft tube and runner cone extensions.

The common perception in the industry is that the effect of the installations are case dependent. This means that some power plants may experience good results with the installations, whereas other will experience no effect or aggravation of the pressure pulsation. Previous publications [28],[29] display how both air and water injection can be beneficial at some operational points and negative effects at others for the same turbine. The publication by March in 2011 showed that turbines have experienced a substantial loss in efficiency, up to 4%.[27] It also states that there is a correlation between the high flows of injected air and increasing losses.

NTNU has conducted several published experiments with runner cone extensions. Ph.D Vekve as well as the ongoing work by Ph.D. Canidate Peter Joachim Gogstad are both noteworthy. Vekve performed initial model test measurements on a Francis turbine with runner cone extensions of different length and diameters in 2004[28]. He concluded that the runner cone with the largest diameter and longest length had the best effect on reducing the pressure pulsations in the model runner. Furthermore, a full-scale test was conducted on the Francis runner at Litjfossen Hydro power Plant in Norway, showing a reduction in pressure pulsation of up to 40% at part load and a relative minor decrease in

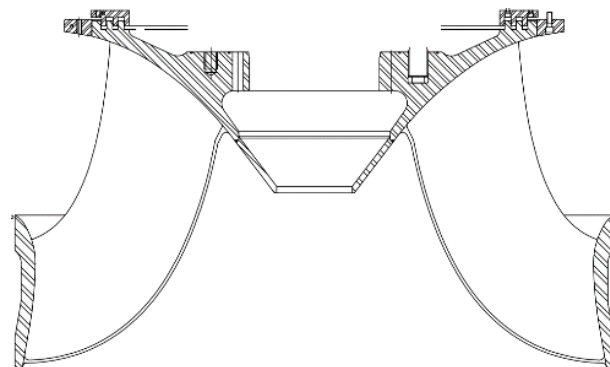


Figure 6 - Runner

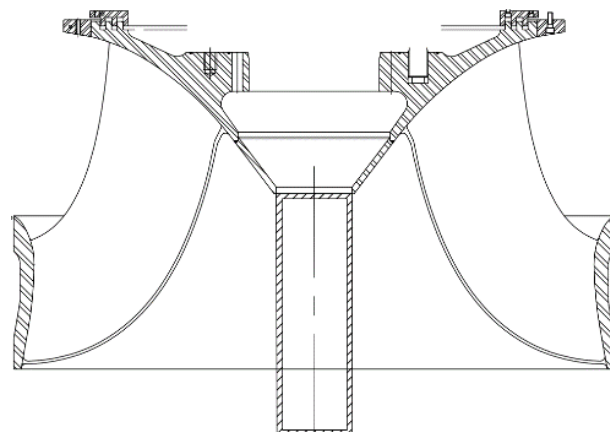


Figure 7 - Runner with runner cone extension

efficiency of 0.5%. Vekve determined that the runner cone extension moved the initialization point of the draft tube vortex rope further downstream in the draft tube. This limits the longitudinal buildup of the vortex rope, reducing the amplitude of the rotating vortex rope and thereby its intensity.

In most recent years, Ph.D. Candidate Gogstad has developed a freely rotating runner cone extension (FRUCE). In 2015 he conducted experiments on a model Francis turbine utilizing a FRUCE with different lengths. His results show a reduction in the pressure amplitude for some cases during part load. It should be pointed out that the non-rotating runner cone extension showed a greater reduction in amplitudes compared to the FRUCE [30]. An observation made by Gogstad is that the highest tangential velocity in the draft tube is at  $0.73Q/Q_{BEP}$ , while the highest peak to peak values is found at flow rates lower than this. Gogstad, in collaboration with Statkraft, is planning to perform a prototype test with a FRUCE at Leirfossene Hydro Power Plant in the third quarter of 2016.

The theory behind the usage of the runner cone extension is that one introduces an object that removes some of the area in the center of the draft tube [Figure 6 and Figure 7]. This forces the axial velocity to increase, reducing the swirl number [30], hopefully reducing the pressure pulsation amplitudes. Experience shows that runner cone extensions with smaller diameters can have a lesser effect. This is possibly because of the runner cone extension not reducing the swirl number as much. Some have experienced that the vortex rope initiates on the extension itself when smaller diameters are used.

## 2.4 Data acquisition

The goal of data acquisition is to sample enough information about the analog signal that one is able to recreate the signal digitally. When acquiring an analog signal it is common to digitalize the signal to be able to store large amounts of data and to have it easily available for data processing. In data processing, it is common to use frequency analysis as a means of displaying and identifying frequencies and their amplitudes in the signal. This chapter will explore the theoretical sampling of analog signals and the post-processing of the digitalized signal.

### 2.4.1 Sampling rate theorem

When a voltage signal is sampled, the data acquisition system reads the values at the given sampling rate. The sampling rate determines how often the sampling device reads the value of the analog signal within one second. This implies that any digital sampling always will be discontinuous [Figure 8]. When the signal is being digitally recreated, an algorithm is used to connect the sampled values to each other creating an interpolated line between the points. The resolution is highly dependent on the amount of sampled points, also known as the sampling frequency.

Today all data acquisition operations are in one way or the other based on the Nyquist-Shannon sampling theorem [37][38]. Nyquist explored the connection between analog signals (continuous-time signals) and digital signals (discrete-time signals). In 1928, Nyquist determined that it is possible to send an independent pulse with a sample twice the systems bandwidth. Shannon proved the sampling theorem in 1949 and applied the theorem to data sampling and the reconstruction of continuous signals. [37]

The sampling rate is commonly referred to as both the Nyquist rate and the Nyquist sampling rate. The sampling rate  $F_s$  defined to be at least twice the highest expected frequency of the analog signal  $f_{high}$  (Eq. 2-9). Figure 9 and Figure 10 show the difference between a rate that is too low and the Nyquist rate.

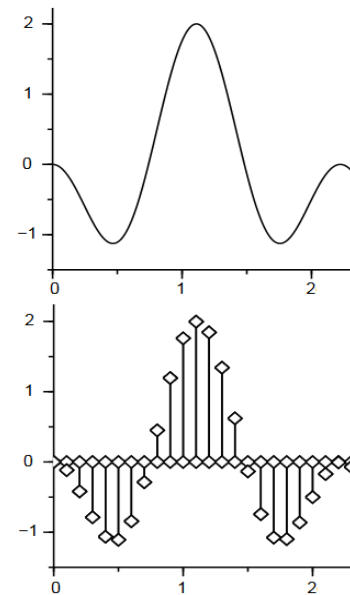


Figure 8 - Analog to digital signal

$$F_s = 2 \cdot f_{high} \quad (\text{Eq. 2-9})$$

## 2. Theory

## Data acquisition

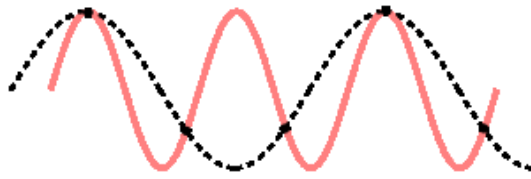


Figure 9 - 1.5 samples per cycle

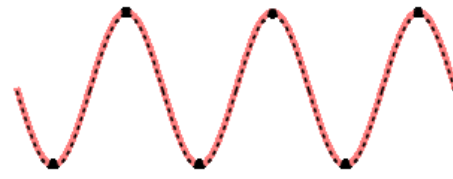


Figure 10 - 2 samples per cycle

The Nyquist-Shannon theorem provides the theoretical minimum sampling rate of any data acquisition system measuring analog signals in order to reconstruct the signal fully. In reality it is difficult to determine an accurate highest frequency of the analog signal. If one is logging at a too low sampling frequency, it will introduce aliases in the measurements and potential spectral leakage in further analysis. This will be discussed later.

### 2.4.2 A/D converter

An analog to digital converter takes a physical signal and converts it to a digital number. This is done to store the recorded analog data, usually stored on binary, on a digital recording device like a computer.

The resolution of the converter is determined by the number of discrete values that can be computed from the range of the analog value. This can be expressed in volt. Equation 2-10 determines the minimum change in voltage needed to result in a change of the digital input, also known as the least significant bit (LSB) [41].

$$Q = \frac{E_{FSR}}{2^M - 1} \quad (\text{Eq. 2-10})$$

$E_{FSR}$  stands for the voltage range used in the measurements  $E_{FSR} = V_{high} - V_{low}$ . For the measurements at Leirfossene, the voltage span used is 0-10V. The exponent “M” stands for the analog to digital converters resolution and is expressed in bits. Table 2 displays the bit rates effect on the LSB value for voltage. Figure 11 displays how the bit resolution effect the sampling of a sinusoid. The 3-bit resolution only follows the main trend, while the 16-bit resolution follows the sinusoid better, especially at its extremal values. [38][45]

Bit resolutions	Distinct values	LSB
8	256	39 mV
10	1024	9.7 mV
12	4096	2.5 mV
14	16384	0.6 mV
16	65536	0.15 mV
24	16777216	0.59 $\mu$ V

Table 2 - Bit resolution

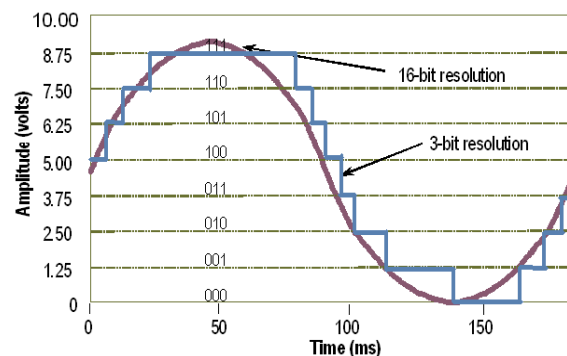


Figure 11 - Bit resolution on a sinusoid [45]



### 2.4.3 Aliasing

Aliasing occurs when an analog signal is sampled with a too low sampling rate relative to the highest frequency component present in the system. This causes a misidentification of frequency components of the signal, where high frequency components are represented as low frequency components. Aliasing will make it impossible to distinguish the different sinusoids of the signal from each other after they have been sampled. This means that it is not possible to recreate the original signal based on the sampled data.

Analog signals are usually modeled as sinusoids. An analog signal will however not have an upper frequency component. This means that the aliasing effect will always be present in the digitalized signal. Figure 12 displays how a signal with a frequency of 9 cycles per second will be represented as a signal with one cycle per second when it is being sampled at a rate of one sample per second. [38][41]

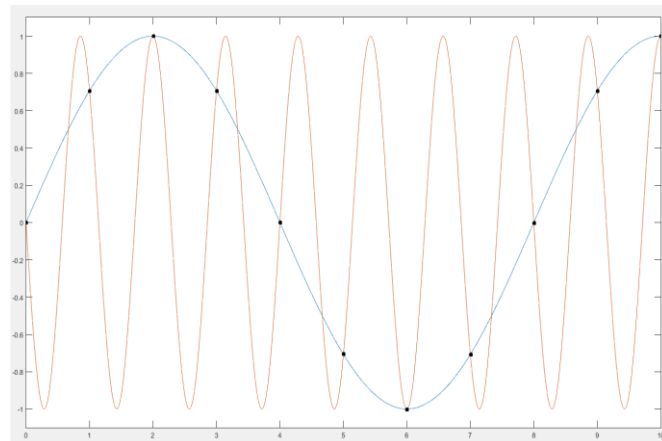


Figure 12 - Aliasing example

To reduce the effect of aliasing, oversampling can be used. Chapter 2.4.1 discussed how the Nyquist sampling theorem allows the discrete-time signal to capture the complete analog signal. Oversampling refers to the sampling of a signal with a significant higher sampling rate than what the Nyquist sampling rate demands. This is commonly referred to as oversampling with the factor  $N$  of the Nyquist rate. In reality, it is common to oversample the signal because it will increase the resolution, reduce the effect of aliasing, phase distortion and noise in the measurements.

An advantage in measurement systems where one utilizes oversampling is that one reduces the need for anti-aliasing filters on the original analog signal. This is because the digital signal has gotten enough information from the sampled analog signal that one can apply anti-aliasing filters digitally. It is common for many of the analog to digital converters to have built in filters that take care of aliasing problems.

Another aspect of oversampling is the noise that will always be present in any sampled data. Research [42] shows that the signal-to-noise ratio, SNR, depends on the samples taken. The larger the sample  $N$ , the lower the SNR will be. Therefore, one will experience less noise in an oversampled signal compared to a signal sampled with the Nyquist rate. This is a cost effective and efficient way of performing signal processing. Oversampling also provides the option of re-sampling the signal to the desired sampling frequency without introducing new aliases.

## 2.5 Post processing

The raw data has to be processed in order to obtain the needed information. In order to achieve the best results, the data is put through statistical and signal enhancement tools to make sure that there are as few outliers present. The next chapter will focus on the post processing of the data used in frequency and peak pressure analysis.

### 2.5.1 Fast Fourier Transform

The Fast Fourier Transform (FFT) is an optimization of the Discrete Fourier Transform (DFT). The DFT describes the connection between analog and digital signals. Multiple DFT optimization algorithms exist today, with the FFT being the most common. When applying the FFT to a time domain signal, one is able to decompose the different sinusoids present in the signal. This is done by taking the signal from the time domain and converting to the frequency domain. The function, in this case the logged signal, is decomposed into sinusoid functions.

The FFT is applied to the continuous signal of the time domain, this will identify all the frequency components of the signal, that otherwise would have been impossible to distinguish from the raw signal. A challenge that will arise in the transformation is that the FFT requires a continuous signal.[40] A logged digital signal does not meet this requirement due to the digital signal being discontinuous. Therefore, the frequency spectrum will experience spectral leakage. Window functions can be applied to compensate for the discontinuity. When the FFT is applied correctly, one is able to recreate the original signal from the frequency domain to the time domain.[39]

### 2.5.2 Window function

The FFT assumes that the signal, which is being transformed into the frequency domain, is periodic. In real life, the sampled signals rarely appear to be periodic. This will cause errors in the transformation. Usually these errors are referred to as spectral leakage or “smearing” of the peaks. In the analysis, this means that the intensity of the frequencies will be distorted.

In order to compensate for the errors in the transformation, one can precondition the original signal in the time domain. Most commonly, window functions are applied. Window functions are mathematical functions that bring the edges of a sampled signal rapidly towards zero. This means that it is the window functions responsibility to make the signal behave periodic and avoid discontinuities by removing the sharp edges. This will in most cases mitigate the spectral leakage. However, some of the information in the signal will be lost when window functions are applied. It can for example reduce the amplitude of the entire frequency spectrum. When processing large data sets it is common to divide the data into smaller data sets and apply individual windows on each set. To limit the loss of data at the edges, the windows overlap. Determining the necessary overlap factor is based on both the applied window function as well as the desire to isolate frequencies in the FFT. A smaller window like the Flat top window will need a higher overlap factor than larger windows like the Hanning window. [39][40]

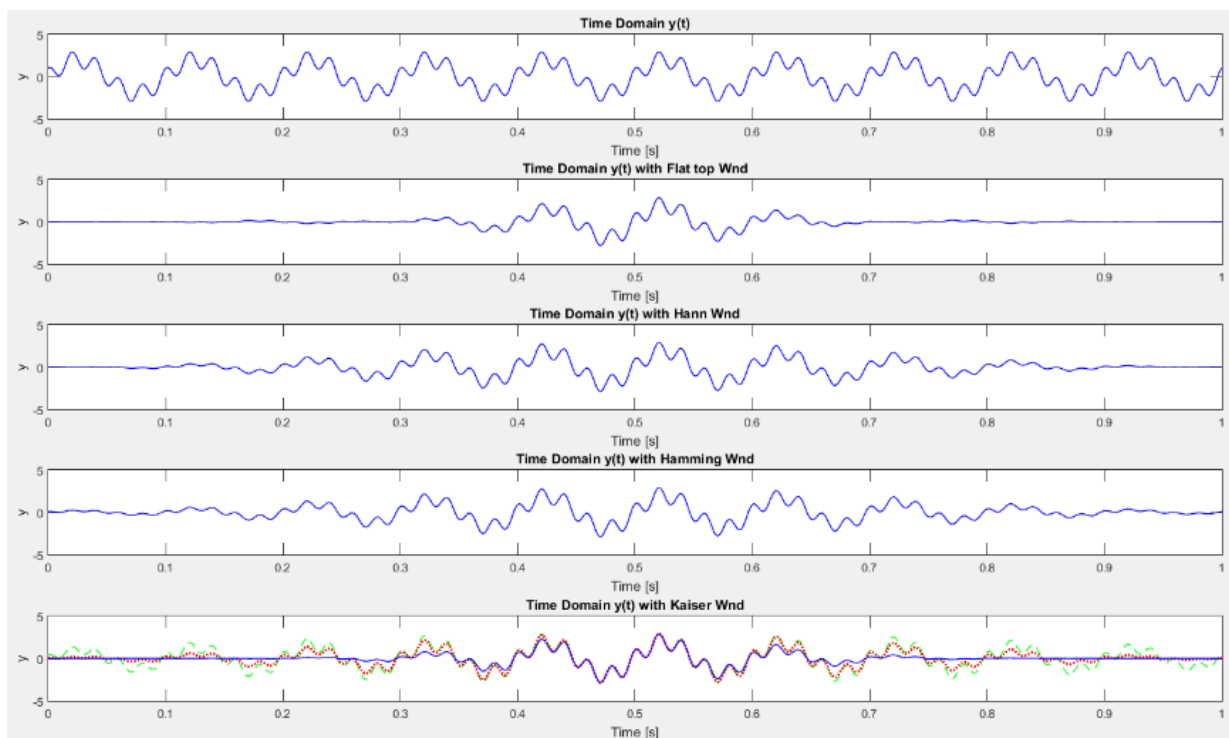


Figure 13 - Window functions-Flat top, Hann, Hamming and Kaiser

Figure 13 shows the effect of the Flat top, Hann, Hamming and Kaiser Window functions on a generated time domain signal. These are some of the most common window functions. Each window has its own frequency response and characteristics that makes it suited for specific applications. When speaking about window functions and its effect on the frequency analysis it is important to be aware of the windows impact on the Fourier transform. Each frequency peak will be exposed to spectral leakage. [40]

Figure 14 displays how the detected frequency, referenced as the main lobe, will be represented in the Fourier transformation. The spectral leakage refers to the smaller lobes present on each side of the main lobe (sidelobes). The sidelobe level describes the intensity of the spectral leakage. A special case with the FFT analysis is that the Rectangular window function is automatically applied to the time domain-signal when no other window function is selected. The rectangular window does however maintain a distinct discontinuity resulting in a high sidelobe level. [40][39]

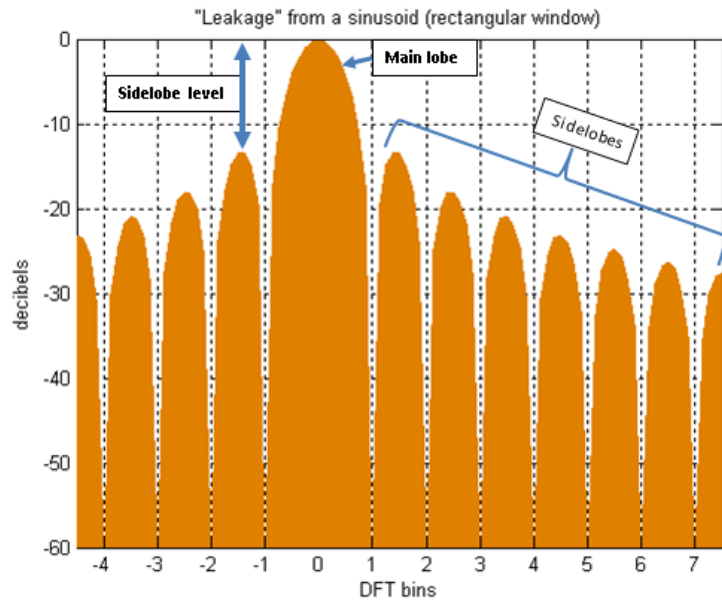


Figure 14 - Spectral leakage [43]

The correct window size has to be determined in order to achieve the best effect of the window function. This can be estimated by knowing the expected frequency in the signal. In order for the FFT analysis to detect the correct frequency and its amplitude, the signal period has to be repeated enough times within the window. A good estimation is that the period should be repeated 10 to 15 within the window for it to be of good accuracy. For example, if one is to investigate a frequency of 1HZ, with the signal sampled at 2000 samples per seconds, the window size then has to be between 20 000 and 30 000 samples to achieve the desired accuracy. [45] Numerous window functions with the ability to mitigate the discontinuity significantly are available. Some of the common window function are explored in the next paragraphs.

### 2.5.2.1 Flat top window

The flat top window is a sinusoidal window function with a negative value because it crosses zero. The function leaves only a small section of the signal intact. Because of this, it needs a large overlap factor to still get enough information for the FFT. Due to the high overlap factor, it is recommended to use larger data sets, enabling larger window lengths to ensure higher resolutions. The result of using a flat top window function is that the main lobe of the frequency spectrum becomes dominant, with low side lobe levels. However, it does result in the main lobe to get a slightly wider peak in the frequency domain. This makes the flat top windows suitable for determining accurate frequency amplitude, especially in sinusoidal signals.[39][40]

### 2.5.2.2 Hann window

The Hann window, commonly referred to as Hanning window, is a window function that is typically used for digital signal processing. The function uses a sinusoidal shape that goes to zero at the edges. Because it uses a sinusoidal shape, the function will let a lot of the signal to pass through. This is both an advantage and a drawback. It will slightly reduce the frequency resolution because it widens the main lobe. The big advantage is that the window function has a low aliasing effect and is known to have a low spectral leakage. This results in low side lobes, which makes it very suitable for signal processing. Many use this window function as their standard function. Because the Hanning window is known to be highly applicable to signals that are sinusoidal or a combination of sinusoidal. The window function is also to utilize for narrowband signals and when content of the signal is unknown. [39][40]

### 2.5.2.3 Hamming Window

The Hamming window is similar to the Hanning window in its sinusoidal shape but differs in that it does not go to zero at the edges of the window. This means that the Hamming window lets through more information, which results in a narrower main lobe, making it easier to distinguish the frequencies that are located close to each other. A drawback is that the sidelobe levels increase slightly because of the hamming window still being discontinuous in Fourier transformation. The overlap of the Hamming window is more or less the same as with the Hanning window. Hamming window does a better job than the Hanning in eliminating the closest sidelobes to the main lobe, but has a poorer performance on removing the rest of the sidelobes. Typically, the Hamming window is used on signals with closely spaced sine waves because of its narrow bandwidth. [39][40]

#### 2.5.2.4 Kaiser window

The Kaiser window belongs to the family of adjustable window functions. Like most adjustable window functions, one can control the Kaiser window by adjusting the variable  $\alpha$  that determines the relationship between the main and side-lobes. Figure 13 shows how the different values of the variable affect the shape of the Kaiser window. The Kaiser window can be adjusted to mimic the same effect as both the Hanning and flat top window functions. It can let the edges of the window go towards zero as well as remain well above zero. The overlap factor of the window is highly depended on the adjustment of the window. A narrow window will result in a higher overlap factor compared to wider windows. Experienced users tend to use adjustable window because of its adjustability and ability to display even the lowest frequencies due to the low sidelobe level. This means that one will be able to display frequencies close to each other but have distinctly different amplitudes. [39][40]

### 2.5.3 Harmonies

Harmonies are a phenomenon that occurs in frequency analysis. It is defined as a frequency that is an integer of the fundamental frequency. This means that harmonies are described as the appearance of frequencies that are directly related to a main frequency by integer multiples of each other. The harmonies can appear with both a greater and smaller amplitude than the main frequency. The amplitudes tend to be decreasing with the increase of frequency. The main frequency is often referred to as the fundamental frequency, and the harmonies as the 2<sup>nd</sup>, 3<sup>rd</sup>, ..., n<sup>th</sup> harmony. [Figure 15][46]

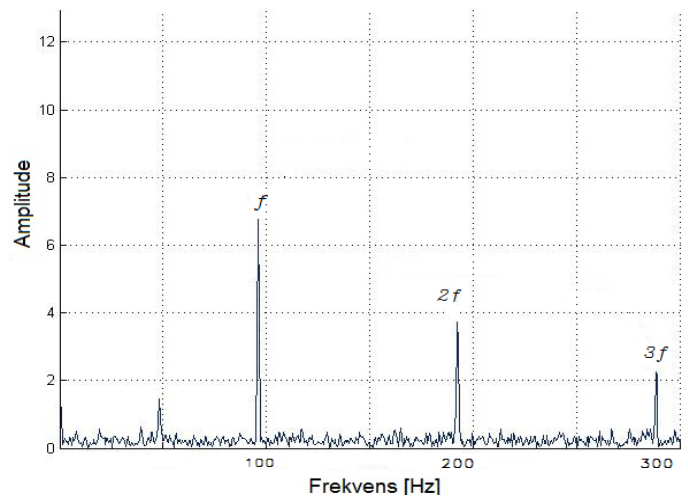


Figure 15 - Harmonies

### 2.5.4 Peak-to-peak analysis

Peak-to-peak analysis is used in post processing to displays the full range of the measured data. It shows the difference between the highest and lowest measured signal, known as the maximum excursion of the signal. Figure 16 displays the histogram of a pressure sensor. The x-axis displays the pressure in kPa while the y-axis displays the number of times the pressure is repeated. The histogram is plotted using a 99% confidence level. This can be observed at the edges of the histogram where the edges are “cut off” to avoid statistically unlikely values. The peak pressure value for the sensor will be the distance from the left side of the histogram to the right side.

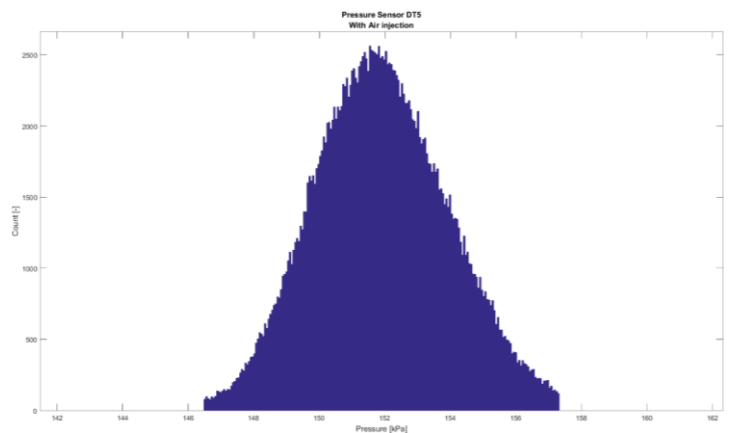


Figure 16 - Histogram- Peak to Peak

The histogram is plotted using a 99%

confidence level. This can be observed at the edges of the histogram where the edges are “cut off” to avoid statistically unlikely values. The peak pressure value for the sensor will be the distance from the left side of the histogram to the right side.

The advantage of post processing the data using the peak-to-peak analysis is that one is able to compare how trends and intensities developments in the system. This can be useful in pressure pulsation analysis because one often is interested to know if the pulsation amplitudes increase or decrease. Applying a confidence interval ensures that there is a high certainty that the amplitudes are within these levels.[28]

## 2.6 Efficiency measurements

Efficiency measurements are performed on both new and old runners. It is common to perform efficiency measurements on newly built units as a method of verifying that the contracted guarantees are fulfilled. On old units, it is used as a method to monitor the condition of the hydraulic units and as a tool to anticipate maintenance and downtime.

When new turbines are commissioned, it is common practice to determine which method and standard is supposed to be used for the acceptance test of the new unit. Different methods are available and some of the methods have requirements that have to be met in order to perform the measurements. When these requirements can not be met on the prototype runner, the standard IEC 60041 recommends performing the acceptance tests on a model runner instead. [1] The equation (Eq. 2-11) for calculating the efficiency of any system, is to calculate the relationship between the available power and actually produced power.

$$\eta = \frac{P_{produced}}{P_{available}} \quad (\text{Eq. 2-11})$$

The total efficiency of a power plant can also be expressed as the combined efficiency of all components in the system. (Eq. 2-12 shows how the total efficiency hydraulic power unit it can be expressed.

$$\eta_{tot} = \eta_{hydraulic} \cdot \eta_{generator} \cdot \eta_{transformer} \cdot \eta_{mechanical} \cdot \eta_{leakage} \quad (\text{Eq. 2-12})$$

Equation 2-13 shows the expression for calculating the efficiency of a turbine. Equation 2-14 and 2-15 show the expressions for the mechanical and hydraulic efficiency.

$$\eta_{turbine} = \eta_{mechanical} \cdot \eta_{hydraulic} \quad (\text{Eq. 2-13})$$

$$\eta_{mechanical} = \frac{P_{mechanical}}{P_{runner}} \quad (\text{Eq. 2-14})$$

$$\eta_{hydraulic} = \frac{P_{runner}}{P_{hydraulic}} \quad (\text{Eq. 2-15})$$

Equation 2-16 and 2-17 shows how the hydraulic and mechanical power is defined.

$$P_{hydraulic} = \rho g H Q \quad (\text{Eq. 2-16})$$

$$P_{generator} = \frac{P_{generator}}{\eta_{generator}} \quad (\text{Eq. 2-17})$$

Equation 2-18 shows the turbine efficiency as a combination of the above listed equations.

$$\eta_{turbine} = \frac{P_{mechanical}}{P_{hydraulic}} = \frac{P_{generator}}{\eta_{generator} \cdot P_{hydraulic}} = \frac{P_{generator}}{\eta_{generator} \cdot \rho g H Q} \quad (\text{Eq. 2-18})$$



### 2.6.1 Methods of flow measurements

The turbine efficiency is computed using equation 2-18 The flow parameter,  $Q$ , is the most difficult to determine accurately. This is because it is often difficult to access the flow itself, or because the measuring methods have limitations. This chapter will take a closer look at the different methods of measuring flow.

IEC 60041 recommends that the flow measurements for an IEC acceptance test should be made with an absolute method. The standard mentions three main factors that affect the choice of which flow-measuring method should be used in the efficiency measurements.

- I. Limitations imposed by the design of the plant
- II. Cost of installation and special equipment
- III. Limitations imposed by plant operating conditions, e.g. draining of the system, constant load or discharge operation, etc.

Table 3 describes the flow measurement methods presented in IEC 69941 and discuss their pros and cons.[1][28][13]

<p><b>Pressure time method (Gibsons method)</b></p>	<p><b>Description</b></p> <p>The pressure time method takes advantage of Newton's law and the derived law of fluid mechanics. The fundamental principle is that one rapidly decelerates the flow meanwhile measuring the pressure rise between two points in a uniform section of the pipe. One can determine the flow knowing that the pressure rise that occurs in the pipe is dependent on the initial velocity of the flow as well as the geometrical properties of the pipe.</p> <p><b>Pros</b></p> <p>It is a fast way of performing the measurements, there is no need to shut down the power plant, the method has a good accuracy and the measurements result in an absolute flow.</p> <p><b>Cons</b></p> <p>Requirements to the geometrical shape of the section where the measurement are performed, e.g. no free surfaces between the sections, minimum length of 10 meters between sections, constant cross-section, no irregularities and an increase in uncertainty with large diameters and short pipes. [18]</p>
---	---

<b>Current-meter method</b>	<p><b>Description</b></p> <p>The current-meter method uses propeller type current-meters that are distributed over a suitable cross section in the conduit. The basic principle is that each current-meter measures the mean velocity proportional to the water velocity at specified points in the cross section. These velocity measurements will then be integrated over the cross section, resulting in the flow.</p> <p><b>Pros</b></p> <p>The current meter method can be used on several different flows and geometries e.g. both in closed and open conduits. The measurements are absolute and are considered accurate.</p> <p><b>Cons</b></p> <p>In order to achieve a good measurement a large amount of current meters have to be installed to cover the cross section. It can become time-consuming to install all of the current-meters, especially in large cross sections.</p> <p>Calibration requires special facilities and can become time consuming.</p>
<b>Pitot tube</b>	<p><b>Description</b></p> <p>The Pitot tube method takes advantage of the dynamic pressure in the flow from which the local velocity can be computed. One has to perform measurements at several points in the cross section to be able to apply the velocity method area to determine the flow.</p> <p><b>Pros</b></p> <p>It is an easy method to apply to any conduits and it results in absolute flow measurements.</p> <p><b>Cons</b></p> <p>The Pitot tube has one big limitation and that is that the accuracy decreases and uncertainty increases with decreasing flow velocity. This limits the use of the pitot tube method with in not too low velocities. Some have also experienced issues with measurements when the water has a high particles content.</p>

<p style="text-align: center;"><b>Tracer methods</b> <b>Transit-time method</b></p>	<p><b>Description</b></p> <p>Multiple different tracer methods exist, essentially they are all based on injecting tracers in the flow. This is done to either take samples and analyses the dilution downstream of the injection point or to track the tracers in the system. The transit-time method is the recommended method by IEC 60041. The methods measures the time the tracers uses to travel between two known cross sections with a known distance between them.</p> <p><b>Pros</b></p> <p>Independent of the conduits geometry. Results in an absolute flow measurement with a good accuracy.</p> <p><b>Cons</b></p> <p>There can not be any leakage, flow extraction or additional supply of flow between the injection and measuring point. It can often be difficult to install a tracer injection and water sampling system. Large amounts of tracers are needed in fast flows and large cross sections.</p>
<p style="text-align: center;"><b>Winter-Kennedy method</b></p>	<p><b>Description</b></p> <p>The core principle of the Winter-Kennedy method is to measure the static differential pressure between the inner and outer wall in the spiral casing, caused by the centrifugal forces. The Winter-Kennedy method is not an absolute method, meaning that it is relative. It can only be used when it has been calibrated against an absolute measurement method. The method uses equation <math>Q = k \cdot h^n</math> to determine the flow, <math>h</math> stands for the differential pressure between the inner and outer wall, whereas <math>k</math> &amp; <math>n</math> has to be determined through calibration.</p> <p><b>Pros</b></p> <p>Fast, easy and cheap to set up. When the Winter-Kennedy method first has been calibrated, one can monitor the flow of the turbine under continuous operation.</p> <p><b>Cons</b></p> <p>It is a relative way of measuring flow and needs calibrating. Has a higher uncertainty than other methods, and can produce high inaccuracy at low flow rates and turbulent flow patterns.</p>

<b>Thermodynamic method</b>	<p><b>Description</b></p> <p>This is technically not a flow measuring method, but it is extensively used because it is easy to set up and one directly computes the losses. The fundamental principle is that one assumes that all the energy extracted from the flow is turned into heat. Therefore, the temperature of the water will rise and the temperature difference can be measured before and after the turbine. Combined with the hydraulic energy (pressure measurements), the efficiency can be calculated.</p> <p><b>Pros</b></p> <p>The method has a good accuracy when performed on high head turbines. It does not need a direct flow measurement to compute the efficiency. It is suited for Nordic conditions due to the low water temperature throughout the year.</p> <p><b>Cons</b></p> <p>With decreasing head, the uncertainty increases. There is a need to shut down the power plant to install temperature sensors. If the water is led through pipes that are located outside and if there is a shallow intake, it is recommended to perform measurement during the night to reduce temperature variation in the water.</p>
-----------------------------	--

*Table 3 - Flow measurements methods*

As seen by the methods listed in Table 3 there is a great diversity in the how to and the advantages and disadvantages with each method. Traditionally the pressure-time and the thermodynamic method have been most common in Norway because high head turbines are common in many plants in addition to the water temperature being ideal for these kinds of measurements.

This thesis will focus on the use of the thermodynamic method in determining the efficiency of Leirfossene power plant. Chapter 2.7 and chapter 2.9 will go through the theory of the thermodynamic efficiency measurements and the uncertainty analysis.

### 2.7 Thermodynamic method

The thermodynamic method uses the fundamental principle of conservation of energy. The first law of thermodynamics states that the total energy of an isolated system is constant. When applying this to the hydro power plant, it is assumed that all energy taken out of the flow through the runner/turbine (loss of energy) is transformed into heat, ergo an increase in water temperature. [1] This means that there is no need to measure the flow of the system to determine the efficiency of the system. One does however need the velocity component at the inlet and outlet of the turbine and must therefore estimate the flow. As will be shown in chapter 2.8, the potential error of the estimation does not influence the mechanical energy term in a significant way, because the flow will be iterated again later.

Standard IEC 60041 covers the experimental application of the thermodynamic method and the setup for its acceptance test for hydraulic turbines. The standards states that the thermodynamic method is limited to the specific hydraulic energy equivalent of a head of 100m or more. It goes on to state that the method can be used for lower heads as well when the conditions are highly favorable, but the accuracy of the measurements have to be taken into account.

A special consideration when using this method is the equipment that is used for measuring pressure but most importantly to measure temperature. The thermometer has to provide an accurate indication of the temperature difference with a sensitivity of a least 0.001K. [1]

## 2.8 Efficiency calculation

By reviewing equation 2-18,  $\eta_{turbine} = \frac{P_{mechanical}}{P_{hydraulic}}$ , it shows that the efficiency is expressed with a mechanical and hydraulic component. Figure 17 shows the enthalpy-entropy diagram, points "11" and "21" illustrate the pressure and temperature before and after the turbine. Point "s" illustrates the pressure and temperature at an ideal process after the turbine. An ideal process, from point "11" to "s", is the theoretical assumption that the process happens without any losses. In reality, this is not possible. The line from point "11" to "21" illustrates the real process as the pressure decreases as energy is extracted through the turbine. The relationship between the real process and the ideal, isentropic process, is the basis of efficiency measurements with the thermodynamic method.[1][13][28]

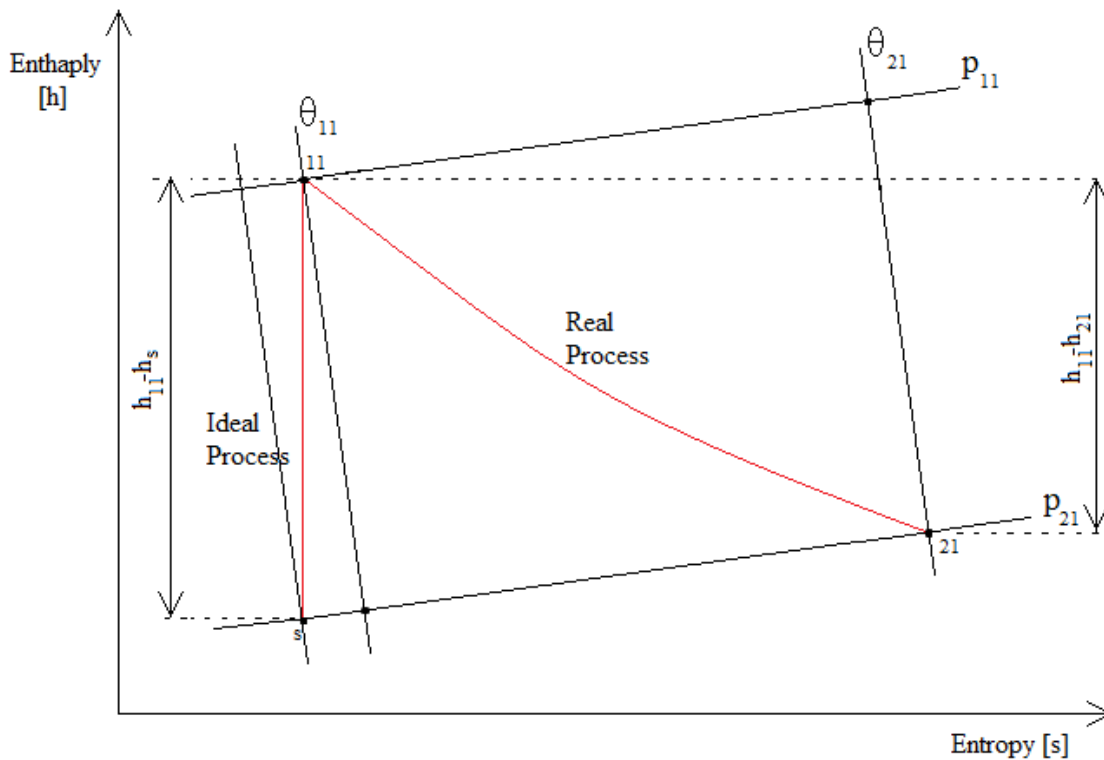


Figure 17 - Enthalpy-Entropy diagram

Equation 2-19 presents the enthalpy difference between inlet and outlet of ideal process.

$$\Delta h_{ideal\ process} = h_{11} - h_s \quad (\text{Eq. 2-19})$$

Equation 2-20 presents the enthalpy difference between inlet and outlet of the real process.

$$\Delta h_{real\ process} = h_{11} - h_{21} \quad (\text{Eq. 2-20})$$

Equation 2-21 expresses the efficiency of the process.

$$\eta = \frac{h_{11} - h_{21}}{h_{11} - h_s} \quad (\text{Eq. 2-21})$$

The real and ideal processes displayed in Figure 17, can be directly related to both the mechanical and hydraulic energy of the system. The mechanical energy,  $E_m$ , takes into account the specific energy exchanged between the turbine/runner and the water. This means that the mechanical energy  $E_m$  in the enthalpy-entropy diagram expressed through the enthalpy difference of the real process, thereby  $E_m = E_{11-21} = \Delta h_{real\ process} = h_{11} - h_{21}$ . The correlation between the mechanical power  $P_m$  and the mechanical energy is shown in equation 2-22.

$$P_m = \rho_1 \cdot Q_1 \cdot E_m \quad (\text{Eq. 2-22})$$

The ideal process is expressed through the hydraulic energy term  $E_h = E_{11-s} = \Delta h_{ideal\ process} = h_{11} - h_s$ . This implies that there are no losses in regards to the hydraulic energy in the system, meaning that  $\Delta P_h = 0$ . The relationship between the hydraulic power and hydraulic energy is governed by equation 2-23.

$$P_h = \rho_1 \cdot Q_1 \cdot E_h \quad (\text{Eq. 2-23})$$

When equation 2-22 and 2-23 are combined the turbine efficiency is expressed through the mechanical energy terms in equation 2-24.

$$\eta_{turbine} = \frac{P_m}{P_h} = \frac{\rho_1 \cdot Q_1 \cdot E_m}{\rho_1 \cdot Q_1 \cdot E_h} = \frac{E_m}{E_h} \quad (\text{Eq. 2-24})$$

The following chapter will present the theory of how to calculate the efficiency of the measurements. When conducting efficiency computations it is important to be aware that most pressures are not measured at their actual location. This means that the pressure measurement have to be numerically adjusted to achieve the real pressure. Chapter 3.1 goes through the specific heights and other information needed to calculate the necessary information regarding the pressure measurements at Leirfossene.

### 2.8.1 Flow

In order to determine the kinetic energy of the both the mechanical and hydraulic energy the flow has to be estimated. Equation 2-26 shows that the turbine power is needed to estimate the flow and is determined from the known efficiency of the generator and the actual power produced by the generator (Eq. 2-25). Equation 2-27 presents the expression to estimated velocity based on the assumed flow.  $A_2$  describes the outlet area where the temperature sensors are located.

$$P_{turbine} = \frac{P_{generator}}{\eta_{generator}} \quad (\text{Eq. 2-25})$$

$$Q_{assumed} = \frac{P_{turbine}}{p_1 - p_{atm}} \quad (\text{Eq. 2-26})$$

$$c_{21\ assumed} = \frac{Q_{assumed}}{A_2} \quad (\text{Eq. 2-27})$$

An iterative process is used to determine a more accurate flow estimate. Equation 2-22 shows that power can be expressed as function of the specific mechanical energy, flow and density of the water. Equation 2-28 shows the expression solved for flow. The variable in equation 2-28 is the mechanical energy of the system, specifically the kinetic energy term (Eq. 2-34) because of the kinetic velocity terms changing when a new flow is calculated. This means that the flow can be iterated until  $Q_{reacalculated\ n} - Q_{reacalculated\ n+1} = 0$

$$Q_{reacalculated} = \frac{P_{turbine}}{\bar{\rho} \cdot E_m} \quad (\text{Eq. 2-28})$$

Based on the now recalculated flow the velocities at the inlet and outlet can be calculated using the continuity equation, displayed in equation 2-29, in order to determine the hydraulic energy of the system.

$$c_1 \cdot A_1 = Q_{reacalculated} = c_2 \cdot A_2 \quad (\text{Eq. 2-29})$$

The outlet velocity terms for both the hydraulic and mechanical energy is measured at the center of the outlet in the same axis. This means that the velocities at the outlet are considered equal (Eq. 2-30).

$$c_2 = c_{21} = \frac{Q_{reacalculated}}{A_2} \quad (\text{Eq. 2-30})$$



### 2.8.2 Mechanical energy

The mechanical energy can be split into terms of pressure, potential, kinetic and thermal energy. (Eq. 2-31).

$$E_m = E_{m \text{ pressure}} + E_{m \text{ potential}} + E_{m \text{ kinetic}} + E_{m \text{ thermal}} \quad (\text{Eq. 2-31})$$

These terms can again be specified in terms listed below.

Pressure energy

$$E_{m \text{ pressure}} = \bar{a} \cdot (p_{11} - p_{21}) \quad (\text{Eq. 2-32})$$

Potential energy

$$E_{m \text{ potential}} = \bar{g} \cdot (z_{11} - z_{21}) \quad (\text{Eq. 2-33})$$

Kinetic energy

$$E_{m \text{ kinetic}} = \frac{1}{2} \cdot (c_{11}^2 - c_{21}^2) \quad (\text{Eq. 2-34})$$

Thermal energy

$$E_{m \text{ thermal}} = \bar{c}_p \cdot (T_{11} - T_{21}) \quad (\text{Eq. 2-35})$$

When combined, the total mechanical energy can be expressed in equation 2-36.

$$E_m = \bar{a} \cdot (p_{11} - p_{21}) + \bar{g} \cdot (z_{11} - z_{21}) + \frac{1}{2} \cdot (c_{11}^2 - c_{21}^2) + \bar{c}_p \cdot (T_{11} - T_{21}) \quad (\text{Eq. 2-36})$$

When calculating the mechanical energy, it is important to consider other losses as well. These types of losses are typically related to leakage water, temperature variation between sections and heat exchange to the surroundings. The corrective term covering all losses will be indicated with “ $\delta E_m$ ” in the specific mechanical energy term as can be seen in equation 25. At Leirfossene, there is no leakage water and no major temperature variation between sections. The heat exchange to its surrounding is also considered negligible.

$$E_m = \bar{a} \cdot (p_{11} - p_{21}) + \bar{g} \cdot (z_{11} - z_{21}) + \frac{1}{2} \cdot (c_{11}^2 - c_{21}^2) + \bar{c}_p \cdot (T_{11} - T_{21}) + \delta E_m \quad (\text{Eq. 2-37})$$

## 2.8.2.1 Mechanical Pressure energy

The mechanical pressure energy uses the pressures measured at the inlet temperature sensor,  $p_{11 \text{ mesurment}}$ , and the atmospheric pressure,  $p_{atm}$ . Equation 2-39 and 2-40 shows how the height difference is taken into account to calculate the correct  $p_{11}$  and  $p_{atm}$ . The isothermal factor  $\bar{a}$  can either be derived from the formulas or the tables presented in the IEC 60041 appendix E5 and E8.

$$E_{m \text{ pressure}} = \bar{a} \cdot (p_{11} - p_{21}) \quad (\text{Eq. 2-38})$$

$$p_{11} = p_{11 \text{ mesurment}} + \rho_{in} \cdot g \cdot \Delta z_{11} \quad (\text{Eq. 2-39})$$

$$p_{21} = p_{atm} + \rho_{out} \cdot g \cdot \Delta h_{21} \quad (\text{Eq. 2-40})$$

## 2.8.2.2 Mechanical Potential energy

The potential mechanical energy is computed based on 2-41, it uses the gravitational constant derived from the formulas or the tables presented in the IEC 60041 appendix E1. The height  $z_{11}$  is measured at the height of the temperatures sensor, while  $z_{21}$  refers to the center height of the outlet measurements.

$$E_{m \text{ potential}} = \bar{g} \cdot (z_{11} - z_{21}) \quad (\text{Eq. 2-41})$$

## 2.8.2.3 Mechanical Kinetic energy

The kinetic energy is dependent on the velocity at both the temperature measurements at inlet and outlet. The inlet sensor velocity,  $c_{11}$ , is computed using equation 2-43, were the flow is expressed in as the time it takes to fill up a bucket with a known volume (Eq. 2-44). The area in 2-43 describes the area of the probe leading the water past the inlet temperature sensor. The outlet velocity  $c_{21}$  has been derived earlier in this chapter.

$$E_{m \text{ kinetic}} = \frac{1}{2} \cdot (c_{11}^2 - c_{21}^2) \quad (\text{Eq. 2-42})$$

$$c_{11} = \frac{Q_{probe}}{A_{probe}} \quad (\text{Eq. 2-43})$$

$$Q_{probe} = \frac{V_{bucket}}{t_{filling}} \quad (\text{Eq. 2-44})$$

## 2.8.2.4 Mechanical Thermal energy

The thermal energy is computed using equation 2-45, it uses the specific heat coefficient derived from the formulas or the tables presented in the IEC 60041 appendix E6 and E8. The temperature inputs  $T_{11}$  is measured at the high pressure inlet through the temperature probe, while the sensors used to compute  $T_{21}$  are located in the draft tube.

$$E_{m \text{ thermal}} = \bar{c}_p \cdot (T_{11} - T_{21}) \quad (\text{Eq. 2-45})$$

### 2.8.3 Hydraulic energy

The hydraulic energy  $E_h$  can in terms be divided between pressure, potential and kinetic energy. (Eq. 2-46).

$$E_h = E_{h \text{ pressure}} + E_{h \text{ potential}} + E_{h \text{ kinetic}} \quad (\text{Eq. 2-46})$$

These terms can again be specified in terms listed below.

Hydraulic Pressure energy

$$E_{h \text{ pressure}} = \frac{1}{\rho} \cdot (p_1 - p_2) \quad (\text{Eq. 2-47})$$

Hydraulic Potential energy

$$E_{h \text{ potential}} = \bar{g} \cdot (z_1 - z_2) \quad (\text{Eq. 2-48})$$

Hydraulic Kinetic energy

$$E_{h \text{ kinetic}} = \frac{1}{2} \cdot (c_1^2 - c_2^2) \quad (\text{Eq. 2-49})$$

When combined the total hydraulic energy can be expressed in equation 2-50.

$$E_h = \frac{1}{\rho} \cdot (p_1 - p_2) + \bar{g} \cdot (z_1 - z_2) + \frac{1}{2} \cdot (c_1^2 - c_2^2) \quad (\text{Eq. 2-50})$$

## 2.8.3.1 Hydraulic Pressure energy

The mechanical pressure energy uses the pressures measured at the inlet temperature sensor,  $p_{1\text{ measurement}}$ , and the atmospheric pressure,  $p_{atm}$ . Equation 2-51 and 2-52 shows how the height difference is taken into account to calculate the correct  $p_1$  and  $p_2$ . Equation 2-53 shows that in order to calculate the correct  $p_2$ , the velocity diffusion between the lower reservoir (Eq. 2-54) [47] and the measured outlet has to be taken into account. The density,  $\rho$ , at both inlet and outlet can either be derived from the formulas or the tables presented in the IEC 60041 appendix E5 and E8.

$$E_{h\text{ pressure}} = \frac{1}{\bar{\rho}} \cdot (p_1 - p_2) \quad (\text{Eq. 2-51})$$

$$p_1 = p_{1\text{ measurement}} + \rho_{in} \cdot g \cdot \Delta z_1 \quad (\text{Eq. 2-52})$$

$$p_2 = p_{atm} + \rho_{out} \cdot g \cdot \Delta h_2 - \rho_{out} \cdot (c_2^2 - c_3^2) \quad (\text{Eq. 2-53})$$

$$c_3 = \frac{Q_{Final}}{A_3} \quad (\text{Eq. 2-54})$$

## 2.8.3.2 Hydraulic Potential energy

The potential hydraulic energy is computed using equation 2-55, it uses the gravitational constant derived from the formulas or the tables presented in the IEC 60041 appendix E1. The height  $z_1$  is measured at center of high pressure inlet pipe before the turbine.  $z_2$  refers to the center height of the outlet.

$$E_{h\text{ potential}} = \bar{g} \cdot (z_1 - z_2) \quad (\text{Eq. 2-55})$$

## 2.8.3.3 Hydraulic Kinetic energy

The kinetic hydraulic energy (Eq. 2-56) is dependent on the velocity at the center of both the at inlet and outlet. The velocity at inlet,  $c_1$ , and outlet,  $c_2$ , are computed using the recalculated flow and their respective areas. This has been derived earlier in this chapter.

$$E_{h\text{ kinetic}} = \frac{1}{2} \cdot (c_1^2 - c_2^2) \quad (\text{Eq. 2-56})$$

## 2.9 Uncertainties

IEC 60041 defines uncertainty as “the range which the true value of a measured quantity can be expected to lie with a suitably high probability”. The standard goes on to state that the probability should have a confidence level of 95% [1- p.87].

When performing measurements and analyzing a set of measurements there are multiple uncertainties that need to be taken into account. The measurement setup, calibration, and environmental factors are some of the factors that have to be reviewed in order to estimate the uncertainty. Errors caused by systematic and random errors will be discussed in the next paragraphs.

The total uncertainty,  $f_{total}$ , is expressed by combining the systematic uncertainties  $f_s$  and the random uncertainties  $f_r$ . This can only be done if both random and systematic uncertainty has been determined using the same type of probability distribution. The true value is assumed to have a probability of 95% to lie within in the range of the measured point. This means that every point that lies within the 95% confidence level is considered equally valid. [1-p.91]

When the uncertainty is calculated it is common practice to combine the uncertainties using the root sum squared method (RSS-method). By squaring the combined uncertainties one avoids a too conservative uncertainty. Equation 2-57 displays the formula for the total uncertainty in the efficiency.  $f_s$  is the expression for the systematic uncertainty, while  $f_r$  expresses the random uncertainty in the efficiency.

$$f_{tot} = \sqrt{f_s^2 + f_r^2} \quad (\text{Eq. 2-57})$$

### 2.9.1 Systematic error

Systematic error describes the error that cannot be reduced by increasing the number of samples. These errors arise because of poor calibration, environmental interference, wrongly used equipment or something being wrong with the equipment. Where systematic error differs from random error is that a systematically obtained error cannot be analyzed statistically in order to compensate for it. Systematic error does not affect the repeatability of the measurements [1-p.89]. These errors usually degenerate by the measurements becoming either too high or too low compared to the measured signal by a fixed value. For example not showing zero when the measured quantity is zero. All measurement equipment has there own systematic uncertainty, this can be found in the equipment data sheet. When equipment requires calibration, it is the systematic uncertainty of the calibration that will be the applicable. Equation 2-58 displays the equation used to determine the systematic uncertainty.

$$f_s = \frac{e_s}{E} \quad (\text{Eq. 2-58})$$

### 2.9.2 Random error

Random error is caused by independent, unpredictable and varying factors, for example measuring the same physical quantity multiple times with different results. Random errors behave in a statistical pattern, are assumed to have a normal (Gaussian) distribution and can be resolved by sampling large amounts of data and analyzing them statistically. For example, in hydro power plants, effects like variation in pressure during the measurements can introduce random error. Equation 2-59 shows the expression to calculate the random uncertainty  $f_r$ .  $E$  describes the relative amount of the uncertainty.  $e_r$  describes the random uncertainty. Equation 2-60 shows that the random uncertainty is calculated with a confidence level of 95% illustrated by the student t factor.  $s_Y$  is the standard deviation of the measurements.  $n$  describes the number of samples. When the random uncertainty is calculated on a large sample, it has a tendency to move towards zero. IEC 60041, Appendix E provides the need tables for the student t value. [1]

$$f_r = \frac{e_r}{E} \quad (\text{Eq. 2-59})$$

$$e_r = \frac{t_{95} \cdot s_Y}{\sqrt{n}} \quad (\text{Eq. 2-60})$$

### 2.9.3 Environmental influences

Many factors have to be taken into account when measurements are performed. The main causes of systematic error is varying temperature and cable noise. Other environmental influences are base strain, radiation, magnetic fields and humidity.

All material properties are temperature dependent, a change in temperature will result in a changed sensitivity. This means that the surrounding temperature can influence material and thereby the sensor. Rule of thumb is that a cold environment will reduce the sensitivity, while a warm environment will increase the sensitivity.

The main cable noise source is tribo-electric noise. The motion of the cable itself causes changes in charge due to the bending, compression and tension of the cables. To reduce cable noise in the measurements, the cable should be taped down as close to the sensor as possible to avoid unnecessary movements.

## 3 Preparation and execution of measurement

### 3.1 Leirfossene hydro power plant

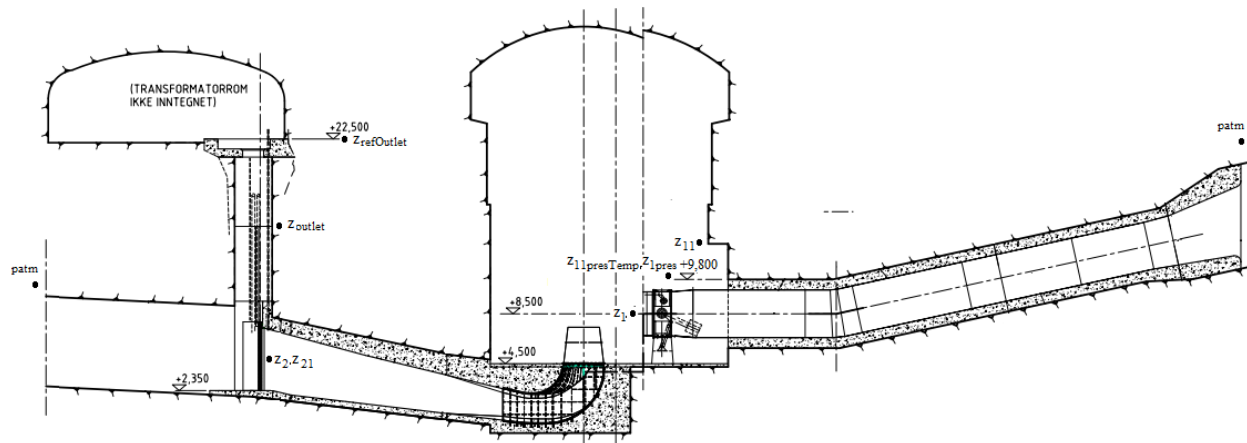


Figure 18 - Leirfossene turbine 2 overview

In order to perform the pressure and efficiency measurements one needs to use several outtakes for pressure and temperature sensors. Eleven pressure sensors and four temperature sensors are needed to perform the measurements. Figure 18 shows the layout of the power plant. The water is led from the upper reservoir at Lake Øvre Leirfoss, through the penstock, to the Francis turbine where the energy is extracted, before the water is transferred via a 1.5km long discharge tunnel to the Lake Nedre Leirfoss.

Symbol	[m]	Description
$Z_1$	8.5	Height turbine center inlet
$Z_2$	3.847	Draft tube center outlet
$Z_{11}$	10.266	Height of temperature sensor at inlet
$Z_{21}$	3.847	Mean Height of temperature sensor at outlet
$Z_{1pres}$	9.595	Height of pressure sensor inlet
$Z_{11presTemp}$	10.011	Height of temp. pressure sensor at inlet
$Z_{refOutlet}$	22.455	Outlet reference height
$Z_{refDiff}$	variable	Height from $Z_{refOutlet}$ to lower reservoir
$Z_{outlet}$	$Z_{refOutlet} - Z_{refDiff}$	Water level at lower reservoir
$\text{deltaz}_1$	$Z_{1pres} - Z_1$	Diff. between pres. meas. and center of inlet pipe
$\text{deltaz}_{11}$	$Z_{11presTemp} - Z_{11}$	Diff. between temp-pres. sensor and temp. sensor
$h_2$	$Z_{refOutlet} - Z_{refDiff} - Z_2$	Diff. between lower reservoir & outlet pipe center
$h_{21}$	$Z_{refOutlet} - Z_{refDiff} - Z_{21}$	Diff. between lower reservoir & outlet temp.sensor

Table 4 - Reference heights at Leirfossene

Figure 18 shows the location of reference heights and sensor locations needed to calculate the thermal efficiency. The denotation 1 and 2 are refer to the center of respectively inlet and outlet. While the denotation 11 and 21 refer to the temperature term at inlet and outlet. Table 4 lists the specific height expression and relationships needed to perform the analysis. These heights are measured at the day of the measurements.

Table 5 displays all the pressure, vibration and temperatures sensor to be installed for the experiments at Leirfossene. Chapter 3.3 and 3.4 will provide technical information regarding the sensors and their locations.

<b>Temperature [°C]</b>		
$T_{11}$	Temperature at inlet	Measured upstream of turbine through probe
$T_{21}$	Temperature at outlet	Measured downstream of turbine in flow
<b>Vibration</b>		
$V_1$	Guide vane	Measuring in axial direction, top mounted
$V_2$	Guide vane	Measuring in radial direction, side mounted
$V_3$	Turbine head cover	Measuring in axial direction, top mounted
$V_4$	Turbine head cover	Measuring in radial direction, side mounted
<b>Pressure [kPa]</b>		
$p_{1pressureSensor}$	Pressure at inlet	Flush mounted with inlet pipe
$p_{11tempSensor}$	Pressure at $T_{11}$ probe	Measured through probe at turbine cover
$p_{atm}$	Atmospheric pressure	Measured through probe at turbine cover
$DT1$	Draft tube pressure 1	Flush mounted with draft tube
$DT2$	Draft tube pressure 2	Flush mounted with draft tube
$DT3$	Draft tube pressure 3	Flush mounted with draft tube
$DT4$	Draft tube pressure 4	Flush mounted with draft tube
$DT5$	Draft tube pressure 5	Flush mounted with draft tube
$DT6$	Draft tube pressure 6	Flush mounted with draft tube
$DT7$	Draft tube pressure 7	Flush mounted with draft tube
$DT8$	Draft tube pressure 8	Flush mounted with draft tube

Table 5 - Overview of temperatures, vibration and pressures



### 3.1.1 Time- and running- schedule

Before going to the power plant, a time schedule and running schedule was developed at NTNU and approved by the plant owners Statkraft. This is done to have an estimated time schedule of the measurements and to make the central control center aware the turbines down time. The measurements will be conducted under steady-state operating conditions. A total of 9 conditions will be logged ranging from part load to high load. The first and last operating point will be the turbines reference point in order to evaluate the measurements repeatability. The international standard IEC 60994 states that parameters like guide-vane opening, power, rotational speed and specific hydraulic energy should be kept constant [12] for a condition to be considered steady-state. For some power plants with small reservoir the specific energy cannot be kept constant, in these cases a deviation up  $\pm 3\%$  in specific hydraulic energy is accepted. [12] At Leirfossene the reservoir is considered large enough that the specific energy is considered constant for the duration of the measurements.

Day	Objective
0	Draining of the power plant
1	Installation of equipment <ul style="list-style-type: none"> <li>- Temperature sensors</li> <li>- Pressure sensors</li> </ul> Refilling of power plant
2	Measurements <ul style="list-style-type: none"> <li>- Temperature sensors</li> <li>- Pressure sensors</li> </ul> Removal of equipment <ul style="list-style-type: none"> <li>- Temperature sensors</li> <li>- Pressure sensors</li> </ul> Refilling of power plant

Table 6 - Time schedule

The measurements were conducted over three days. Table 6 shows that the initial task is to drain the power plant of water in the draft tube and spiral casing. When this is done the equipment needed for the measurements is installed in the. On the third day, the measurements are conducted in accordance with the running schedule presented in Table 7. For each measurement point, the system was adjusted to a new steady-state operating condition. It takes an estimated 35minutes for each measurement to be conducted. This includes 2 minutes to adjust to its new operating condition, 18 minutes to stabilize and 15 minutes to sample the measurements.

Run nr.	Generator Power [MW]	Time at run [min]
1	13.4	35
2	15.8	35
3	10.3	35
4	12.1	35
5	9.3	35
6	14.2	35
7	7.3	35
8	16.5	35
9	13.3	35
		5.83 hours

Table 7 - Running schedule

### 3.2 Measurement setup

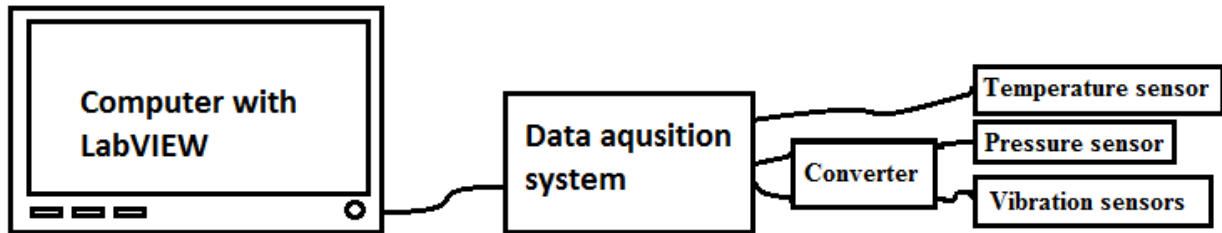


Figure 19 - Measurements setup

The purpose of the measurement setup is to make sure that the desired data is sampled in a secure way and to ensure a repeatable experiment with a high accuracy. Figure 19 presents the simplified measurement setup from sensors to sampling device.

#### 3.2.1 LabVIEW

A unique LabVIEW program has been created to sample the temperature, vibration and pressure measurements. The created program has the ability to simultaneously monitor the efficiency of the turbine as well as display a simple FFT analysis. It is important to remember that the efficiency displayed is calculated based on the simultaneous logging of pressure and temperature and that the data has not been statistically analyzed. The block-diagram and the programs layout is shown in the Appendix G.

#### 3.2.2 Sampling Rate

Based on the theory presented in chapter 2.4 the needed sampling rate is calculate based on the expected highest frequencies in the system. The Nyquist sampling theorem says that the sampling rate should be at least two times greater than the highest expected frequency of the system. However, there are benefits of oversampling, chapter 2.4.1. By oversampling, the risk of having sampled with a two low frequency is removed. Therefore, it is better to be on the safe side, considering that it is not possible to repeat the measurements on another day due to the power plant being in daily operation. Another factor that is important when deciding on the sampling rate is the limitations equipment as well as the desire not accumulate to large data sets. Based on experience and corroborated by Einar Kobro [22], a sampling rate,  $F_s$ , 10 times greater than the expected highest frequency ensures good measurements series.

Runner frequency	$f_n = 5.55 \text{ Hz}$
Runner vane frequency	$f_{rv} = 61.11 \text{ Hz}$
Guide vane frequency	$f_{gv} = 133.33 \text{ Hz}$
Rheingans frequency	$f_R = 1.3875 - 2.775 \text{ Hz}$
Elastic fluctuations – Turbine to lower reservoir	$f_{e-TP} = 4.81 - 6.86 \text{ Hz}$

Table 8 - Calculated expected frequencies

Table 8 presents the expected frequencies in the system. These frequencies are calculated based on the theory presented in chapter 2.1. The highest expected frequency to be measured at Leirfossene is the guide vane frequency  $f_{gv} = 133.2\text{Hz}$ . This leads to a recommended sampling rate of  $F_s = 1332\text{Hz}$  for the system. Taking into account the acceptable data rates of the analog input module from national instrument, the more suitable sampling rate of  $F_s = 2000\text{Hz}$  is selected. This is 15 times greater than the highest expected frequency and 7 times greater than Nyquist sampling theorem states.

### 3.3 Equipment

In order to perform the measurements of efficiency, pressure pulsation and vibration several different components have been used. Different sensors, charge converters, analog to digital input modules, data acquisition chassis, wiring and computers to mention some. The next chapter will present the equipment used for the measurements and its setup.

#### 3.3.1 Temperature sensors

The temperature sensors are all of the type Seabird Electronics 38. Table 4 shows the technical specifications of the sensors. All sensors are highly accurate with an accuracy of  $0.001K$ . The manufacturer calibrated all sensors in March of 2016. This calibration is according to the manufacturer certified for up to six months, due to the stability of the sensor changing over time. The sensors has a limited update rate of one sample every 3-4 seconds. Therefore, it is important to conduct the measurements over a longer period to achieve a good reading. By performing the measurements over longer periods, the random uncertainty will decrease as the measurement points increase. The calibration reports are available in Appendix M, while Appendix L presents the technical specifications of the sensor.

As part of the quality assurance of the temperature sensors, a measurement test with the sensors submersed in ice water is performed. The result of the test showed that the deviation between the sensors is negligible and within the maximum error aloud according to IEC 60041.

Ref #	Temp. sensor	SN	Range	Resolution	Placement	Notations
01	SBE 38	3832689-0199	-5 to 35°C	0.00025°C	Inlet	$T_{in}$
02	SBE 38	3844844-0315	-5 to 35°C	0.00025°C	Outlet 1	$T_{out1}$
04	SBE 38	3839551-0242	-5 to 35°C	0.00025°C	Outlet 2	$T_{out2}$
05	SBE 38	3832689-0196	-5 to 35°C	0.00025°C	Outlet 3	$T_{out3}$

Table 9 - Temperature sensor overview

In order to sample the data form the temperature sensors, each sensor is connected to a data acquisition unit using an ADAM RS-485/USB signal converter.

### 3.3.2 Pressure Transducers

During the measurements at Leirfossene 11 pressure sensors are used. The pressure measurements are conducted for three different area of interest. Each sensor has been chosen based on the expected pressure range at its location, a more accurate measurement can be performed with a designated sensor. Table 10 presents the different pressures that are measured and the thought behind the selected sensor.

Area of interest	Description
Atmospheric pressure	The atmospheric pressure is measured at the height of the turbine cover and is used in the efficiency measurement. The expected atmospheric pressure is usually between 98kPa to 103kpa. Therefore, a sensor with a range of 0-2.5 bara is selected to ensure its resolution.
Inlet and temp.-sensor pressure	The inlet and temperature sensor pressure is respectively measured at the height of the turbine cover and at the temperature sensor pressure outlet. Both measurements are used in the efficiency measurement. The expected pressure is between 600kPa to 750kpa, with pressure peaks up to 900kPa. Therefore, a sensor with a range of 0-10 bara is selected.
Draft tube pressure	The draft tube pressure is measured flush with draft tube wall. The measurements are going to be used for the analysis of pressure pulsation in the draft tube. The expected pressure in the draft tube can be lower than the atmospheric pressure and has been observed to be as low as 50kPa. However, previous measurements have shown pressure pulsations in the draft tube up to 600kpa. Therefore, a sensor with a range of 0-10 bara is selected to be able to cover the whole range.

Table 10 - Pressure-Area of interests

All of the selected pressure sensors are piezo-resistive static pressure sensors [Table 11]. The advantage of using static pressure transducer is that they are able to show the current pressure, compared to the dynamic pressure transducer that only display the difference in pressure. For the computation of the efficiency, one is dependent on having the static pressure. Table 11 displays the different pressure sensors that were used in the measurements. Appendix L shows the technical data sheet, while Appendix M shows the corresponding calibration report for each sensor.

Ref	Transducer	SN	Range [bara]	Placement	Max Uncertainty [%]	Symbol
-----	------------	----	--------------	-----------	---------------------	--------

1	Druck PTX 1830	2313100	0 – 5	Draft Tube	0.032	$p_{DT1}$
2	Druck PTX 1830	2313099	0 – 5	Draft Tube	0.043	$p_{DT2}$
3	Druck PTX 1830	2313103	0 – 5	Draft Tube	0.045	$p_{DT3}$
4	Druck PTX 1830	2313105	0 – 5	Draft Tube	0.058	$p_{DT4}$
5	Druck PTX 1830	2309837	0 – 5	Draft Tube	0.069	$p_{DT5}$
6	Druck PTX 1830	2313101	0 – 5	Draft Tube	0.057	$p_{DT6}$
7	Druck PTX 1830	2313104	0 – 5	Draft Tube	0.073	$p_{DT7}$
8	Druck PTX 1830	2313102	0 – 5	Draft Tube	0.061	$p_{DT8}$
9	Druck PTX 610	2184827	0 – 10	Inlet pipe	0.053	$p_{in}$
10	Druck PTX 610	4091551	0 – 10	Temp. sensor	0.052	$p_{temp}$
11	Druck PTX 610	2480173	0 – 2.5	Turbine cover	0.067	$p_{atm}$

Table 11 - Pressure transducer overview

The piezo-resistive pressure transducer all output the raw pressure signal in current, in order for the signal to be logged the current has to be converted to voltage. In order to sample the analog pressure signal it is connected to a National Instrument Data Acquisition System (NI DAQ) Analog input modules are used to digitalize the analog pressure signal from the sensors. These modules are connected to a data acquisition chassis which in terms is connected to the LabVIEW logging program. Table 12 displays the equipment used to digitalize the analog signal.

Hardware	Type	Quantity	Range
Data acquisition chassis	NI-cDAQ-9172	1	400k samples per seconds
Analog Input module	NI 9239	3	50k samples per seconds
Voltage Converter	-	1	$\pm 10$ V

Table 12 - Pressure measurements hardware overview

### 3.3.3 Equipment Vibration sensors

The chapter about vibration sensors has been gotten directly from the Semester thesis “Pressure Pulsation and Vibrations in Francis Turbines” written in collaboration with Magomed Selmurzaev during the fall of 2015[21]. Some modifications have been made to fit the purpose of the measurements performed at Leirfossene.

Table 13 displays the four sensors used in the vibration measurements. Due to availability in the laboratory, three different types of sensors had to be utilized. The sensors produced by Brüel & Kjær are piezoelectric accelerometers. Inside the sensor, a piezoelectric material exhibits an electric current proportional to the applied force when it is stressed.

The Entran International EGAS sensors are bridge-type piezo-resistive accelerometers. In contrast to the piezoelectric accelerometer, the Entran accelerometer produces a change in resistance depending on the strain on the sensor. The piezo-resistive accelerometers have a superior low frequency range compared to the piezoelectric accelerometers from Brüel & Kjær.

#	Type	Serial number	Resonance frequency	Upper limit
V1	Entran International EGAS	W5486	723 Hz	±25 [g]
V2	Entran International EGAS	W5485	733 Hz	±25 [g]
V3	Brüel & Kjær Type 4397A	32166	53 000 Hz	±750 [g]
V4	Brüel & Kjær Type 4397A	32168	53 000 Hz	±750 [g]

Table 13 - Accelerometer information

A common feature between the sensors is that they are all uniaxial accelerometers, only displaying vibration in one axis. The sensors are considered miniature accelerometers with a very low self weight. This means that the sensors can be used to measure high frequencies without the mass of the accelerometers to influence the vibration levels.

It is important to consider the frequency range of the accelerometers when they are used. The Nyquist sampling theorem states that the needed sampling rate for the measurement have to be at least two times the highest expected frequency. Equation 3-1 determines the highest frequency that the accelerometer is suited for. By sampling with a higher sampling rate than given by the equation 3-1 the measurements could experience higher sensitivity due to resonance of the sensor.

$$\text{Highest sensor frequency} = \frac{f_{\text{resonance}}}{3} \quad (\text{Eq. 3-1})$$

The signal from the sensors have to be converter to voltage and amplified before being connected to the analog input module. The analog input modules of the accelerometers are connected to the same NI DAQ chassis as the pressure transducers. The equipment used for sampling of vibrations is displayed in Table 14.

<b>Hardware</b>	<b>Type</b>	<b>Quantity</b>	<b>Bandwidth</b>
Data acquisition chassis	NI-cDAQ-9172	1	400k samples per seconds
Analog input module	NI9239	1	50k samples per seconds
Analog input module	NI9233	1	50k samples per seconds
Charge converter	MGA II DA12	1	100k samples per seconds
Control element	MGA II ME10	3	Range 0kHz 10 kHz

*Table 14 - Vibration measurements hardware overview*



### 3.4 Location of sensors

IEC 60041 has been used for the efficiency measurements ergo the placement of pressure and temperature sensors needed for the calculation of the efficiency. Both the pressure and the vibration sensors have been placed based on what is expected to measure and or the area of interest. The overall objective is that an operator should be able to monitor how and where trends develop and how they propagate in the system. For the measurements done at Leirfossene power plant one is interested in the draft tube section as to this is the area where the low frequency pressure pulsation originate and propagate from.

#### 3.4.1 Efficiency measurement

In total four temperature sensor and three pressure sensors are used in order to calculate the efficiency. The inlet temperature sensors is located at the high pressure side of the turbine, placed inside the high pressure probe. Figure 21 shows the design of the probe, while Figure 20 illustrates the location of the probe at the inlet of the turbine. The flow through the probe was derived by timing how long it took to fill up a bucket with a known volume. As displayed in Figure 21 the pressure at the temperature sensor is measured through an outtake of the probe.

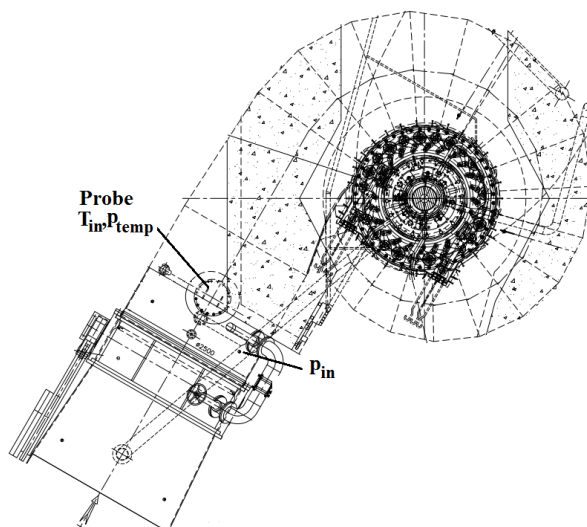


Figure 20 - Location of inlet temperature sensor, pressure inlet-, pressure temperature inlet sensors

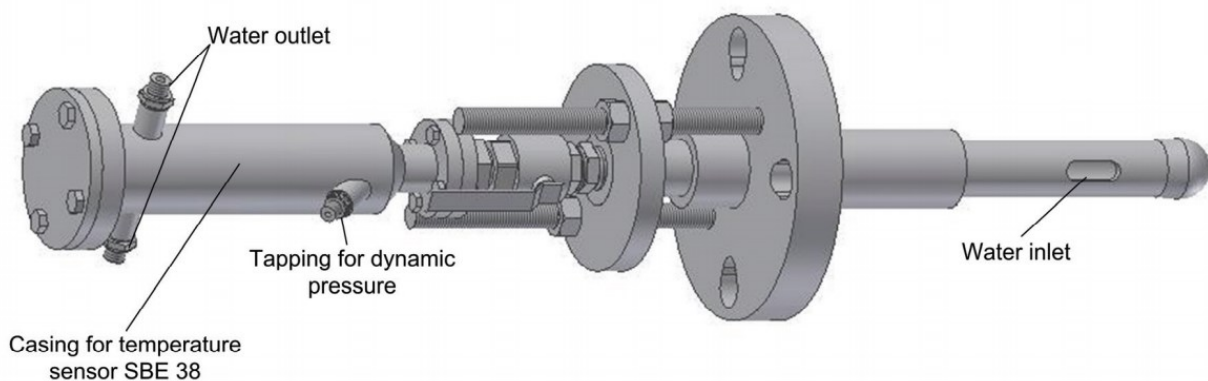


Figure 21 - High pressure probe [49]

The inlet pressure is measured flush with the pipe wall at the inlet, illustrated in Figure 20. The pressure has to be numerically compensated in order to achieve the inlet pressure at the center of the pipe. The atmospheric pressure is measured at the deck of the turbine cover. Based on the atmospheric pressure the outlet pressure can be computed.

The three remaining temperature sensors are located in the outlet after the draft tube. Figure 22 shows that the three sensors are located in the center of the outlet in the same vertical axis. The sensors are spaced with an equal distance between each other. The average height of the temperature sensors corresponds with the center height of the outlet.

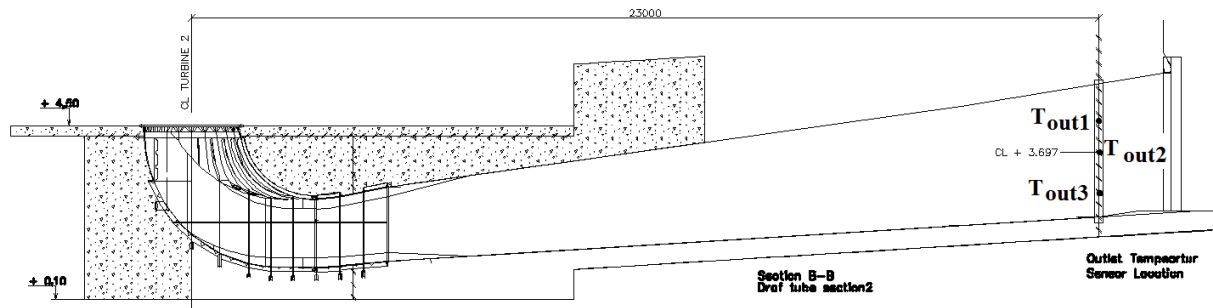


Figure 22 - Location of outlet temperature sensor

As mentioned in chapter 2.8.2, the total mechanical energy is calculated as part of the efficiency analysis. The thermal energy term is dependent on the temperature difference between inlet and outlet of the turbine. IEC 60041 [1] states that there is a need for multiple temperature at the inlet as there is a danger of improper mixing and or when the inlet diameter becomes too large. At Leirfossene the inlet diameter is 2.5m, has a uniform flow pattern and the flow goes through a uniform cross-section. The need for additional temperature sensors at the inlet is therefore deemed unnecessary. Figure 23 shows how the probe and temperature sensor is insulated at the inlet, to avoid external influences.



Figure 23 - Temperature sensor at inlet

After the turbine, the flow passes through a bend and through an expanding cross-section. This can potentially give temperature differences between the outlet because there is a potential flow separation. Therefore, three temperature sensors are used to cover a larger area at the outlet

### 3.4.2 Pressure measurements

Two types of pressure measurements are conducted, one for the computation of efficiency and one for the pressure pulsation analysis. The measurement of the inlet, atmospheric and temperature pressure was discussed in the previous paragraph.

The objective of the pressure pulsation measurements at Leirfossene is to track and analyze the pressure pulsations in the draft tube. Previous pressure measurements have been performed in the draft tube, therefore the same pressure outtakes were used again. Figure 24 shows the placement of the eight pressure sensor in the draft tube. The sensors locations are placed in accordance to IEC 60994. The standard states that pressure sensor "At a distance of  $0.2D_5 - 0.8D_5$  from the bottom face of the band of a Francis runner/impeller,  $D_5$  being the suction diameter" [1].

As mentioned earlier, there were eight sensor installed in the draft tube. Respectively four sensors are placed in the same vertical axis, on each side of the draft tube by an average vertical distance of 860mm downstream of each other. This means that two sensors will be in the same horizontal axis, offset by 180degree. Figure 24 shows the location of each sensor in the draft tube. The pressure transducers on the draft tube and inlet

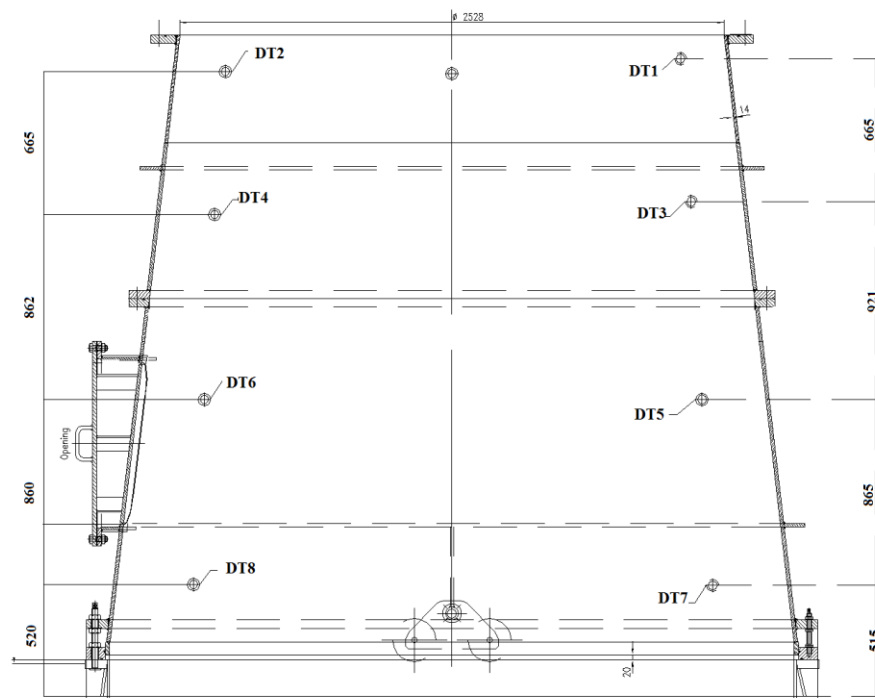


Figure 24 - Location of pressure sensors in draft tube

are flush mounted with the tube wall. All sensor used at Leirfossene are static pressure transducer and were calibrated both before and after measurements to assure repeatability.

### 3.4.3 Vibration Sensors

Four uniaxial accelerometers are used to measure vibrations on the unit. The sensors are mounted on the outside of machine components and are distributed according to target areas. The objective of the vibration measurements is to observe the frequency components present in the system and correlate these with the pressure pulsation measurements. IEC 60994 [12] states that the housing of each guide bearing, the support frame of the thrust bearing, the head cover of the turbine and guide vanes are most likely to experience significant vibrations. The vibration measurements at Leirfossene will focus on the head cover and guide vanes. The accelerometers have been mounted at the following locations [Figure 25]. Figure 26 shows how V3 and V4 are cemented (chapter 2.2.1) on the turbine cover.

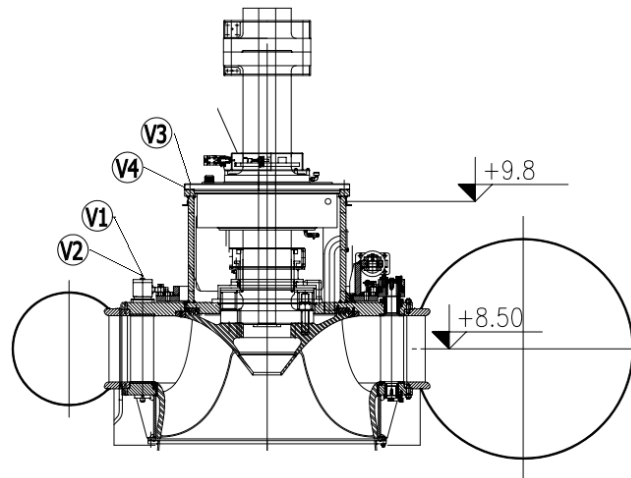


Figure 25 - Location of vibration sensors

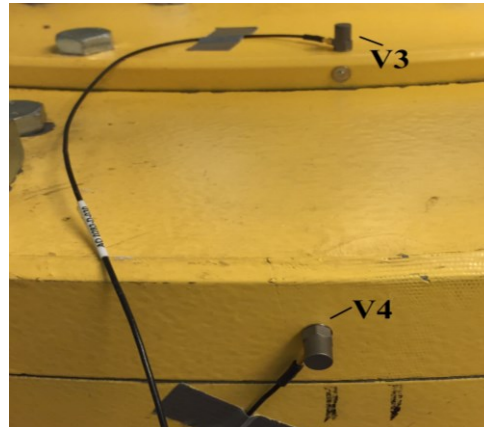


Figure 26 - Location vibration sensor V3 & V4

	Sensor	Description
<b>Guide vane</b>	V1-Axial	V1 is mounted on top of guide vane number 1 in its axial direction. V2 is mounted on the same guide vane in its axial direction. It is expected that the runner dependent frequencies will be most obvious, especially the frequencies from the rotor stator interaction
	V2-Radial	
<b>Head cover of the turbine</b>	V3-Axial	V3 is mounted in the axial direction of the turbine, on the head cover. V4 is mounted on the side of the cover in the runner's radial direction. It is expected to detect frequencies related to the rotor stator interaction, as well as the Rheingans frequency .
	V4-Radial	

Table 15 - Vibration sensor mounting information

### 3.5 Analysis of measurements

All of the measurements have been analyzed using MATLAB. The following paragraphs will provide more information about the methods used to evaluate and compute the results. All of the scripts used in the analysis are available in the Appendix H.

#### 3.5.1 Efficiency measurements

The analysis of the thermodynamic efficiency measurements consist of determining the hydraulic and mechanical energy of the system. This is done by applying the theory presented in chapter 2.6 with the measured quantities of the pressure and temperature at both the inlet and outlet. Initially the measured data will be statistically evaluated using MATLAB in order to get rid of outliers and noise in the signal.

Based on the standard IEC60041, the temperature measurements have to be averaged at both the inlet and outlet of the turbine. The same goes for the pressure measurements at both the temperature sensor, inlet sensor and atmospheric sensor. Some of the pressure values used in the calculations have to be numerically compensated in order to ensure that the correct value is used at the correct location. Therefore, the accurate height measurements are important.

The temperature also needs to be adjusted. There is a certain distance between the temperature sensors at inlet and outlet. This means that it takes some time for the water measured at inlet to transit to the outlet. In order to compensate for this a time delay has to be calculated. The offset

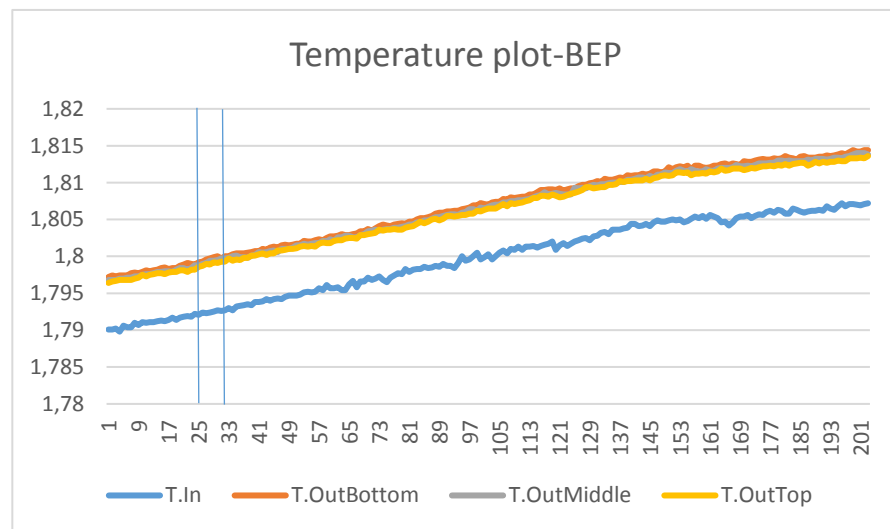


Figure 27 - Raw temperature output

is dependent on the flow at the operational point, for example at the turbines best point (BEP), the time delay is 8.7 seconds, meanwhile at part load the delay is 15 seconds. The blue lines in Figure 27 display the delay that has to be taken into account at BEP.

The IEC standard allows a maximum drift in the temperature to be  $\Delta T = 0005 \text{ K}/_{min}$ . It also states that the temperature sensors used need to have an accuracy of at least  $0.001K$ . Figure 27 displays the raw temperature plot of a previously performed measurement. Based on the graph one can already now state that the drift in temperature is within the limit stated by IEC60041. It will take further analysis to check for eventually outliers in the measurements.

A specially designed MATLAB script, Appendix H, with built in flow iteration has been created to perform the numerical calculation of the efficiency and perform the necessary compensation for the temperature and pressure measurements. An uncertainty analysis has also been implemented in the same script computing both the random and systematic uncertainty.

Due to confidentiality reasons, relative values have been used to calculate the efficiency. The relative efficiency measurements are displayed as a plot showing the efficiency curve, with its uncertainty band, related to the turbines power output at its rated head.

### 3.5.2 Pressure and vibration measurements

The purpose of the pressure and vibration measurements at Leirfossene is to conduct a frequency analysis, focusing on the lower frequency range and the frequency amplitude in the draft tube. The measurements are performed at different operating conditions. The measured data of both the vibrations and pressure pulsations will consist of raw data. The raw data is the outputted volt signal from the sensors. In order to achieve a data set that is logical, the raw data has to be processed with its coherent calibration constant. Furthermore the data will be examined using statistical tools and signal processing methods in a designated MATLAB script. This is done as an effort to remove outliers and ensure a good data-set has been achieved before further analysis is conducted.

Subsequently the processed data will be analyzed using the MATLAB PWELCH function to display the frequency spectra. A peak-to-peak analysis will be used to show the magnitude of the pressure measurements [chapter 2.5.4]. The PWELCH function takes advantage of window functions to further enhance the quality of the analysis. For the analysis, the Hanning widow with an overlap factor of 0.5 is used. The widow length between 20k to 30k samples has been used in order to focus on the lower frequency ranges. [Chapter 2.5.2] Peak to peak values were found using a 99% confidence level. [Appendix J]

The frequency resolution  $f_{res}$ , describes the distance between two data points that are adjacent in the FFT analysis. The resolution is defined by the relationship between the sampling rate  $F_s$ , and the total number of samples in the data-series,  $N = F_s \cdot t$ . Which as seen in equation 3-2 is derived to be only be dependent on the sampling time  $t$  in seconds. This means that the only way to increase the frequency resolution is to sample over longer periods. For example a signal sampled at  $F_s = 2000$  for  $t = 10s$  will have a  $f_{res} = 0.1Hz$ . [Chapter 2.5] The length of the window used in the FFT analysis are all with a  $f_{res} = 0.1Hz$  or higher. [48]

$$f_{res} = \frac{F_s}{F_s \cdot t} = \frac{1}{t} \quad (\text{Eq. 3-2})$$

Various representational methods are used to present the result, waterfall-plots and heat-plots are used to display the trend of the system meanwhile 2D-plots and tables are used to display specific values. It should be pointed out that the measurements of vibration sensors V1, V2 and V4 did not yield provide any results due to unforeseen errors in the measurements .

### 3.5.3 Uncertainty

After the measurements have been analyzed, it is important to evaluate the uncertainty of the efficiency measurements. Both the systematic and random uncertainty has to be evaluated. This is done in an effort to determine the accuracy of the measurements. Appendix D displays how to theoretically derive uncertainty of efficiency.

The uncertainty in the efficiency measurements is dependent on several variables and will therefore need a complex uncertainty analysis. The result of the pressure pulsation measurements are only dependent on the sensor itself because no other variables or constants are applied. This means that it is the uncertainty of each sensors is the uncertainty from the calibration report. The calibration reports are found in Appendix P, Appendix N and Appendix M.

### 3.5.4 Calibration

The calibration is performed to make sure that two sensors measuring the same quantity display the same result. To reduce the uncertainty of the measurement the same equipment, cables, modules and sampling devices are used in the actual field measurements as was used in the calibration. The equipment has been calibrated in accordance to IEC 60041. In the Appendix P, Appendix N and Appendix M covers respectively the calibration report of the pressure, vibration and temperature sensors. The calibrated data has been used to present all the results in chapter 3 and in the Appendix F.



## 4 Experimental results and discussion

The following chapter will present and discuss the results of the efficiency and pressure pulsation measurements performed on Turbine 2 at Leirfossene power plant.

The efficiency measurements are performed in accordance with the international IEC 60041 standard. In the following chapter, the efficiency measurements are presented with regards to the turbines power output at its rated head. The efficiency measurements will be compared to previous measurements performed by Norconsult in 2009. The measurements conditions are deemed satisfactory, with the temperature not increasing more than the 0.005K per minutes as stated by the IEC standard. The pressure pulsation measurements

will give an overview of the frequency components occurring in the draft tube. Figure 1 displays the location of the pressure sensors in the draft tube. An investigation of the pressure intensity, as well as a discussion of the pressure difference between the inner and outer radius of the draft tube bend will be presented. The effects of air injection will

also be evaluated. In the analysis, the operational points are discussed relative to the nominal discharge,  $Q_n = 30 \text{ m}^3/\text{s}$ , of the turbine. The turbines Best Efficiency Point (BEP) is considered to be  $0.84 \cdot Q_n$ . All measurements were performed under steady-state conditions, with constant generator output and constant flow.

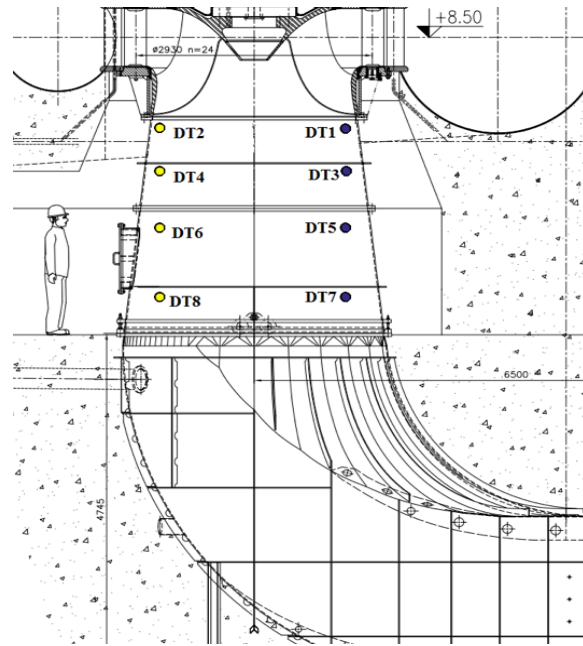


Figure 1 - Location of draft tube pressure

Description	Nomenclature	Value
Nominal Head	$H_n [m]$	58
Nominal Discharge	$Q_n [m^3/s]$	30
Nominal Output	$P_n [MW]$	16
Nominal Speed	$n_n [rpm]$	333.3
Runner blades	[-]	11
Guide vanes	[-]	24

Table 16 - Nominal parameters Turbine 2 Leirfossene

Measurement	1	2	3	4	5	6	7	8	9
$P_n [MW]$	7.29	9.35	10.38	12.26	13.55	13.64	14.49	16.3	17.08
$H [MW]$	58.6	58.34	58	57.8	57.9	57.2	57.8	57.4	57.2
$Q/Q_n$	0.46	0.58	0.64	0.76	0.83	0.84	0.89	0.99	1.03

Table 17 - The performed measurement points

### 4.1 Efficiency measurements

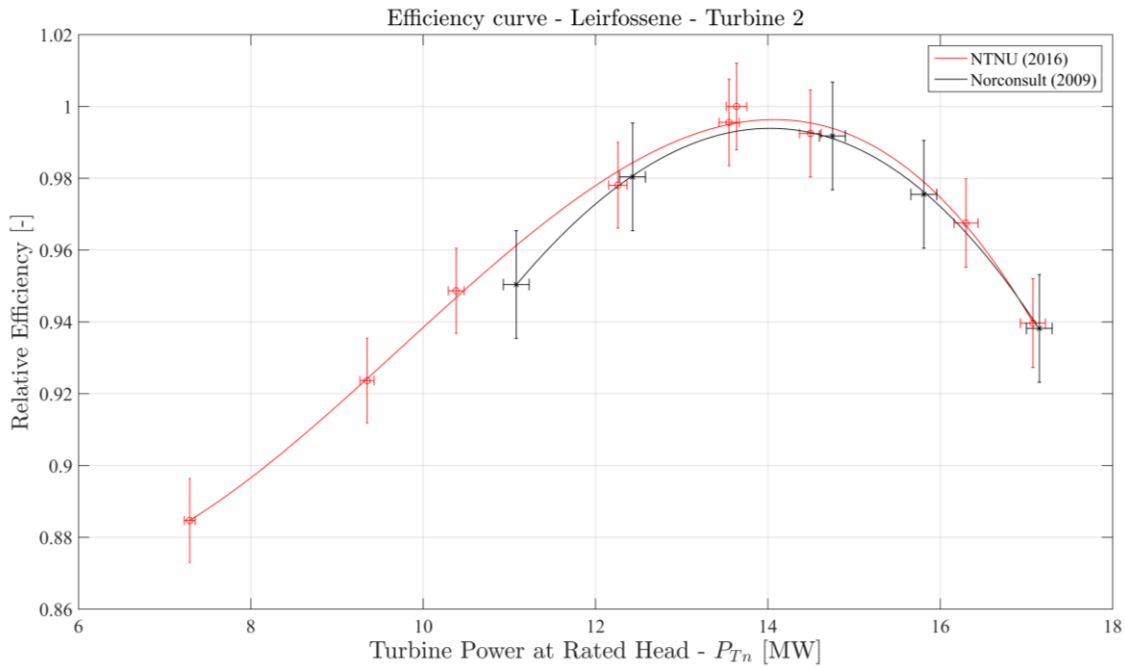


Figure 28 - Efficiency measurement Leirfossene

$P_n$ [MW]	7.29	9.35	10.38	12.26	13.55	13.64	14.49	16.3	17.08
$\eta$ [-]	0.885	0.924	0.948	0.978	0.995	1	0.992	0.967	0.939
Uncertainty [%]	$\pm 1,37$	$\pm 1,32$	$\pm 1,29$	$\pm 1,26$	$\pm 1,25$	$\pm 1,25$	$\pm 1,26$	$\pm 1,31$	$\pm 1,36$

Table 18 - Normalized efficiency values

Figure 28 displays two efficiency curves. The red line represents the measurements performed by the thesis author in May of 2016 using the thermodynamic method. The black line represents the guarantee measurements performed with the Gibson method by Norconsult in 2009. The results presented are normalized using the highest efficiency point measured with the thermodynamic method. This is done to not reveal confidential information.

Figure 28 and Table 18 show that both efficiency measurements present the same trend. Both the thermodynamic method and Gibson's method display the peak efficiency to be at 14MW. The maximum uncertainty in the measurement performed by NTNU is calculated to be 1.4% while the measurements by Norconsult have an uncertainty of 1.6%. Figure 28 shows that the deviation between the measurements varies from 1.12% at part load to -0,13% at high load. This means that the efficiency lies within each others uncertainties.

### 4.1.1 Uncertainty

Figure 29 shows the total uncertainty of the measurements based on the nominal turbine efficiency. The biggest contributor to the total uncertainty is the uncertainty of the measured temperature difference. The uncertainty in the temperature difference is due to the low head, as the total losses are small. The temperature losses are therefore small compared to

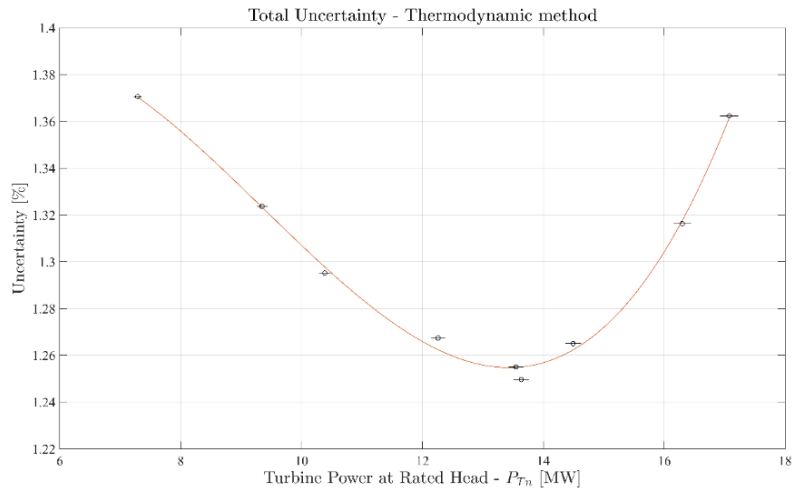


Figure 29 - Efficiency measurement - Total uncertainty

the accuracy of the temperature sensors. It is because of the small increase in temperature over low-head turbines that the IEC 60041 standard recommends that the thermodynamic measurements should be performed on heads over 100 meters. It also recommends to use temperature sensors with an as high as possible accuracy, to reduce the overall uncertainty in the measurements. Figure 29 clearly shows how the uncertainty increases as one moves away from the turbines best efficiency point. This is because of the increasing instability in the flow, causing the uncertainty of the pressure measurements to increase.

### 4.1.2 Head loss

Figure 4 displays the head loss for the turbine related to the nominal power of the turbine. An increase in power will result in an increase of flow. This shows that the head loss will increase with an increase in turbine power. The head loss at BEP is determined to be 0.95m. The head loss coefficient is dependent on the actual head loss and the volume flow at that point. The head loss coefficient for turbine 2 at Leirfossene is calculated to be  $K = \frac{H_{loss}}{Q^2} = 0.00153$ .

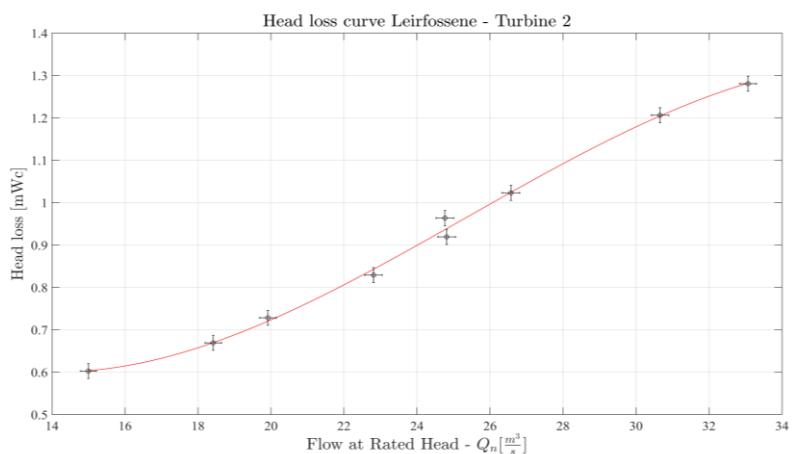


Figure 30 - Head loss curve Leirfossene turbine 2

## 4.2 Pressure pulsation measurement

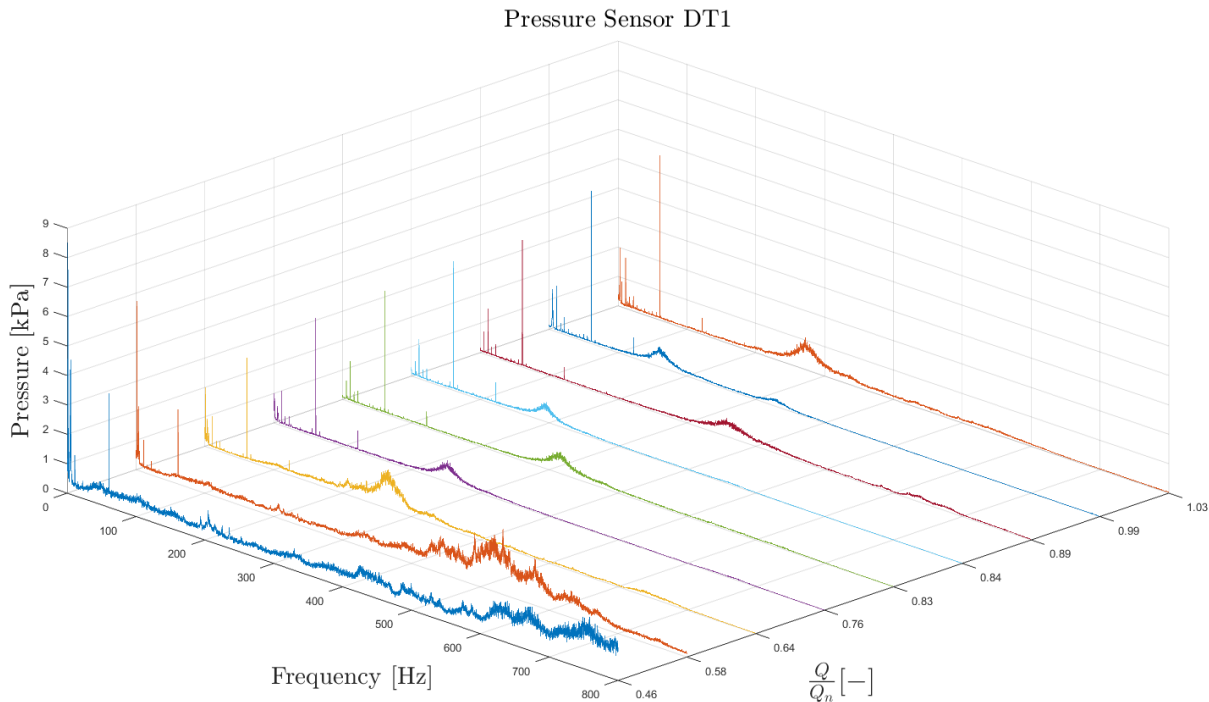


Figure 31 - FFT for all measured operational points - DT1 [0Hz-800Hz]

Figure 31 displays the Fast Fourier Transform, FFT from 1Hz to 800Hz, based on the pressure sensor DT1, located closest to the turbine outlet. The figure shows the measurements for all measured operational load points. Based on the peaks displayed for the different operational points one can see that there are some overlaying trends. The highest intensities are measured at the part load points of  $0.46 \cdot Q_n$  and  $0.58 \cdot Q_n$ . At part load, high frequency components over 400Hz can be seen that appear to have a high intensity. As the loads increase it appears as if the high frequency components are greatly reduced. This coincides with the flow becoming less turbulent and more stable when it increases.

An interesting observation is the fluctuation of frequencies between 200Hz and 350Hz depending on the turbines load. It is most likely not related to any rotational dependent frequencies because of its fluctuations. Therefore, it is likely to be related to the elastic fluctuations in the system.

The guide vane frequency at 122.3Hz can be observed with an increasing intensity for all operational loads over  $0.64 \cdot Q_n$ . The guide vane frequency is only observed in the measurements from sensor DT1, DT2, DT3 and DT4. These are the sensor located closest to the turbine outlet. Intensity is relatively low compared to the other rotational dependent frequency.

In the further analysis, the main focus will be on the lower frequency ranges. This is the area of interest believed to generate the greatest vibrations in the machinery.

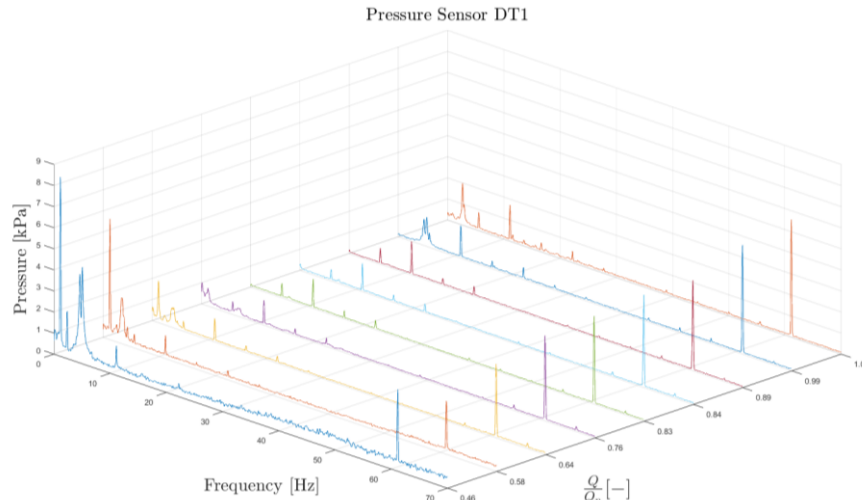


Figure 32 - FFT for all measured operational points - DT1

Figure 32 shows an enlarged section of Figure 31, displaying the frequencies from 0Hz to 70Hz. The plot shows that the runner dependent frequencies are dominant. The most dominant frequency at part load is the Rheingans frequency at 1.16Hz. Figure 33 shows how the intensity of the Rheingans frequency decreases as the flow moves toward the best efficiency point and disappears entirely. The highest intensity of the Rheingans frequency will be at low part loads. This is related to the high tangential velocity in the draft tube.

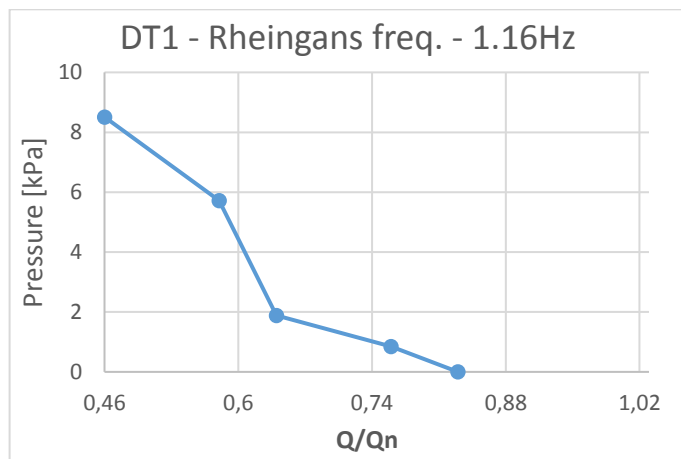


Figure 33 - Rheingans frequency intensity DT1

Figure 34 shows the intensity of the runner frequency measured at 5.55Hz. The trend shows that the intensity of the runner frequency decreases as the flow moves towards BEP, before increasing as it moves towards high load. This is expected considering the flow is becoming less turbulent at BEP. The figure shows that the relative intensity compared to the Rheingans and runner vane frequency is low. This said, the second

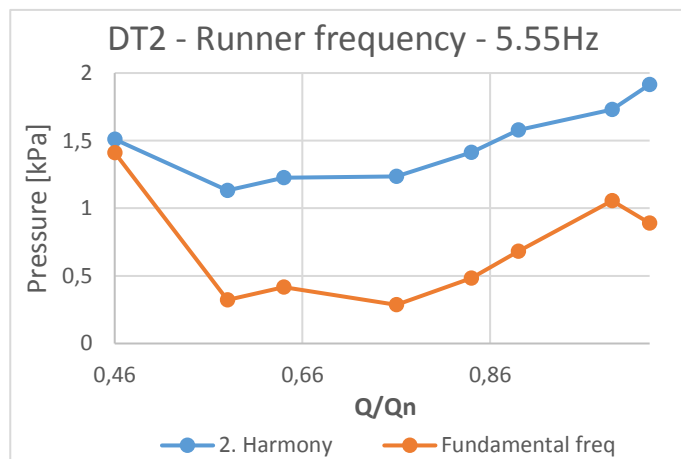


Figure 34 - Runner frequency intensity DT2

harmony of the runner frequency, measured at 11.11Hz, is measured to have an intensity greater than the fundamental frequency. It should be noted that the multiple harmonies with smaller intensity can be observed as far up as to the runner frequency.

Figure 35 shows the runner vane frequency measured at 61.1Hz. The plot shows that the intensity of this frequency intensifies as the flow increases at higher loads. The same trend is observed with pressure sensor DT2. However, as can be seen in Figure 10, the sensor located further downstream in the draft tube shows that the intensity moves towards zero.

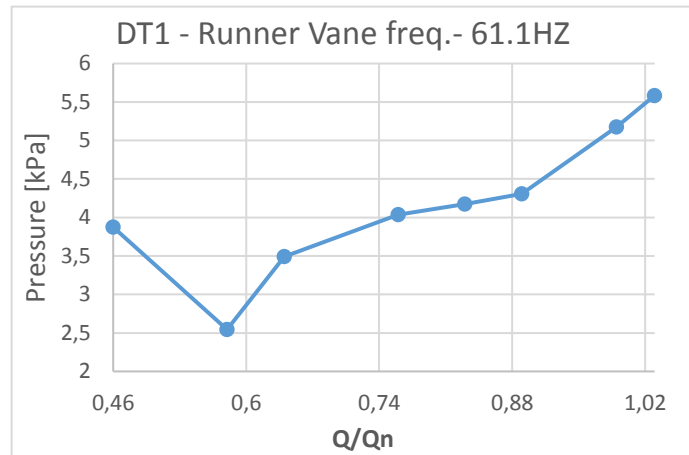


Figure 35 - Runner vane frequency

Figure 37 shows how the Rheingans frequency develops in the draft tube as the load increases from part load towards BEP. Sensor DT2 is located close to the outlet of the turbine, while DT8 is at the bottom of the draft tube. DT4 and DT6 are spaced in between DT2 and DT8, in the same vertical axis. An interesting observation that can be made is how the intensity measured by DT1 changes as the load increases. The intensity of the Rheingans frequency is the highest during low part load operation. The highest amplitude is measured at DT2, during part load. This is most likely a result of the tangential in the draft tube being at its highest at low part loads. This enables the vortex rope to move further away the draft tubes centerline.

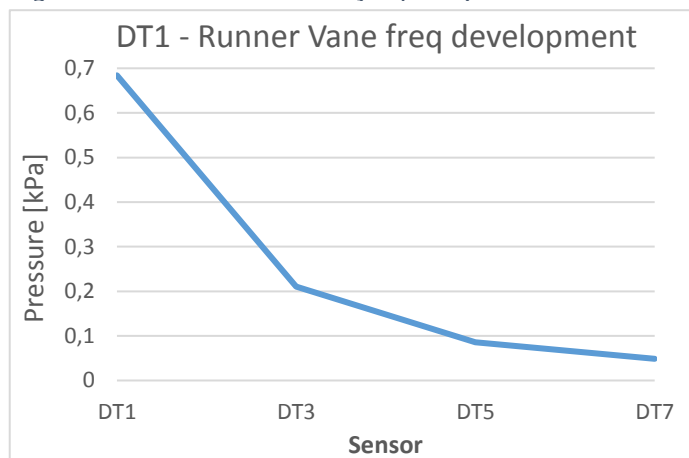


Figure 36 - Runner vane intensity at 0.83·Q<sub>n</sub>

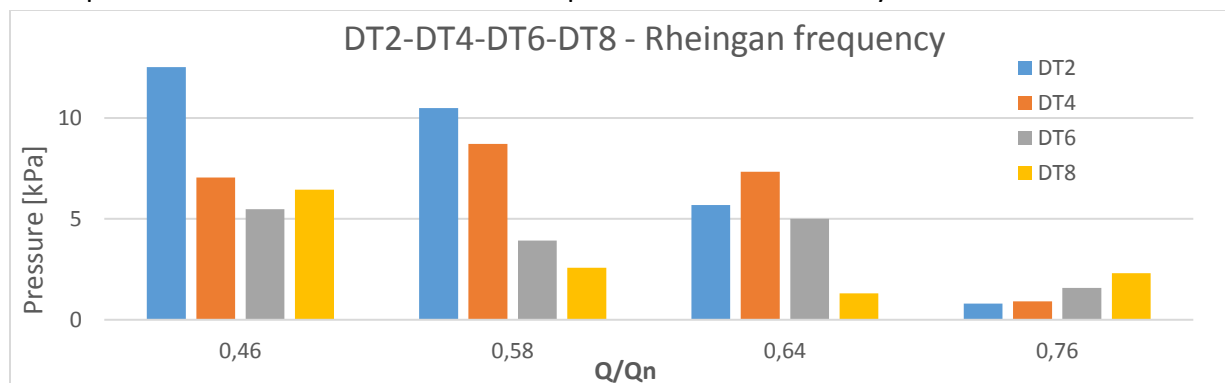


Figure 37 - Rheingans frequency intensity development

The axial velocity will increase when the load is increased, reducing the tangential velocity. As the tangential velocity decreases, the size and reach of the vortex rope will decrease, thereby lessening the intensity of the Rheingans frequency. This can be seen in Figure 37. The same figure displays that the intensity of DT8 increases relative to the other sensors at  $0.76 \cdot Q_n$ . DT8 is located furthest down in the draft tube. The higher intensity at DT8 is possibly because of the centrifugal forces moving the vortex rope away from the draft tube center as it moves downstream from the turbine.

4.2.1 Pressure intensity

Figure 38 to Figure 41 illustrate the peak pressure that each sensor in the draft tube experienced per operational point. The values that are shown have a confidence level of 99%. The confidence level is used in an effort to remove outliers and avoid over- estimation of the pressure peaks. The figures present two sensors in pair, that both are placed in the same horizontal axis, on either side of the draft tube. Figure 1 illustrates how each set of sensors are placed with a given distance between them. The blue bar represents the sensors located closest to the inner radius of the bend, while the yellow bar represents the sensors located closest to the outer radius of the bend.

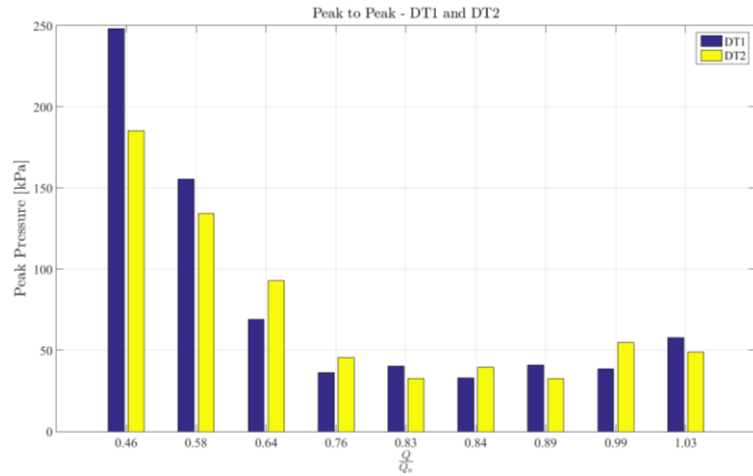


Figure 38 - Peak pressure comparison sensor DT1 and DT2

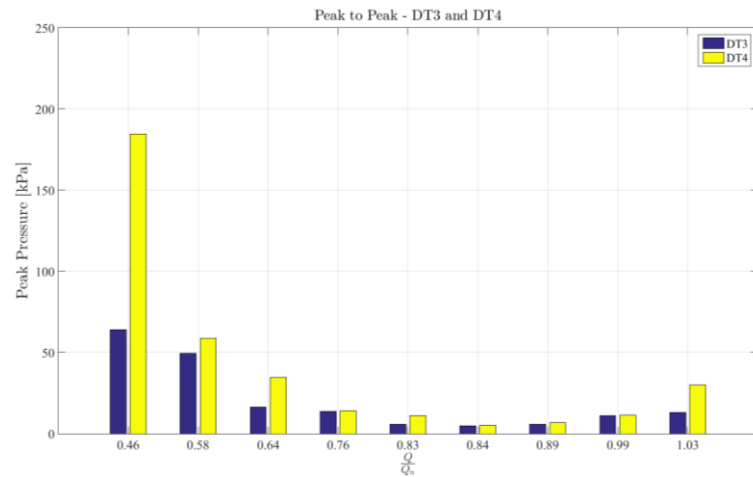


Figure 39 - Peak pressure comparison sensor DT3 and DT4

The maximum pressure peak of 250kPa was measured by sensor DT1 during part load operation at  $0.46 \cdot Q_n$ . The lowest pressure peak was 2kPa, measured by sensor DT7 at BEP. A trend that is displayed in all of the bar plots is that the peak pressure is reduced significantly when the flow moves towards the turbines best efficiency point at  $0.84 \cdot Q_n$ . All sensors measure the highest pressure peaks at low part load operation.

Pressure Sensor $r_{inside}$	DT1	DT3	DT5	DT7
Peak pressure [kPa]	250	60	48	50
Pressure Sensor $r_{outside}$	DT2	DT4	DT6	DT8
Peak pressure [kPa]	185	185	65	232
Diff $r_{inside}/r_{outside}$	-35%	67%	26%	78%

Table 19 - Peak Pressures all sensors for  $0.46 \cdot Q_n$



An interesting phenomenon is that there appears to be a difference in the pressure peaks between each side of the draft tube. Comparing the pressure peaks as the flow moves down the draft tube shows that there is a significant difference between the sides. The blue bar in Figure 38 shows a higher intensity for sensor DT1 than for DT2. Table 19 presents the pressure values for the part load point of  $0.46 \cdot Q_n$ . If one tracks the development of the peak pressure through the draft tube at  $0.46 \cdot Q_n$ , it can be seen that the pressure measured closest to the outside radius of the draft tube bend has peaks up to 78% higher.

Sensor DT1 and DT2 are located directly under the outlet of the turbine. Due to their placement, they are prone to be in direct wake of the flow exiting the blades. This cause the sensors to experience higher peak pressure relative to the other sensors further down in the draft tube. Figure 39 and Figure 41 show that the pressure measured with DT4 and DT8 are between two and four times greater than the peaks measured with DT3 and DT7. This is observed at all operational points. Figure 42 illustrates the results of a previously performed CFD analysis of a laminar flow through a uniform circular bend. The figure displays the inlet velocity conditions of the flow right before the bend and is expected to be similar to the flow at BEP. The figure shows how the highest flow velocity has a tendency

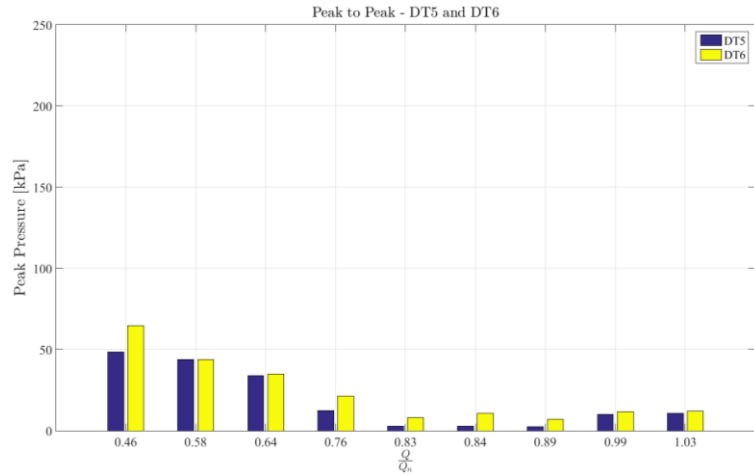


Figure 40 - Peak pressure comparison sensor DT5 and DT6

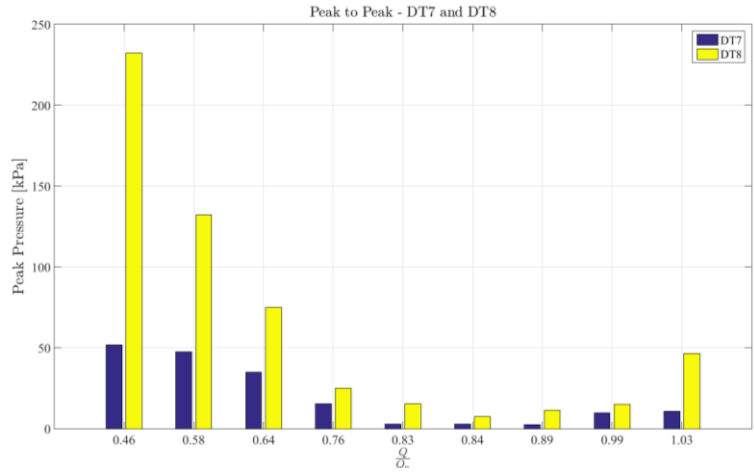


Figure 41 - Peak pressure comparison sensor DT7 and DT8

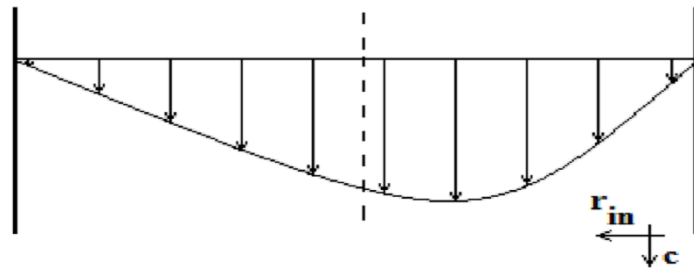


Figure 42 - Inlet velocity condition before bend

to curve towards the outer radius of the bend. The figure shows how the highest flow velocity has a tendency

to be towards the inner radius of the bend. The outer radius experiences a lower velocity and thereby a higher pressure. The bend at Leirfossene does not have the same uniform shape, however it is assumed that the bend at Leirfossene has a similar flow pattern, where the inner radius experiences a lower pressure due to higher velocities than the outer radius. This assumption is the basis for further discussion.

It is determined that there is a difference between different the operating conditions, part load (PL) at  $0.46 \cdot Q_n$ , the best efficiency point (BEP) at  $0.84 \cdot Q_n$  and high load (HL) at  $1.03 \cdot Q_n$ .

Of these, it is the PL that experiences the highest peak

pressures. BEP shows the lowest peak pressures for all sensors. This is expected as the flow during the turbines BEP does not have a tangential velocity component. HL has a higher peak pressure than BEP due to the added tangential velocity. The peak pressures at HL are however far less than at PL.

	Inner radius Pressure [kPa]	Outer radius Pressure [kPa]	Diff $r_{inside}/r_{outside}$
<b>DT1-DT2</b>	32	39	18%
<b>DT3-DT4</b>	4.9	5.2	6%
<b>DT5-DT6</b>	2.8	10.1	72%
<b>DT7-DT8</b>	2.7	11.2	74%

*Table 20 - Peak Pressure at BEP all sensors*

BEP and HL both display the same trend of different peak pressures on either side of the wall. Knowing that the inner radius of the bend has a higher velocity, ergo lower pressure than the outer radius and assuming that this propagates into the draft tube, it would cause one side to experience a higher pressure than the other. This could explain why the sensors located on either side of the draft tube wall would experience a deviation in pressure while operating at BEP. Table 20 appears to confirm the theory of the pressure being lower closer to the inner radius of the bend. It is believed that the tendency of the flow to move towards the inner diameter of the bend increases gradually as the flow travels down the draft tube. This theory is partly supported in the data, showing that the difference in pressure peaks at DT3 and DT4 is small, but rapidly increases as the flow moves further down the draft tube. The pressure peaks at sensors DT1 and DT2 are believed to be mainly influenced by the flow exiting the turbine and the turbines operational point.

At part load the flow has a high tangential velocity in the draft tube. Under these conditions a rotating vortex rope can develop in the draft tube. The higher the relative tangential velocity to the flows axial velocity, the higher up in the draft tube the vortex rope can develop. This is

supported by the result from the previous chapter, as it can be seen that the Rheingans frequency decreases as one moves towards the BEP.

All pressure sensors measure their highest peaks at PL. It is believed that the flow still has a higher velocity closer to the inner radius at PL. It can be assumed that the inner radius experiences lower pressure peaks because of the main flow, with the highest velocity, being located closer to the sensors. In the draft tube, the high velocity flow will act similar to a stable flow and less turbulent, causing less pressure pulsation.

This implies that the vortex rope will move towards the lower velocity area at the outer radius of the bend, causing higher pressure pulsations on this side. This can be supported by the data presented in figures 12 and 13, which shows that the vortex rope is initiated at the outlet of the turbine with a high pressure peak. As the rope moves downstream in the tube it follows its natural movement towards sensor DT4, showing a still high pressure peak, moving towards the center imposing equal pressure on each sensors, before moving towards the low velocity area at the inlet of the bend.

### 4.2.2 Effects of air injection

In order to evaluate the effect of air injection on the system, the peak value of the pressure pulsation as well as the frequency spectrum has been evaluated. Air was injected during two part-load operational points, respectively  $0.46 \cdot Q_n$  and  $0.58 \cdot Q_n$ . In the following chapter, both operational points will be presented and evaluated.

#### 4.2.2.1 Part load $0.46 \cdot Q_n$

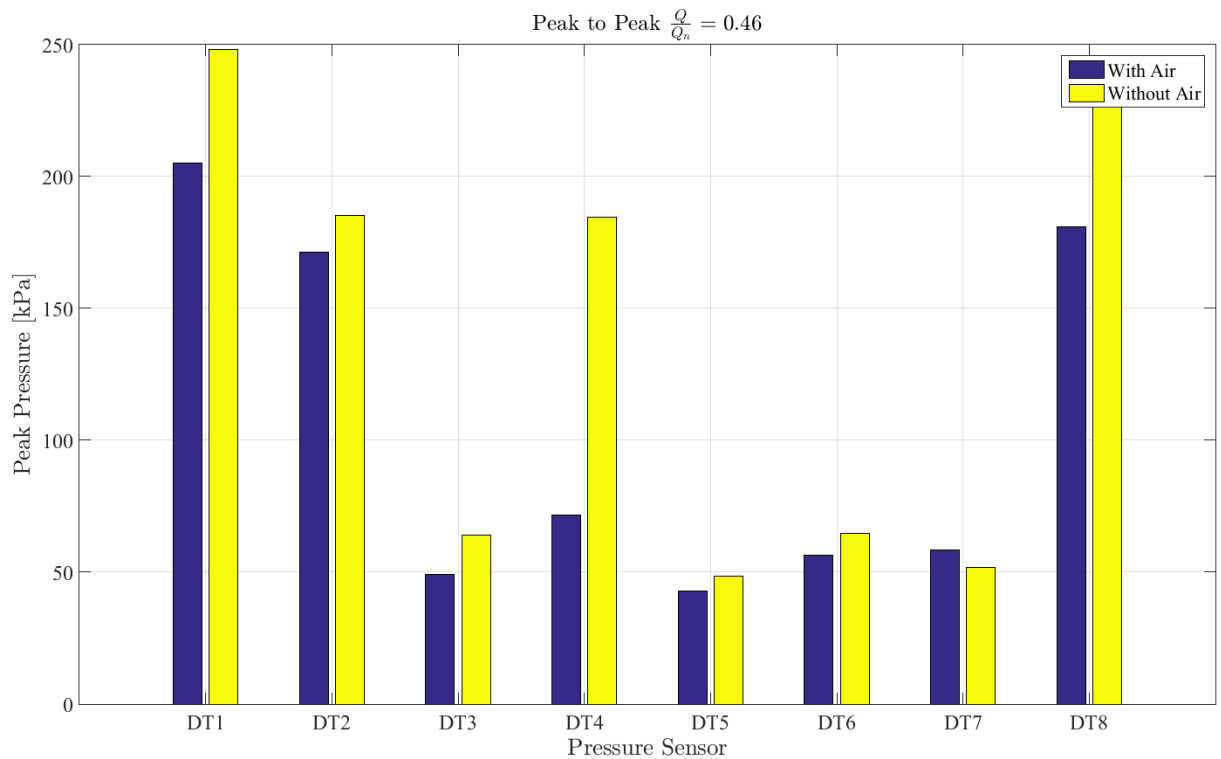


Figure 43 - Pressure peak Values w/without air injection –  $0.46 \cdot Q_n$

Figure 43 displays the peak values of the recorded pressure pulsations at  $0.46 \cdot Q_n$ . The vertical axis represents the peak pressure in kPa. The higher the bar in the plot, the greater the pressure pulsations. The blue bar represents the peak pressure with air injection while the yellow bar represents the peak pressure without air injection. The horizontal axis displays the pressure sensors that are being analyzed.

Figure 43 and Table 21 show the effect that the air injection has on the pressure pulsation. Table 21 lists the peak values and difference in % for the measurements with and without air injection. Pressure sensor DT3, DT4 and DT8 experience a reduction in the pressure pulsation between 20% and 60% with air injection. Sensor DT2, DT5 and DT6 experience a more moderate reduction of 7% to 13%, whereas DT7 displays an increase of 13% in pressure pulsation when air is injected. The sensor

Sensor	With [kPa]	Without [kPa]	Diff [%]
DT1	205	248	17,4
DT2	171	185	7,6
DT3	49	64	23,1
DT4	72	185	61,3
DT5	43	48	11,7
DT6	56	65	13,0
DT7	59	52	13,2
DT8	181	232	22,2
<b>Mean</b>	<b>104</b>	<b>135</b>	<b>22,6</b>

Table 21 - Peak pressure values  $0.46 \cdot Q_n$

DT7, which experiences a slight increase after the air injection, has to be evaluated as part of the whole system. The main purpose was to reduce the strong pulsations in the system. The results from sensors DT3, DT4 and DT8 show that a great reduction has been achieved when injecting air.

The overall trend for seven out of eight sensors is a reduction in peak pressure when air is injected. This shows that the relatively low pressure peak from sensor DT7 does not influence the whole system because its effect can be considered to be marginal in the greater picture. In total a reduction of 22% in the overall peak pressure has been observed after air injection.

Figure 44 and Figure 45 display the frequency spectrum at  $0.46 \cdot Q_n$  without and with air injected. The left side of the figures display the four sensors closest to the inner radius of draft tube bend, while the right side displays the four pressure sensors that are located at the outer radius of the bend. The horizontal axis describes the computed frequency in Hertz, while the vertical axis shows which pressure sensor is displayed. The spectrogram displays the intensity of the frequency in colors. The color blue represents the lowest intensity and the color red the highest intensity.

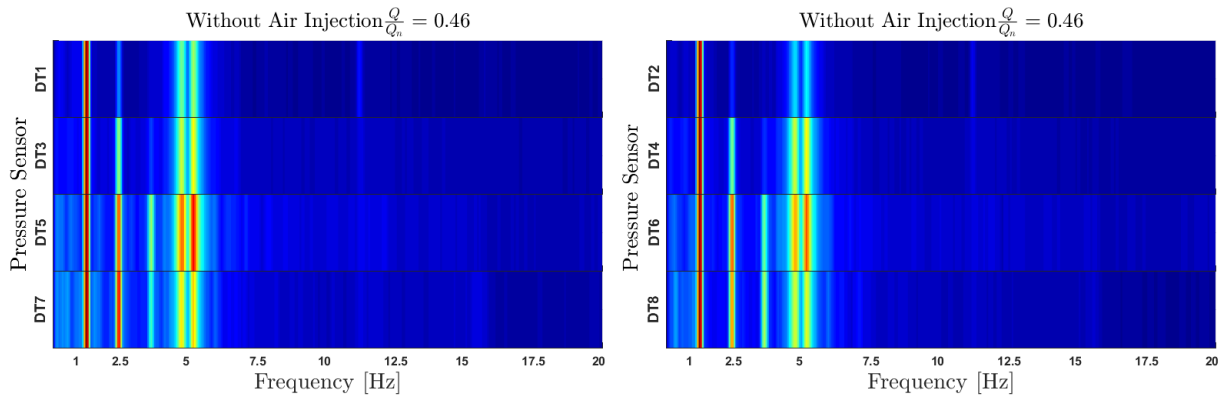


Figure 44 - Spectrogram Without air injection

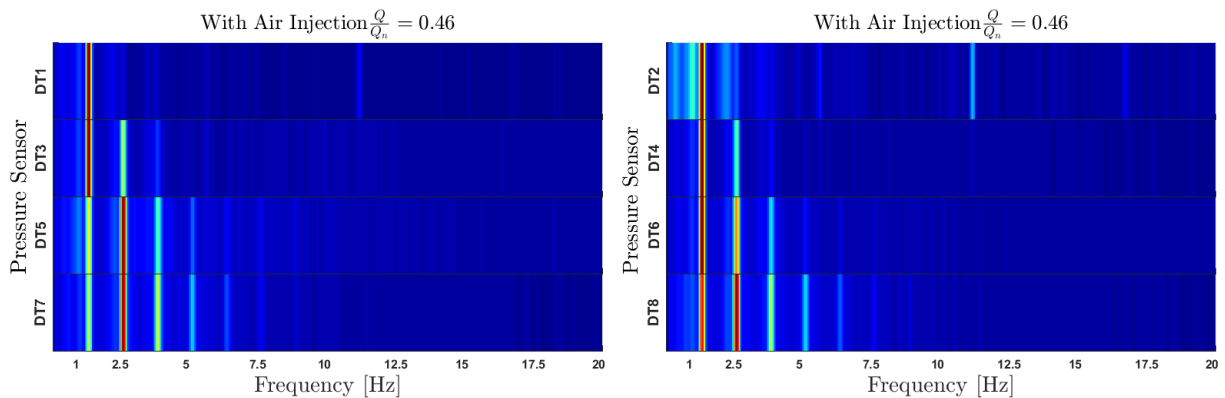


Figure 45 - Spectrogram With air injection

By comparing Figure 44 and Figure 45, some similarities can be observed between the measurements with and without air injection. Both figures show the second harmonic of the runner frequency at 11.11Hz at sensors DT1 and DT2, as well as the fundamental frequency of the Rheingans frequency for all eight sensors. The Rheingans frequency appears to have a slight shift in its frequency from 1.16Hz to 1.2Hz when air is injected.

When comparing sensor DT5 and DT7, it can be seen that the intensity in the fundamental Rheingans frequency is somewhat reduced in the measurements with air injection. That said, the first and second harmonic in the measurements with air injected seem to be of a higher intensity compared to the ones without air injected. Sensors DT1 and DT2, located closest to the outlet of the runner, detect the first harmonic of the Rheingans frequency when no air is injected, but not after air injection. This can possibly be attributed to the initializing point of the vortex rope to be pushed further down into the draft tube when air is being injected.

An interesting phenomenon is that both measurements show a growing number of harmonics related to the Rheingans frequency as the flow moves downstream in the draft tube. This is assumed to be because of the increasing number of turns of the rotating vortex rope in the draft tube, thereby increasing the number of harmonics that are created downstream in the draft tube.

Figure 44 shows that all sensors in the draft tube observe two distinct frequencies at 4.64Hz and 5.06Hz during part load at  $0.46 \cdot Q_n$  without air injection. Figure 45 shows that these frequencies are not present when air is injected into the system. It is believed that these frequencies are not rotational dependent because they do not appear in the measurements with air injection. It also does not match with the runner frequency of 5.55Hz or any of the harmonics of the Rheingans frequency. Both frequencies are likely related to the elastic fluctuations from the lower reservoir. Theoretically, frequencies 4.64Hz and 5.06Hz correlate with the level of the reference outlet reservoir and the area transition between the outlet reference reservoir and outlet, respectively. The air injected into the water appears to reduce the presumed elastic fluctuations.

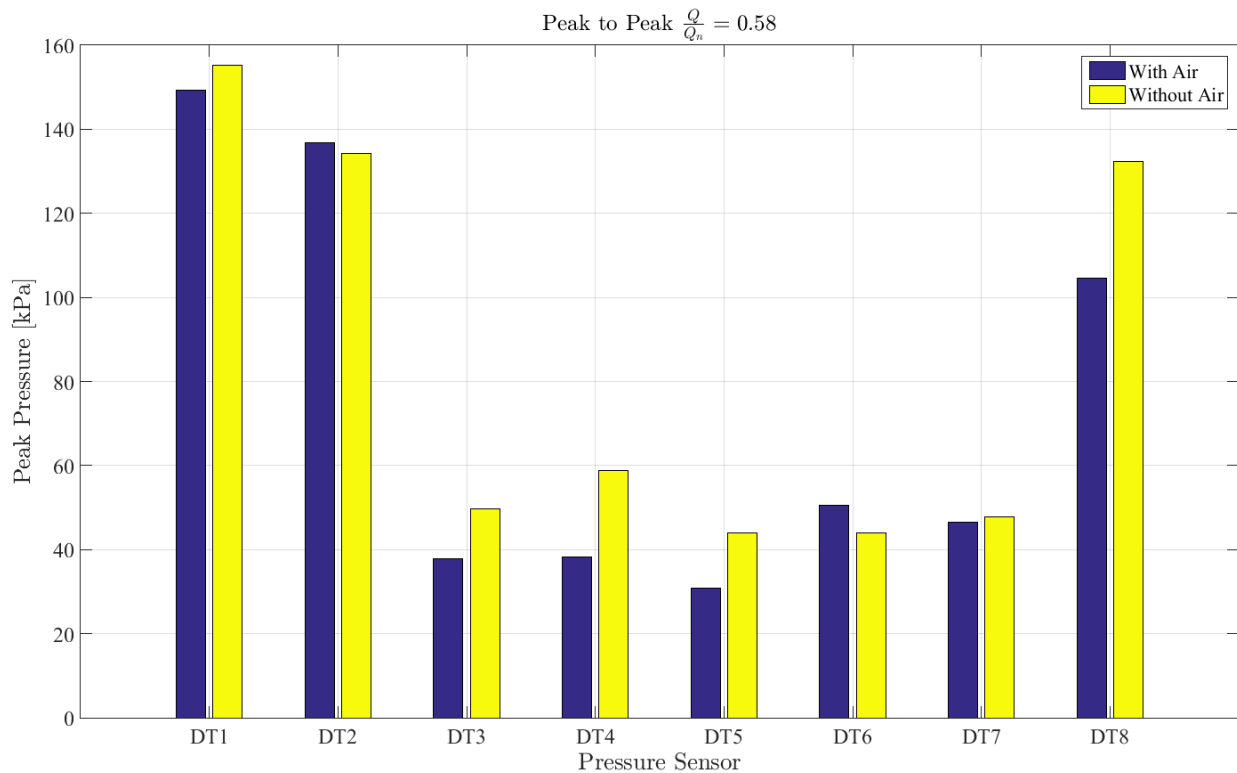
4.2.2.2 Part load  $-0.58 \cdot Q_n$ 

Figure 46 - Pressure peak Values w/without air injection –  $0.58 \cdot Q_n$

Figure 46 shows the effect of the air injection on the peak values of the pressure pulsation at  $0.58 \cdot Q_n$ . Table 22 lists the peak pressures values measured with and without air injection as well as the difference presented in percentage.

Sensor	With [kPa]	Without [kPa]	Diff [%]
DT1	149	155	3,9
DT2	137	134	-1,9
DT3	38	49	23,2
DT4	38	59	34,9
DT5	31	44	29,7
DT6	50	44	-14,6
DT7	46	48	2,6
DT8	105	132	20,9
<b>Mean</b>	<b>74</b>	<b>83</b>	<b>10,7</b>

Table 22 - Peak pressure values  $0.58 \cdot Q_n$

The effects are most noticeable on the sensors DT3, DT4, DT5 and DT8 with a peak reduction of 20% to 34% when air is injected. Sensor DT1 and DT7 both showed a minimal reduction of about 3%. Sensor DT2 and DT6 experienced an

increase in the peak pressure between 2% and 14% when air is injected. The total intensity of the peaks pressure at  $0.58 \cdot Q_n$  is reduced by 10% when air is injected.



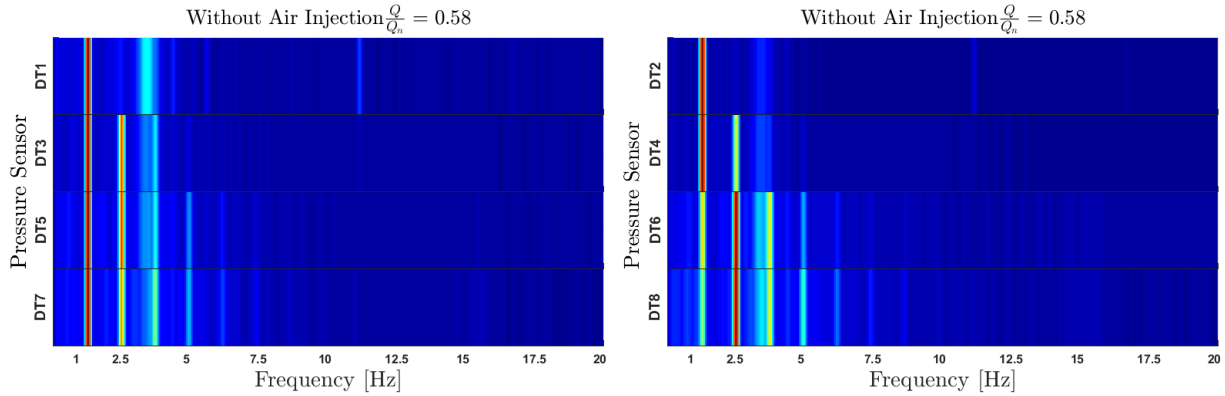


Figure 47 - Spectrogram Without air injection

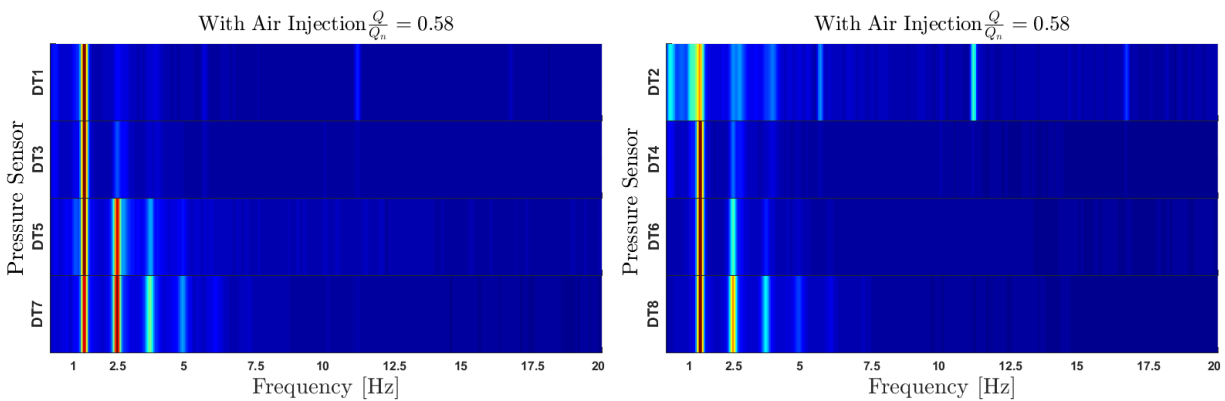


Figure 48 - Spectrogram With air injection

The effect of air injection on the pressure pulsations seems to not be as clear at the higher load compared to the results presented for  $0.46 \cdot Q_n$  load. This is most likely because the flow present at the lower load will be more turbulent, thereby more prone to develop greater pressure pulsations compared to a higher load with a more stable flow. Comparing the trends at both operating points, shows that the overall peak pressure intensity for all sensors are reduced by 20% to 40% when operating at the higher load. This complies with the theory that tangential velocity in the draft tube decreases and the flow becomes more laminar as one moves towards the turbines best efficiency point, thereby reducing the peaks of the pressure pulsations.

The spectrograms presented in Figure 47 and Figure 48 display the part load point of  $0.58 \cdot Q_n$  with and without air injection, respectively. When analyzing the frequency spectra, it can be seen that both measurements clearly display the fundamental Rheingans frequency of 1.2Hz with- and 1.19Hz without air injection. Both measurements display the second harmony of the runner frequency at 11.11Hz.

There are two main differences between the measurements with and without air injection. The first, is the frequency detected next to the third harmonic of the Rheingans frequency, at 3Hz, during operations without air injections. The 3Hz frequency is clearly visible for sensor DT1 and decreases in intensity as it moves downstream in the draft tube. On the other side of the draft tube the 3Hz frequency seems to have the opposite behavior with the highest intensity measured by the DT8 sensors. This can possibly be attributed to a local flow phenomenon where the intensity crosses from the DT1 located at the top of the draft tube, to the DT8 sensor located on the other side at the bottom of the draft tube. This frequency is not present when air is injected, nor is it present at the lower operating point of  $0.46 \cdot Q_n$ .

The second difference is related to the harmonics of the Rheingans frequency. The measurements with air injected seem to delay the formation of harmonics in the draft tube. When comparing sensor DT3 with and without air injected, it can be seen that the measurements with air injected display three prominent harmonics whereas the measurements without air injected display only the fundamental frequency. It should also be noted that the intensity of the harmonics seems to follow the same pattern of being reduced for the fundamental frequency before increasing in intensity in the second harmonic. The same trend was observed for the previously discussed part load operation of  $0.46 \cdot Q_n$ . This said, pressure sensor DT2 displays some frequency in the below 1Hz range that have not been successfully identify.

### 4.2.3 Comment on the total pressure intensity

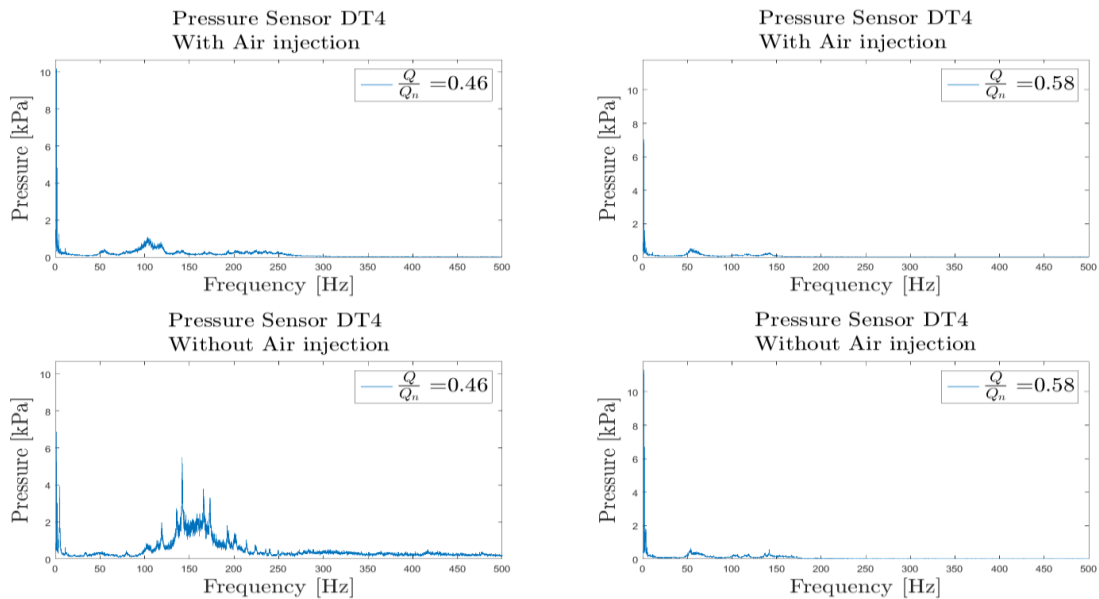


Figure 49 - FFT with and without air injection-Sensor DT4

Figure 49 displays the frequency spectrum from 0Hz to 500Hz for measurements with and without air injections. The two figures on the left represent the part load operational point of  $0.46 \cdot Q_n$ , while figures on the right represent  $0.58 \cdot Q_n$ . Comparing the overall intensity of the measurements at  $0.46 \cdot Q_n$  with and without air injection shows that the intensity without air injection is much greater. The peaks between 100Hz and 200Hz in the measurements with air injection are up to four times greater, and cover a much larger area in the frequency spectra than the measurements without air injection. However, the intensity of Rheingans frequency with air injection appears to be 30% larger compared to the measurements without air injection. The measurements at  $0.58 \cdot Q_n$  display an opposite trend when it comes to the Rheingans frequency. Measurement without air injection appear to have a 40% stronger Rheingans frequency when no air is injected.

In evaluating the means of reducing pressure pulsations and vibrations, one has to look at the totality and the actual impact each frequency has on the system. In theory, a higher frequency will contain more energy than a lower frequency with the same amplitude. This implies that the desired frequency range should be as low as possible. In reality, this is not entirely true. The low frequency range, 0-10Hz, is associated with relatively large movement of the machinery. When comparing the pressure pulsation with the vibration measurements presented in the next chapter, a trend of increasing vibrations intensity can be seen at part load operation. This said, the high frequencies also cause vibrations and are most dangerous when they resonate with the natural frequency of the machinery. The total reduction of the pressure pulsation is still the main objective. One has to be aware that some frequencies may be more harmful than others.

#### 4.2.4 Vibration measurement

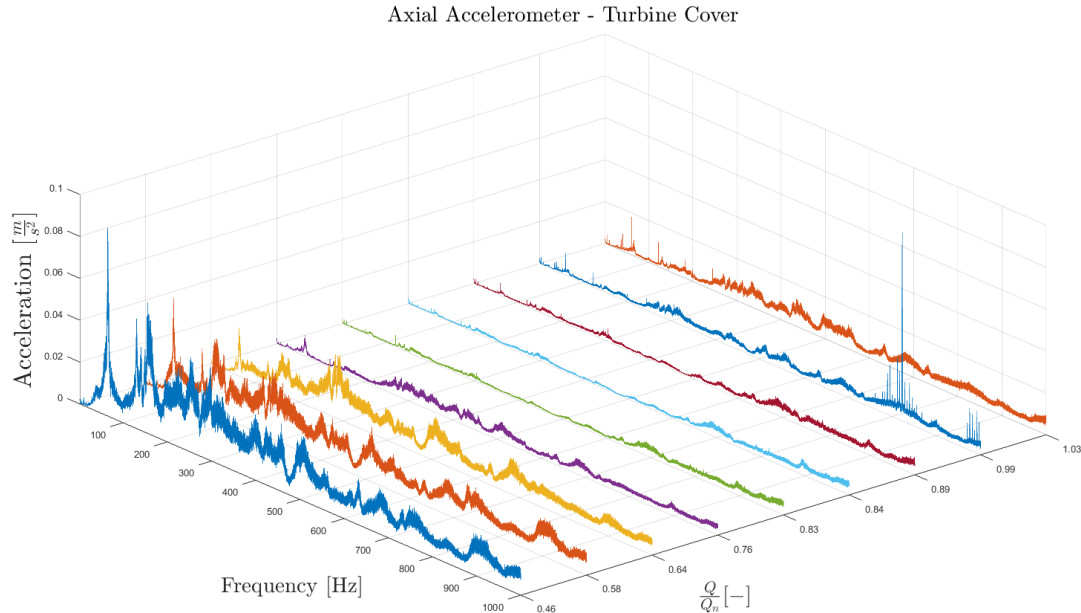


Figure 50 - Vibration at turbine cover for all loads

Figure 50 displays the frequency spectrum from 0Hz and 1000Hz for vibrations at different operational points. Based on the plot it is obvious that the machine experiences most vibrations during part load operation from  $0.46 \cdot Q_n$  to  $0.64 \cdot Q_n$ . It can also be seen that the high load points of  $0.90 \cdot Q_n$  and  $1.03 \cdot Q_n$  experience higher vibrations than the best efficiency point at  $0.84 \cdot Q_n$ .

The data from the vibration measurements shows that the runner frequency, runner vane frequency and guide vane frequency are visible at all operational points. The Rheingans frequency has not been successfully detected because of the vibration sensors lower frequency range being limited to 1Hz, resulting in “ski slope” distortion on the frequencies under 2Hz [222]. It can be seen in the vibration measurements that the highest vibration levels are present in the frequency range under 200Hz. The runner vane frequency is the most intense source of vibration for all operating points.

### 4.2.5 Comparing pressure and vibration measurements

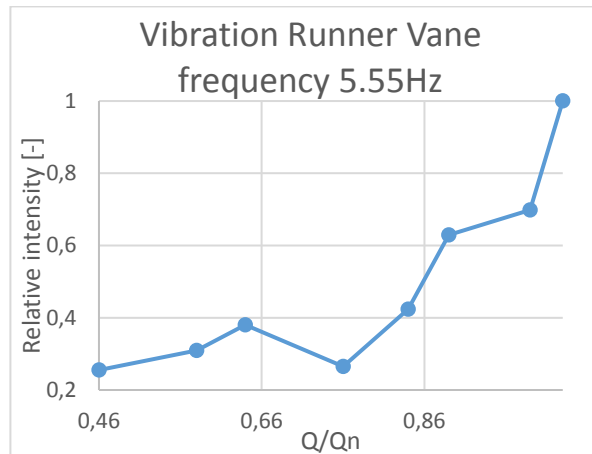


Figure 51 - Vibration intensity of Runner frequency

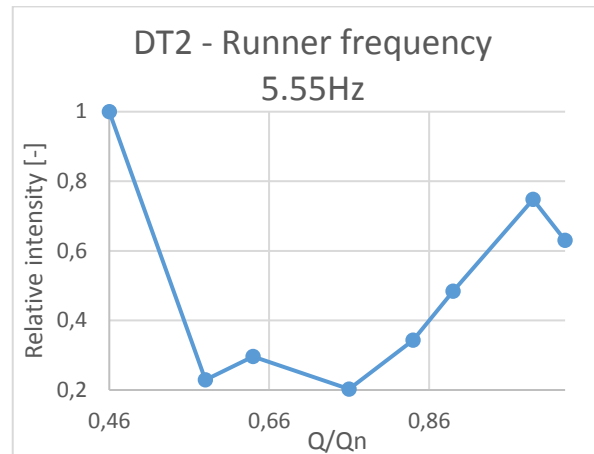


Figure 52 - Pressure intensity of Runner frequency-DT2

Comparing the vibration and pressure pulsation measurements can give an indication if the intensity of the frequency analysis correlates across measurements. Figure 51 and Figure 52 display the relative intensity, to the highest intensity peak, of the runner frequency at 5.55Hz of the vibration and pressure measurements, respectively. The graphs show that both measurements mostly display the same trend. There are some differences at the part load point of  $0.46 \cdot Q_n$  and the high load point of  $0.90 \cdot Q_n$ . This could mean that the intensity of the runner frequency displayed in the pressure measurements at part load does not have a big impact on the actual vibration experienced by the machine.

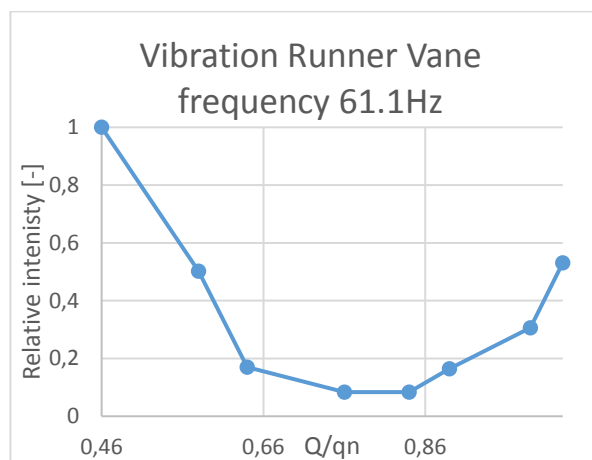


Figure 53 - Vibration intensity of Runner vane frequency

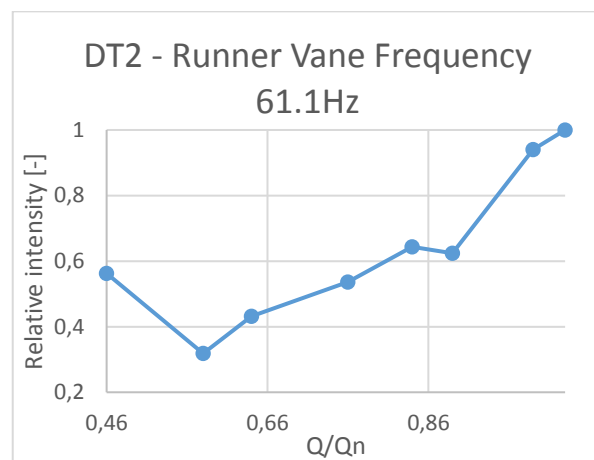


Figure 54 - Pressure intensity of Runner vane frequency DT2

Figure 53 and Figure 54 display the intensity of the runner vane frequency at 61.1Hz from the vibration and pressure measurements, respectively. Both figures show the same trend. However, the frequency intensity shows that the pressure sensor detects a higher amplitude compared to

the relative amplitudes of the vibrations at the turbines BEP. The opposite is observed at part load, where the vibration sensor displays a relative intensity almost two times higher. This supports the theory of lower frequencies causing more severe vibration in the machinery.

Figure 55 and Figure 56 display the lower frequency ranges at  $0.46 \cdot Q_n$  for both the pressure and the vibration sensor. The graph has been plotted from 2Hz to 12 Hz in order to compare the two sets without them being influenced by the “ski-slope” of the vibration measurements. The end of the “ski-slope” can be seen at 3Hz in Figure 55. The vibration measurements display four main peaks at 4.64Hz, 5.06Hz, 9.98Hz and 11.1Hz. The peak at 9.98Hz does not appear to have an obvious source, but is most likely a harmony of a 5Hz frequency that cannot be clearly distinguished in the frequency spectrum. The 11.1Hz peak is also observed in the pressure pulsation measurements and is most likely the second harmony of the runner frequency, 5.55Hz.

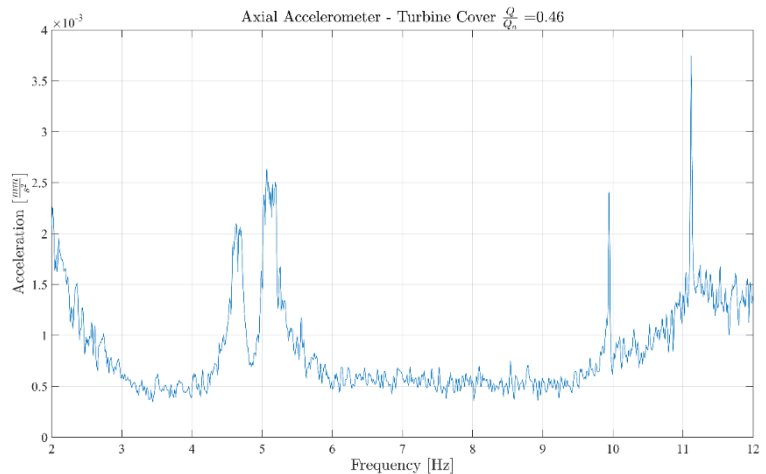


Figure 55 - Axial vibration on turbine cover at  $0.46 \cdot Q_n$

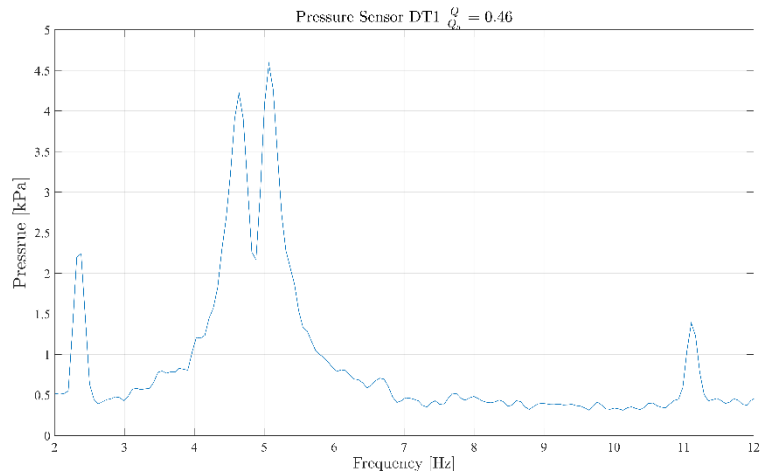


Figure 56 - Pressure pulsation DT1 at  $0.46 \cdot Q_n$

The main area of interest are the two peaks located at 4.64Hz and 5.06Hz. Both frequencies have previously been discussed in chapter 4.2.2.1 about air injection. The interesting part is that it is clearly visible in the vibration measurement as well. Both the vibration and pressure measurements only detect these frequencies at  $0.46 \cdot Q_n$ . This implies that both frequencies most likely are dependent on the behavior of the both flow and the elastic fluctuations under low part-load operation.

## 5 Conclusion

Efficiency Measurements have been carried out for turbine 2 at Leirfossene power plant. The thermodynamic method was used to calculate the turbine efficiency. The measurements have been carried out in accordance with the International Standard IEC 60041, 3.ed 19991-11 [1]. The relative efficiency displays the highest efficiency when the turbines power at its rated head is 14MW. The calculated efficiency deviates between 1.2%, at part load, to 0.13%, at high load, compared to previously performed measurements by Norconsult in 2009. The maximum uncertainty in efficiency is calculated to be 1.4%. The measurements were conducted on a nominal head lower than the 100m the IEC standard demands. They did fulfill the requirement of not having an temperature increase of more than  $0.005 K/min$ .

Pressure pulsation measurements have been performed in the draft tube on turbine 2. The pressure pulsation measurements show that the Rheingans frequency, runner frequency and runner vane frequency are present in the draft tube. The Rheingans frequency is the dominant frequency while operating at part load. The runner frequency displays a high intensity at both part- and high- load compared to the relatively low intensity at its best efficiency point (BEP). The runner vane frequency shows a high intensity at the outlet of the turbine.

The analysis of the pressure intensity shows the highest pressure pulsations measured for BEP, part load and high load are  $45kPa$ ,  $250kPa$ ,  $55kPa$ , respectively. The sensors located closest to the inner radius of the draft tube bend experience a lower intensity than the sensors at the outer radius of the bend. The intensity difference between the sides is up to 4 times greater during part load operation. This is probably a flow-specific phenomenon that occurs in the draft tube bend. Data with and without air injection from two operating point at  $0.46 \cdot Q_n$  and  $0.58 \cdot Q_n$  have been compared. The analysis shows that the air injection reduces the overall intensity by 22% at  $0.46 \cdot Q_n$  and 10% at  $0.58 \cdot Q_n$ . The most powerful pulsations are reduced by 20% to 60%, while the remaining pulsations experienced a change from  $-14\%$  to  $17\%$ . Frequency analysis at part load,  $0.46 \cdot Q_n$ , shows two distinct frequencies at 4.64Hz and 5.06Hz when the turbine runs without air injection. When air is injected into the draft tube, these frequencies disappear altogether. The frequencies are probably related to elastic fluctuations in the system, which are lessened by the injected air.

## 6 Further work

One of the more interesting observations made was the difference in pressure between each side of the draft tube. Further work should be focused on establishing the flow phenomenon that occurs in the draft tube. A theoretical flow study involving computational fluid dynamics (CFD) should be conducted. It can be wise to install more pressure sensors between the existing ones. The sensors should be located 90 degrees apart in the same horizontal axis. By gathering more experimental data, one will be able to better determine how the flow behaves and develops under different operational points.

A key interest that can be researched is how the centrifugal force affects the discharge when it has a high tangential velocity in the draft tube. Other flow phenomena, like the Magnus effect, should be investigated. These phenomena can possibly be a contributor to the pressure difference between the sides, and can influence how the flow behaves in the draft tube.

Another noteworthy observation was the two frequencies of 4.64Hz and 5.06Hz that were present during part load at  $0.46 \cdot Q_n$ . Both frequencies were present during operation when no air was injected. However, when air was injected both frequencies completely disappeared. It was assumed that these frequencies are related to the elastic fluctuations between the lower reservoir and turbine. Further work should try to determine a more accurate speed of sound in order to pinpoint the frequencies origin with a higher certainty.

So far, only air injection has been used as a means of reducing pressure pulsations during part load operation. Other options like a freely rotating runner cone extensions or a fixed runner cone extensions should be explored. Runner cone extensions will increase the axial velocity of the flow at the turbines outlet, ideally moving the start of the vortex rope further downstream. The use of fins in the draft tube should also be explored, in order to guide the flow more efficiently. Efficiency measurements should be performed again if new means of reducing pressure pulsations are tested, in order to review the effect on the system.

The vibration analysis performed in this report focused mainly on the frequency analysis of the measurements. However, the analysis of displacement can potentially give useful information about the intensity and severity of the vibration. The vibration measurements should be performed on different components of the hydraulic unit. This should include measurements on the shaft bearing, generator and the draft tube. A triaxial sensors setup should be considered in the measurements of guide vane, head cover and draft tube vibrations to accurately analyze the movements in all directions.



## 7 Bibliography

- [1] IEC 60041:1991 Field acceptance tests to determine the hydraulic performance of hydraulic performance of hydraulic turbines, storage pumps and pump turbines. International Standard. Geneva, Switzerland 1991
- [2] Brænd, Tore J.. (2013, 14. juni). Energiloven. I Store norske leksikon. Hentet 24. juni 2016 fra <https://snl.no/energiloven>.
- [3] Statkraft (2016), leirfossene. Hentet 24. juni 2016 fra <http://www.statkraft.no/Energikilder/vaare-kraftverk/norge/Leirfossene/>
- [4] W.J. Rheingans, Power swings in hydroelectric power plants, ASME, Vol.62,1940.
- [5] Oftebro, I., Lønning, A., 1967, "Pressure oscillations in Francis turbines", Institution of Mechanical Engineers, 1966-1967, Vol 181 Pt3a, 1967.
- [6] E. Kobro, "Measurement of Pressure Pulsations in Francis Turbines," Norwegian University of Science and Technology, Trondheim, 2010.
- [7] A. M. Tørklep, "Pressure oscillations during start and stop of a high head Francis turbine," NTNU, Trondheim, 2012.
- [8] S. Haga, "Dynamic load on High Head francis turbines during start/stop", NTNU, Trondheim, 2014.
- [9] F. Kjøsnes, "Measurement of Natural Frequency in a circular disk in air and water" NTNU, Trondheim, 2013.
- [10] Wang, Fujun, et al. "Experimental investigation of pressure fluctuation and vibration in a large Francis turbine." *ASME/JSME 2007 5th Joint Fluids Engineering Conference*. American Society of Mechanical Engineers, 2007.
- [11] Dörfler, Sick and Coutu, "Flow induced pulsation and Vibration in Hydroelectric Machinery", 2006
- [12] IEC 60994:1991 Guide for field measurement of vibrations and pulsations in hydraulic machines (turbines, storage pumps and pump-turbines). International Standard. Geneva, Switzerland 1991
- [13] J. Ramsdal, "Efficiency measurements in low head hydro power plants", NTNU 2011
- [14] Alming, Knut, Thermodynamic method of measuring turbine efficiency -Correction for heat transfer in a probe. Report VL 130. The Waterpower Laboratory NTH, Trondheim 1964
- [15] Rögener, H., Herbst., G., Properties of water and equations of state with special respect to the "Thermodynamic Method" of testing hydraulic turbines and pumps. Technical University of Hanover, Germany 1978

## Bibliography

- [16] Hulaas, H., Vinnogg, L., IEC 60041 – 1991, "Field acceptance tests to determine the hydraulic performance of hydraulic turbines, storage pumps and pumpturbines". Clause 14 "Thermodynamic method for measuring efficiency" Comments. Proceeding from the 8<sup>th</sup> IGHEM conference, Roorkee, India 2010
- [17] Hulaas, Harald, and O. G. Dahlhaug. "Uncertainty analysis of Pressure-Time measurements." Proceedings from the 6<sup>th</sup> IGHEM conference. 2006.
- [18] Ramdal, Jørgen. "Efficiency measurements in low head hydro power plants". 2011
- [19] Dahlhaug, Ole G., Torbjørn K. Nielsen, and H. H. Fracke. "Comparison between pressure-time and thermodynamic efficiency measurements on a low head turbine." Proceedings of 6<sup>th</sup> IGHEM symposium. Portland, USA. 2006.
- [20] *Introduction to Engineering Experimentation* by Anthony and J. Weeler and Ahmad R. Ganji, 2004
- [21] Solvik, S. & Selmurzaev, M. "Pressure oscillations and Vibration in Francis Turbines". 2015
- [22] 26<sup>th</sup> IAHR *Symposium on Hydraulic Machinery and Systems* IOP Publishing IOP Conf. Series: Earth and Environmental Science 15 (2012) 022003 doi:10.1088/1755-1315/15/2/022003
- [23] Brekke, H. «Pumper og Turbiner». Vannkraftlaboratoriet NTNU. 2013
- [24] Tovslid, A. «Trykkpulsasjoner i Francistrubiner sammenligning av modell og prototypmålinger». 20134
- [25] Brekke, Hermod. "A Review on Oscillatory Problems in Francis Turbine." *New Trends in Technologies: Devices, Computer, Communication and Industrial Systems*, Sciyo (2010): 217-232.
- [26] Measuring vibration.(September 1982) Brüel & Kjær. Hentet 02. feb 2015 fra <http://bksv.com/doc/br0094.pdf>
- [27] March, P., Hydraulic and Environmental Performance of Aerating Turbine Technologies EPRI, Palo Alto, California, Proceedings of EPRI/DOE Conference on Environmentally-Enhanced Hydropower Turbines: Technical Papers Report, 2011
- [28] Vekve, Thomas. "An experimental investigation of draft tube flow." (2004).
- [29] Papillon B, Sabourin M, Couston M and Deschenes C 2002 Methods for Air Admission in Hydro Turbines 21<sup>st</sup> IAHR Symposium on Hydraulic Machinery and Systems, Lausanne, Switzerland, September pp 9–12
- [30] Gogstad, P. J., Dahlhaug, O. G., „Methods of mitigating pressure pulsations in a francis turbine”, 2016
- [31] J. Haugen, "Laboratoriet - Typiske frekvenser i strømningsmaskiner," 1994.
- [32] Kari Haugan. Master thesis, "Pressure pulsations in Francis Turbines, ". NTNU, 2007.
- [33] Julie Hovland, "Pressure Pulsations and Stress in a High Head Francis Model Turbine", NTNU, 2013.
- [34] Einar Kobro. Master thesis: Pressure pulsations in Francis turbines. NTNU, 2006.
- [35] Resonans. (2012, 23. desember). I Store norske leksikon. Hentet 18. march 2016 fra <https://snl.no/resonans>.

- [36] Nielsen, 1990] Nielsen, T. K. (1990). Dynamisk dimensjonering av vannkraftverk. SINTEF, Strømningsmaskiner.
- [37] Robert J. Marks II, Introduction to Shannon Sampling and Interpolation Theory, Springer-Verlag, New York, 1991
- [38] National Instruments, 2014 "Acquiring an Analog Signal: Bandwidth, Nyquist Sampling Theorem, and Aliasing". Hentet 03. april 2016 fra <http://www.ni.com/white-paper/2709/en/>
- [39] National Instruments, 04. may 2014 "Understanding FFTs and Windowing"
- [40] Heinzl, Gerhard, Albrecht Rüdiger, and Roland Schilling. "Spectrum and spectral density estimation by the Discrete Fourier transform (DFT), including a comprehensive list of window functions and some new at-top windows." (2002).
- [41] Bruxton Corporation, "Data Acquisition. An introduction".2013
- [42] Poole, I., Radio-electronics.com, 2016 "Signal to noise Ratio,SNR". Hentet 03. March 2016, fra <http://www.radio-electronics.com/info/rf-technology-design/rf-noise-sensitivity/receiver-signal-to-noise-ratio.php>
- [43] Maksim, 2015 "Spectral leakage from a sinusoid and rectangular window", Hentet 03. March 2016 fra [https://upload.wikimedia.org/wikipedia/commons/f/f6/Spectral\\_leakage\\_from\\_a\\_sinusoid\\_and\\_rectangular\\_window.png](https://upload.wikimedia.org/wikipedia/commons/f/f6/Spectral_leakage_from_a_sinusoid_and_rectangular_window.png)
- [44] MasterHD,2015, "Resonance", Hentet 03. March 2016 fra <https://upload.wikimedia.org/wikipedia/commons/0/07/Resonance.PNG>
- [45] National Instruments, 2016, "Understanding Resolution in High speed Digitizers/Oscilloscopes", Hentet 04.may2016 fra <http://www.ni.com/white-paper/4806/en/>
- [46] "Harmonics", Electronics tutorial, 2015, Hentet 22. May 2016 fra <http://www.electronics-tutorials.ws/accircuits/harmonics.html>
- [47] Gogstad, P.J., Conversation about efficiency calculation, June 2016, NTNU
- [48] National Instruments, 2007, "FFt Fundamentals (sound and vibration measurement suite)", Hentet 20.may 2016 fra [http://zone.ni.com/reference/en-XX/help/372416A-01/svtconcepts/fft\\_funda/](http://zone.ni.com/reference/en-XX/help/372416A-01/svtconcepts/fft_funda/)
- [49] Francke, H. H and Wiborg, E. J. Falltaps- og virkningsgradsmålinger ved Svean Kraftverk. Master thesis, Norwegian University of Science and Technology. 2005



**Appendix A Calculations of expected frequencies**

Runner frequency  $f_n = \frac{n}{60} [Hz] = \frac{333}{60} = 5.55 Hz$

Runner vane frequency  $f_{rv} = f_n * z_{rv} [Hz] = 5.55 * 11 = 61.05 Hz$

Guide vane frequency  $f_{gv} = f_n * z_{gv} [Hz] = 5.55 * 24 = 133.2 Hz$

Rheingans frequency  $f_R \cong \frac{f_n}{2} \rightarrow \frac{f_n}{4} [Hz] = 2.775 Hz \rightarrow 1.3875 Hz$

Elastic fluctuation  $f = \frac{1}{t} = \frac{a}{8L} [Hz] = 4.63 Hz \rightarrow 6.83 Hz$

## Appendix B Calculation example Efficiency

Generator Power	$P_{generator}$	<i>withheld</i>	Measured
Generator efficiency	$\eta_{generator}$	<i>withheld</i>	Data sheet
Pressure atmospheric pres.	$P_{atm}$	<i>withheld</i>	Measured
Pressure inlet sensor	$p_1$ mesurment	<i>withheld</i>	Measured
Pressure temp sensor	$p_{11}$ mesurment	<i>withheld</i>	Measured
Temperature inlet	$T_{11}$	<i>withheld</i>	Measured
Temperature outlet	$T_{21}$	<i>withheld</i>	Measured
Pipe center inlet	$z_1$	8,5 m	Measured
Draft tube center outlet	$z_2$	3,847 m	Measured
Height temp sensor inlet	$z_{11}$	10.266 m	Measured
Height temp sensor outlet	$z_{21}$	3,847 m	Measured
Height $z_{refout}$ to lower res	$z_3$	8,73 m	Measured
Outlet ref height	$z_{refoutlet}$	22,455 m	Measured
Height pressure measurement inlet	$z_{1pres}$	9,595 m	Measured
Height temp pressure measurement inlet	$z_{11presTemp}$	10,0109 m	Measured
Diff. center pipe and pressure sensor	$\Delta z_1 = z_{1pres} - z_1$	1,095 m	Calculated
Diff. temperature and temp pressure sensor	$\Delta z_{11} = z_{11presTemp} - z_{11}$	-0,2551 m	Calculated
Head at outlet to center of outlet pipe	$\Delta h_2 = z_{refoutlet} - z_3 - z_2$	9,878 m	Calculated
Head at outlet to temp sensor at outlet	$\Delta h_{21} = z_{refoutlet} - z_3 - z_{21}$	9,878 m	Calculated
Gravitational constant	$g_{mean}$	9,8217 $m/s^2$	Calculated
Density inlet	$\rho_{in}$	1000,3 $kg/m^3$	IEC 60041
Density outlet	$\rho_{out}$	1000 $kg/m^3$	IEC 60041
Density outlet	$\bar{\rho}$	1000.15 $kg/m^3$	Calculated
Isothermal factor - Inlet	$a_{in}$	$0,9965 * 10^{-3} m^3/kg$	IEC 60041
Isothermal factor - Outlet	$a_{out}$	$0,9974 * 10^{-3} m^3/kg$	IEC 60041
Isothermal factor - Mean	$a_{mean}$	$0,99695 * 10^{-3} m^3/kg$	Calculated
Specific heat capacity - Inlet	$c_{pIn}$	4199,8 $J/kg \cdot K$	IEC 60041
Specific heat capacity - Outlet	$c_{pout}$	4201,8 $J/kg \cdot K$	IEC 60041

Specific heat capacity - Mean	$\bar{c}_p$	4200,8 J/kg · K	Calculated
Bucket filling time	$t_{filling}$	103,58 s	Measured
Bucket Volume	$V_{bucket}$	0,011 m <sup>3</sup>	Data sheet
Area - Inlet	$A_1$	4,9087	Calculated
Area - Outlet at temperature sensor	$A_2$	14,868 m <sup>2</sup>	Calculated
Area - Outlet at lower reservoir	$A_3$	15,75 m <sup>2</sup>	Calculated
Area - Probe	$A_{probe}$	0,000227 m <sup>2</sup>	Calculated

### Procedure for calculating the efficiency using the thermodynamic method

- Initial Estimation of flow
- Initial calculation of the total mechanical energy
- Recalculation of the flow
- Recalculation the total mechanical energy
- Recalculation of the flow
- Calculation of the Hydraulic Energy
- Computation of the efficiency

### Estimating flow

$$Q_{assumed} = \frac{P_{turbine}}{p_1 - p_{atm}} \quad (\text{Eq. A. 1})$$

$$p_1 = p_{1 \text{ mesurment}} + \rho_{in} \cdot g \cdot \Delta z_1 \quad (\text{Eq. A. 2})$$

$$P_{turbine} = \frac{P_{generator}}{\eta_{generator}} \quad (\text{Eq. A. 3})$$

### Computing the Mechanical energy

$$E_m = E_{m \text{ pressure}} + E_{m \text{ potential}} + E_{m \text{ kinetic}} + E_{m \text{ thermal}} \quad (\text{Eq. A. 4})$$

$$E_m = \bar{a} \cdot (p_{11} - p_{21}) + \bar{g} \cdot (z_{11} - z_{21}) + \frac{1}{2} \cdot (c_{11}^2 - c_{21}^2) + \bar{c}_p \cdot (T_{11} - T_{21}) \quad (\text{Eq. A. 5})$$

### Mechanical pressure energy

$$E_{m \text{ pressure}} = \bar{a} \cdot (p_{11} - p_{21}) \quad (\text{Eq. A. 6})$$

$$p_{11} = p_{11 \text{ mesurment}} + \rho_{in} \cdot g \cdot \Delta z_{11} \quad (\text{Eq. A. 7})$$

$$p_{21} = p_{atm} + \rho_{out} \cdot g \cdot \Delta h_{21} \quad (\text{Eq. A. 8})$$

### Mechanical Potential energy

$$E_{m \text{ potential}} = \bar{g} \cdot (z_{11} - z_{21}) \quad (\text{Eq. A. 9})$$

### Mechanical Kinetic energy

$$E_{m \text{ kinetic}} = \frac{1}{2} \cdot (c_{11}^2 - c_{21}^2) \quad (\text{Eq. A. 10})$$

$$Q_{\text{probe}} = \frac{V_{\text{bucket}}}{t_{\text{filling}}} \quad (\text{Eq. A. 11})$$

$$c_{11} = \frac{Q_{\text{probe}}}{A_{\text{probe}}} \quad (\text{Eq. A. 12})$$

$$c_{21} = \frac{Q_{\text{assumed}}}{A_2} \quad (\text{Eq. A. 13})$$

### Mechanical Thermal energy

$$E_{m \text{ thermal}} = \bar{c}_p \cdot (T_{11} - T_{21}) \quad (\text{Eq. A. 14})$$

### Total mechanical energy

$$E_m = E_{m \text{ pressure}} + E_{m \text{ potential}} + E_{m \text{ kinetic}} + E_{m \text{ thermal}} \quad (\text{Eq. A. 15})$$

### Recalculation of Flow

$$Q_{\text{recalculated}} = \frac{P_{\text{turbine}}}{\bar{\rho} \cdot E_m} \quad (\text{Eq. A. 16})$$



**Recalculation of total Mechanical energy**

$$E_m = E_{m \text{ pressure}} + E_{m \text{ potential}} + E_{m \text{ kinetic new}} + E_{m \text{ thermal}} \quad (\text{Eq. A. 17})$$

$$E_{m \text{ kinetic new}} = \frac{1}{2} \cdot (c_{11}^2 - c_{21}^2) \quad (\text{Eq. A. 18})$$

$$c_{21} = c_2 = \frac{Q_{\text{recalculated}}}{A_2} \quad (\text{Eq. A. 19})$$

**Recalculation of final flow**

$$Q_{\text{Final}} = \frac{P_{\text{turbine}}}{\bar{\rho} \cdot E_m} \quad (\text{Eq. A. 20})$$

**Computation of the hydraulic Energy**

$$E_h = E_{h \text{ pressure}} + E_{h \text{ potential}} + E_{h \text{ kinetic}} \quad (\text{Eq. A. 21})$$

$$E_h = \frac{1}{\bar{\rho}} \cdot (p_1 - p_2) + \bar{g} \cdot (z_1 - z_2) + \frac{1}{2} \cdot (c_1^2 - c_2^2) \quad (\text{Eq. A. 22})$$

**Hydraulic Pressure energy**

$$E_{h \text{ pressure}} = \frac{1}{\bar{\rho}} \cdot (p_1 - p_2) = \frac{1}{1000,15} \quad (\text{Eq. A. 23})$$

$$p_2 = p_{\text{atm}} + \rho_{\text{out}} \cdot g \cdot \Delta h_2 - \rho_{\text{out}} \cdot (c_2^2 - c_3^2) \quad (\text{Eq. A. 24})$$

$$c_2 = \frac{Q_{\text{Final}}}{A_2} \quad (\text{Eq. A. 25})$$

$$c_3 = \frac{Q_{\text{Final}}}{A_3} \quad (\text{Eq. A. 26})$$

**Hydraulic Potential energy**

$$E_{h\ potential} = \bar{g} \cdot (z_1 - z_2) \quad (\text{Eq. A. 27})$$

**Hydraulic Kinetic energy**

$$E_{h\ kinetic} = \frac{1}{2} \cdot (c_1^2 - c_2^2) \quad (\text{Eq. A. 28})$$

$$c_1 = \frac{Q_{Final}}{A_1} \quad (\text{Eq. A. 29})$$

**Total Hydraulic Energy**

$$E_h = E_{h\ pressure} + E_{h\ potential} + E_{h\ kinetic} \quad (\text{Eq. A. 30})$$

**Turbine efficiency**

$$\eta_{turbine} = \frac{E_m}{E_h} \quad (\text{Eq. A. 31})$$

**Calculation of flow at turbine Design point**

$$H = \frac{E_h}{\bar{g}} \quad (\text{Eq. A. 32})$$

$$Q_{Design} = \sqrt{\frac{H_{Design}}{H}} \cdot Q_{Final} \quad (\text{Eq. A. 33})$$

**Calculation of turbine power at turbine Design point**

$$P_{Design} = \left(\frac{H_{Design}}{H}\right)^{3/2} \cdot P_{turbine} \quad (\text{Eq. A. 34})$$

## Appendix C Example of Head loss and Friction coefficient

### Head loss

$$H_{loss} = \frac{1}{\rho g} \cdot (p - p_1) + \frac{1}{2g} (c_{u_{reservoir}}^2 - c_1^2) + (z_{u_{reservoir}} - z_1) \quad (\text{Eq. A. 35})$$

$$c_{u_{reservoir}} = 0 \text{ m/s} \quad (\text{Eq. A. 36})$$

### Friction coefficient

$$K = \frac{H_{loss}}{Q^2} \quad (\text{Eq. A. 37})$$

## Appendix D Uncertainty Efficiency calculation

Time filling bucket	$e_{t_{probe}}$	0,1 s	IEC 60041
Volume Bucket	$e_{V_{Bucket}}$	$0,000001 \text{ m}^3$	Data sheet
Density inlet	$f_{\rho_{in}}$	0,1 %	IEC 60041
Density inlet	$e_{\rho_{in}} = f_{\rho_{in}} \cdot \rho_{in}$	$1,0003 \text{ kg/m}^3$	Calculated
Density outlet	$f_{\rho_{out}}$	0,1 %	IEC 60041
Density outlet	$e_{\rho_{out}} = f_{\rho_{out}} \cdot \rho_{out}$	$1 \text{ kg/m}^3$	Calculated
Density Mean	$e_{\rho_{mean}}$	$1,416 \text{ kg/m}^3$	Calculated
Isothermal factor inlet	$f_{\bar{a}_{tabelIn}}$	0,2 %	IEC 60041
Isothermal factor inlet	$e_{a_{in}} = f_{\bar{a}_{tabelIn}} \cdot a_{in}$	$1,993 \cdot 10^{-6} \text{ m}^3/\text{kg}$	Calculated
Isothermal factor outlet	$f_{\bar{a}_{tabelOut}}$	0,2 %	IEC 60041
Isothermal factor outlet	$e_{a_{out}} = f_{\bar{a}_{tabelOut}} \cdot a_{out}$	$1,9948 \cdot 10^{-6} \text{ m}^3/\text{kg}$	Calculated
Isothermal factor Mean	$e_{a_{mean}}$	$2,8198 \cdot 10^{-6} \text{ m}^3/\text{kg}$	Calculated
Specific Heat Capacity, Inlet	$f_{c_{p_{in}}}$	0,5 %	IEC 60041
Specific Heat Capacity, Inlet	$e_{c_{p_{in}}} = f_{c_{p_{in}}} \cdot c_{p_{in}}$	$20,99 \text{ J/kg} \cdot \text{K}$	Calculated
Specific Heat Capacity, Outlet	$f_{c_{p_{out}}}$	0,5 %	IEC 60041
Specific Heat Capacity, Outlet	$e_{c_{p_{out}}} = f_{c_{p_{out}}} \cdot c_{p_{out}}$	$21,009 \text{ J/kg} \cdot \text{K}$	Calculated
Specific Heat Capacity, Mean	$e_{c_{p_{mean}}}$	$29,697 \text{ J/kg} \cdot \text{K}$	Calculated
Area Probe	$f_{A_{probe}}$	0,025%	Data sheet
Area Probe	$e_{A_{probe}} = f_{A_{probe}} \cdot A_{probe}$	$5,6785 \cdot 10^{-8} \text{ m}^2$	Calculated
Atmospheric pressure	$e_{p_{atm}}$	$0,005297 \text{ kPa}$	Calibration sheet
Inlet pressure	$e_{p_{1 \text{ mesurment}}}$	$0,009828 \text{ kPa}$	Calibration sheet
Temperature pressure	$e_{p_{11 \text{ mesurment}}}$	$0,009149 \text{ kPa}$	Calibration sheet
Pipe center inlet	$e_{z_1}$	$0,02 \text{ m}$	IEC 60041
Draft tube center outlet	$e_{z_2}$	$0,02 \text{ m}$	IEC 60041
Height temp sensor inlet	$e_{z_{11}}$	$0,02 \text{ m}$	IEC 60041
Height temp sensor outlet	$e_{z_{21}}$	$0,02 \text{ m}$	IEC 60041
Height $Z_{refout}$ to lower res.	$e_{z_3}$	$0,02 \text{ m}$	IEC 60041
Outlet ref height	$e_{z_{refoutlet}}$	$0,05 \text{ m}$	IEC 60041

Height pressure measurement inlet	$e_{z_{1pres}}$	0,03 m	IEC 60041
Height temp pressure measurement inlet	$e_{z_{11presTemp}}$	0,03 m	IEC 60041
Generator Efficiency	$f_{\eta_{Generator}}$	0,5%	IEC 60041
Generator Power	$f_{P_{Generator}}$	0,71%	IEC 60041

### Combined Systematic Uncertainty

$$f_s = \pm \sqrt{f_{E_m}^2 + f_{E_{h_s}}^2} \quad (\text{Eq. A. 38})$$

### Total Mechanical systematic Uncertainty

$$f_{E_{m_s}} = \frac{e_{E_{m_s}}}{E_m} \quad (\text{Eq. A. 39})$$

$$e_{E_{m_s}} = \pm \sqrt{e_{E_{m_{p_s}}}^2 + e_{E_{m_{pot_s}}}^2 + e_{E_{m_{k_s}}}^2 + e_{E_{m_{t_s}}}^2} \quad (\text{Eq. A. 40})$$

### Mechanical Pressure

$$E_{m_p} = \bar{a} \cdot (p_{11} - p_{21}) \quad (\text{Eq. A. 41})$$

$$e_{E_{m_{p_s}}} = \sqrt{\left(\frac{e_{\bar{a}}}{\bar{a}}\right)^2 + \left(\frac{\sqrt{e_{p_{11}}^2 + e_{p_{21}}^2}}{(p_{11} - p_{21})}\right)^2} \cdot E_{m_p} \quad (\text{Eq. A. 42})$$

Inlet Pressure at temperature sensor

$$p_{11} = p_{11 \text{ measurement}} + \rho_{in} \cdot g \cdot \Delta z_{11} \quad (\text{Eq. A. 43})$$

$$e_{p_{11}} = \sqrt{\left(\frac{e_{p_{11 \text{ measurement}}}}{p_{11 \text{ measurement}}}\right)^2 + (f_{\rho_{in}})^2 + \left(\frac{\left(\sqrt{e^2_{z_{11 \text{ presTemp}}} + e^2_{z_{11}}}\right)^2}{z_{11 \text{ presTemp}} - z_{11}}\right)^2} \cdot p_{11}$$

( Eq. A. 44)

**Outlet Pressure at temperature sensor**

$$p_{21} = p_{atm} + \rho_{out} \cdot g \cdot (z_{refoutlet} - z_3 - z_{21}) \quad (\text{Eq. A. 45})$$

$$e_{p_{21}} = \sqrt{\left(\frac{e_{p_{atm}}}{p_{atm}}\right)^2 + (f_{\rho_{out}})^2 + \left(\frac{\left(\sqrt{e^2_{z_{refoutlet}} - e^2_{z_3} - e^2_{z_{21}}}\right)^2}{z_{refoutlet} - z_3 - z_{21}}\right)^2} \cdot p_{21}$$

(Eq. A. 46)

**Mechanical Kinetic Energy**

$$E_{m\ kinetic} = \frac{1}{2} \cdot (c_{11}^2 - c_{21}^2) \quad (\text{Eq. A. 47})$$

$$e_{Em_{ks}} = \sqrt{\left(\frac{2 \cdot e_{c_{11}}}{c_{11}}\right)^2 + \left(\frac{2 \cdot e_{c_{21}}}{c_{21}}\right)^2} \cdot E_{m_k} \quad (\text{Eq. A. 48})$$

**Inlet velocity at temperature sensors**

$$c_{11} = \frac{Q_{probe}}{A_{probe}} = \frac{V_{Bucket}}{t_{probe}} \quad (\text{Eq. A. 49})$$

$$e_{c_{11}} = \sqrt{\left(\frac{e_{V_{Bucket}}}{V_{Bucket}}\right)^2 + \left(\frac{e_{t_{probe}}}{t_{probe}}\right)^2 + \left(\frac{e_{A_{probe}}}{A_{probe}}\right)^2} \cdot c_{11} \quad (\text{Eq. A. 50})$$

**Outlet velocity at temperature sensors**

$$c_{21} = \frac{Q_{assumed}}{A_2} = \frac{Q_{assumed}}{B_2 \cdot H_2} \quad (\text{Eq. A. 51})$$

$$e_{c_{21}} = \sqrt{\left(\frac{e_{Q_{assumed}}}{Q_{assumed}}\right)^2 + \left(\frac{e_{B_2}}{B_2}\right)^2 + \left(\frac{e_{H_2}}{H_2}\right)^2} \cdot c_{21} \quad (\text{Eq. A. 52})$$

**Inlet pressure at the inlet of the turbine**

$$p_1 = p_{1 \text{ measurement}} + \rho_{in} \cdot g \cdot \Delta z_1 \quad (\text{Eq. A. 53})$$

$$e_{p_1} = \sqrt{\left(\frac{e_{p_{1 \text{ measurement}}}}{p_{1 \text{ measurement}}}\right)^2 + (f_{\rho_{in}})^2 + \left(\frac{\left(\sqrt{e^2_{z_{z_{1pres}}} + e^2_{z_1}}\right)^2}{z_{1pres} - z_1}\right)^2} \cdot p_1 \quad (\text{Eq. A. 54})$$

**Turbine**

$$P_{turbine} = \frac{P_{generator}}{\eta_{generator}} \quad (\text{Eq. A. 55})$$

$$e_{P_{turbine}} = \sqrt{(f_{P_{Generator}})^2 + (f_{\eta_{Generator}})^2} \cdot P_{turbine} \quad (\text{Eq. A. 56})$$

**Flow**

$$Q_{assumed} = \frac{P_{turbine}}{p_1 - p_{atm}} \quad (\text{Eq. A. 57})$$

$$e_{Q_{assumed}} = \sqrt{\left(\frac{e_{P_{turbine}}}{P_{turbine}}\right)^2 + \left(\frac{\sqrt{e^2_{p_1} + e^2_{p_{atm}}}}{(p_1 - p_{atm})}\right)^2} \cdot Q_{assumed} \quad (\text{Eq. A. 58})$$



**Mechanical Potential energy**

$$E_{m\ potential} = \bar{g} \cdot (z_{11} - z_{21}) \quad (\text{Eq. A. 59})$$

$$e_{Em_{pot_s}} = \sqrt{e_{z_{11}}^2 + e_{z_{21}}^2} \quad (\text{Eq. A. 60})$$

**Mechanical Thermal energy**

$$E_{m_t} = \bar{c}_p \cdot (T_{11} - T_{21}) \quad (\text{Eq. A. 61})$$

$$e_{Em_{t_s}} = \sqrt{\left(\frac{e_{\bar{c}_{p\ mean}}}{\bar{c}_{p\ mean}}\right)^2 + (f_{E_{in}})^2 + (f_{E_{out}})^2 + \left(\frac{\left(\sqrt{e^2_{T_{11}} + e^2_{T_{21}}}\right)^2}{(T_{11} - T_{21})}\right)^2} \cdot E_{m_t} \quad (\text{Eq. A. 62})$$

**Total Systematic Uncertainty – Mechanical Energy**

$$e_{E_{m_s}} = \sqrt{e_{Em_{p_s}}^2 + e_{Em_{pot_s}}^2 + e_{Em_{k_s}}^2 + e_{Em_{t_s}}^2} \quad (\text{Eq. A. 63})$$

$$f_{E_{m_s}} = \frac{e_{E_{m_s}}}{E_m} \quad (\text{Eq. A. 64})$$

**Total Hydraulic Systematic uncertainty**

$$f_{E_{hs}} = \frac{e_{E_{hs}}}{E_h} \quad (\text{Eq. A. 65})$$

$$e_{E_{hs}} = \pm \sqrt{e_{E_{hp_s}}^2 + e_{E_{hp_{ot_s}}}^2 + e_{E_{hk_s}}^2} \quad (\text{Eq. A. 66})$$

**Hydraulic Pressure energy**

$$E_h = \frac{1}{\rho} \cdot (p_1 - p_2) \quad (\text{Eq. A. 67})$$

$$e_{E_{hp_s}} = \sqrt{\left(\frac{e_{\rho}}{\rho}\right)^2 + \left(\frac{\sqrt{e_{p_1}^2 + e_{p_2}^2}}{(p_1 - p_2)}\right)^2} \cdot E_{hp} \quad (\text{Eq. A. 68})$$

**Outlet pressure term**

$$p_2 = p_{atm} + \rho_{out} \cdot g \cdot \Delta h_2 - \rho_{out} \cdot (c_2^2 - c_3^2) \quad (\text{Eq. A. 69})$$

$$e_{p_2} = \sqrt{\left(\frac{e_{p_{atm}}}{p_{atm}}\right)^2 + (f_{\rho_{out}})^2 + \left(\frac{\left(\sqrt{e_{z_{refoutlet}}^2 - e_{z_3}^2 - e_{z_2}^2}\right)^2}{z_{refoutlet} - z_3 - z_2}\right)^2 + \left(\frac{\sqrt{e_{c_2}^2 + e_{c_3}^2}}{(c_2 - c_3)}\right)^2} \cdot p_2 \quad (\text{Eq. A. 70})$$

**Velocity at outlet and lower reservoir**

$$e_{c_2} = e_{c_{21}} \quad (\text{Eq. A. 71})$$

$$e_{c_3} = \sqrt{\left(\frac{e_{Q_{assumed}}}{Q_{assumed}}\right)^2 + \left(\frac{e_{B_2}}{B_3}\right)^2 + \left(\frac{e_{H_2}}{H_3}\right)^2} \cdot c_{21} \quad (\text{Eq. A. 72})$$

**Hydraulic Pressure energy**

$$e_{Eh_{p_s}} = \sqrt{\left(\frac{e_{\bar{p}}}{\bar{p}}\right)^2 + \left(\frac{\sqrt{e_{p_1}^2 + e_{p_2}^2}}{(p_1 - p_2)}\right)^2} \cdot E_{h_p} \quad (\text{Eq. A. 73})$$

**Hydraulic Potential energy**

$$E_{h_{potential}} = \bar{g} \cdot (z_1 - z_2) \quad (\text{Eq. A. 74})$$

$$e_{Eh_{pot_s}} = \sqrt{e_{z_1}^2 + e_{z_2}^2} \quad (\text{Eq. A. 75})$$

**Hydraulic Kinetic energy**

$$E_{h_{kinetic}} = \frac{1}{2} \cdot (c_1^2 - c_2^2) \quad (\text{Eq. A. 76})$$

$$e_{Eh_{k_s}} = \sqrt{\left(\frac{2 \cdot e_{c_1}}{c_1}\right)^2 + \left(\frac{2 \cdot e_{c_2}}{c_2}\right)^2} \cdot E_{h_k} \quad (\text{Eq. A. 77})$$

**Inlet velocity**

$$c_1 = \frac{Q}{A_1} = \frac{Q}{\pi r^2} \quad (\text{Eq. A. 78})$$

$$e_{c_1} = \sqrt{\left(\frac{e_Q}{Q}\right)^2 + \left(\frac{2 \cdot e_r}{r}\right)^2} \cdot c_1 \quad (\text{Eq. A. 79})$$

**Hydraulic Kinetic energy**

$$e_{Eh_{k_s}} = \sqrt{\left(\frac{2 \cdot e_{c_1}}{c_1}\right)^2 + \left(\frac{2 \cdot e_{c_2}}{c_2}\right)^2} \cdot E_{h_k} \quad (\text{Eq. A. 80})$$

**Systematic Uncertainty - Total Hydraulic Energy**

$$e_{Eh_s} = \pm \sqrt{e_{Eh_{p_s}}^2 + e_{Eh_{pot_s}}^2 + e_{Eh_{k_s}}^2} \quad (\text{Eq. A. 81})$$

$$f_{Eh_s} = \frac{e_{Eh_s}}{E_h} \quad (\text{Eq. A. 82})$$

## Appendix E Random uncertainty efficiency calculation

$$e_r = \frac{t_{95} \cdot s_Y}{\sqrt{n}} \quad (\text{Eq. A. 83})$$

$t_{95}$  = Student t – factor with 95% confidence interval

$s_Y$  = Standard deviation

$n$  = number of samples

$$s_Y = \sqrt{\frac{\sum(\bar{Y} - Y_i)^2}{n - 1}} \quad (\text{Eq. A. 84})$$

Student t factor for measurements with samples larger than 120 samples have a  $t_{95} = 1,96$ .

Variable	$f$	%
Generator output	$f_{P_{generator}}$	$\pm 0,1\%$
heights	$f_{z_r}$	$\sim 0\%$
Density	$f_{\rho_r}$	$\sim 0\%$
Isothermal factor	$f_{a_r}$	$\sim 0\%$
Heat capacity	$f_{cp_r}$	$\sim 0\%$
Gravity	$f_{g_r}$	$\sim 0\%$
Probe flow	$f_{Q_{probe}}$	$\sim 0\%$

Table 23 - Random uncertainty according to IEC60041

Sensor	$t_{95}$	$s_Y$	$e_r$
$p_{atm}$	1,96	$2,0508 \cdot 10^{-5} J/kg$	$2,9960 \cdot 10^{-6} J/kg$
$p_1$ mesurment	1,96	$7,1548 \cdot 10^{-4} J/kg$	$1,0452 \cdot 10^{-6} J/kg$
$p_{11}$ mesurment	1,96	$0,0024 J/kg$	$3,5191 \cdot 10^{-6} J/kg$
$temp_{11-21}$	1,96	$0,7773 J/kg$	$0,0952 J/kg$

Table 24 - Random uncertainty of measured quantities

Table 24 presents the calculated random uncertainty of the sensors. The random uncertainty in the pressure measurements is low due to the number of samples for performed for each sensor. The diff temperature has fewer samples, and will therefore display a higher uncertainty.

**Random uncertainty Mechanical Energy**

$$E_m = \bar{a} \cdot (p_{11} - p_{21}) + \bar{g} \cdot (z_{11} - z_{21}) + \frac{1}{2} \cdot (c_{11}^2 - c_{21}^2) + \bar{c}_p \cdot (T_{11} - T_{21}) \quad (\text{Eq. A. 85})$$

**Mechanical Pressure Energy**

$$e_{E_{mp_r}} = \sqrt{e^2_{p_{11 \text{ mesurment}_r}} + e^2_{p_{atm_r}}} \quad (\text{Eq. A. 86})$$

**Mechanical Potential Energy**

$$e_{E_{mpot_r}} = \sqrt{e^2_{c_{11}} + e^2_{c_{21}}} \quad (\text{Eq. A. 87})$$

**Mechanical thermal Energy**

$$e_{E_{mtr}} = \sqrt{e^2_{T_{11}} + e^2_{T_{21}}} \quad (\text{Eq. A. 88})$$

$$f_{P_{Turbine_r}} = f_{P_{Generator_r}} \quad (\text{Eq. A. 89})$$

**Flow**

$$e_{Q_{assumed_r}} = \sqrt{e^2_{P_{Turbine_r}} + e^2_{p_{11 \text{ mesurment}_r}} + e^2_{p_{atm_r}}} \quad (\text{Eq. A. 90})$$

**Velocity**

$$e_{c_r} = e_{Q_r} \quad (\text{Eq. A. 91})$$

**Total Random Uncertainty – Mechanical Energy**

$$f_{Em_r} = \frac{\sqrt{(e_{Empr}^2 + e_{Emkr}^2 + e_{Emtr}^2)}}{E_m} \quad (\text{Eq. A. 92})$$

**Random uncertainty Hydraulic Energy**

$$E_h = \frac{1}{\rho} \cdot (p_1 - p_2) + \bar{g} \cdot (z_1 - z_2) + \frac{1}{2} \cdot (c_1^2 - c_2^2) \quad (\text{Eq. A. 93})$$

**Hydraulic Pressure Energy**

$$e_{E_{hp_r}} = \sqrt{e_{p_{1\text{mesurment}_r}}^2 + e_{p_{atm_r}}^2} \quad (\text{Eq. A. 94})$$

**Hydraulic potential Energy**

$$e_{E_{hpot_r}} = 0 \quad (\text{Eq. A. 95})$$

**Hydraulic Kinetic Energy**

$$e_{E_{hk_r}} = \sqrt{e_{c_{1r}}^2 + e_{c_{2r}}^2} \quad (\text{Eq. A. 96})$$

**Total Random Uncertainty – Hydraulic Energy**

$$f_{Eh_r} = 100 \cdot \frac{\sqrt{(e_{E_{hp_r}}^2 + e_{E_{hk_r}}^2)}}{E_m} \quad (\text{Eq. A. 97})$$

**Combined Random Uncertainty**

$$f_r = \sqrt{f_{Em_r}^2 + f_{Eh_r}^2} \quad (\text{Eq. A. 98})$$

**Total Uncertainty**

$$f_{tot} = \sqrt{f_s^2 + f_r^2} \quad (\text{Eq. A. 99})$$

### Appendix F Pressure pulsations plots

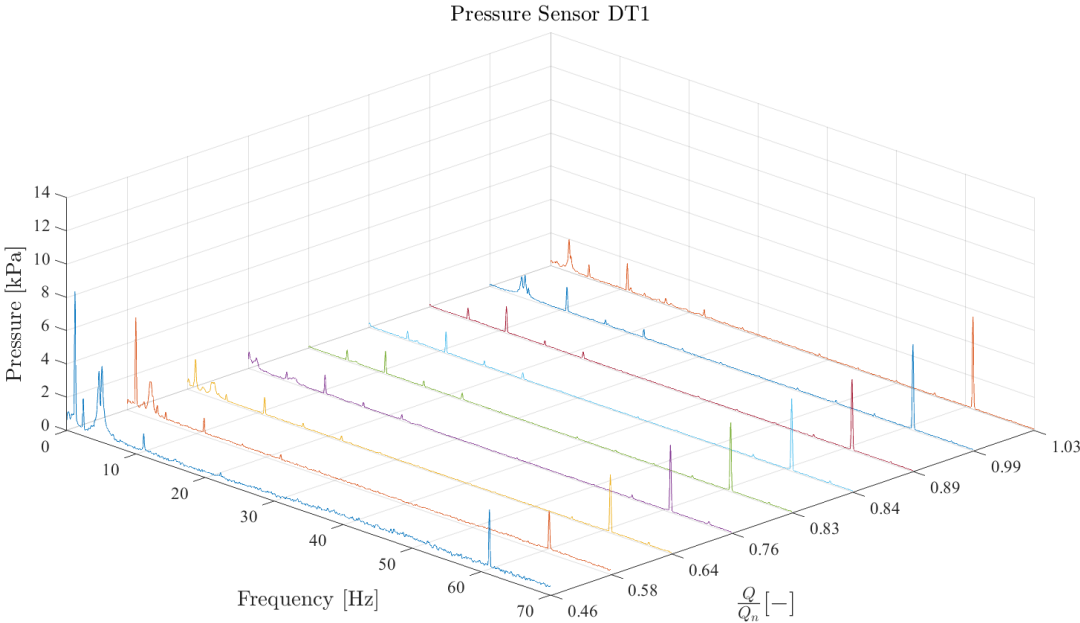


Figure 57 - Waterfall plot -Pressure sensor DT1

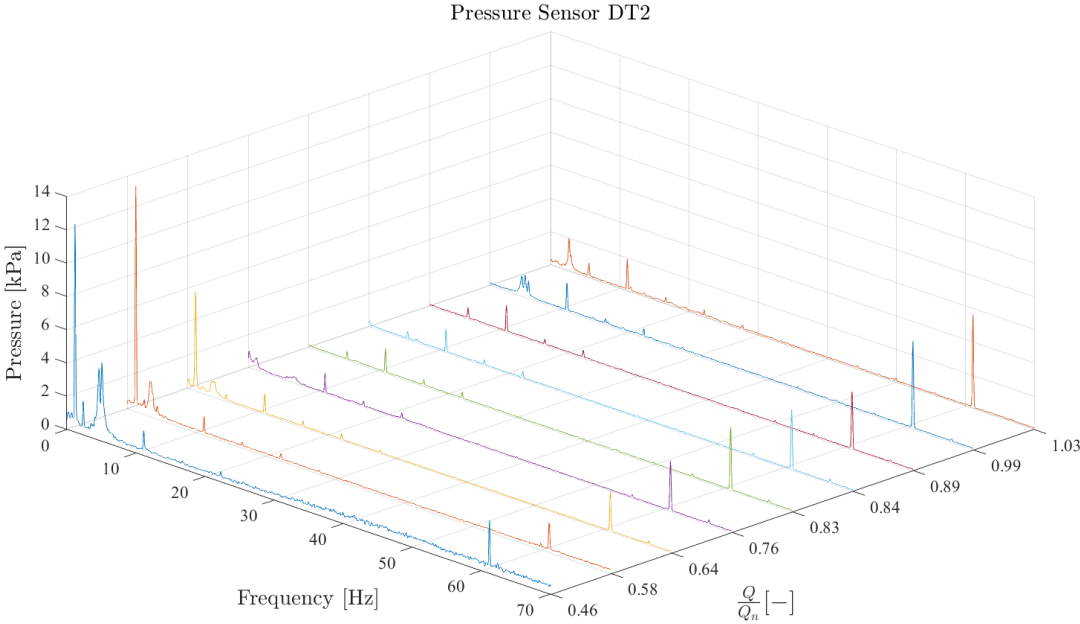


Figure 58 - Waterfall plot -Pressure sensor DT2

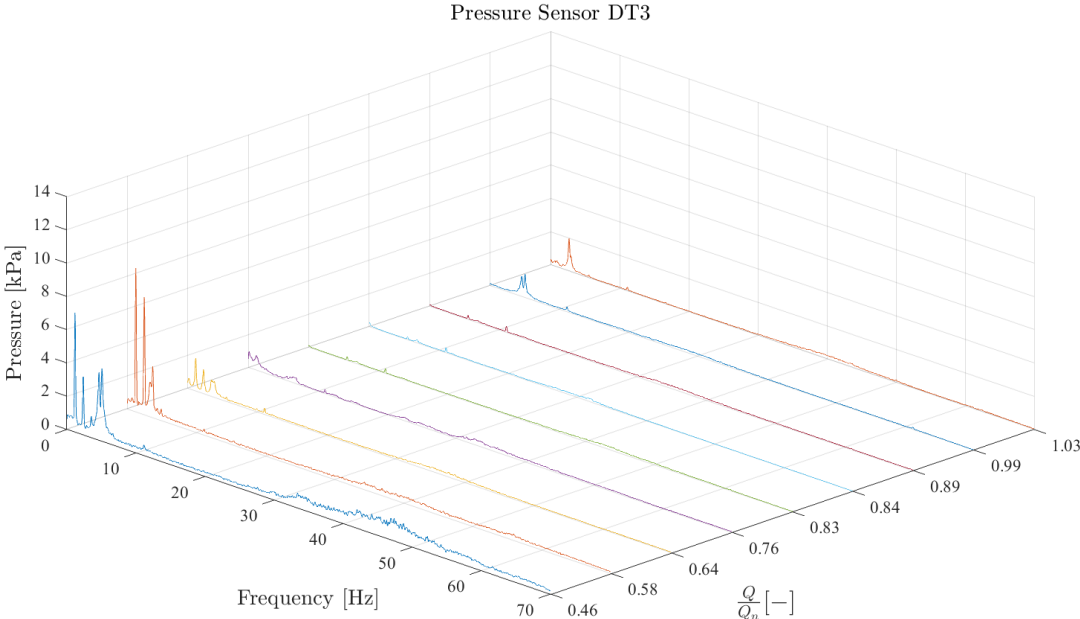


Figure 59 - Waterfall plot -Pressure sensor DT3

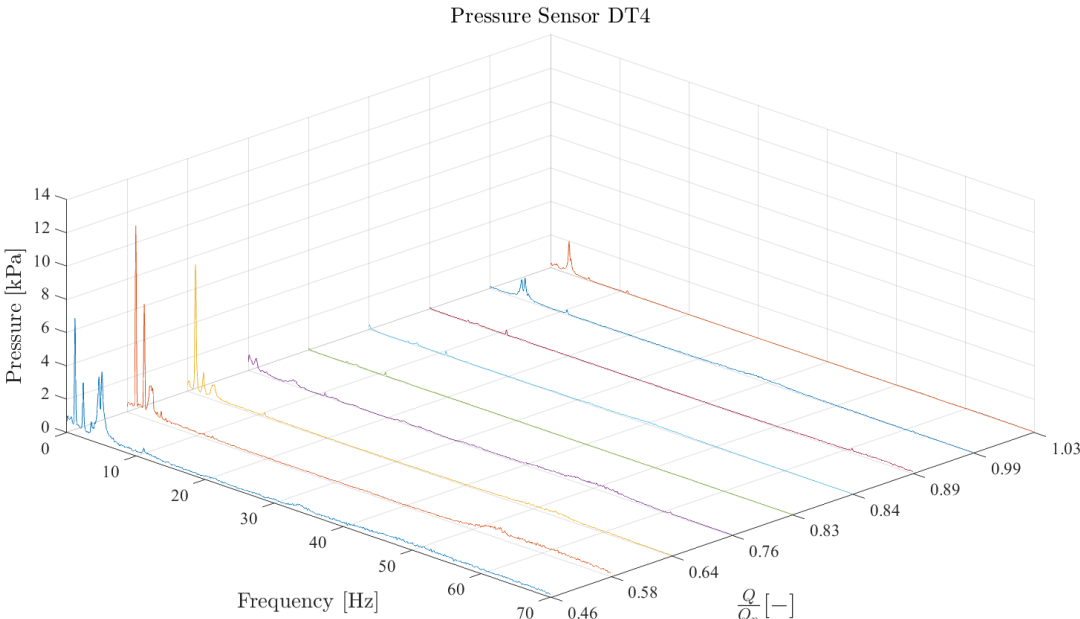


Figure 60 - Waterfall plot -Pressure sensor DT4



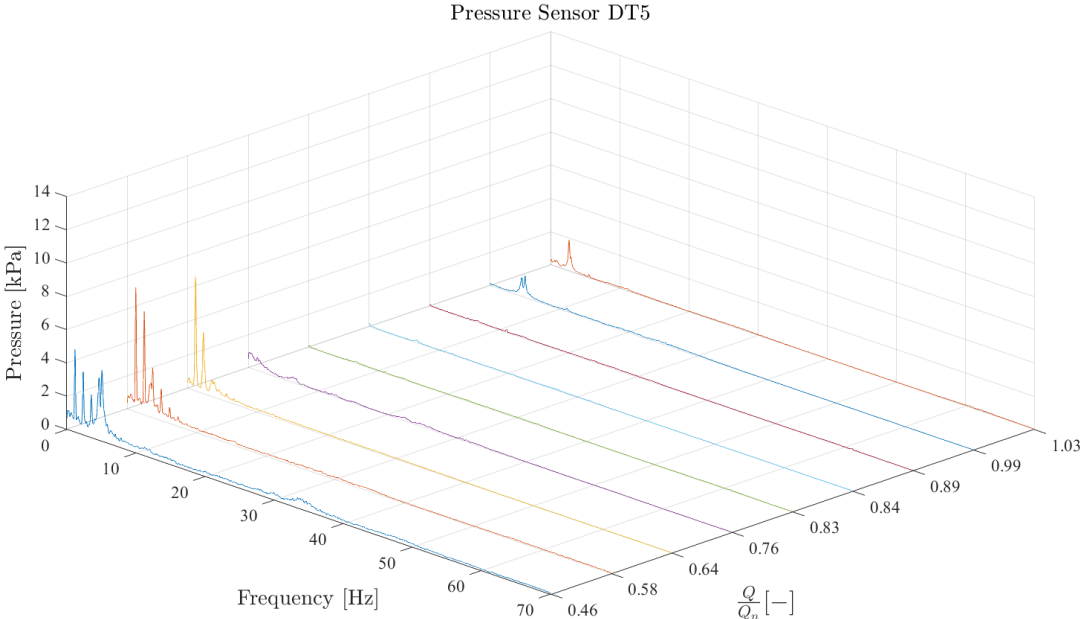


Figure 61 - Waterfall plot -Pressure sensor DT5

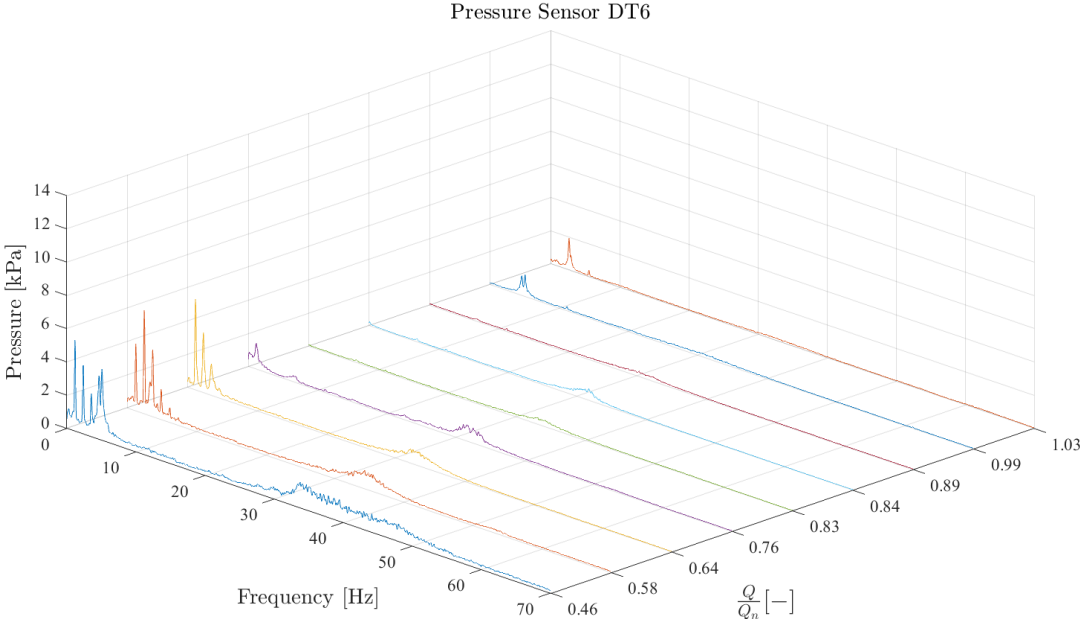


Figure 62 - Waterfall plot -Pressure sensor DT6

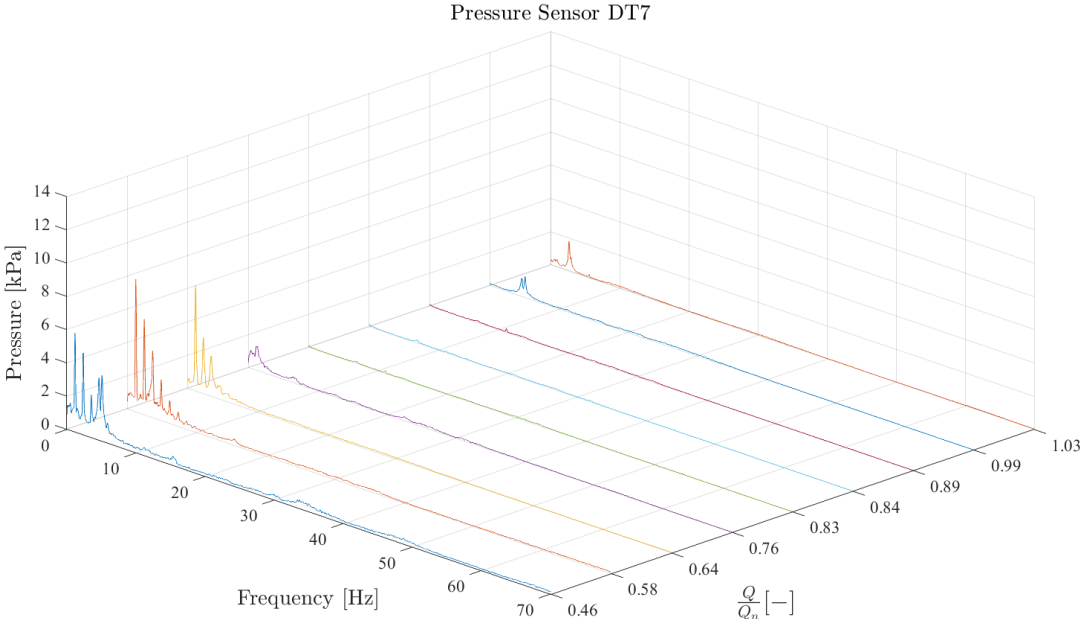


Figure 63 - Waterfall plot -Pressure sensor DT7

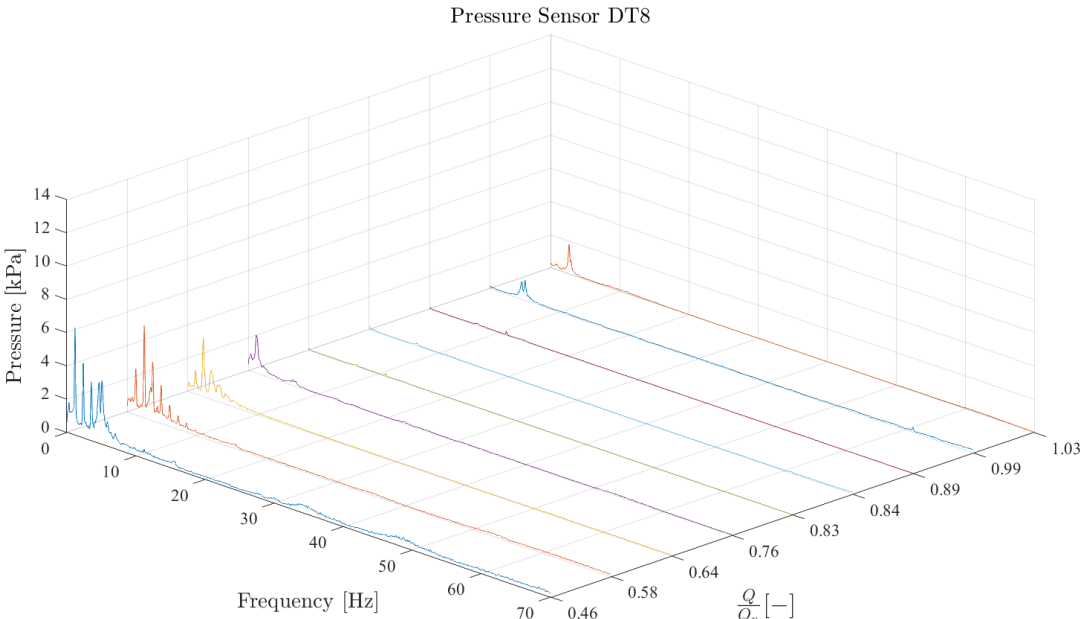


Figure 64 - Waterfall plot -Pressure sensor DT8

# Appendix G LabVIEW Program

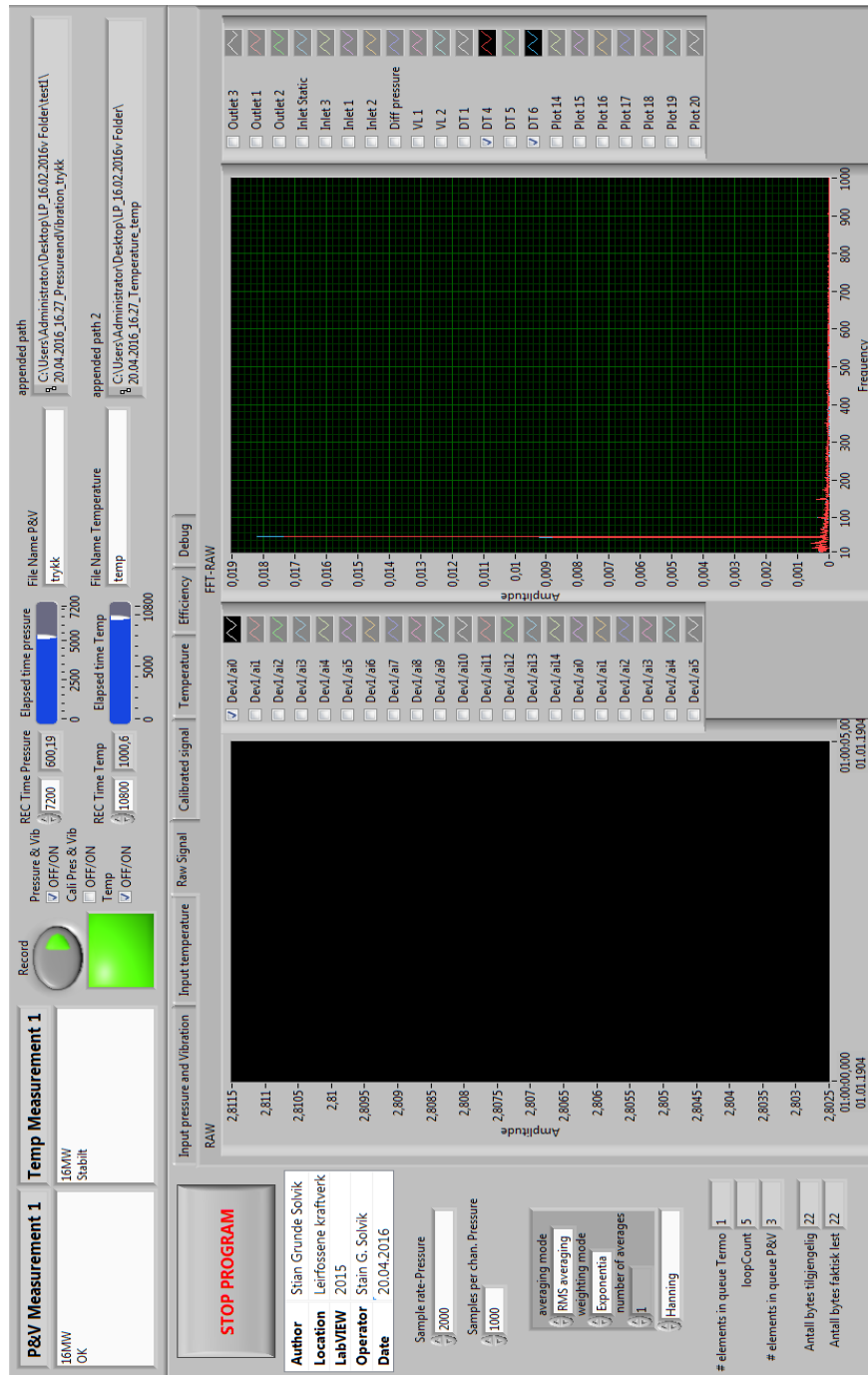


Figure 65 - LABVIEW front panel pressure

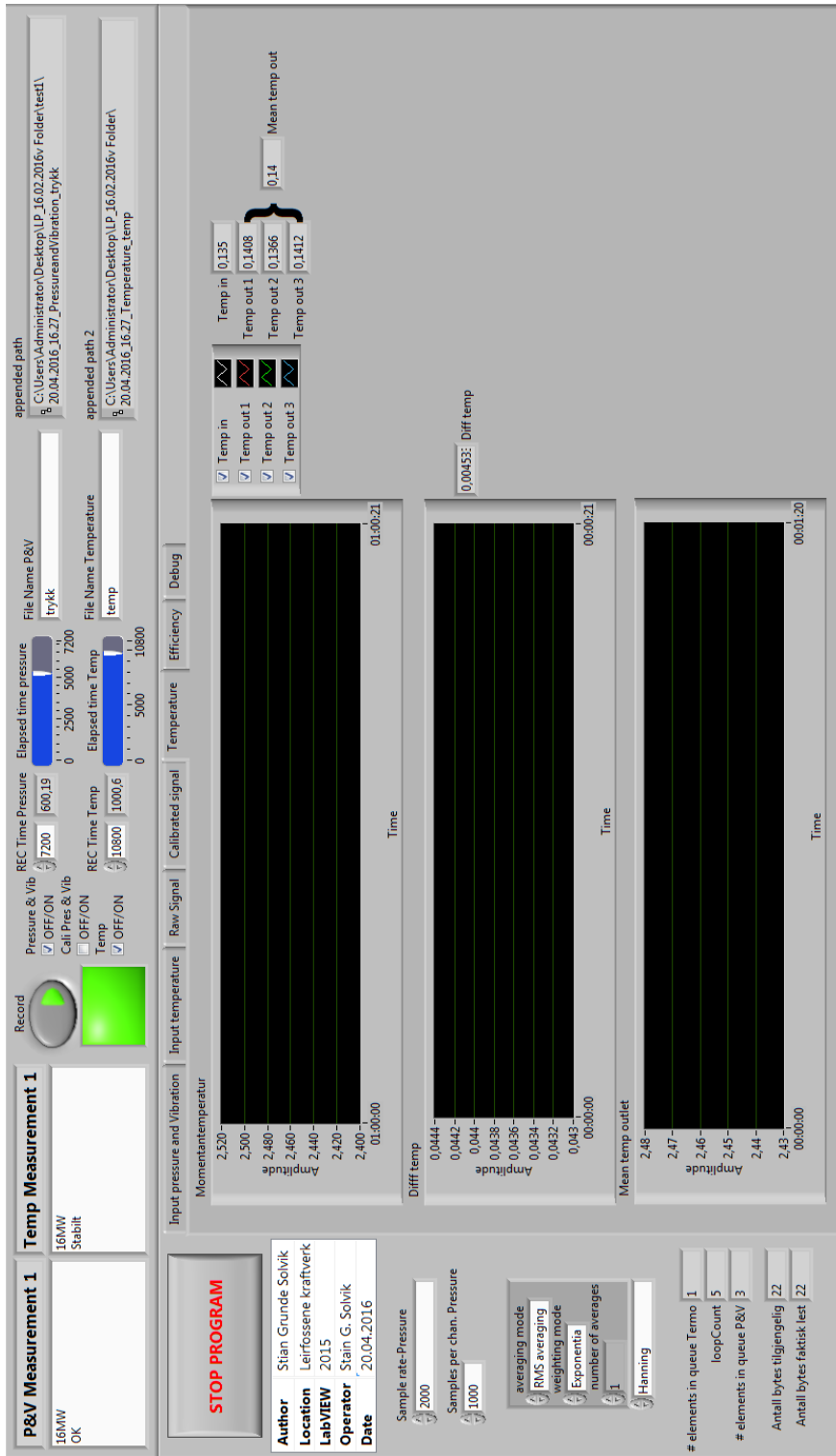


Figure 66 - LABVIEW front panel temperature

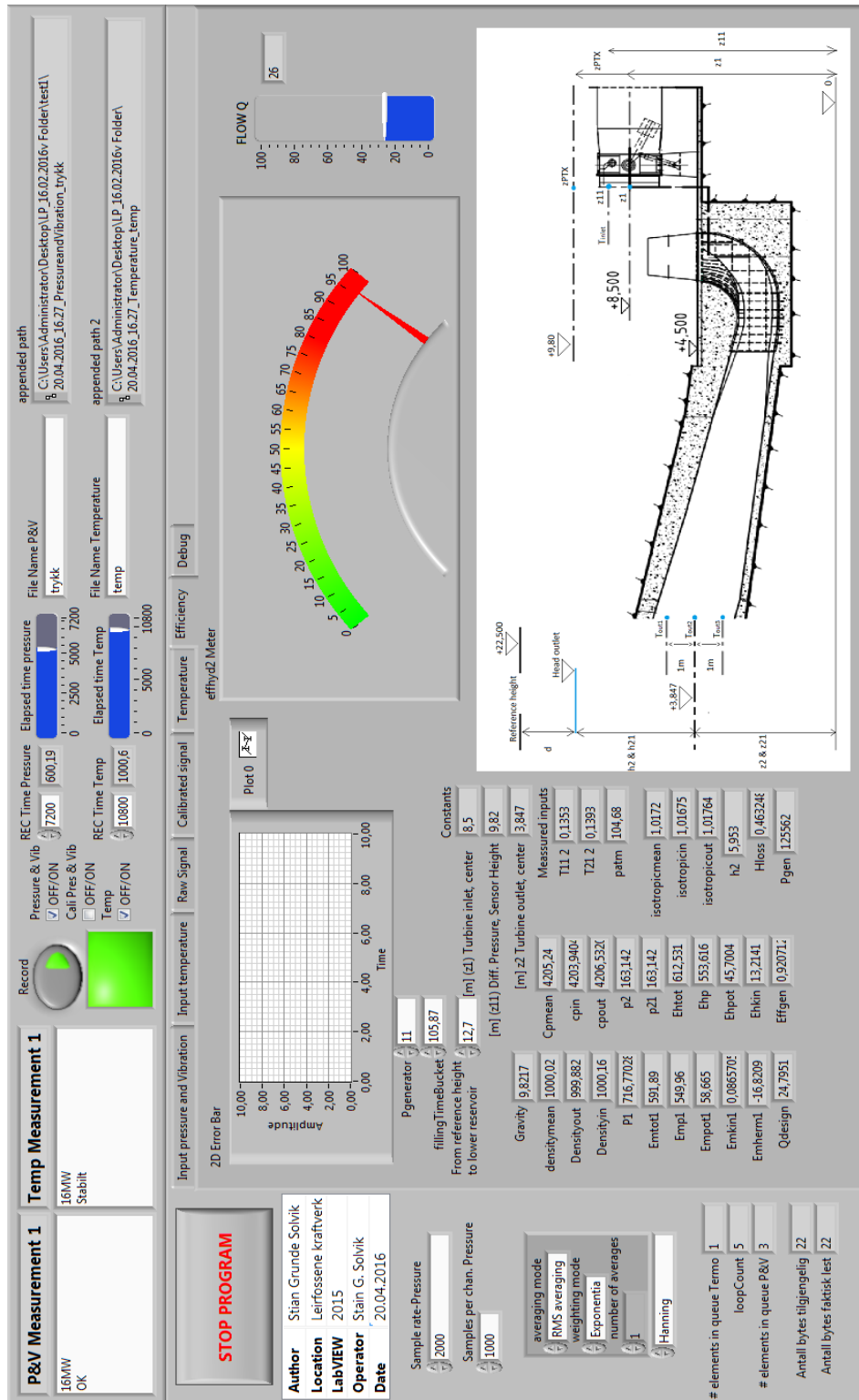


Figure 67 - LABVIEW front panel efficiency

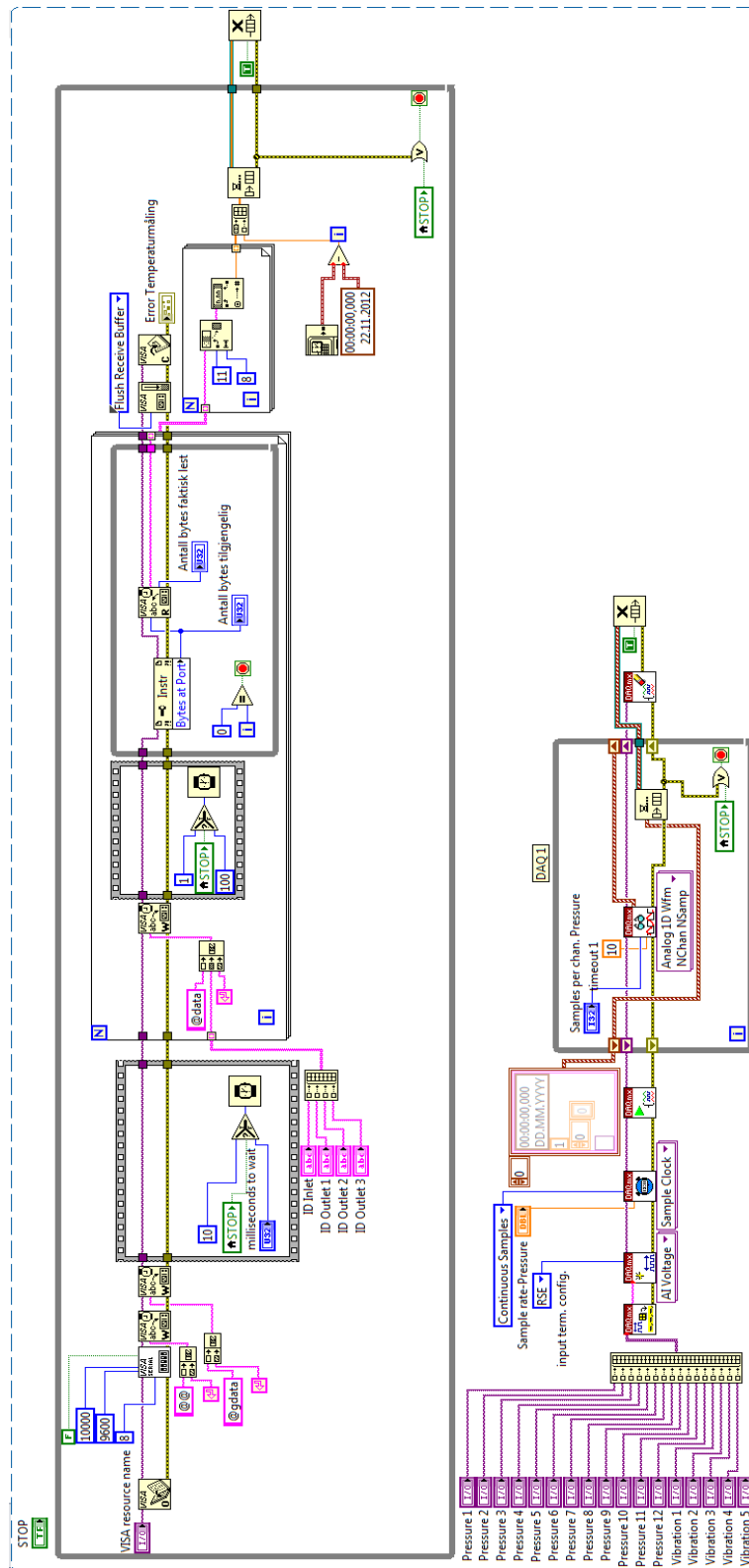


Figure 68 - LABVIEW signal input

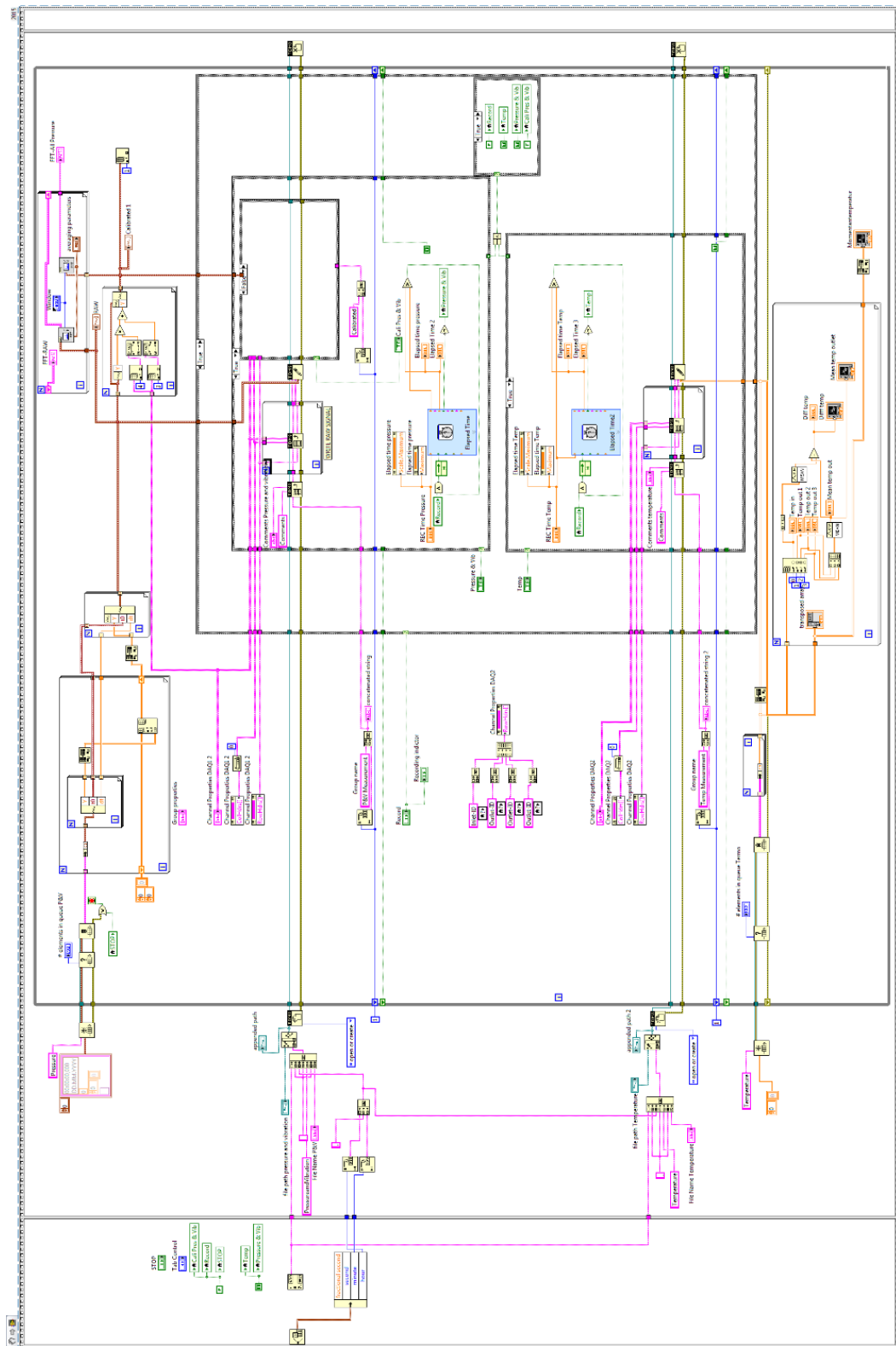


Figure 69 - LABVIEW blockdiagram - Write to TDMS -Timer

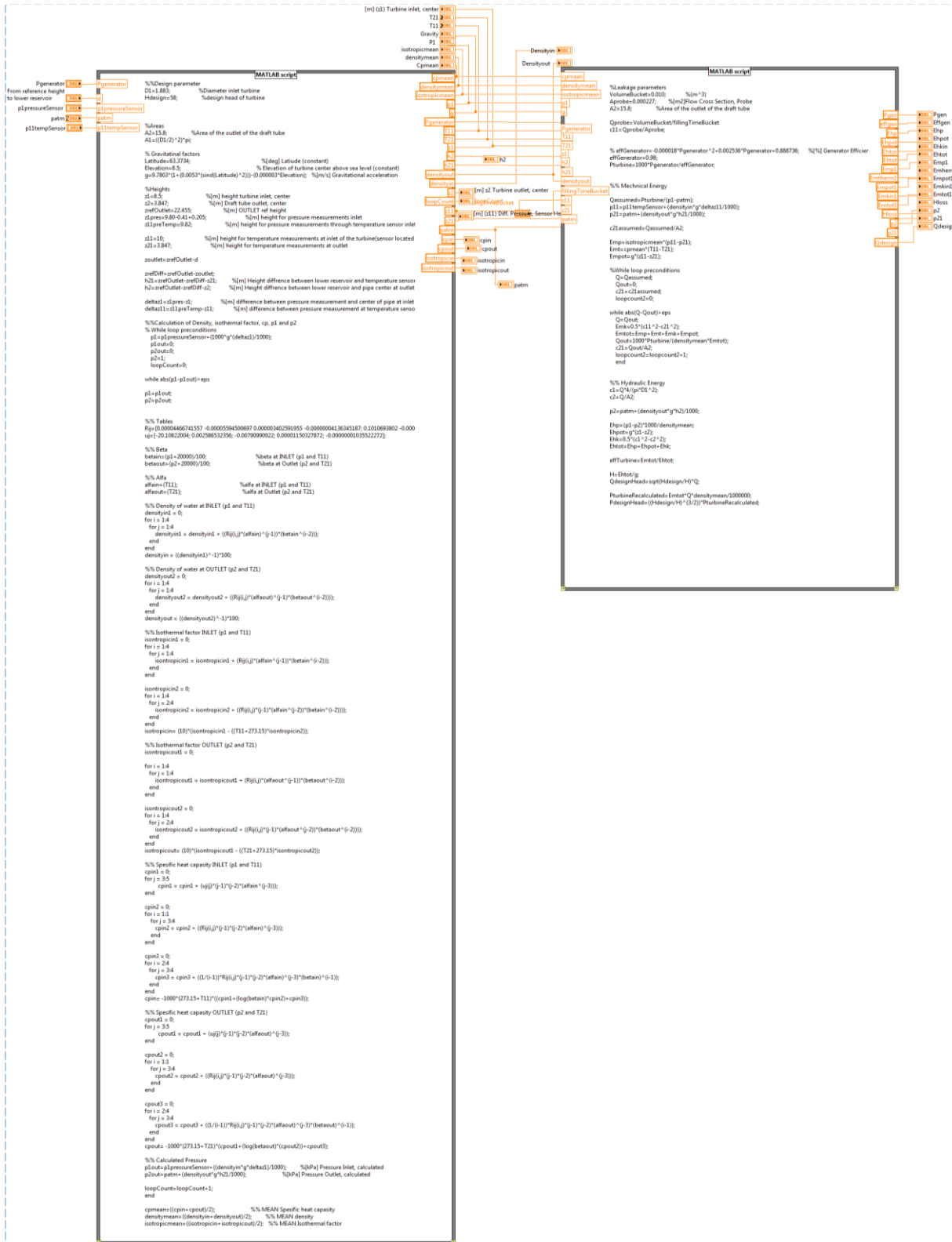


Figure 70 - LABVIEW code to calculate the efficiency

### Appendix H MATLAB script Efficiency

```

load('AllTemperatureLeirfossene.mat')
load('PressureEfficiency.mat')

```



```

tdiff=[13.36, 16.65, 15.23, 19.80, 11.54, 9.47, 12.34, 12.33, 10.11]; %time diff temp in and temp out

RowStartOut=[floor(tdiff/3.4)]; %adjusting vector size
RowStartIn=1;
LengthRowEndOut=256;
dd=max(RowStartOut);
RowEndOut(1,:)=[256+RowStartOut];
RowEndInRow=[RowEndOut-RowStartOut];
RowEndIn=min(RowEndInRow);

for j=1:9
T11(:,j)=T(j).InletT;
T11R(:,j)=[T11(RowStartIn:RowEndIn,j)];
Lt11=length (T11R);
T21Top(:,j)=T(j).OutletT1;
T21TopR(:,j)=[T21Top(RowStartOut+1:RowEndOut,j)];
T21Mid(:,j)=T(j).OutletT2;
T21MidR(:,j)=[T21Mid(RowStartOut+1:RowEndOut,j)];
T21Low(:,j)=T(j).OutletT3;
T21LowR(:,j)=[T21Low(RowStartOut+1:RowEndOut,j)];
end

TempDiff=T11R-((T21TopR+T21MidR+T21LowR)/3);
MeanT21TopR=mean(T21TopR);
MeanT21MidR=mean(T21MidR);
MeanT21LowR=mean(T21LowR);
T11=mean(T11R);
T21=(MeanT21TopR+MeanT21MidR+MeanT21LowR)/3;

D1=2.5; %Diameter inlet turbine m
Hdesign=58; %design head of turbine m
VolumeBucket=0.011; %Bucket volume m3
Aprobe=0.000227; %Flow Cross Section, Probe [m2]
A2=14.868; %Area of the outlet of the draft tube m2
A1=((D1/2)^2)*pi; %Area inlet

%Heights
z1=8.5; %[m] height turbine inlet, center
z2=3.847; %[m] Draft tube outlet, center
z1pres=9.80-0.41+0.205; %[m] height pressure measurements inlet
z11preTemp=9.80+0.192+0.0189; %[m] height pressure measurements through temperature sensor
inlet

```

```

z11=10.266;           %[m] height temperature measurements at inlet of the turbine(sensor located on floor
of turbine cover)
z21=3.847;           %[m] height temperature measurements at outlet
zrefOutlet=22.5-0.045;    %[m] OUTLET ref height

% Gravitational factors
Latitude=63.3734;      %[deg] Latitude
gin=9.7803*(1+(0.0053*(sind(Latitude)^2)))-(0.000003*z1);    %[m/s2]
gout=9.7803*(1+(0.0053*(sind(Latitude)^2)))-(0.000003*z2);    %[m/s2]
gmean=(gin+gout)/2;    %[m/s2]

%% %VARIABLES% %VARIABLES% %VARIABLES% %VARIABLES% %VARIABLES%
Operational_point =[0.76, 0.58, 0.64, 0.46, 0.89, 1.03, 0.83, 0.84, 0.99];
%Leakage parameters
fillingTimeBucket=[105.31, 105, 105, 103.25, 104.09, 104.9, 105.35, 103.58, 102.66];
Pgenerator=[12.1, 9.3, 10.3, 7.3, 14.2, 16.5, 13.3, 13.4, 15.80];    %Generator

%Pressures
p1pressureSensor=-248.82636108+124.83442086*[p(:).Inlet];
p11tempSensor=-250.33220162+124.84051990*[p(:).InletTemp];
patm=-62.80378168+31.22750987*[p(:).atm];
Meanp1=mean(p1pressureSensor);
Meanp11=mean(p11tempSensor);
Meanpatm=mean(patm);

%Heights
z3=[8.76, 8.81, 8.83, 8.94, 8.71, 8.58, 8.7, 8.73, 8.62];    %[m] height from zref to water level at
outlet
z0=[72.70, 72.76, 72.70, 72.79, 72.70, 72.63, 72.70, 72.67, 72.61]; % height upper reservoir

for k=1:numel(T11)

h21(k)=zrefOutlet-z3(k)-z21;    %[m] Height difference between lower reservoir and temperature sensor at
outlet
h2(k)=zrefOutlet-z3(k)-z2;    %[m] Height difference between lower reservoir and pipe center at outlet
deltaz1=z1pres-z1;    %[m] difference between pressure measurement and center of pipe at inlet
deltaz11=z11preTemp-z11;    %[m] difference between pressure measurement at temperature sensor and
temp sensor

%%Calculation of Density, isothermal factor, cp, p11 and p21
% While loop preconditions
p11(k)=Meanp11(k)+(1000*gin*deltaz11/1000);
p11out(k)=0;
p21out(k)=0;

```

```

p21(k)=1;
loopCount=0;

while abs(p11(k)-p11out(k))>eps

p11(k)=p11out(k);
p21(k)=p21out(k);
% Tables
Rij=[0.00004466741557 -0.00005594500697 0.000003402591955 -0.00000004136345187; 0.1010693802 -
0.00001513709263 0.000001063798744 -0.000000008146078995;-0.000005398392119 0.00000004672756685
-0.000000001194765361 -0.00000000001366322053;0.0000000007780118121 -0.00000000001619391322
0.0000000000005883547485 0.000000000000008754014287];
uj=[-20.10822004; 0.002586532356; -0.00790990922; 0.00001150327872; -0.00000001035522272];
%% Beta
betain(k)=(p11(k)+20000)/100; %beta at tempINLET (p11 and T11)
betaout(k)=(p21(k)+20000)/100; %beta at tempOutlet (p21 and T21)
%% Alfa
alfain(k)=(T11(k)); %alfa at tempINLET (p11 and T11)
alfaout(k)=(T21(k)); %alfa at tempOutlet (p21 and T21)

densityin1 = 0;
for i = 1:4
for j = 1:4
densityin1 = densityin1 + ((Rij(i,j))*(alfain(k))^(j-1))*(betain(k)^(i-2)));
end
end
densityin(k) = ((densityin1)^-1)*100; % Density of water at INLET

densityout2 = 0;
for i = 1:4
for j = 1:4
densityout2 = densityout2 + ((Rij(i,j))*(alfaout(k))^(j-1))*(betaout(k)^(i-2)));
end
end
densityout(k) = ((densityout2)^-1)*100; % Density of water at OUTLET

%% Isothermal factor INLET (p1 and T11)
isothermalin1 = 0;
for i = 1:4
for j = 1:4
isothermalin1 = isothermalin1 + (Rij(i,j))*(alfain(k))^(j-1))*(betain(k)^(i-2)));
end
end

```

```

isothermalin2 = 0;
for i = 1:4
    for j = 2:4
isothermalin2 = isothermalin2 + ((Rij(i,j)*(j-1)*(alfain(k)^(j-2))*(betain(k)^(i-2))));
    end
end
isothermalin(k)= (10)*(isothermalin1 - ((T11(k)+273.15)*isothermalin2));

%% Isothermal factor OUTLET (p2 and T21)
isothermalout1 = 0;
for i = 1:4
    for j = 1:4
isothermalout1 = isothermalout1 + (Rij(i,j)*(alfaout(k)^(j-1))*(betaout(k)^(i-2))));
    end
end
isothermalout2 = 0;
for i = 1:4
    for j = 2:4
isothermalout2 = isothermalout2 + ((Rij(i,j)*(j-1)*(alfaout(k)^(j-2))*(betaout(k)^(i-2))));
    end
end
isothermalout(k)= (10)*(isothermalout1 - ((T21(k)+273.15)*isothermalout2));

%% Specific heat capacity INLET (p1 and T11)
cpin1 = 0;
for j = 3:5
    cpin1 = cpin1 + (uj(j)*(j-1)*(j-2)*(alfain(k)^(j-3)));
end
cpin2 = 0;
for i = 1:1
    for j = 3:4
        cpin2 = cpin2 + ((Rij(i,j)*(j-1)*(j-2)*(alfain(k)^(j-3))));
    end
end
cpin3 = 0;
for i = 2:4
    for j = 3:4
cpin3 = cpin3 + ((1/(i-1))*Rij(i,j)*(j-1)*(j-2)*(alfain(k)^(j-3))*(betain(k)^(i-1)));
    end
end
cpin(k)= -1000*(273.15+T11(k))*((cpin1+(log(betain(k))*cpin2)+cpin3));

%% Specific heat capacity OUTLET (p2 and T21)

```

```
cpout1 = 0;
for j = 3:5
    cpout1 = cpout1 + (uj(j))*(j-1)*(j-2)*(alfaout(k))^(j-3));
end
cpout2 = 0;
for i = 1:1
    for j = 3:4
        cpout2 = cpout2 + ((Rij(i,j))*(j-1)*(j-2)*(alfaout(k))^(j-3)));
    end
end
cpout3 = 0;
for i = 2:4
    for j = 3:4
        cpout3 = cpout3 + ((1/(i-1))*Rij(i,j))*(j-1)*(j-2)*(alfaout(k))^(j-3)*(betaout(k))^(i-1));
    end
end
cpout(k) = -1000*(273.15+T21(k))*(cpout1+(log(betaout(k))*(cpout2))+cpout3);
```

```

%% Calculated Pressure
p11out(k)=Meanp11(k)+((densityin(k)*gin*deltaz11)/1000); %[kPa]p Inlet
p21out(k)=Meanpatm(k)+(densityout(k)*gout*h21(k)/1000); %[kPa]p Outlet
loopCount=loopCount+1;
end
%mean values
cpmean(k)=(cpin(k)+cpout(k))/2; % MEAN cp
densitymean(k)=(densityin(k)+densityout(k))/2; % MEAN density
isothermalmean(k)=(isothermalin(k)+isothermalout(k))/2 % MEAN Isothermal factor

Qprobe(k)=VolumeBucket/fillingTimeBucket(k); % Flow probe
c11(k)=Qprobe(k)/Aprobe; % Probe
effGenerator=0.985;
Pturbine(k)=1000*Pgenerator(k)/effGenerator; % Turbine power
p1(k)=Meanp1(k)+(densityin(k)*gin*deltaz1/1000);
Qassumed(k)=Pturbine(k)/(p1(k)-Meanpatm(k)); % Flow assumed
c21assumed(k)=Qassumed(k)/A2;

%% Mechanical Energy
Emp(k)=isothermalmean(k)*(p11(k)-p21(k)); %Pressure Mechanical Energy
Emt(k)=cpmean(k)*(T11(k)-T21(k)); %Thermal Mechanical Energy
Empot(k)=gmean*(z11-z21); %Potential Mechanical Energy

%While loop preconditions
Q(k)=Qassumed(k);
Qout(k)=0;
c21(k)=c21assumed(k);
loopcount2=0;

while abs(Q(k)-Qout(k))>eps
    Q(k)=Qout(k); %Flow recalculated
    c21(k)=Qout(k)/A2; %Velocity recalculated
    Emk(k)=0.5*(c11(k)^2-c21(k)^2); %Kinematic mechanical energy
    Emtot(k)=Emp(k)+Emt(k)+Emk(k)+Empot(k); %Total mechanical energy
    Qout(k)=1000*Pturbine(k)/(densitymean(k)*Emtot(k)); %New Flow
    loopcount2=loopcount2+1;
end

c1(k)=Q(k)/A1; %Velocity inlet
c2(k)=Q(k)/A2; %Velocity outlet
c3(k)=Q(k)/(4.5*3.5); %Velocity lower reservoir
p2(k)=Meanpatm(k)+(densityout(k)*gout*h2(k))/1000-(densityout(k)*(c2(k).^2-c3(k).^2)/2)/1000;

```

```

%% Hydraulic Energy
Ehp(k)=(p1(k)-p2(k))*1000/densitymean(k);           %Pressure Hydraulic energy
Ehpot(k)=gmean*(z1-z2);                            %potential Hydraulic energy
Ehk(k)=0.5*(c1(k)^2-c2(k)^2);                      %Kinematic Hydraulic energy
Ehtot(k)=Ehp(k)+Ehpot(k)+Ehk(k);                  %total Hydraulic energy

effTurbine(k)=Emtot(k)/Ehtot(k);                   % Turbine Efficiency
H(k)=Ehtot(k)/gmean;                               % Head
Qnom(k)=sqrt(Hdesign/H(k))*Q(k);                   % Nominal flow
PTnom(k)=Pturbine(k)*((Hdesign/H(k))^(3/2));        % Nominal Turbine Power

%% Head Loss
Hloss(k)=(((Meanpatm(k)-p1(k))*1000)/(gin*densityin(k)))-((c1(k)^2)/(2*gin))+z0(k)-z1;

%% Systematic Uncertainty terms
fp11measurment=0.00045576;
fdensity=0.001;
ez=0.02;
ezrefoutlet=0.03;
epatm=0.005297;
ez3=0.05;
ep11(k)=sqrt((fp11measurment)^2+fdensity^2+((ez^2+ez^2)/deltaz11)^2)*p11(k);
ep21(k)=p21(k)*(sqrt((epatm/Meanpatm(k)).^2+fdensity^2+((ez^2+ezrefoutlet^2+ez3^2)/h21(k)).^2));

eVbucket=1*10^-6;
etprobe=0.1;
eAprobe=5.6785*10^-8;
ec11(k)=c11(k)*sqrt((eVbucket/VolumeBucket)^2+(etprobe/fillingTimeBucket(k)).^2+(eAprobe/Aprobe)^2);

fp1measurment=0.00042519;
ez1pres=0.03;
ep1(k)=(sqrt((fp1measurment)^2+fdensity^2+((ez1pres^2+ez^2)/deltaz1)^2))*p1(k);
ePturbine(k)=(sqrt(0.0071^2+0.005^2))*Pturbine(k);
eQassumed(k)=Qassumed(k)*sqrt((ePturbine(k)/Pturbine(k)).^2+((sqrt(ep1(k).^2+epatm)/(p1(k)-patm(k))).^2));
ec21(k)=c21(k)*sqrt((eQassumed(k)/Qassumed(k)).^2+(ez/4.5)^2+(ez/3.304)^2);

fEin=0.002;
fEout=0.006;
ecpmean=sqrt(2*0.005^2);
eT=0.001;
edensitymean(k)=sqrt((fdensity*densityin(k)).^2+(fdensity*densityout(k)).^2);
ec2(k)=ec21(k);
ec3(k)=c3(k)*(sqrt((eQassumed(k)/Qassumed(k)).^2+(ez/4.5)^2+(ez/3.5)^2));

```

```
ep2(k)=p2(k)*(sqrt((epatm/Meanpatm(k)).^2+fdensity^2+((ez^2+ez^2+ez3^2)/h2(k)).^2+(((ec2(k).^2)+(ec3(k).^2))/(c2(k)-c3(k)).^2)));
```

```
eQ(k)=eQassumed(k);
```

```
ec1(k)=c1(k)*sqrt((eQ(k)/Q(k)).^2+(2*0.01/1.25)^2);
```

```
%% Random Uncerainty terms%%
```

```
ep1r(k)=sqrt((sum((mean(p1pressureSensor(:,k))-p1pressureSensor(:,k)).^2)/(1800000-1))*(1.96/sqrt(1800000))/densityin(k);
```

```
ep11r(k)=sqrt((sum((mean(p11tempSensor(:,k))-p11tempSensor(:,k)).^2)/(1800000-1))*(1.96/sqrt(1800000))/densityin(k);
```

```
epatmr(k)=sqrt((sum((mean(patm(:,k))-patm(:,k)).^2)/(1800000-1))*(1.96/sqrt((1800000-1)))/densityin(k);
```

```
eTr(k)=sqrt((sum((mean(TempDiff(:,k))-TempDiff(:,k)).^2)/(256-1))*(1.96/sqrt(256))*cpmean(k);
```

```
ePturbiner(k)=0.001*(Pturbine(k)/(densitymean(k)*Q(k)));
```

```
eQr(k)=sqrt(ePturbiner(k).^2+ep11r(k).^2+epatmr(k).^2);
```

```
ec11r(k)=eQr(k);
```

```
ec21r(k)=eQr(k);
```

```
ec1r(k)=ec21r(k);
```

```
ec2r(k)=ec21r(k);
```

```
end
```

```
%%Systematic Uncertainty%%
```

```
for k=1:9
```

```
eEmps(k)=Emp(k)*(sqrt((sqrt(2*0.002^2)^2)+((sqrt(ep11(k).^2+ep21(k).^2))/(p11(k)-p21(k))).^2)));
```

```
eEmks(k)=Emk(k)*(sqrt((2*ec11(k)/c11(k)).^2+(2*ec21(k)/c21(k)).^2)));
```

```
eEmpots(k)=sqrt(ez^2+ez^2);
```

```
eEmts(k)=Emt(k)*sqrt((ecpmean/cpmean(k)).^2+(fEin)^2+(fEout)^2+(sqrt(eT^2+eT^2)/(T11(k)-T21(k)))^2);
```

```
eEms(k)=sqrt(eEmps(k).^2+eEmpots(k).^2+eEmks(k).^2+eEmts(k).^2);
```

```
fEms(k)=100*eEms(k)/Emtot(k); % in [%]
```

```
eEhps(k)=Ehp(k)*(sqrt((edensitymean(k)/(densitymean(k))).^2+(sqrt(ep1(k).^2+ep2(k).^2)/(p1(k)-p2(k))).^2)));
```

```
eEhpots(k)=sqrt(ez^2+ez^2);
```

```
eEhks(k)=Ehk(k)*(sqrt((2*ec1(k)/c1(k)).^2+(2*ec2(k)/c2(k)).^2)));
```

```
eEhs(k)=sqrt(eEhps(k).^2+eEhpots(k).^2+eEhks(k).^2);
```

```
fEhs(k)=100*eEhs(k)/Ehtot(k); % in [%]
```

```
fS(k)=sqrt(fEms(k).^2+fEhs(k).^2); % Total systematic Uncertainty in [%]
```

```
fQ(k)=100*sqrt((eQr(k)).^2+(eQ(k)).^2)/Q(k); % Uncertainty in flow [J/kg]
```

```
fPturbine(k)=100*sqrt((ePturbiner(k)).^2+(ePturbine(k)).^2)/Pturbine(k); % in [J/kg]
```

```
eHloss(k)=sqrt((epatm/Meanpatm(k)).^2+(ep1(k)/p1(k)).^2+(ec1(k)/c1(k)).^2+((ez^2+ez^2)/(z0(k)-z1)).^2);
```

```
fHloss(k)=100*eHloss(k)/Hloss(k); % in [J/kg]
```

```
end
```



```

%%Random Uncertainty%%
for k=1:9
eEmpr(k)=sqrt(ep11r(k).^2+epatmr(k).^2);           % in [J/kg]
eEhkr(k)=sqrt(ec11r(k).^2+ec21r(k).^2);           % in [J/kg]
eEmr(k)=sqrt(eEmpr(k).^2+eEhkr(k).^2);           % in [J/kg]
eEmr(k)=eTr(k);                                   % in [J/kg]

eEhpr(k)=sqrt(ep1r(k).^2+epatmr(k).^2);           % in [J/kg]
eEhkr(k)=sqrt(ec1r(k).^2+ec2r(k).^2);           % in [J/kg]
eEhr(k)=sqrt(eEhpr(k).^2+eEhkr(k).^2);           % in [J/kg]

fEmr(k)=100*eEmr(k)/Emtot(k);                     % in [%]
fEhr(k)=100*eEhr(k)/Ehtot(k);                     % in [%]

fR(k)=sqrt(fEmr(k).^2+fEhr(k).^2);                %Total Random Uncertainty in [%]
fTotalEm(k)=sqrt(fEmr(k).^2+fEms(k).^2);          % in [%]
fTotalEh(k)=sqrt(fEhr(k).^2+fEhs(k).^2);          % in [%]
fTotal(k)=sqrt(fR(k).^2+fS(k).^2);                 % Total Uncertainty in [%]
end

```

```
%% Rearranging the values in order to create figures
```

```
[TempQnom I]= sort(Operational_point);
for i=1:length(effTurbine);
    TempEff(i)=effTurbine(I(i));
    TempError(i)=fTotal(I(i)); % in [%]
    TempfS(i)=fS(I(i));
    TempfR(i)=fR(I(i));
    TempPnom(i)=PTnom(I(i))/1000;
    error(i)=TempError(i)*TempEff(i)/100; % in [-] eff
    errx(i)=error(i)*10;
    erry(i)=error(i);
end
```

```
[TempQnom K]= sort(Qnom);
for i=1:length(Hloss);
    TempHloss(i)=Hloss(K(i));
    TempEmtot(i)=Emtot(K(i));
    TempEhtot(i)=Ehtot(K(i));
    TempfHloss(i)=fHloss(K(i));
    TempFTotalEm(i)=fTotalEm(K(i));
    TempfTotalEh(i)=fTotalEh(K(i));
    Tempfpturbine(i)=fPtrubine(K(i));
    TempfQ(i)=fQ(K(i));

    errorHloss(i)= TempfHloss(i)*TempHloss(i)/100;
    errorHlossy(i)=errorHloss(i);
    errorEm(i)=TempEmtot(i)*TempFTotalEm(i)/100;
    errorEmy(i)=errorEm(i);
    errorEh(i)=TempEhtot(i)*TempfTotalEh(i)/100;
    errorEhy(i)=errorEh(i);
    errorQ(i)=(TempfQ(i)/100)*Q(k);
    errorPturbine(i)=(Tempfpturbine(i)/100)*Ptrubine(K(i))/1000;
end
```

```
%% Efficiency Curve
```

```
pp=polyfit(TempPnom,TempEff/max(TempEff),3);
x1 = linspace(min(TempPnom),max(TempPnom));
y1 = polyval(pp,x1);
dfig ('Efficiency_1')
plot(TempPnom, TempEff/max(TempEff),'o')
hold on
```

```
%% Efficiency Curve
```

```

Author=plot(x1,y1, 'r');
hold on
for i=1:9
errorbarxy(TempPnom(i),TempEff(i)/max(TempEff),errorPturbine(i),erry(i),{'ro-', 'r', 'r'})
hold on
end
hold on

%% Efficiency Curve NORCONSULT           %% Efficiency Curve NORCONSULT
NorOP=[information subtracted due to confidentiality]
NorEff=[information subtracted due to confidentiality];

ppNOR=polyfit(NorOP,NorEff/max(TempEff),3);
x1NOR = linspace(min(NorOP),max(NorOP));
y1NOR = polyval(ppNOR,x1NOR);
dfig ('Efficiency_1')
plot(NorOP, NorEff/max(TempEff),'k*')
hold on
NORC=plot(x1NOR,y1NOR,'k');
hold on
errxNor=0.15;
erryNor=0.015;
for i=1:5
errorbarxy(NorOP(i),NorEff(i)/max(TempEff),errxNor,erryNor,{'k-', 'k', 'k'})
hold on
end
hold on

```

```

title(['Efficiency curve - Leirfossene - Turbine 2'],'FontSize',22,'FontWeight','bold','Interpreter','Latex')
xlim([6 18])
ylim([0.86 1.02])
xlabel(['Turbine Power at Rated Head - ','${P_{Tn}} }$'],'FontSize',23,'FontWeight','bold','Interpreter','Latex')
ylabel(['Relative Efficiency [-]'],'FontSize',22,'FontWeight','bold','Interpreter','Latex')
grid on
a = get(gca,'XTickLabel');
set(gca,'XTickLabel',a,'FontName','Times','fontSize',18);
legend([Author,NORC],'NTNU (2016)','Norconsult (2009)','Location','northeast')

set(gcf,'PaperPositionMode','auto');
print('Efficiency Curve Leirfossene gibson','-dpng','-r400');

%% Head Loss Qnom % Head Loss Qnom
p=polyfit(TempQnom,TempHloss,3);
x1 = linspace(min(TempQnom),max(TempQnom));
y1 = polyval(p,x1);

dfig ('Hloss')
plot(TempQnom, TempHloss, 'o')
hold on
plot(x1,y1,'r')
hold on
for i=1:9
errorbarxy(TempQnom(i),TempHloss(i),errorQ(i),errorHlossy(i),{'ko-', 'k', 'k'})
end
hold on

title(['Head loss curve Leirfossene - Turbine 2'],'FontSize',24,'FontWeight','bold','Interpreter','Latex')
xlim([14 34])
ylim([0.5 1.4])
xlabel(['Flow at Rated Head - ','${Q_n}\frac{m^3}{s}$'],'FontSize',23,'FontWeight','bold','Interpreter','Latex')
ylabel(['Head loss [mWc]'],'FontSize',22,'Interpreter','Latex')
a = get(gca,'XTickLabel');
set(gca,'XTickLabel',a,'FontName','Times','fontSize',18);
grid on
set(gcf,'PaperPositionMode','auto');
print('Head Loss Leirfossene1','-dpng','-r400');

```

```

%% Total Uncertainty
p=polyfit(TempPnom,TempError,3);
x1 = linspace(min(TempPnom),max(TempPnom));
y1 = polyval(p,x1);
dfig('Total Uncertainty')
plot(TempPnom, TempError, 'o')
hold on
plot(x1,y1)
hold on
title(['Total Uncertainty - Thermodynamic method'],'FontSize',24,'FontWeight','bold','Interpreter','Latex')
xlim([6 18])
ylim([1.22 1.4])

for i=1:9
errorbarxy(TempPnom(i),TempError(i),errorPturbine(i),0,{'ko', 'k', 'k'})
end
hold on
xlabel(['Turbine Power at Rated Head - ', '$P_{Tn}$'],
'FontSize',23,'FontWeight','bold','Interpreter','Latex')
ylabel(['Uncertainty [%]'],'FontSize',22,'Interpreter','Latex')
grid on
a = get(gca, 'XTickLabel');
set(gca, 'XTickLabel', a, 'FontName', 'Times', 'fontSize', 18);
% set(gcf, 'PaperPositionMode', 'auto');
% print('Total Uncertainty', '-dpng', '-r600');

```

## Appendix I MATLAB script for 3D plots

```

load('DTPressure_2000SRate_UtenLuft.mat')

Fs=2000; %Sample rate
ov=0.5; %Window overlapFactor
conf_l=0.95; %confidence level
na = 12; %na=number of windows

f_min=0; %frequency values x-axis
f_max=100; % frequency values x-axis

%Select sensor
disp('1: DT1 ')
disp('2: DT2 ')
disp('3: DT3 ')
disp('4: DT4 ')
disp('5: DT5 ')
disp('6: DT6 ')
disp('7: DT7 ')
disp('8: DT8 ')

prompt = 'Chose sensor, Please ';
inputN = input(prompt,'s');
inputN = str2num(inputN);

if isempty(inputN)
    kk=1:8;
else
    kk=inputN;
end

for inputN=kk;

    switch inputN
        case 1
            sensorInput='DT1';
            NameX=fieldnames(P);
            FignameT=NameX(inputN);
            Figname=FignameT{1};
            FigTitle = 'Draft Tube Pressure 1'; %DT1
            a=61.30880908; %calibration const.
            b=-121.61051306; %calibration const.
        case 2

```

```
sensorInput='DT2';
NameX=fieldnames(P);
FignameT=NameX(inputN);
Figname=FignameT{1};
FigTitle = 'Draft Tube Pressure 2';           %DT2
a=61.17379911;                               %calibration const.
b=-121.42918313;                             %calibration const.
case 3
sensorInput='DT3';
NameX=fieldnames(P);
FignameT=NameX(inputN);
Figname=FignameT{1};
FigTitle = 'Draft Tube Pressure 3';           %DT3
a=61.21574205;                               %calibration const.
b=-122.53410606;                             %calibration const.
case 4
sensorInput='DT4';
NameX=fieldnames(P);
FignameT=NameX(inputN);
Figname=FignameT{1};
FigTitle = 'Draft Tube Pressure 4';           %DT4
a=61.25759912;                               %calibration const.
b=-123.19199928;                             %calibration const.
case 5
sensorInput='DT5';
NameX=fieldnames(P);
FignameT=NameX(inputN);
Figname=FignameT{1};
FigTitle = 'Draft Tube Pressure 5';           %DT5
a=61.27267521;                               %calibration const.
b=-121.91624464;                             %calibration const.
```

```

case 6
    sensorInput='DT6';
    NameX=fieldnames(P);
    FignameT=NameX(inputN);
    Figname=FignameT{1};
    FigTitle = 'Draft Tube Pressure 6';           %DT6
    a=61.20854518;                               %calibration const.
    b=-122.27875129;                             %calibration const.
case 7
    sensorInput='DT7';
    NameX=fieldnames(P);
    FignameT=NameX(inputN);
    Figname=FignameT{1};
    FigTitle = 'Draft Tube Pressure 7';           %DT7
    a=61.23005606;                               %calibration const.
    b=-121.82442935;                             %calibration const.
case 8
    sensorInput='DT8';
    NameX=fieldnames(P);
    FignameT=NameX(inputN);
    Figname=FignameT{1};
    FigTitle = 'Draft Tube Pressure 8';           %DT8
    a=61.11306315;                               %calibration const.
    b=-121.75310005;                             %calibration const.
end

for i = 1:numel(P)
    x(:,i) = P(i).(sensorInput)*a+b;
end

Operational_point =[0.6438, 0.7563, 0.575, 0.8875, 0.4625, 0.83125, 1.0313, 0.8375, 0.9875];
[TempOperational I]= sort(Operational_point);    %Sort elements
for k=1:length(Operational_point);
    Tempx(:,k)=[x(:,I(k))];
    t = (1:length(Tempx(:,k)))';
    opol = 7;
    [p,s,mu] = polyfit(t,Tempx(:,k),opol);
    f_y(:,k)= polyval(p,t,[],mu);
    dt_x(:,k) = Tempx(:,k) - f_y(:,k);
end

```



```

[n m] = size(dt_x);
z = 1:n;
for j=1:m
nx = max(size(dt_x(:,j)));
w = hanning(floor(nx/na)); %window function and size
num_win=na/(1-ov);
[PSD(:,j),f1,PSDc]=pwelch(dt_x(:,j),w,floor(ov*(nx/na)),[],Fs,'ConfidenceLevel',conf_); %PSD=Power
Spectral density V^2/Hz

fbin=f1(2)-f1(1); %frequency resolution
S1=sum(w);
S2=sum(w.^2);
ENBW=Fs*(S2/(S1^2)); %E active Noise andWidth,
PS1=PSDc(:,1)*ENBW; %PS Confidence level
PS2=PSDc(:,2)*ENBW; %PS Confidence level
PS(:,j)=PSD(:,j)*ENBW; %Power spectrum

RMS1=sqrt(PS1); %RMS Confidence level
RMS2=sqrt(PS2); %RMS Confidence level
RMS(:,j)=sqrt(PS(:,j)); %RMS

Peak1=sqrt(PS1)*sqrt(2);
Peak2=sqrt(PS2)*sqrt(2);
Peak(:,j)=sqrt(PS(:,j))*sqrt(2); %Peak amplitude
LL=length(Peak(:,j));
i1 = ones(LL,1);
i1 = i1(1:LL);

dfig('046') %Plot figure
plot(f1,Peak(:,1))
xlim([f_min,f_max])
title(['Pressure Sensor ' Figname , ' $\frac{Q}{Q_n}=0.46$'], 'FontSize',22, 'Interpreter','Latex')
ylabel(['Pressrue [kPa]'],'FontSize',25,'Interpreter','Latex')
xlabel('Frequency [Hz'],'FontSize',22,'Interpreter','Latex')
grid on
a = get(gca,'XTickLabel');
set(gca,'XTickLabel',a,'FontName','Times','fontsize',18)
% set(gcf,'PaperPositionMode','auto'); %Export Figure
% print(['0-46'],'-dpng','-r500');

dfig(Figname) %Plot figure
hold on
plot3(z(j+3)*i1,f1,Peak(:,j))
title(['Pressure Sensor ' Figname]'],'FontSize',22,'Interpreter','Latex')

```

```
grid on
xlabel(['$\frac{Q}{Q_n}$'], 'FontSize', 25, 'Interpreter', 'Latex')
ylabel('Frequency [Hz]', 'FontSize', 22, 'Interpreter', 'Latex')
zlabel('Pressure [kPa]', 'FontSize', 22, 'Interpreter', 'Latex')
ylim([f_min, f_max])
set(gca, 'XTickLabel', {'0.46', '0.58', '0.64', '0.76', '0.83', '0.84', '0.89', '0.99', '1.03'})
end

set(gca, 'Xdir', 'reverse', 'view', [135, 45])           %rotate figure
set(gcf, 'PaperPositionMode', 'auto');
print([Figname, '0-800'], '-dpng', '-r0');           %Export Figure
end
```

## Appendix J MATLAB script Peak analysis

```

load('Pressure_with_air.mat')
load('Pressure_without_air.mat')

Fs=2000;                                %sampling rate

%Select sensor
disp('1: DT1 ')
disp('2: DT2 ')
disp('3: DT3 ')
disp('4: DT4 ')
disp('5: DT5 ')
disp('6: DT6 ')
disp('7: DT7 ')
disp('8: DT8 ')

prompt = 'Chose sensor, Please ';
inputN = input(prompt,'s');
inputN = str2num(inputN);

if isempty(inputN)
    kk=1:8;
else
    kk=inputN;
end

for inputN=kk;

    switch inputN
    case 1
        sensorInput='DT1';
        NameX=fieldnames(P);
        FignameT=NameX(inputN);
        Figname=FignameT{1};
        FigTitle = 'Draft Tube Pressure 1';           %DT1
        a=61.30880908;                               %calibration const.
        b=-121.61051306;                             %calibration const.
    case 2
        sensorInput='DT2';
        NameX=fieldnames(P);
        FignameT=NameX(inputN);
        Figname=FignameT{1};
        FigTitle = 'Draft Tube Pressure 2';           %DT2

```

```
a=61.17379911; %calibration const.
b=-121.42918313; %calibration const.
case 3
sensorInput='DT3';
NameX=fieldnames(P);
FignameT=NameX(inputN);
Figname=FignameT{1};
FigTitle = 'Draft Tube Pressure 3'; %DT3
a=61.21574205; %calibration const.
b=-122.53410606; %calibration const.

case 4
sensorInput='DT4';
NameX=fieldnames(P);
FignameT=NameX(inputN);
Figname=FignameT{1};
FigTitle = 'Draft Tube Pressure 4'; %DT4
a=61.25759912; %calibration const.
b=-123.19199928; %calibration const.

case 5
sensorInput='DT5';
NameX=fieldnames(P);
FignameT=NameX(inputN);
Figname=FignameT{1};
FigTitle = 'Draft Tube Pressure 5'; %DT5
a=61.27267521; %calibration const.
b=-121.91624464; %calibration const.

case 6
sensorInput='DT6';
NameX=fieldnames(P);
FignameT=NameX(inputN);
Figname=FignameT{1};
FigTitle = 'Draft Tube Pressure 6'; %DT6
a=61.20854518; %calibration const.
b=-122.27875129; %calibration const.
```

```
case 7
    sensorInput='DT7';
    NameX=fieldnames(P);
    FignameT=NameX(inputN);
    Figname=FignameT{1};
    FigTitle = 'Draft Tube Pressure 7';           %DT7
    a=61.23005606;                               %calibration const.
    b=-121.82442935;                             %calibration const.
case 8
    sensorInput='DT8';
    NameX=fieldnames(P);
    FignameT=NameX(inputN);
    Figname=FignameT{1};
    FigTitle = 'Draft Tube Pressure 8';           %DT8
    a=61.11306315;                               %calibration const.
    b=-121.75310005;                             %calibration const.
end

for i = 1:numel(P)
    x(:,i) = PL(i).(sensorInput)*a+b;
    y(:,i) = P(i).(sensorInput)*a+b;
end

%%Sort elements
Operational_point =[0.575, 0.4625];
[TempOperational I]= sort(Operational_point);

for j=1:length(PL);
    Tempx(:,j)=[x(:,I(j))];
    Tempy(:,j)=[y(:,I(j))];
end
```

```
%%To detrend the signal if it is in- or de-creasing over time
```

```
% t = (1:length(Tempx(:,j)))';
% opol = 7;
% [p,s,mu] = polyfit(t,Tempx(:,j),opol);
% f_y(:,j)= polyval(p,t,[],mu);
% dt_x(:,j) = Tempx(:,j) - f_y(:,j);
% Meanx(:,j)=dt_x(:,j)-mean(dt_x(:,j));

% ty = (1:length(Tempy(:,j)))';
% [py,sy,muy] = polyfit(ty,Tempy(:,j),opol);
% f_y(:,j)= polyval(py,ty,[],muy);
% dt_y(:,j) = Tempy(:,j) - f_y(:,j);
% Meany(:,j)=dt_y(:,j)-mean(dt_y(:,j));
```

```
meanx(:,j)=mean(Tempx(:,j));
StandardDeviationx(:,j)=std(Tempx(:,j));
SD1x(:,j)=2.58*StandardDeviationx(:,j);
```

```
%99confident interval;
```

```
Cl1x(:,j)=meanx(:,j)+SD1x(:,j);
Cl2x(:,j)=meanx(:,j)-SD1x(:,j);
diffx(:,j)=Cl1x(:,j)-Cl2x(:,j);
```

```
meany(:,j)=mean(Tempy(:,j));
StandardDeviationy(:,j)=std(Tempy(:,j));
SD1y(:,j)=2.58*StandardDeviationy(:,j);
```

```
%99confident interval;
```

```
Cl1y(:,j)=meany(:,j)+SD1y(:,j);
Cl2y(:,j)=meany(:,j)-SD1y(:,j);
diffy(:,j)=Cl1y(:,j)-Cl2y(:,j);
```

```
%with air
Lmx=length(Tempx(:,j));
maxmx=Cl1x(:,j);
mimx=Cl2x(:,j);
diffmx=maxmx-mimx;
Binsmx=diffmx/200;
binrangemx(:,j) = mimx:Binsmx:maxmx;
[bincountmx(:,j)] = histc(Tempx(:,j),binrangemx(:,j));
```

```
%without air
Lmy=length(Tempy(:,j));
mamy=Cl1y(:,j);
```

```

mimy=Cl2y(:,j);
diffmy=mamy-mimy;
Binsmy=diffmy/200;
binrangemy(:,j) = mimy:Binsmy:mamy;
[bincountmy(:,j)] = histc(Tempy(:,j),binrangemy(:,j));

```

```

dfig(['P2PM ',Figname])
    subplot(2,2,j);
    bar(binrangemx(:,j),bincountmx(:,j),'histc')
    title(['Pressure Sensor ',Figname], 'With Air injection');
    ylabel('Count [-]')
    xlabel('Pressure [kPa]')
    xlim ([mimx-5 maxmx+5])
    ylim([0 max(bincountmx(:,j))+100])

    subplot(2,2,j+2);
    bar(binrangemy(:,j),bincountmy(:,j),'histc')
    title(['Pressure Sensor ',Figname], 'Without Air injection');
    ylabel('Count [-]')
    xlabel('Pressure [kPa]')
    xlim ([mimy-5 mamy+5])
    ylim([0 max(bincountmy(:,j))+100])

```

end

```

dfig(['Bar-P2P',Figname])
    barP2P=[diffx; diffy];
    bar(barP2P)
    title(['Pressure Sensor ',Figname], 'Peak to peak comparison');
    legend('With Air','Without Air')
    set(gca,'XTickLabel',{'0.46' '0.58'})
    t=xlabel([' $\frac{P}{P_n}$  [-]'],);
    set(t,'FontSize',19,'FontWeight','bold','Interpreter','Latex');
    xlabel(['Frequency [Hz]'],'FontSize',16,'FontWeight','bold')
    P2Px(inputN,:)=diffx;
    P2Py(inputN,:)=diffy;

```

end

## Appendix K MATLAB script for Heat plot

```

load('Pressure_with_air.mat')
load('Pressure_without_air.mat')
Fs=2000; %Sample rate
ov=0.5; %Window overlap Factor
conf_l=0.95; %confidence level
na = 12; %na=number of windows
f_min=0; %determines min in plot
f_max=20; %determines min in plot

% xtick=[0:2.5:25];%
% xtick=linspace(f_min,f_max,10);
% xtick=[1 5 10 15 20 25 30 35 40 45 50 55 60 65 70 75];
xtick=[1 2.5 5 7.5 10 12.5 15 17.5 20]; % X-labels

names={'0.46', '0.58'}; % Sensors names
disp('1: DT1 ')
disp('2: DT2 ')
disp('3: DT3 ')
disp('4: DT4 ')
disp('5: DT5 ')
disp('6: DT6 ')
disp('7: DT7 ')
disp('8: DT8 ')

prompt = 'Chose sensor, Please ';
inputN = input(prompt,'s');
inputN = str2num(inputN);
if isempty(inputN)
    kk=1:8;
else
    kk=inputN;
end
for inputN=kk;
    switch inputN
        case 1
            sensorInput='DT1';
            NameX=fieldnames(P);
            FignameT=NameX(inputN);
            Figname=FignameT{1};
            FigTitle = 'Draft Tube Pressure 1'; %DT1
            a=61.30880908; %calibration const.
            b=-121.61051306; %calibration const.

```



```
case 2
    sensorInput='DT2';
    NameX=fieldnames(P);
    FignameT=NameX(inputN);
    Figname=FignameT{1};
    FigTitle = 'Draft Tube Pressure 2';           %DT2
    a=61.17379911;                               %calibration const.
    b=-121.42918313;                             %calibration const.

case 3
    sensorInput='DT3';
    NameX=fieldnames(P);
    FignameT=NameX(inputN);
    Figname=FignameT{1};
    FigTitle = 'Draft Tube Pressure 3';           %DT3
    a=61.21574205;                               %calibration const.
    b=-122.53410606;                             %calibration const.

case 4
    sensorInput='DT4';
    NameX=fieldnames(P);
    FignameT=NameX(inputN);
    Figname=FignameT{1};
    FigTitle = 'Draft Tube Pressure 4';           %DT4
    a=61.25759912;                               %calibration const.
    b=-123.19199928;                             %calibration const.

case 5
    sensorInput='DT5';
    NameX=fieldnames(P);
    FignameT=NameX(inputN);
    Figname=FignameT{1};
    FigTitle = 'Draft Tube Pressure 5';           %DT5
    a=61.27267521;                               %calibration const.
    b=-121.91624464;                             %calibration const.
```

```

case 6
    sensorInput='DT6';
    NameX=fieldnames(P);
    FignameT=NameX(inputN);
    Figname=FignameT{1};
    FigTitle = 'Draft Tube Pressure 6';           %DT6
    a=61.20854518;                               %calibration const.
    b=-122.27875129;                             %calibration const.
case 7
    sensorInput='DT7';
    NameX=fieldnames(P);
    FignameT=NameX(inputN);
    Figname=FignameT{1};
    FigTitle = 'Draft Tube Pressure 7';         %DT7
    a=61.23005606;                               %calibration const.
    b=-121.82442935;                             %calibration const.
case 8
    sensorInput='DT8';
    NameX=fieldnames(P);
    FignameT=NameX(inputN);
    Figname=FignameT{1};
    FigTitle = 'Draft Tube Pressure 8';         %DT8
    a=61.11306315;                               %calibration const.
    b=-121.75310005;                             %calibration const.
end

for i = 1:numel(PL)
    x(:,i) = PL(i).(sensorInput)*a+b;
    y(:,i) = P(i).(sensorInput)*a+b;
end

%Sorting of elements

Operational_point =[0.575, 0.4625];
[TempOperational I]= sort(Operational_point);

```

```

for k=1:length(Operational_point);
    Tempx(:,k)=x(:,l(k));
    Tempy(:,k)=y(:,l(k));
    t = (1:length(Tempx(:,k)))';
    opol = 7;
    [p,s,mu] = polyfit(t,Tempx(:,k),opol);
    f_y(:,k)= polyval(p,t,[],mu);
    dt_x(:,k) = Tempx(:,k) - f_y(:,k);

    ty = (1:length(Tempy(:,k)))';
    [py,sy,muy] = polyfit(ty,Tempy(:,k),opol);
    f_y(:,k)= polyval(py,ty,[],muy);
    dt_y(:,k) = Tempy(:,k) - f_y(:,k);
end
%%
[n m] = size(dt_x);
for j=1:m

    nx = max(size(dt_x(:,j)));
    w = hanning(floor(nx/na));
    num_win=na/(1-ov);
    [PSD(:,j),f1,PSDc]=pwelch(dt_x(:,j),w,floor(ov*(nx/na)),[],Fs,'ConfidenceLevel',conf_l);
    %PSD=Power Spectral density V^2/Hz
    [PSDy(:,j),f1y,PSDcy]=pwelch(dt_y(:,j),w,floor(ov*(nx/na)),[],Fs,'ConfidenceLevel',conf_l);
    %PSD=Power Spectral density V^2/Hz

    fbin=f1(2)-f1(1);
    S1=sum(w);
    S2=sum(w.^2);
    ENBW=Fs*(S2/(S1^2));
    PS1=PSDc(:,1)*ENBW;
    PS2=PSDc(:,2)*ENBW;
    PS(:,j)=PSD(:,j)*ENBW;
    PSy(:,j)=PSDy(:,j)*ENBW;

    RMS1=sqrt(PS1);
    RMS2=sqrt(PS2);
    RMS(:,j)=sqrt(PS(:,j));

    Peak1=sqrt(PS1)*sqrt(2);
    Peak2=sqrt(PS2)*sqrt(2);
    Peak(:,j)=sqrt(PS(:,j))*sqrt(2);
    Peaky(:,j)=sqrt(PSy(:,j))*sqrt(2);
    ymax=max([max(Peak(:,j)) max(Peaky(:,j))]);

```

```

y1 = [0 1];
A1 = Peak(:,j);
A1(:,2) = Peak(:,j);

y1y = [0 1];
A1y = Peaky(:,j);
A1y(:,2) = Peaky(:,j);

% Plot one operational point with all the sensors

z=length (NameX);
if j==1
    if mod(inputN,2)==0
        dfig([names{j}]);
        subtightplot(z,2,inputN,[0.002,0.05])
        surf(f1,y1,A1,'linestyle','none')
        hold on
        set(gca,'view',[0 90]);
        xlim([f_min f_max])
        ylabel(Figname,'FontSize',14,'FontWeight','bold')
        set(gca,'XTickLabel',[]);
        set(gca,'YTickLabel',[]);
        colormap jet
        if inputN==2
            title(['With Air Injection', '\frac{Q}{Q_n}=0.46$'],'FontSize',20,'Interpreter','Latex');
        end
        if inputN==8
            xlabel(['Frequency [Hz]'],'FontSize',22,'Interpreter','Latex')
            ax=gca;
            ax.XTick=xtick;
            ax.XTickLabel=round(xtick,1);
            ax.FontSize=12;
            ax.FontWeight='bold';
        end
    end
else
    dfig([names{j}]);
    subtightplot(z,2,inputN,[0.002,0.05])
    surf(f1,y1,A1,'linestyle','none')
    hold on
    set(gca,'view',[0 90]);
    xlim([f_min f_max])
    ylabel(Figname,'FontSize',14,'FontWeight','bold')
    set(gca,'XTickLabel',[]);

```

```
set(gca,'YTickLabel',[]);
colormap jet
if inputN==1
    title(['With Air Injection', '\frac{Q}{Q_n}=0.46$'], 'FontSize', 20, 'Interpreter', 'Latex');
end
if inputN==7
    xlabel(['Frequency [Hz]'], 'FontSize', 22, 'Interpreter', 'Latex');
    t=text(-1.2, 1, 'Pressure Sensor', 'rotation', 90, 'FontSize', 22, 'Interpreter', 'Latex');
    t1=text(21.1, 1, 'Pressure Sensor', 'rotation', 90, 'FontSize', 21, 'Interpreter', 'Latex');
    ax=gca;
    ax.XTick=xtick;
    ax.XTickLabel=round(xtick,1);
    ax.FontSize=12;
    ax.FontWeight='bold';
end
% set(gcf,'PaperPositionMode','auto');
% print('mLuft0-46','-dpng','-r0');
end
```

## Appendix L Technical information Pressure Sensor

GE  
Sensing

### Features

- Ranges from 1 psi to 900 psi
- Accuracy  $\pm 0.06\%$  full scale (FS) best straight line (BSL)
- Fully welded 0.69 in titanium construction
- Integral lightning surge arrestor
- Polyurethane and fluoropolymer cables
- Full range of installation accessories
- 5 year anti corrosion warranty

The PDCR 1830/1880 transducer (mV output) and PTX 1830/1880 transmitter (4 to 20 mA output) are the latest generation of fully submersible titanium high performance sensors for measurement of hydrostatic liquid levels.

## 1830/1880 Series

### Druck High Performance Level Pressure Sensors

1830/1880 is a Druck product.  
Druck has joined other  
GE high-technology sensing  
businesses under a new  
name—GE Sensing.



## GE Sensing

### Applications

The PDCR/PTX 1830/1880 Series incorporates many enhanced features gained from experience in supplying thousands of sensors for small and large scale installations worldwide. Example applications include:

- **Potable water**  
From ground water borehole to surface water level measurements in rivers, canals and reservoirs.
- **Waste water and remediation**  
Monitoring of secondary and outflow sewage levels within certified hazardous areas and contaminated ground water levels in land fill sites.
- **Tank Level**  
From land based liquid storage vessels to on-board ship ballast tank monitoring within safe and certified hazardous areas.
- **Sea Water**  
Marine environmental applications including tide gauging, coastal flood protection and wave profiling amongst others.

### Reliability and Data Quality

The combination of a high technology sensor, together with advanced signal conditioning and packaging techniques, provides an ideal long term solution for reliable, accurate and economical level measurements.

The Druck micromachined silicon element is sealed within an all-titanium pressure module assembly, fully isolated from the pressure media. This is contained in a slimline, welded titanium body, terminated in an injection molded cable assembly. The cable features a Kevlar® strain cord and is IP68/Type 6 rated for indefinite immersion in pressure of 1000 psi.

### Lightning Surge Protection

An optional integral lightning surge arrester is available, qualified to the highest standard IEC 61000-4-5 (level 4). This protects the sensor from raised earth potentials caused by lightning strikes, which often occur in surface water applications.

### Ease of Use

A simple datum marked cable system is provided for ease of installation. 1 ft datum points are clearly marked for quick and accurate cable alignment below ground level. In addition, a full range of related accessories simplifies installation, operation and maintenance.

- Quick-release cable clamp assembly
- Slimline and short profile sink weights
- Moistureproof Sensor Termination Enclosure
- In-situ pressure test/calibration adaptors



GE  
Sensing

# 1830/1880 Specifications

## Pressure Measurement

### Operating Pressure Ranges

#### PDCR 1830/1880 (mV)

- 1, 2.5 psi gauge
- 5, 10, 15, 20, 30, 50, 75, 100, 150, 200, 300, 500, 900 psi gauge or absolute

#### PTX 1830/1880 (mA)

Any zero based FS from 1 to 900 psi gauge, 5 to 900 psi absolute.

### Overpressure

The operating FS pressure range may be exceeded by the following multiples with negligible effect on calibration:

- 8 x for ranges 1, 2.5 psi
- 6 x for range 2.5 to 5 psi
- 4 x for ranges above 5 psi (2000 psi maximum).

### Pressure Containment

- 10 x for ranges up to 5 psi gauge
- 6 x for ranges above 5 psi gauge (2000 psi maximum)
- 2900 psi for absolute ranges.

### Media Compatibility

Fluids compatible with titanium (body), acetyl (nose cone) and polyurethane or Tefzel (cable assembly)

### Pulse Power Excitation

Recommended power-on-time before output sample

PDCR 1830/1880: 10 ms

PTX 1830/1880: 30 ms

For pulse power operation refer to technical note.

The minimum supply voltage ( $V_{min}$ ) which must appear across the pressure transmitter terminals is 9 V and is given by the following equation:

$$V_{min} = V_{sup} - (0.02 \times R_{loop})$$

Where  $V_{sup}$  is supply voltage in Volts,  $R_{loop}$  is total loop resistance in Ohms

### Excitation Voltage

PDCR 1830/1880 (mV)

10 V at 5 mA nominal

Output is fully ratiometric to supply within 2.5 V to 12 V limits.

PTX 1830/1880 (mA)

9 to 30 V

9 to 28 V for Intrinsically Safe version.

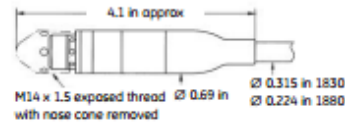
### Common Mode Voltage - PDCR 1830/1880

Typically +3.5 V to +9 V with respect to the negative supply

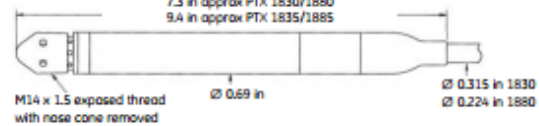
### Output Impedance - PDCR 1830/1880

2 k $\Omega$  nominal

### PDCR 1830/1880



### PTX 1830/1880



### Electrical Connections

#### PDCR 1830

Red: Supply positive  
White: Supply negative  
Yellow: Output positive  
Blue: Output negative  
Screen wire connected to case  
(S version - screen not connected)  
Remaining cores not connected

#### PTX 1830/1880 Lightning protection

Red: Supply positive  
Black: Supply negative  
Screen wire connected to case  
(S version - screen not connected)  
Remaining cores not connected

### Output Signal

#### PDCR 1830/1880

- 25 mV for 1 psi range
- 50 mV for 2.5 and 5 psi ranges
- 100 mV for ranges 10 psi and above

#### PTX 1830/1880

4 to 20 mA proportional, for zero to FS pressure.

## Performance Specification

### Accuracy

Combined effects of Non-linearity, Hysteresis and Repeatability:

- Standard:  $\pm 0.1\%$  FS BSL maximum
- Option D:  $\pm 0.06\%$  FS BSL maximum ( $\pm 0.08\%$  maximum for 1.5 psi and below).

### Zero Offset and Span Setting

#### PDCR 1830/1880

- Typical:  $\pm 1.5$  mV
- Maximum:  $\pm 3$  mV

#### PTX 1830/1880

Maximum:  $\pm 0.05$  mA

### Long-Term Stability

$\pm 0.1\%$  typically per annum

### Operating Temperature Range

-5 to 140 °F (-21 to 60°C)

### Compensated Temperature Range

30 to 86 °F (-1 to 30°C)

### Temperature Effects

- $\pm 0.3\%$  FS Temperature Error Band (TEB) for 5 psi range and above
- $\pm 0.6\%$  FS TEB for ranges below 5 psi.



# GE Sensing

## Intrinsic Safety

### PDCR 1830/1880:

CSA/UL: Class I Div I Groups A, B, C, D

Class II Div I Groups E, F, & G

Class III

FM: Class I, II, III Div I Groups A, B, C, D, E, F, G.

### PTX 1830/1880:

CSA: Class I Div I Groups A, B, C, D

Class II Div I Groups E, F, & G

Class III

FM: Class I, II, III Div I Groups A, B, C, D, E, F, G.

**Lightning surge arrester** (optional on PTX only) Integral lightning protection assembly certified to standard IEC 61000-4-5 (level 4)

## Shock and Vibration

MIL-STD-810E, method 514.4, Category 10 min. integrity

Figure 514.4-16

Product will withstand 20 g peak shock half sine wave 9 ms duration in all axes, also 2000 g peak shock 0.5 ms duration in all axes.

## Insulation

Standard: >100 MΩ at 500 VDC

Intrinsically Safe version: <5 mA at 500 Vac

## Physical Specification

### Pressure Connection

Standard: Radial holed M14 x 1.5 mm male thread fitted with protective acetyl nose cone.

### Electrical Connection

**1830:** Vented polyurethane cable with integral Kevlar® strain relief cord rated to 119 lb load.

**1880:** Vented flourpolymer

### Ingress Protection

Type 6/IP68 to 1000 psi

### Cable Lengths

To be specified as required in 1 ft increments up to 1600 ft. For longer lengths refer to GE Sensing.

### CE marking

CE marked for electromagnetic compatibility and pressure equipment directive.

### Documentation

Detailed user instructions are provided with specific calibration data.

## Accessories

A full range of accessories is available to enhance installation, operation and maintenance of the 1830/1840 Series as listed below:

- STE moistureproof sensor termination enclosure (STE 110)
- Slimline sink weight Ø17.5 mm (DA2608-1-01)
- Short sink weight Ø25 mm (DAA068-1-01)
- Cable clamp system (192-373-01)
- 360° Rotatable calibration adaptor to:
  - G1/8 (DA4112-1-01) 1/8 NPT (DA4112-2-01)
- Economical direct calibration adaptor to:
  - G1/8 (DA2537-1-01) 1/8 NPT (DA2537-2-01)
- Accessory pack contains (TAS-A187)
  - STE box Slimline sink weight
  - Cable clamp Direct calibration adaptor

## Options

- FM/CSA certification
- Threaded pressure port (welded) 1/4, 1/8 NPT male, 7/16 UNF male, G1/4, G1/8 male.

## Ordering Information

Code	Model	Cable type	Lightning protection
PDCR18	mV output	Polyurethane	Not fitted
PTX 18	mA output	Flourpolymer	Fitted
	Code	Code	
	3	0	
	8	5	

- (1) Select model number
- (2) Pressure range and scale units
- (3) Options (if required)
- (4) Cable length required
- (5) Accessories (order as separate items).
- (6) Supporting Services (order as separate items)

## Supporting Services

Our highly trained staff can support you, no matter where you are in the world. We can provide training, nationally accredited calibration - both initially and at periodic intervals - extended warrantee terms and even rental of portable or laboratory calibrators. Further details can be found in [www.gesensing.com/productservices/service.htm](http://www.gesensing.com/productservices/service.htm)



©2008 GE All rights reserved.  
920-0940

All specifications are subject to change for product improvement without notice. GE® is a registered trademark of General Electric Co. Other company or product names mentioned in this document may be trademarks or registered trademarks of their respective companies, which are not affiliated with GE.

[www.gesensing.com](http://www.gesensing.com)

## Appendix M Calibration -Pressure sensors

All the pressure sensors are calibrated at the Waterpower laboratory at NTNU, using designated deadweight testers. The following appendix will present the calibration report of all 12 sensors used in the measurements at Leirfossene power plant.



Figure a) Low pressure deadweight tester.



Figure b) High Pressure deadweight tester

Table 25 displays the range and uncertainty of the equipment used to calibrate the sensors. This means that if a sensor is supposed to measure values between 100mbar to 10bar both testers have to be used in order to calibrate the correct area it is supposed to measure.

Type	Classification	Range	Uncertainty
GE deadweight tester, P3023-6-P	Pneumatic	30 – 2000 mbar	0,008 %
GE deadweight tester, P3223-1	Hydraulic	1 – 350 bar	0,008 %

Table 25 - Deadweight calibration tester

## I. Draft tube sensor 1

**CALIBRATION REPORT****CALIBRATION PROPERTIES**

Calibrated by: Stian Solvik  
 Type/Producer: Druck PTX 1830  
 SN: 23131000-ref\_1  
 Range: 0-5 bar a  
 Unit: kPa  
 The king had a son  
 Druck PTX 1830  
 2867610  
 0-10 bar a  
 kPa

**CALIBRATION SOURCE PROPERTIES**

Type/Producer: Pressurements deadweight tester P3023-6-P  
 SN: 66611  
 Uncertainty [%]: 0,01

**POLY FIT EQUATION:**

$Y = -121.51345376E+0X^0 + 61.20876242E+0X^1$

**CALIBRATION SUMMARY:**

Max Uncertainty : 0.032618 [%]  
 Max Uncertainty : 0.007991 [kPa]  
 RSQ : 1.000000  
 Calibration points : 16

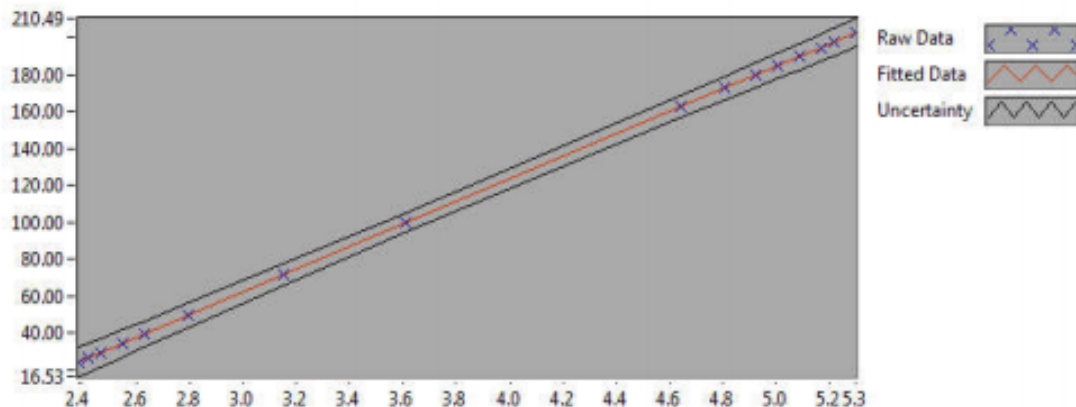


Figure 1 : Calibration chart (The uncertainty band is multiplied by 1000 )

---

Stian Solvik

**CALIBRATION VALUES**

<b>Value [kPa]</b>	<b>Voltage [V]</b>	<b>Best Poly Fit [kPa]</b>	<b>Deviation [kPa]</b>	<b>Uncertainty [%]</b>	<b>Uncertainty [kPa]</b>
24.498774	2.385894	24.524156	-0.025383	0.032618	0.007991
26.501795	2.418213	26.502391	-0.000595	0.029735	0.007880
29.506327	2.467304	29.507156	-0.000829	0.026172	0.007722
34.513881	2.549038	34.509992	0.003889	0.021618	0.007461
39.521434	2.630824	39.515998	0.005436	0.018240	0.007209
49.536542	2.794398	49.528175	0.008366	0.013576	0.006725
71.569777	3.154475	71.568033	0.001744	0.008128	0.005817
99.612077	3.612292	99.590491	0.021586	0.005094	0.005074
162.647252	4.642568	162.652361	-0.005109	0.003649	0.005935
172.662359	4.806143	172.664588	-0.002229	0.003657	0.006315
179.672934	4.920697	179.676311	-0.003378	0.003685	0.006621
184.680487	5.002563	184.687213	-0.006726	0.003714	0.006859
189.688041	5.084385	189.695463	-0.007422	0.003744	0.007102
194.695594	5.165988	194.690250	0.005344	0.003772	0.007344
197.700127	5.215103	197.696523	0.003603	0.003794	0.007501
202.707680	5.296945	202.705980	0.001700	0.003839	0.007782

**COMMENTS:**

2313102-ref\_8 ikke kalibrert

---

The uncertainty is calculated with 95% confidence. The uncertainty includes the randomness in the calibrated instrument during the calibration, systematic uncertainty in the instrument or property which the instrument under calibration is compared with (dead weight manometer, calibrated weights etc.), and due to regression analysis to fit the calibration points to a linear calibration equation. The calculated uncertainty can be used as the total systematic uncertainty of the calibrated instrument with the given calibration equation.

## II. Draft tube sensor 2

**CALIBRATION REPORT****CALIBRATION PROPERTIES**

Calibrated by: Stian Solvik  
 Type/Producer: Druck PTX 1830  
 SN: 2313099-ref\_2  
 Range: 0-5 bar a  
 Unit: kPa  
 test  
 Druck PTX 1830  
 2867610  
 0-10 bar a  
 kPa

**CALIBRATION SOURCE PROPERTIES**

Type/Producer: Pressurements deadweight tester P3023-6-P  
 SN: 66611  
 Uncertainty [%]: 0,01

**POLY FIT EQUATION:**

$Y = -121.36396347E+0X^0 + 61.06785291E+0X^1$

**CALIBRATION SUMMARY:**

Max Uncertainty : 0.043397 [%]  
 Max Uncertainty : 0.010632 [kPa]  
 RSQ : 1.000000  
 Calibration points : 16

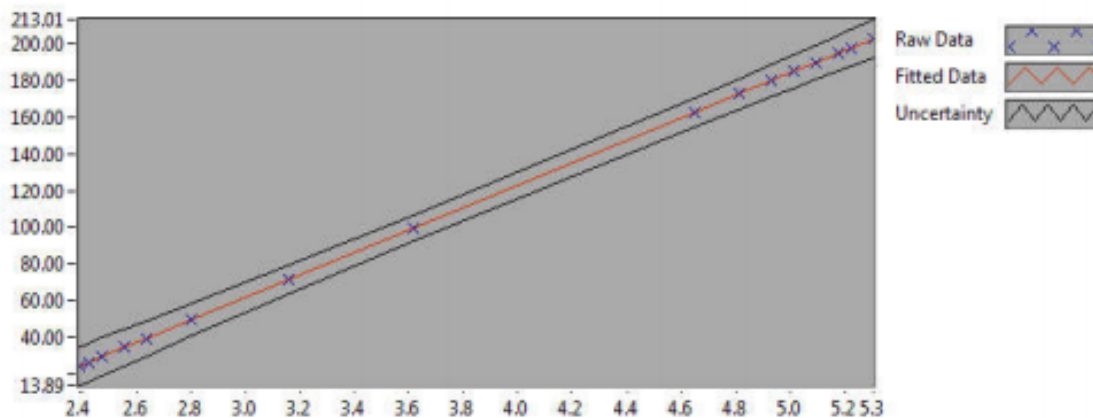


Figure 1 : Calibration chart (The uncertainty band is multiplied by 1000 )

---

Stian Solvik

**CALIBRATION VALUES**

<b>Value [kPa]</b>	<b>Voltage [V]</b>	<b>Best Poly Fit [kPa]</b>	<b>Deviation [kPa]</b>	<b>Uncertainty [%]</b>	<b>Uncertainty [kPa]</b>
24.498774	2.388975	24.525596	-0.026822	0.043397	0.010632
26.501795	2.421459	26.509366	-0.007571	0.039568	0.010486
29.506327	2.470609	29.510819	-0.004491	0.034824	0.010275
34.513881	2.552535	34.513853	0.000027	0.028766	0.009928
39.521434	2.634473	39.517640	0.003794	0.024270	0.009592
49.536542	2.798272	49.520494	0.016048	0.018065	0.008949
71.569777	3.159223	71.562978	0.006799	0.010806	0.007734
99.612077	3.617967	99.577542	0.034535	0.006772	0.006746
162.647252	4.650827	162.652059	-0.004807	0.004831	0.007858
172.662359	4.814846	172.668373	-0.006014	0.004849	0.008372
179.672934	4.929569	179.674233	-0.001299	0.004889	0.008783
184.680487	5.011695	184.689518	-0.009030	0.004925	0.009096
189.688041	5.093634	189.693315	-0.005274	0.004965	0.009417
194.695594	5.175589	194.698161	-0.002567	0.005005	0.009745
197.700127	5.224712	197.697998	0.002128	0.005033	0.009950
202.707680	5.306673	202.703136	0.004544	0.005087	0.010311

**COMMENTS:**

2313102-ref\_8 ikke kalibrert

---

The uncertainty is calculated with 95% confidence. The uncertainty includes the randomness in the calibrated instrument during the calibration, systematic uncertainty in the instrument or property which the instrument under calibration is compared with (dead weight manometer, calibrated weights etc.), and due to regression analysis to fit the calibration points to a linear calibration equation. The calculated uncertainty can be used as the total systematic uncertainty of the calibrated instrument with the given calibration equation.



## III. Draft tube sensor 3

**CALIBRATION REPORT****CALIBRATION PROPERTIES**

Calibrated by: Stian Solvik  
 Type/Producer: Druck PTX 1830  
 SN: 2313103\_3  
 Range: 0-5 bar a  
 Unit: kPa2313102-ref\_8  
 test  
 Druck PTX 1830  
 2867610  
 0-10 bar a  
 kPa

**CALIBRATION SOURCE PROPERTIES**

Type/Producer: Pressurements deadweight tester P3023-6-P  
 SN: 66611  
 Uncertainty [%]: 0,01

**POLY FIT EQUATION:**

$Y = -121.65119602E+0X^0 + 61.12072043E+0X^1$

**CALIBRATION SUMMARY:**

Max Uncertainty : 0.045557 [%]  
 Max Uncertainty : 0.011161 [kPa2313102-ref\_8]  
 RSQ : 1.000000  
 Calibration points : 16

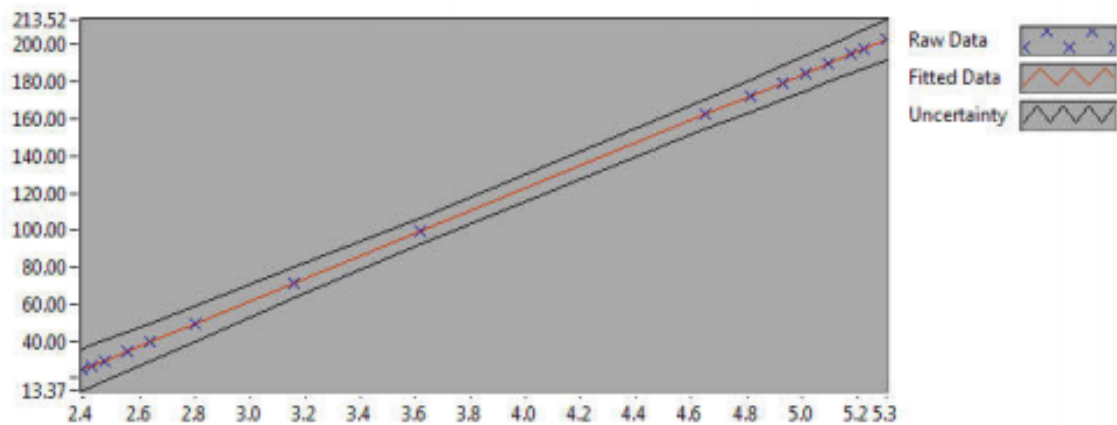


Figure 1 : Calibration chart (The uncertainty band is multiplied by 1000 )

---

Stian Solvik

**CALIBRATION VALUES**

<b>Value [kPa2313102- ref_8]</b>	<b>Voltage [V]</b>	<b>Best Poly Fit [kPa2313102- ref_8]</b>	<b>Deviation [kPa2313102- ref_8]</b>	<b>Uncertainty [%]</b>	<b>Uncertainty [kPa2313102- ref_8]</b>
24.498774	2.391690	24.530643	-0.031869	0.045557	0.011161
26.501795	2.424094	26.511171	-0.009375	0.041538	0.011008
29.506327	2.473092	29.505964	0.000363	0.036560	0.010788
34.513881	2.554989	34.511548	0.002333	0.030200	0.010423
39.521434	2.636889	39.517366	0.004069	0.025479	0.010070
49.536542	2.800537	49.519653	0.016889	0.018965	0.009395
71.569777	3.161156	71.560921	0.008856	0.011343	0.008118
99.612077	3.619583	99.580354	0.031723	0.007109	0.007081
162.647252	4.651591	162.657387	-0.010136	0.005068	0.008243
172.662359	4.815418	172.670592	-0.008233	0.005090	0.008788
179.672934	4.929963	179.671721	0.001213	0.005130	0.009218
184.680487	5.012025	184.687371	-0.006883	0.005170	0.009548
189.688041	5.093916	189.692615	-0.004574	0.005210	0.009883
194.695594	5.175792	194.696964	-0.001369	0.005254	0.010228
197.700127	5.224892	197.697968	0.002159	0.005280	0.010439
202.707680	5.306777	202.702843	0.004837	0.005336	0.010816

**COMMENTS:**

2313102-ref\_8 ikke kalibrert

---

The uncertainty is calculated with 95% confidence. The uncertainty includes the randomness in the calibrated instrument during the calibration, systematic uncertainty in the instrument or property which the instrument under calibration is compared with (dead weight manometer, calibrated weights etc.), and due to regression analysis to fit the calibration points to a linear calibration equation. The calculated uncertainty can be used as the total systematic uncertainty of the calibrated instrument with the given calibration equation.



## IV. Draft tube sensor 4

**CALIBRATION REPORT****CALIBRATION PROPERTIES**

Calibrated by: Stian Solvik  
 Type/Producer: Druck PTX 1830  
 SN: 2313105ref\_4  
 Range: 0-5 bar a  
 Unit: kPa  
 The son had a cat  
 Druck PTX 1830  
 2867610  
 0-10 bar a  
 kPa

**CALIBRATION SOURCE PROPERTIES**

Type/Producer: Pressurements deadweight tester P3223-1  
 SN: 66611  
 Uncertainty [%]: 0,01

**POLY FIT EQUATION:**

$Y = -123.19662076E+0X^0 + 61.24274144E+0X^1$

**CALIBRATION SUMMARY:**

Max Uncertainty : 0.058246 [%]  
 Max Uncertainty : 0.012595 [kPa]  
 RSQ : 1.000000  
 Calibration points : 18

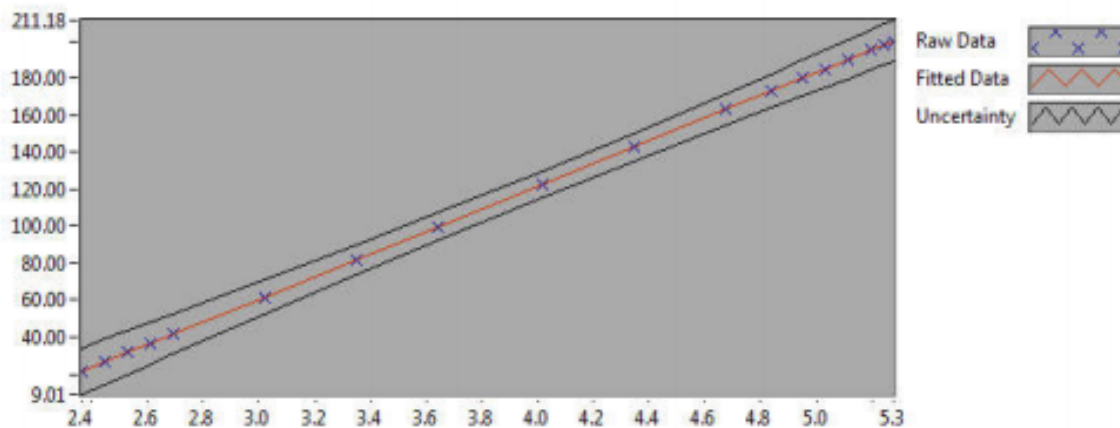


Figure 1 : Calibration chart (The uncertainty band is multiplied by 1000 )

---

Stian Solvik

**CALIBRATION VALUES**

<b>Value [kPa]</b>	<b>Voltage [V]</b>	<b>Best Poly Fit [kPa]</b>	<b>Deviation [kPa]</b>	<b>Uncertainty [%]</b>	<b>Uncertainty [kPa]</b>
21.624251	2.364358	21.603143	0.021108	0.058246	0.012595
26.631804	2.446379	26.626336	0.005468	0.045652	0.012158
31.639358	2.528390	31.648903	-0.009545	0.037076	0.011731
36.646911	2.610171	36.657401	-0.010490	0.030864	0.011311
41.654465	2.692021	41.670106	-0.015641	0.026177	0.010904
61.684679	3.019382	61.718595	-0.033916	0.015246	0.009405
81.774893	3.346615	81.759275	0.015618	0.010024	0.008197
99.812086	3.640911	99.782746	0.029340	0.007427	0.007413
122.846832	4.017385	122.839036	0.007797	0.005808	0.007135
142.887056	4.344663	142.882441	0.004615	0.005283	0.007548
162.917270	4.671825	162.918769	-0.001499	0.005215	0.008496
172.952377	4.835619	172.949973	0.002405	0.005274	0.009121
179.962952	4.950025	179.956508	0.006445	0.005336	0.009603
184.970506	5.031982	184.975763	-0.005258	0.005391	0.009972
189.998048	5.113880	189.991391	0.006658	0.005453	0.010360
195.005602	5.195751	195.005429	0.000172	0.005511	0.010746
198.010134	5.244871	198.013686	-0.003552	0.005547	0.010984
200.013155	5.277842	200.032881	-0.019726	0.005574	0.011148

**COMMENTS:**


---

The uncertainty is calculated with 95% confidence. The uncertainty includes the randomness in the calibrated instrument during the calibration, systematic uncertainty in the instrument or property which the instrument under calibration is compared with (dead weight manometer, calibrated weights etc.), and due to regression analysis to fit the calibration points to a linear calibration equation. The calculated uncertainty can be used as the total systematic uncertainty of the calibrated instrument with the given calibration equation.

## V. Draft tube sensor 5

### CALIBRATION REPORT

---

#### **CALIBRATION PROPERTIES**

Calibrated by: Stian Solvik  
 Type/Producer: Druck PTX 1830  
 SN: 2309837ref\_5  
 Range: 0-5 bar a  
 Unit: kPa  
 The king had a son  
 Druck PTX 1830  
 2867610  
 0-10 bar a  
 kPa

#### **CALIBRATION SOURCE PROPERTIES**

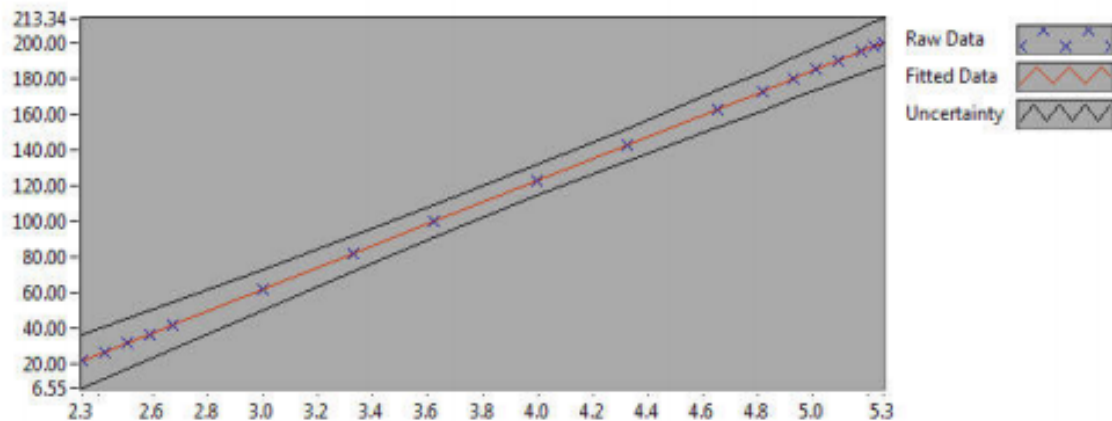
Type/Producer: Pressurements deadweight tester P3223-1  
 SN: 66611  
 Uncertainty [%]: 0,01

#### **POLY FIT EQUATION:**

$Y = -121.94593216E+0X^0 + 61.26314142E+0X^1$

#### **CALIBRATION SUMMARY:**

Max Uncertainty : 0.069590 [%]  
 Max Uncertainty : 0.015048 [kPa]  
 RSQ : 1.000000  
 Calibration points : 18




---

Stian Solvik

**CALIBRATION VALUES**

<b>Value [kPa]</b>	<b>Voltage [V]</b>	<b>Best Poly Fit [kPa]</b>	<b>Deviation [kPa]</b>	<b>Uncertainty [%]</b>	<b>Uncertainty [kPa]</b>
21.624251	2.343035	21.595748	0.028503	0.069590	0.015048
26.631804	2.425159	26.626950	0.004854	0.054542	0.014525
31.639358	2.507070	31.645066	-0.005708	0.044295	0.014015
36.646911	2.589034	36.666431	-0.019520	0.036871	0.013512
41.654465	2.670692	41.669026	-0.014561	0.031272	0.013026
61.684679	2.998105	61.727419	-0.042740	0.018205	0.011230
81.774893	3.325223	81.767651	0.007243	0.011960	0.009780
99.812086	3.619260	99.781288	0.030798	0.008872	0.008855
122.846832	3.995433	122.826830	0.020003	0.006933	0.008516
142.887056	4.322663	142.873983	0.013073	0.006306	0.009011
162.917270	4.649761	162.913059	0.004211	0.006224	0.010141
172.952377	4.813515	172.945137	0.007240	0.006296	0.010889
179.962952	4.928140	179.967423	-0.004471	0.006370	0.011464
184.970506	5.009864	184.974105	-0.003600	0.006436	0.011906
189.998048	5.091857	189.997246	0.000802	0.006509	0.012367
195.005602	5.173615	195.005993	-0.000391	0.006580	0.012832
198.010134	5.222742	198.015628	-0.005495	0.006623	0.013113
200.013155	5.255678	200.033398	-0.020243	0.006654	0.013310

**COMMENTS:**


---

The uncertainty is calculated with 95% confidence. The uncertainty includes the randomness in the calibrated instrument during the calibration, systematic uncertainty in the instrument or property which the instrument under calibration is compared with (dead weight manometer, calibrated weights etc.), and due to regression analysis to fit the calibration points to a linear calibration equation. The calculated uncertainty can be used as the total systematic uncertainty of the calibrated instrument with the given calibration equation.

## VI. Draft tube sensor 6

**CALIBRATION REPORT****CALIBRATION PROPERTIES**

Calibrated by: Stian Solvik  
 Type/Producer: Druck PTX 1830  
 SN: 2313101ref\_6  
 Range: 0-5 bar a  
 Unit: kPa  
 test  
 Druck PTX 1830  
 2867610  
 0-10 bar a  
 kPa

**CALIBRATION SOURCE PROPERTIES**

Type/Producer: Pressurements deadweight tester P3223-1  
 SN: 66611  
 Uncertainty [%]: 0,01

**POLY FIT EQUATION:**

$Y = -122.38721122E+0X^0 + 61.20034395E+0X^1$

**CALIBRATION SUMMARY:**

Max Uncertainty : 0.057716 [%]  
 Max Uncertainty : 0.012481 [kPa]  
 RSQ : 1.000000  
 Calibration points : 18

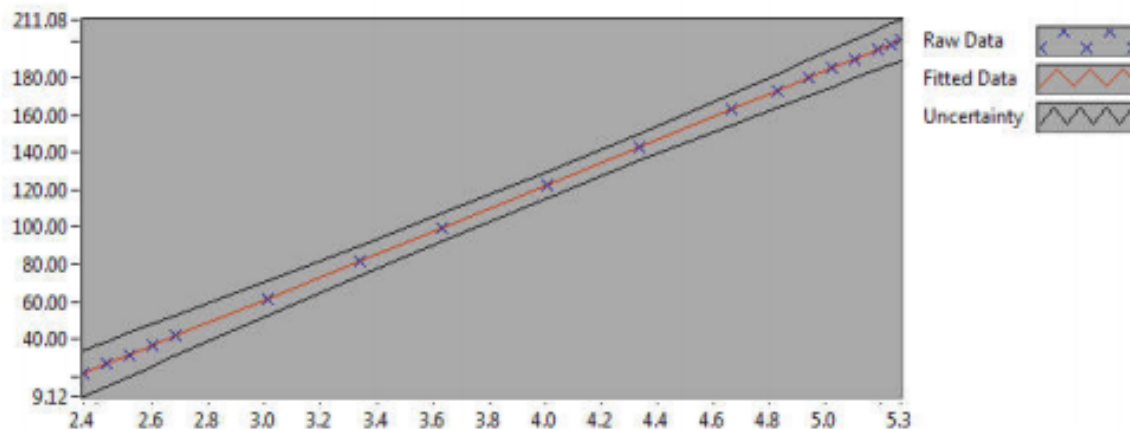


Figure 1 : Calibration chart (The uncertainty band is multiplied by 1000 )

---

Stian Solvik

**CALIBRATION VALUES**

<b>Value [kPa]</b>	<b>Voltage [V]</b>	<b>Best Poly Fit [kPa]</b>	<b>Deviation [kPa]</b>	<b>Uncertainty [%]</b>	<b>Uncertainty [kPa]</b>
21.624251	2.352807	21.605415	0.018836	0.057716	0.012481
26.631804	2.434875	26.627973	0.003831	0.045239	0.012048
31.639358	2.516884	31.646952	-0.007595	0.036740	0.011624
36.646911	2.598772	36.658512	-0.011601	0.030584	0.011208
41.654465	2.680670	41.670687	-0.016222	0.025939	0.010805
61.684679	3.008215	61.716570	-0.031891	0.015107	0.009319
81.774893	3.335740	81.761222	0.013671	0.009934	0.008124
99.812086	3.630237	99.784520	0.027566	0.007360	0.007347
122.846832	4.006846	122.833112	0.013720	0.005755	0.007070
142.887056	4.334401	142.879603	0.007453	0.005235	0.007480
162.917270	4.661800	162.916537	0.000733	0.005168	0.008419
172.952377	4.825653	172.944416	0.007961	0.005226	0.009039
179.962952	4.940200	179.954738	0.008214	0.005290	0.009519
184.970506	5.022308	184.979761	-0.009256	0.005343	0.009883
189.998048	5.104286	189.996873	0.001175	0.005404	0.010268
195.005602	5.186161	195.007617	-0.002015	0.005461	0.010650
198.010134	5.235277	198.013567	-0.003433	0.005497	0.010885
200.013155	5.268296	200.034305	-0.021150	0.005524	0.011050

**COMMENTS:**


---

The uncertainty is calculated with 95% confidence. The uncertainty includes the randomness in the calibrated instrument during the calibration, systematic uncertainty in the instrument or property which the instrument under calibration is compared with (dead weight manometer, calibrated weights etc.), and due to regression analysis to fit the calibration points to a linear calibration equation. The calculated uncertainty can be used as the total systematic uncertainty of the calibrated instrument with the given calibration equation.



## VII. Draft tube sensor 7

**CALIBRATION REPORT****CALIBRATION PROPERTIES**

Calibrated by: Stian Solvik  
 Type/Producer: Druck PTX 1830  
 SN: 2313104ref\_7  
 Range: 0-5 bar a  
 Unit: kPa  
 test  
 Druck PTX 1830  
 2867610  
 0-10 bar a  
 kPa

**CALIBRATION SOURCE PROPERTIES**

Type/Producer: Pressurements deadweight tester P3223-1  
 SN: 66611  
 Uncertainty [%]: 0,01

**POLY FIT EQUATION:**

$Y = -121.85450572E+0X^0 + 61.16953912E+0X^1$

**CALIBRATION SUMMARY:**

Max Uncertainty : 0.073985 [%]  
 Max Uncertainty : 0.016213 [kPa]  
 RSQ : 1.000000  
 Calibration points : 16

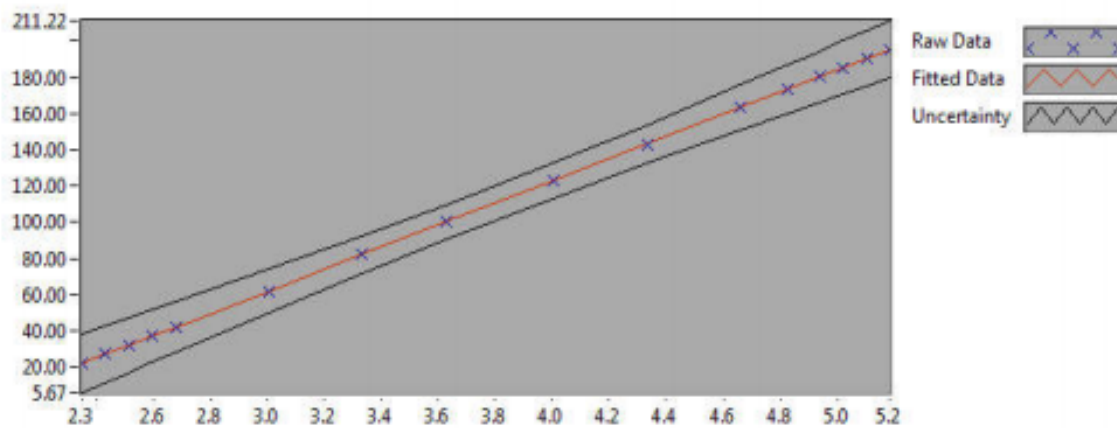


Figure 1 : Calibration chart (The uncertainty band is multiplied by 1000 )

Stian Solvik

**CALIBRATION VALUES**

<b>Value [kPa]</b>	<b>Voltage [V]</b>	<b>Best Poly Fit [kPa]</b>	<b>Deviation [kPa]</b>	<b>Uncertainty [%]</b>	<b>Uncertainty [kPa]</b>
21.914248	2.349797	21.881487	0.032761	0.073985	0.016213
26.921802	2.431818	26.898682	0.023120	0.058008	0.015617
31.929355	2.514002	31.925864	0.003491	0.047084	0.015034
36.936909	2.596098	36.947624	-0.010715	0.039165	0.014467
41.944462	2.678095	41.963350	-0.018888	0.033180	0.013917
61.974677	3.005664	62.000547	-0.025871	0.019262	0.011938
82.004891	3.333268	82.039977	-0.035086	0.012754	0.010459
100.082084	3.628023	100.069971	0.012113	0.009686	0.009694
123.116830	4.004792	123.116795	0.000035	0.007959	0.009798
143.147044	4.332386	143.155553	-0.008509	0.007543	0.010798
163.217258	4.660039	163.197921	0.019337	0.007636	0.012463
173.232365	4.823806	173.215454	0.016911	0.007767	0.013456
180.242940	4.938446	180.227950	0.014990	0.007882	0.014208
185.250494	5.020601	185.253370	-0.002876	0.007974	0.014771
190.258047	5.102525	190.264611	-0.006564	0.008068	0.015350
195.265601	5.184514	195.279850	-0.014249	0.008161	0.015936

**COMMENTS:**

9 and 10 calibrated for high pres as well

---

The uncertainty is calculated with 95% confidence. The uncertainty includes the randomness in the calibrated instrument during the calibration, systematic uncertainty in the instrument or property which the instrument under calibration is compared with (dead weight manometer, calibrated weights etc.), and due to regression analysis to fit the calibration points to a linear calibration equation. The calculated uncertainty can be used as the total systematic uncertainty of the calibrated instrument with the given calibration equation.



## VIII. Draft tube sensor 8

**CALIBRATION REPORT****CALIBRATION PROPERTIES**

Calibrated by: Stian Solvik  
 Type/Producer: Druck PTX 1830  
 SN: 2313102ref\_8  
 Range: 0-5 bar a  
 Unit: kPa  
 test  
 Druck PTX 1830  
 2867610  
 0-10 bar a  
 kPa

**CALIBRATION SOURCE PROPERTIES**

Type/Producer: Pressurements deadweight tester P3223-1  
 SN: 66611  
 Uncertainty [%]: 0,01

**POLY FIT EQUATION:**

$Y = -121.88827335E+0X^0 + 61.06822182E+0X^1$

**CALIBRATION SUMMARY:**

Max Uncertainty : 0.061411 [%]  
 Max Uncertainty : 0.013280 [kPa]  
 RSQ : 1.000000  
 Calibration points : 18

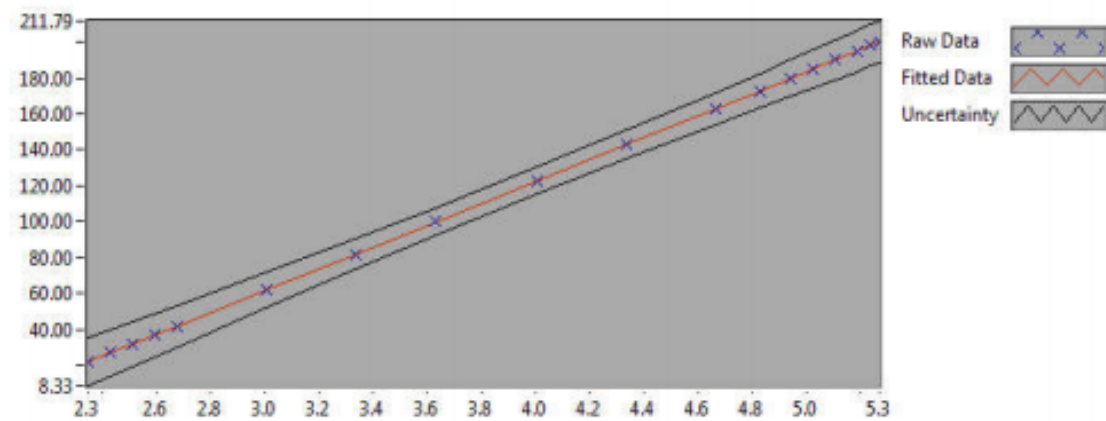


Figure 1 : Calibration chart (The uncertainty band is multiplied by 1000 )

Stian Solvik

**CALIBRATION VALUES**

<b>Value [kPa]</b>	<b>Voltage [V]</b>	<b>Best Poly Fit [kPa]</b>	<b>Deviation [kPa]</b>	<b>Uncertainty [%]</b>	<b>Uncertainty [kPa]</b>
21.624251	2.349759	21.607332	0.016919	0.061411	0.013280
26.631804	2.431996	26.629375	0.002429	0.048134	0.012819
31.639358	2.514135	31.645500	-0.006142	0.039093	0.012369
36.646911	2.596203	36.657229	-0.010318	0.032543	0.011926
41.654465	2.678306	41.671090	-0.016625	0.027600	0.011497
61.684679	3.006561	61.717082	-0.032402	0.016071	0.009914
81.774893	3.334823	81.763420	0.011473	0.010565	0.008639
99.812086	3.629948	99.786196	0.025890	0.007831	0.007816
122.846832	4.007352	122.833564	0.013268	0.006122	0.007521
142.887056	4.335497	142.872807	0.014249	0.005568	0.007956
162.917270	4.663684	162.914640	0.002630	0.005497	0.008955
172.952377	4.827821	172.938185	0.014192	0.005559	0.009615
179.962952	4.942640	179.949966	0.012986	0.005625	0.010123
184.970506	5.024955	184.976778	-0.006272	0.005683	0.010512
189.998048	5.107172	189.997623	0.000425	0.005747	0.010920
195.005602	5.189271	195.011296	-0.005695	0.005809	0.011329
198.010134	5.238548	198.020549	-0.010415	0.005848	0.011580
200.013155	5.271613	200.039746	-0.026591	0.005877	0.011755

**COMMENTS:**


---

The uncertainty is calculated with 95% confidence. The uncertainty includes the randomness in the calibrated instrument during the calibration, systematic uncertainty in the instrument or property which the instrument under calibration is compared with (dead weight manometer, calibrated weights etc.), and due to regression analysis to fit the calibration points to a linear calibration equation. The calculated uncertainty can be used as the total systematic uncertainty of the calibrated instrument with the given calibration equation.

## IX. Inlet Pressure sensor

**CALIBRATION REPORT****CALIBRATION PROPERTIES**

Calibrated by: Stian Solvik  
 Type/Producer: Druck PTX 610  
 SN: 2184827ref\_9  
 Range: 0-10 bar a  
 Unit: kPa  
 test  
 Druck PTX 1830  
 2867610  
 0-10 bar a  
 kPa

**CALIBRATION SOURCE PROPERTIES**

Type/Producer: Pressurements deadweight tester P3223-1  
 SN: 66611  
 Uncertainty [%]: 0,01

**POLY FIT EQUATION:**

$Y = -248.95239552E+0X^0 + 124.84354439E+0X^1$

**CALIBRATION SUMMARY:**

Max Uncertainty : 0.053905 [%]  
 Max Uncertainty : 0.011813 [kPa]  
 RSQ : 1.000000  
 Calibration points : 16

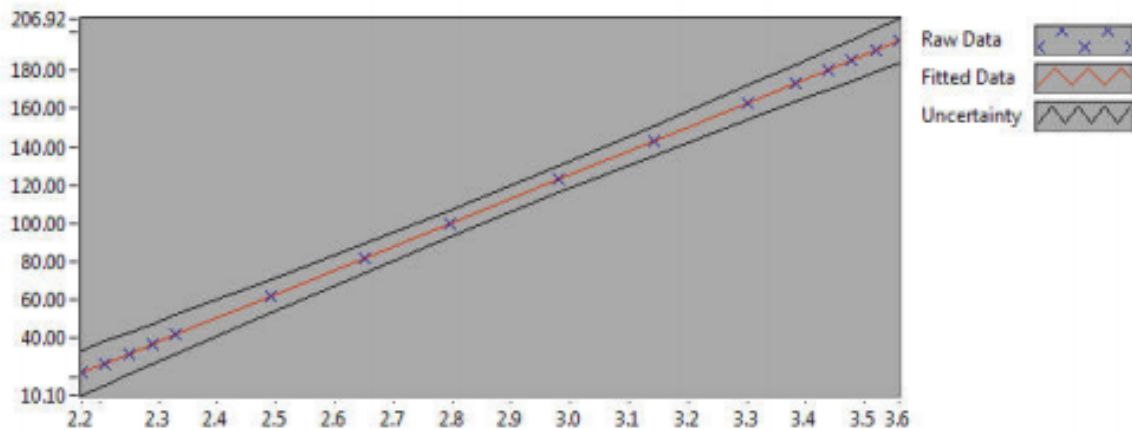


Figure 1 : Calibration chart (The uncertainty band is multiplied by 1000 )

Stian Solvik

**CALIBRATION VALUES**

<b>Value [kPa]</b>	<b>Voltage [V]</b>	<b>Best Poly Fit [kPa]</b>	<b>Deviation [kPa]</b>	<b>Uncertainty [%]</b>	<b>Uncertainty [kPa]</b>
21.914248	2.169599	21.908040	0.006208	0.053905	0.011813
26.921802	2.209730	26.918171	0.003631	0.042267	0.011379
31.929355	2.249798	31.920401	0.008954	0.034314	0.010956
36.936909	2.289981	36.936994	-0.000085	0.028544	0.010543
41.944462	2.330182	41.955782	-0.011320	0.024182	0.010143
61.974677	2.490651	61.989289	-0.014612	0.014043	0.008703
82.004891	2.651137	82.024972	-0.020081	0.009315	0.007639
100.082084	2.795562	100.055493	0.026591	0.007063	0.007069
123.116830	2.980306	123.119581	-0.002751	0.005803	0.007144
143.147044	3.140812	143.157653	-0.010608	0.005507	0.007883
163.217258	3.301317	163.195724	0.021534	0.005575	0.009099
173.232365	3.381561	173.213712	0.018653	0.005669	0.009821
180.242940	3.437843	180.240140	0.002800	0.005753	0.010369
185.250494	3.478023	185.256381	-0.005887	0.005821	0.010783
190.258047	3.518160	190.267163	-0.009115	0.005894	0.011214
195.265601	3.558309	195.279513	-0.013912	0.005959	0.011636

**COMMENTS:**

9 and 10 calibrated for high pres as well

---

The uncertainty is calculated with 95% confidence. The uncertainty includes the randomness in the calibrated instrument during the calibration, systematic uncertainty in the instrument or property which the instrument under calibration is compared with (dead weight manometer, calibrated weights etc.), and due to regression analysis to fit the calibration points to a linear calibration equation. The calculated uncertainty can be used as the total systematic uncertainty of the calibrated instrument with the given calibration equation.

## X. Pressure sensor at temperature inlet sensor

### CALIBRATION REPORT

---

#### **CALIBRATION PROPERTIES**

Calibrated by: Stian Solvik  
 Type/Producer: Druck PTX 610  
 SN: 4091551ref\_10  
 Range: 0-10 bar a  
 Unit: kPa  
 The king had a son  
 Druck PTX 1830  
 2867610  
 0-10 bar a  
 kPa

#### **CALIBRATION SOURCE PROPERTIES**

Type/Producer: Pressurements deadweight tester P3223-1  
 SN: 66611  
 Uncertainty [%]: 0,01

#### **POLY FIT EQUATION:**

$Y = -250.49471911E+0X^0 + 124.86102018E+0X^1$

#### **CALIBRATION SUMMARY:**

Max Uncertainty : 0.052476 [%]  
 Max Uncertainty : 0.011500 [kPa]  
 RSQ : 1.000000  
 Calibration points : 16

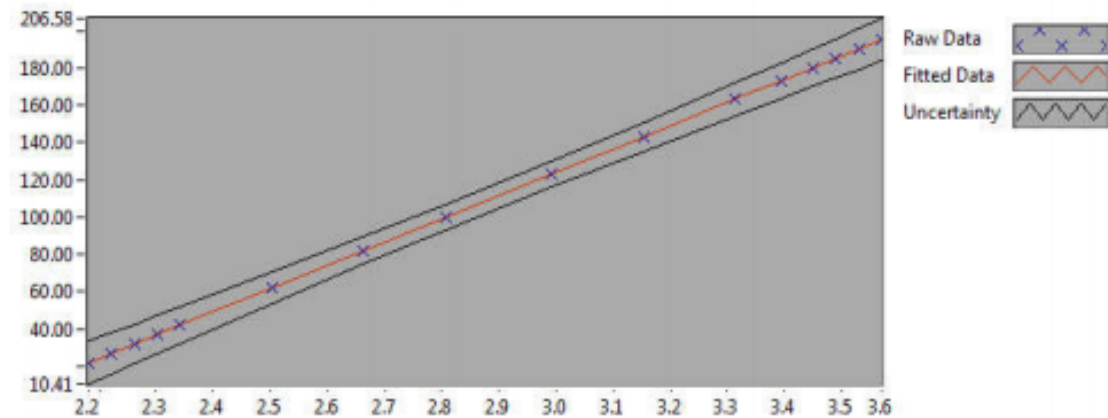


Figure 1 : Calibration chart (The uncertainty band is multiplied by 1000 )

---

Stian Solvik

**CALIBRATION VALUES**

<b>Value [kPa]</b>	<b>Voltage [V]</b>	<b>Best Poly Fit [kPa]</b>	<b>Deviation [kPa]</b>	<b>Uncertainty [%]</b>	<b>Uncertainty [kPa]</b>
21.914248	2.181665	21.910223	0.004025	0.052476	0.011500
26.921802	2.221798	26.921289	0.000513	0.041147	0.011077
31.929355	2.261842	31.921135	0.008220	0.033404	0.010666
36.936909	2.302009	36.936523	0.000385	0.027787	0.010264
41.944462	2.342191	41.953616	-0.009154	0.023539	0.009873
61.974677	2.502595	61.981886	-0.007209	0.013663	0.008467
82.004891	2.663143	82.028054	-0.023163	0.009038	0.007411
100.082084	2.807527	100.055942	0.026141	0.006869	0.006875
123.116830	2.992223	123.117259	-0.000429	0.005641	0.006945
143.147044	3.152736	143.159133	-0.012089	0.005349	0.007657
163.217258	3.313242	163.200040	0.017218	0.005413	0.008836
173.232365	3.393428	173.212101	0.020264	0.005508	0.009542
180.242940	3.449680	180.235883	0.007057	0.005592	0.010078
185.250494	3.489902	185.257962	-0.007468	0.005654	0.010475
190.258047	3.530042	190.269906	-0.011859	0.005722	0.010886
195.265601	3.570152	195.278054	-0.012453	0.005788	0.011301

**COMMENTS:**

9 and 10 calibrated for high pres as well

---

The uncertainty is calculated with 95% confidence. The uncertainty includes the randomness in the calibrated instrument during the calibration, systematic uncertainty in the instrument or property which the instrument under calibration is compared with (dead weight manometer, calibrated weights etc.), and due to regression analysis to fit the calibration points to a linear calibration equation. The calculated uncertainty can be used as the total systematic uncertainty of the calibrated instrument with the given calibration equation.



## XI. Atmospheric pressure sensor

### CALIBRATION REPORT

---

#### **CALIBRATION PROPERTIES**

Calibrated by: Stian Solvik  
 Type/Producer: Druck PTX 610  
 SN: 2480173ref\_11  
 Range: 0-2.5 bar a  
 Unit: kPa  
 The son had a cat  
 Druck PTX 1830  
 2867610  
 0-10 bar a  
 kPa

#### **CALIBRATION SOURCE PROPERTIES**

Type/Producer: Pressurements deadweight tester P3223-1  
 SN: 66611  
 Uncertainty [%]: 0,01

#### **POLY FIT EQUATION:**

$Y = -62.82826789E+0X^0 + 31.23197418E+0X^1$

#### **CALIBRATION SUMMARY:**

Max Uncertainty : 0.067928 [%]  
 Max Uncertainty : 0.014886 [kPa]  
 RSQ : 1.000000  
 Calibration points : 16

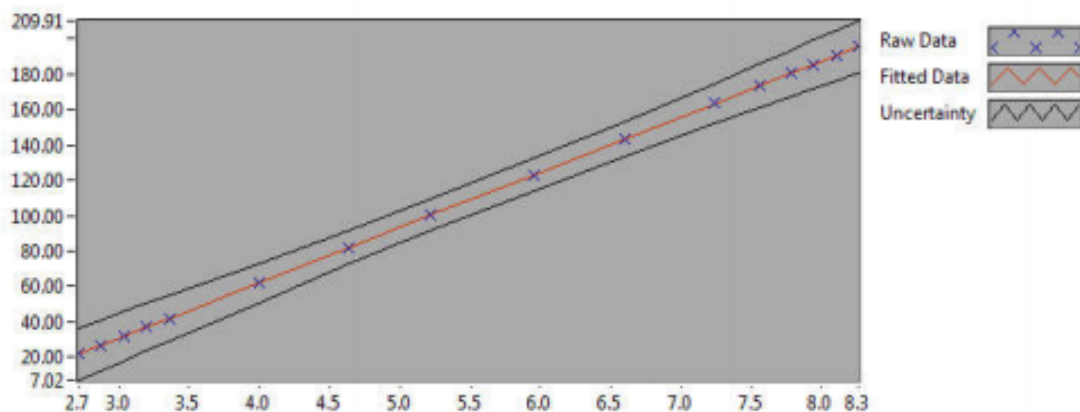


Figure 1 : Calibration chart (The uncertainty band is multiplied by 1000 )

---

Stian Solvik

**CALIBRATION VALUES**

<b>Value [kPa]</b>	<b>Voltage [V]</b>	<b>Best Poly Fit [kPa]</b>	<b>Deviation [kPa]</b>	<b>Uncertainty [%]</b>	<b>Uncertainty [kPa]</b>
21.914248	2.712905	21.901105	0.013143	0.067928	0.014886
26.921802	2.873195	26.907292	0.014510	0.053264	0.014340
31.929355	3.034100	31.932663	-0.003308	0.043233	0.013804
36.936909	3.194740	36.949775	-0.012866	0.035963	0.013283
41.944462	3.355276	41.963634	-0.019171	0.030466	0.012779
61.974677	3.996427	61.988031	-0.013354	0.017684	0.010959
82.004891	4.637815	82.019854	-0.014964	0.011695	0.009590
100.082084	5.215253	100.054376	0.027708	0.008890	0.008898
123.116830	5.953390	123.107864	0.008966	0.007299	0.008986
143.147044	6.595188	143.152460	-0.005416	0.006920	0.009906
163.217258	7.236801	163.191300	0.025958	0.007003	0.011430
173.232365	7.557640	173.211752	0.020613	0.007126	0.012345
180.242940	7.782384	180.230953	0.011988	0.007233	0.013036
185.250494	7.943489	185.262572	-0.012078	0.007315	0.013551
190.258047	8.103956	190.274281	-0.016233	0.007402	0.014083
195.265601	8.264587	195.291098	-0.025497	0.007488	0.014622

**COMMENTS:**

9 and 10 calibrated for high pres as well

---

The uncertainty is calculated with 95% confidence. The uncertainty includes the randomness in the calibrated instrument during the calibration, systematic uncertainty in the instrument or property which the instrument under calibration is compared with (dead weight manometer, calibrated weights etc.), and due to regression analysis to fit the calibration points to a linear calibration equation. The calculated uncertainty can be used as the total systematic uncertainty of the calibrated instrument with the given calibration equation.



# Appendix N Data sheet -Accelerometers

## I. Accelerometer 1

**Calibration Chart for DeltaTron<sup>®</sup> Accelerometer Type 4397**

Serial No.: .....**32166**.....

Reference Sensitivity<sup>1)</sup> at 159.2 Hz ( $\omega = 1000 \text{ s}^{-1}$ ), 20 ms<sup>2</sup> RMS, 4 mA supply current and 23.1 °C: .....**9.918**..... mV/g

Frequency Range: .....**1 Hz to 25 kHz**.....  
 Amplitude ( $\pm 10\%$ ): .....**0.12**..... mV/ms<sup>2</sup> ( $\pm 10\%$ )  
 Phase ( $\pm 5^\circ$ ): .....**0.12**..... Hz to 2.5 kHz

Mounted Resonance Frequency: .....**53**..... kHz

Transverse Sensitivity<sup>2)</sup>: .....**0.12**..... %  
 Maximum (at 50 Hz, 100 ms<sup>-2</sup>): .....**0.12**..... %  
 Angle of minimum,  $\alpha$ : (see drawing) .....**1.30**..... °

Transverse Resonance Frequency: .....**17**..... kHz

Calculated values for TEDS<sup>3)</sup>:

Resonance frequency: .....**53.2**..... kHz  
 Quality factor  $Q_{1dB}$ : .....**1.2**.....  
 Amplitude slope: .....**-2.2**..... dB/octave  
 High pass cut-off frequency: .....**0.12**..... Hz  
 Low pass cut-off frequency: .....**3.9**..... kHz

Measuring Range:  $T < 100^\circ\text{C}$ :  $\pm 7500 \text{ ms}^{-2}$  peak ( $\pm 750 \text{ g}$  peak)  
 $T < 125^\circ\text{C}$ :  $\pm 5000 \text{ ms}^{-2}$  peak ( $\pm 500 \text{ g}$  peak)

Polarity of the electrical signal is positive for an acceleration in the direction of the arrow on the drawing.

**Electrical:**

Bias Voltage: .....**+12 V  $\pm$  0.5 V**..... at full temperature and current range; .....**+8 V to +15 V**..... at 25°C and 4 mA;  
 Power Supply requirements: Constant Current:  $T < 100^\circ\text{C}$ : .....**+2 to +20 mA**.....  
 $T < 125^\circ\text{C}$ : .....**+2 to +10 mA**.....  
 Unloaded Supply Voltage: .....**+24 V to +30 V**.....

Output Impedance: .....**10  $\Omega$** .....

Start-up time (to final bias  $\pm 10\%$ ): .....**5**..... s

Inherent Noise (RMS): .....**< 15  $\mu\text{V}$** .....  
 Broadband (1 Hz to 22 kHz): .....**corresponding to  $< 0.015 \text{ ms}^{-2}$  ( $< 1500 \mu\text{g}$ )**.....  
 Spectral: .....**7.9  $\times 10^{-4} \text{ ms}^{-2}/\sqrt{\text{Hz}}$  ( $79 \mu\text{g}/\sqrt{\text{Hz}}$ )**..... at 10 Hz  
 .....**2.1  $\times 10^{-4} \text{ ms}^{-2}/\sqrt{\text{Hz}}$  ( $21 \mu\text{g}/\sqrt{\text{Hz}}$ )**..... at 100 Hz  
 .....**1.4  $\times 10^{-4} \text{ ms}^{-2}/\sqrt{\text{Hz}}$  ( $14 \mu\text{g}/\sqrt{\text{Hz}}$ )**..... at 1000 Hz

Ground Loops can introduce error signals. These can be avoided by insulating the accelerometer from the mounting surface using Insulating Stud UA 1216.

Recommended cable: .....**AO 1381**.....

**Environmental:**

Temperature Range: .....**-50 to +125°C (-58 to +257**.....  
 Temperature Coefficient of Sensitivity: .....**+0.05%**.....  
 Temp. Transient Sensitivity (3 Hz Low Lim. Freq. (-3 dB, 6 dB/oct)): .....**2 ms<sup>2</sup>**.....  
 Magnetic Sensitivity (50 Hz, 0.038 T): .....**50 ms**.....  
 Acoustic Sensitivity (154 dB SPL): .....**0.01 #**.....

Base Strain Sensitivity (at 250  $\mu\text{r}$  in base plane): .....**0.065 ms<sup>-2</sup>**.....  
 Max. Non-destructive Shock: Axial: .....**100 kms<sup>-2</sup> peak (10000 g peak)**.....  
 Transverse: .....**50 kms<sup>-2</sup> peak (5000 g peak)**.....  
 Humidity: .....**90 % RH non-condens**.....

**Mechanical:**

Case Material: .....**Titanium ASTM Grac**.....  
 Sensing Element: .....**Piezoelectric, Type P2**.....  
 Construction: .....**Delta She**.....  
 Sealing: .....**Wet**.....  
 Weight: .....**2.4 gram (0.085**.....  
 Electrical Connector: .....**Coaxial**.....  
 Mounting Thread: .....**M3, Depth 2.4**.....

Mounting Surface Flatness: .....**Max. 0.6 Nm (5.3 lbf-in), Min. 0.2 Nm (1.8 lb**.....  
 Mounting Torque: .....**< 3**.....

<sup>1)</sup> This calibration is obtained on a modified Brüel & Kjær Calibration System Type 9610 System No. 150187.3 and is traceable (amplitude only) to the National Institute of Standards and Technology, USA and Physikalisch-Technische Bundesanstalt, Germany.

The expansion uncertainty is 5 Hz to 4 kHz: 10%, 4 kHz to 7 kHz: 1.4% and 7 kHz to 10 kHz: 2.0% is determined in accordance with IEC 61221. A coverage factor  $k=2$  is used. This corresponds to a coverage probability of 95% for a normal distribution.

<sup>2)</sup> The uncertainty is 0.3% of Reference Sensitivity and 5° on the angle.

<sup>3)</sup> Transducer Electronic Data Sheet according to IEEE P451.4. Built-in ID-information not included.

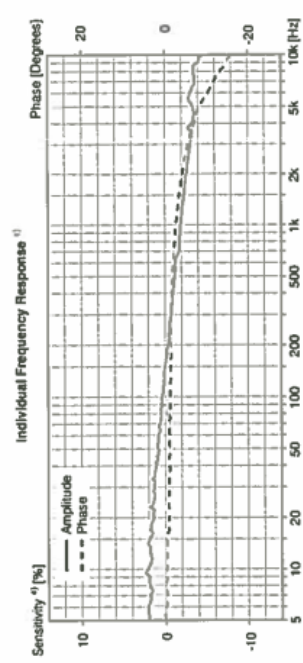
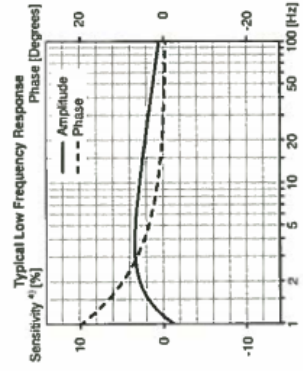
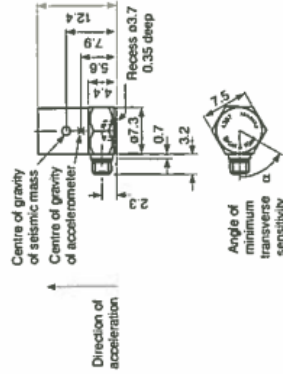
<sup>4)</sup> Division from Reference Sensitivity.

For further information, please see <http://www.bkbr.com> and Product Data Sheet BP 1268 and BP 1848.

**Mounting Technique:**

Examine the mounting surface for cleanliness and smoothness. If necessary, machine surface to a flatness  $< 10 \mu\text{m}$  and a roughness  $< 2 \mu\text{m}$ . Fasten the accelerometer using the appropriate stud. Take care not to exceed the recommended mounting torque and that the stud does not bottom in the mounting hole.

A thin film of oil or grease between the accelerometer and the mounting surface helps achieve good contact and improves mounting stiffness. For other types of mounting, see the Brüel & Kjær handbook "Piezoelectric Accelerometers and Vibration Preamplifiers" (available from your local Brüel & Kjær representative).



Date **07 Feb 2014**, 07.13 Operator .....**JF**.....  
 Specifications obtained in accordance with ANSI S2.11-1959 and parts of ISO 5347.  
 All values are typical at 25°C (77°F) unless measurement uncertainty is specified. BC 0025-13

## II. Accelerometer 2

### Calibration Chart for DeltaTron® Accelerometer Type 4397



**Brüel & Kjær**

Serial No.: 32166

Reference Sensitivity <sup>1)</sup> at 159.2 Hz ( $\omega = 1000 \text{ s}^{-1}$ ): 20  $\text{ms}^{-2}$  RMS.  
4 mA supply current and 23.1°C: 1.011  $\text{mV/ms}^2$  ( 9.918  $\text{mV/g}$ )

Frequency Range: Amplitude ( $\pm 10\%$ ): 1 Hz to 25 kHz  
Phase ( $\pm 5^\circ$ ): 4 Hz to 2.5 kHz

Mounted Resonance Frequency: 53 kHz  
Transverse Sensitivity <sup>2)</sup>:  
Maximum (at 30 Hz, 100  $\text{ms}^{-2}$ ): 2.2 % re Reference Sensitivity  
Angle of minimum,  $\alpha$ : (see drawing) 1.30°

Transverse Resonance Frequency:  
Calculated values for TEDS <sup>3)</sup>: Resonance frequency: 59.2 kHz  
Quality factor  $Q_{\text{ref}}$ : 1.78  
Amplitude slope: -2.2%/decade  
High pass cut-off frequency: 0.12 Hz  
Low pass cut-off frequency: 39 kHz

Measuring Range: T < 100°C:  $\pm 7500 \text{ ms}^{-2}$  peak ( $\pm 750 \text{ g}$  peak)  
T < 125°C:  $\pm 5000 \text{ ms}^{-2}$  peak ( $\pm 500 \text{ g}$  peak)

Polarity of the electrical signal is positive for an acceleration in the direction of the arrow on the drawing.

### Electrical:

Bias Voltage: at 25°C and 4 mA: +12 V  $\pm 0.5$  V  
at full temperature and current range: +6 V to +15 V  
Power Supply requirements: Constant Current: T < 100°C: +2.10 to +20 mA  
T < 125°C: +2.10 to +10 mA  
Unloaded Supply Voltage: +24 V to +30 V  
Output Impedance: 10  $\Omega$   
Start-up time (to final bias  $\pm 10\%$ ): 5 s  
Inherent Noise (RMS): < 15  $\mu\text{V}$   
Bandwidth (1 Hz to 22 kHz): corresponding to < 0.015  $\text{ms}^{-2}$  ( $< 15000 \mu\text{g}$ )  
Spectral: 10 Hz: 7.9x10<sup>-4</sup>  $\text{ms}^{-2}/\sqrt{\text{Hz}}$  (79  $\mu\text{g}/\sqrt{\text{Hz}}$ )  
100 Hz: 2.1x10<sup>-4</sup>  $\text{ms}^{-2}/\sqrt{\text{Hz}}$  (21  $\mu\text{g}/\sqrt{\text{Hz}}$ )  
1000 Hz: 1.4x10<sup>-4</sup>  $\text{ms}^{-2}/\sqrt{\text{Hz}}$  (14  $\mu\text{g}/\sqrt{\text{Hz}}$ )  
Ground Loops can introduce error signals. These can be avoided by insulating the accelerometer from the mounting surface using Insulating Stud UA 1216.  
Recommended cable: AO 1381

### Environmental:

Temperature Range: -50 to +125°C (-58 to +257°F)  
Temperature Coefficient of Sensitivity: +0.05%/°C  
Temp. Transient Sensitivity (3 Hz Low Lim. Freq. (-3 dB, 6 dB/oct)): 2  $\text{ms}^{-2}/\text{°C}$   
Magnetic Sensitivity (50 Hz, 0.038 T): 50  $\text{ms}^{-2}/\text{T}$   
Acoustic Sensitivity (154 dB SPL): 0.01  $\text{ms}^{-2}$   
Base Strain Sensitivity (at 250  $\mu\text{r}$  in base plane): 0.005  $\text{ms}^{-2}/\mu\text{r}$   
Max. Non-destructive Shocks: Axial: 100  $\text{kms}^{-2}$  peak (10000 g peak)  
Transverse: 50  $\text{kms}^{-2}$  peak (5000 g peak)  
90 % RH non-condensing  
Humidity: 90 % RH non-condensing

### Mechanical:

Case Material: Titanium ASTM Grade 2  
Sensing Element: Piezoelectric, Type PZ 23  
Construction: Delta Shear<sup>®</sup>  
Sealing: Welded  
Weight: 2.4 gram (0.085 oz)  
Electrical Connector: Coaxial M3  
Mounting Thread: M3, Depth 2.4 mm  
Mounting Surface Flatness: < 3  $\mu\text{m}$   
Mounting Torque: Max. 0.6 Nm (5.3 lbf-in). Min. 0.2 Nm (1.8 lbf-in)

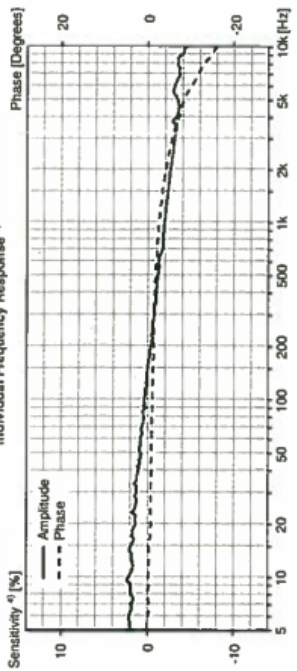
<sup>1)</sup> This calibration is obtained on a modified Brüel & Kjær Calibration System Type 9610.5, item No. 150157.9 and is traceable (unlike only) to the National Institute of Standards and Technology, USA and Physikalisch-Technische Bundesanstalt, Germany.  
The excluded uncertainty 5 Hz to 4 kHz: 1.0%, 4 kHz to 7 kHz: 1.4%, 7 kHz to 10 kHz: 2.0%. It is determined in accordance with EAL-PZ. A coverage factor k=2 is used. This corresponds to a coverage probability of 95% for a normal distribution.

<sup>2)</sup> The uncertainty is 0.2% of Reference Sensitivity and 5° on the angle.

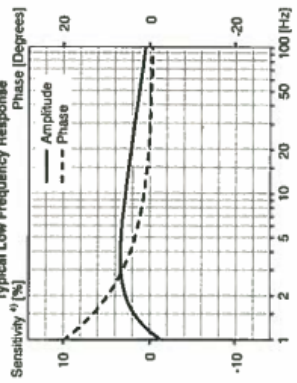
<sup>3)</sup> Transducer Electronic Data Sheet according to IEEE P1451.4. Built-in ID-information not included.  
<sup>4)</sup> Deviation from Reference Sensitivity.  
For further information, please see <http://www.bkav.com> and Product Data Sheet BP 1268 and BP 1043.



Individual Frequency Response <sup>1)</sup>

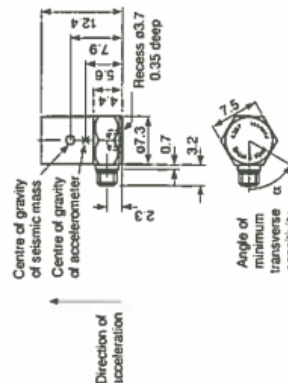


Typical Low Frequency Response



### Mounting Technique:

Examine the mounting surface for cleanliness and smoothness.  
If necessary, machine surface to a flatness < 10  $\mu\text{m}$  and a roughness < 2  $\mu\text{m}$ .  
Fasten the accelerometer using the appropriate stud. Take care not to exceed the recommended mounting torque and that the stud does not bottom in the mounting hole.  
A thin film of oil or grease between the accelerometer and the mounting surface helps achieve good contact and improves mounting stiffness.  
See also ISO 5348. For other types of mounting, see the Brüel & Kjær handbook 'Piezoelectric Accelerometers and Vibration Preamplifiers' (available from your local Brüel & Kjær representative).



Serial No.: 32166

Date: 07 Feb 2014, 07:13 Operator: JF  
Specifications obtained in accordance with ANSI S2.11-1989 and parts of ISO 5347.  
All values are typical at 25°C (77°F) unless measurement uncertainty is specified. BC 0026-13

III. Accelerometer 3, 4 and 5

**Entran<sup>®</sup> International**  
 EUROPEAN HEADQUARTERS 14365 Les Clayes-sous-Bois, FRANCE

**Accelerometer**

Model: EGAS-FS-25 Range (X/Y/Z): + 25 g  
 S/N: W5486 Useful Frequency: \*\* Hz, Do Not Exceed: \_\_\_\_\_ Hz  
 Sensitivity (X/Y/Z): 3.620 mV/g mV/g Excitation: 15 V  
 Input Imped. (X/Y/Z): 1325 ohms  
 Output Imped. (X/Y/Z): 1481 ohms  
 Leg 1 / Leg 2: \_\_\_\_\_ ohms

Wiring Code:  +In=Red +Out=Gm  
                    -In=Blk -Out=Wht  
 +In=Red +Out=Gm  
 -In=Blk

Bridge Compl:  
 See Calibration Sheet

**\*\* : See curve**

**SENSITIVE INSTRUMENT - DO NOT DROP  
 READ INSTRUCTION MANUAL BEFORE USE**



**Entran<sup>®</sup> International**  
 EUROPEAN HEADQUARTERS 11179 Les Clayes-sous-Bois, FRANCE

**Accelerometer**

Model: EGAS-FS-50D Range (X/Y/Z): + 50 g  
 S/N: X3-131 Useful Frequency: \*\* Hz, Do Not Exceed: \_\_\_\_\_ Hz  
 Sensitivity (X/Y/Z): 1.78 mV/g mV/g Excitation: 15 V  
 Input Imped. (X/Y/Z): 1309 ohms  
 Output Imped. (X/Y/Z): 1436 ohms  
 Leg 1 / Leg 2: \_\_\_\_\_ ohms

Wiring Code:  +In=Red +Out=Gm  
                    -In=Blk -Out=Wht  
 +In=Red +Out=Gm  
 -In=Blk

Bridge Compl:  
 See Calibration Sheet

**\*\* : SEE CURVE**

**SENSITIVE INSTRUMENT - DO NOT DROP  
 REA**



ITE Vannkrftlaboratoriet  
 NTNU 4421-4

**Entran<sup>®</sup> International**  
 EUROPEAN HEADQUARTERS 14365 Les Clayes-sous-Bois, FRANCE

**Accelerometer**


Model: EGAS-FS-25 Range (X/Y/Z): + 25 g  
 S/N: W5485 Useful Frequency: \*\* Hz, Do Not Exceed: \_\_\_\_\_ Hz  
 Sensitivity (X/Y/Z): 3.496 mV/g mV/g Excitation: 15 V  
 Input Imped. (X/Y/Z): 1313 ohms  
 Output Imped. (X/Y/Z): 1455 ohms  
 Leg 1 / Leg 2: \_\_\_\_\_ ohms

Wiring Code:  +In=Red +Out=Gm  
                    -In=Blk -Out=Wht  
 +In=Red +Out=Gm  
 -In=Blk

Bridge Compl:  
 See Calibration Sheet

**\*\* : See curve**

**SENSITIVE INSTRUMENT - DO NOT DROP  
 READ INSTRUCTION MANUAL BEFORE USE**





## Appendix O Data sheet-Temperature Sensors



sea-birdscientific.com  
info@sea-birdscientific.com

### SBE 38 Digital Oceanographic Thermometer

Sophisticated A/D acquisition electronics, ultra-stable thermistor, and state-of-the-art calibration provide the standards-level performance of an expensive AC bridge and platinum thermometer at a small fraction of the cost. The SBE 38 is unaffected by shock and vibration, has high accuracy and stability, and is easy to use. It has a rugged, 10,500 m titanium housing. Real-time temperature is transmitted via the RS-232 or RS-485 serial interface in ASCII characters (°C or raw counts). The SBE 38 must be externally powered, and its data logged or telemetered by a computer, data logger, or instrument.

Applications include calibration baths, oceanographic/aquatic research, and environmental monitoring. The SBE 38 is frequently integrated as a remote temperature sensor with an SBE 21 Thermosalinograph or SBE 45 MicroTSG, to provide accurate sea surface temperature. It can also be integrated as a secondary temperature sensor with an SBE 16plus, 16plus-IM, 16plus V2, 16plus-IM V2, 19plus V2, or 25plus CTD.



#### Features

- Programmable sampling:
  - Continuous (begins when power applied or on command);  
interval between samples (sec) =  $(0.133 * N_{Avg}) + 0.339$  where  $N_{Avg}$  is number of acquisition cycles/sample.
  - Polled.
- Serial output:
  - RS-232 (full duplex) with one SBE 38 connected to the interface;
  - RS-485 (half duplex) with one SBE 38 connected to the interface; or
  - RS-485 (half duplex) with several RS-485 sensors sharing one pair of wires (cannot sample continuously).
- No batteries or memory.
- Compatible with Sea-Bird thermosalinographs and some Sea-Bird CTDs.
- Titanium housing; depths to 10,500 m.
- Seasoft® V2 Windows software package (instrument setup and data display).
- Five-year limited warranty.

#### Options

- RS-232 or RS-485 output.
- XSG or wet-pluggable MCBH connector.

www.seabird.com

sales@seabird.com

+1 425-643-9866

**SBE** Sea-Bird  
Electronics

**Calibration**

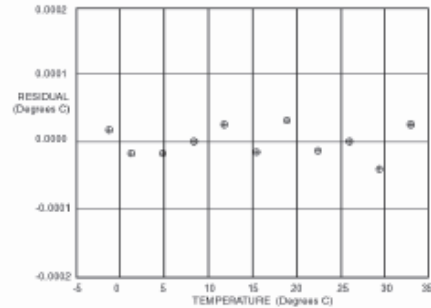
The SBE 38 is calibrated in Sea-Bird's state-of-the-art calibration laboratory, which maintains primary temperature standards (water triple point [TPW] and gallium melting point [GaMP] cells), ITS-90 certified and standards-grade platinum resistance thermometers, and a low-gradient temperature bath. Temperature is computed using the Steinhart-Hart polynomial (Steinhart and Hart, 1968; Bennett, 1972). The equation characterizes the non-linear temperature versus resistance response of the sensor. Thermistors require individualized coefficients to the Steinhart-Hart equation, because the material is an individualized mix of dopants:

$$t_{\text{out}} = \left[ \frac{1.0}{(a_0 + a_1 \cdot \ln(n) + a_2 \cdot \ln^2(n) + a_3 \cdot \ln^3(n))} - 273.15 \right] \cdot \text{Slope} + \text{Offset } [^{\circ}\text{C}]$$

where n is SBE 38 output.

**Example Calibration Data** (sensor serial number 80, 02 Sept 1997):  
 a0 = -2.809379e-05    a2 = -2.619655e-06    a1 = 2.783483e-04    a3 = 1.598734e-07

Bath Temperature [°C]	Instrument Output [n]	Instrument Temperature [°C]	Residual (Instrument - Bath) [°C]
-1.52985	824162.7	-1.52983	0.00002
1.03108	733633.1	1.03106	-0.00002
4.80520	625547.1	4.80518	-0.00002
8.11169	536776.4	8.11169	-0.00000
11.61533	462132.6	11.61536	0.00003
15.17575	398167.3	15.17574	-0.00001
18.63931	345476.6	18.63934	0.00003
22.14032	300170.8	22.14031	-0.00001
25.66793	261276.6	25.66793	0.00000
29.13948	228549.1	29.13944	-0.00004
32.61481	200420.3	32.61484	0.00003



**Performance**

Measurement Range	-5 to +35 °C
Initial Accuracy <sup>1</sup>	± 0.001 °C (1 mK)
Typical Stability	0.001 °C (1 mK) in six months, certified
Resolution	0.00025 °C (0.25 mK)
Response Time <sup>2</sup>	500 msec
Self-heating Error	< 200 µK

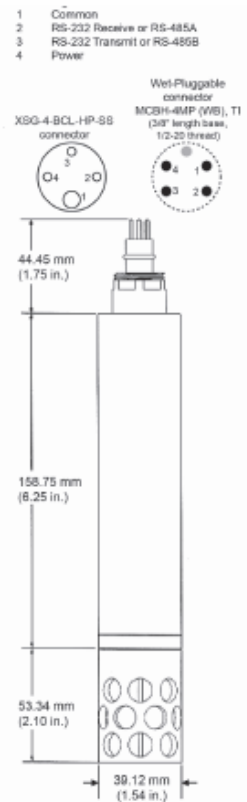
<sup>1</sup> NIST-traceable calibration applying over the entire range.  
<sup>2</sup> Time to reach 63% of final value following a step change in temperature

**Electrical**

Output Signal	RS-232 or RS-485 (half-duplex)
Input Power	8-15 VDC at 15 mA average for RS-232 output; 8-15 VDC at 10 mA average for RS-485 output

**Mechanical**

Housing & Depth rating	Titanium, 10,500 m
Weight	0.9 kg in air, 0.5 kg in water



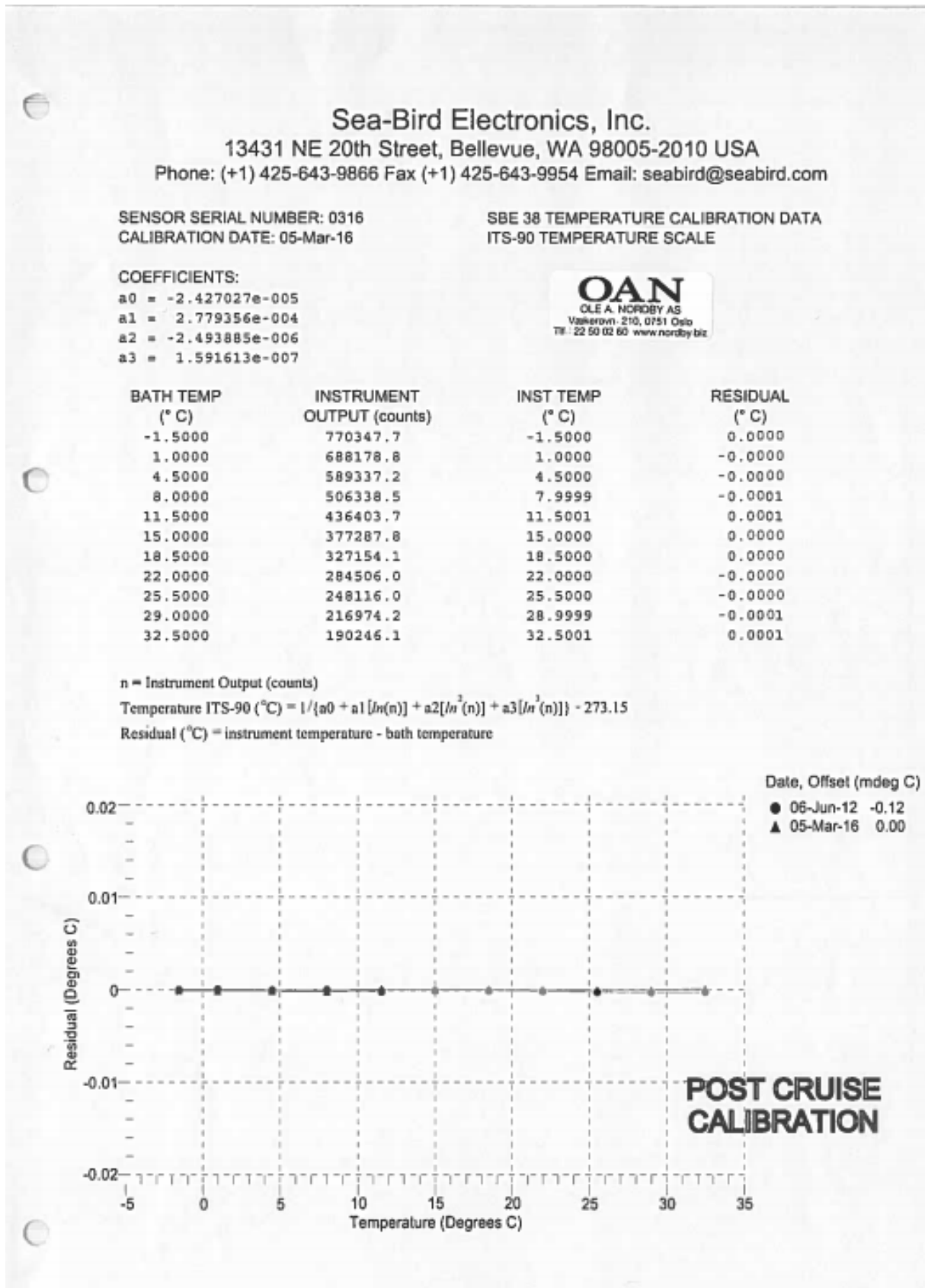
Specifications subject to change without notice. ©2014 Sea-Bird Scientific. All rights reserved. Rev. August 2015



Sea-Bird Electronics  
 +1 425-643-9866  
 sales@seabird.com  
 www.seabird.com

# Appendix P Calibration Temperature Sensor

## I. Temperature sensor nr.01



**SBE** SEA-BIRD ELECTRONICS, INC.  
 13431 NE 20th St. Bellevue, Washington 98005 USA  
 Phone: (425) 643-9866 Fax: (425) 643-9954 www.seabird.com

### Temperature Calibration Report

Customer:	Ole A. Nordby AS		
Job Number:	88645	Date of Report:	3/8/2016
Model Number:	SBE 38	Serial Number:	3844844-0316

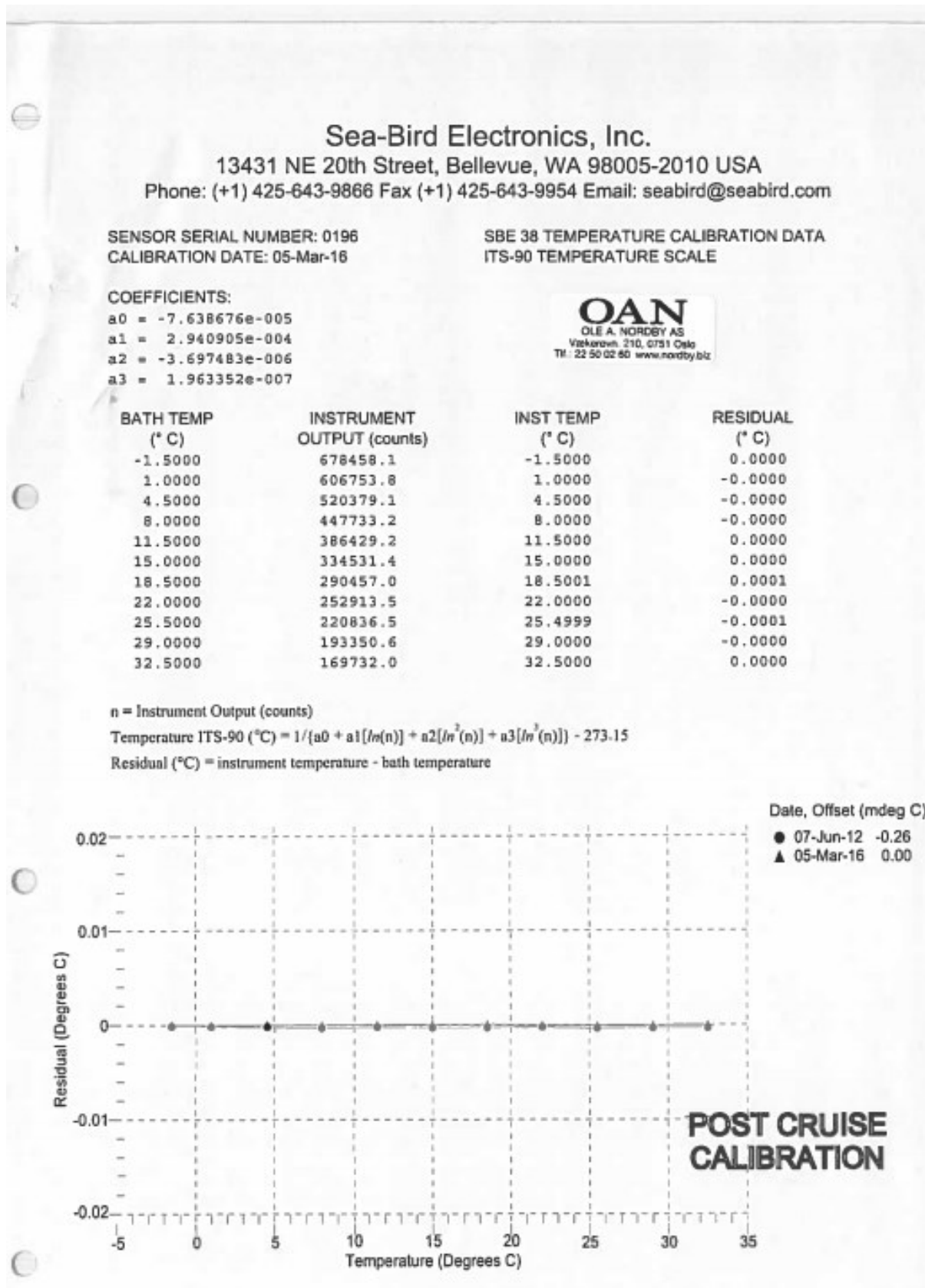
*Temperature sensors are normally calibrated 'as received', without adjustments, allowing a determination sensor drift. If the calibration identifies a problem, then a second calibration is performed after work is completed. The 'as received' calibration is not performed if the sensor is damaged or non-functional, or by customer request.*

*An 'as received' calibration certificate is provided, listing coefficients to convert sensor frequency to temperature. Users must choose whether the 'as received' calibration or the previous calibration better represents the sensor condition during deployment. In SEASOFT enter the chosen coefficients. The coefficient 'offset' allows a small correction for drift between calibrations (consult the SEASOFT manual). Calibration coefficients obtained after a repair apply only to subsequent data.*

'AS RECEIVED CALIBRATION'  Performed  Not Performed  
 Date:  Drift since last cal:  Degrees Celsius/year  
 Comments:

'CALIBRATION AFTER REPAIR'  Performed  Not Performed  
 Date:  Drift since Last cal:  Degrees Celsius/year  
 Comments:

II. Temperature sensor nr-02





**SBE** SEA-BIRD ELECTRONICS, INC.  
 13431 NE 20th St. Bellevue, Washington 98005 USA  
 Phone: (425) 643-9866 Fax: (425) 643-9954 www.seabird.com

### Temperature Calibration Report

Customer:	Ole A. Nordby AS		
Job Number:	88673	Date of Report:	3/7/2016
Model Number:	SBE 38	Serial Number:	3832689-0196

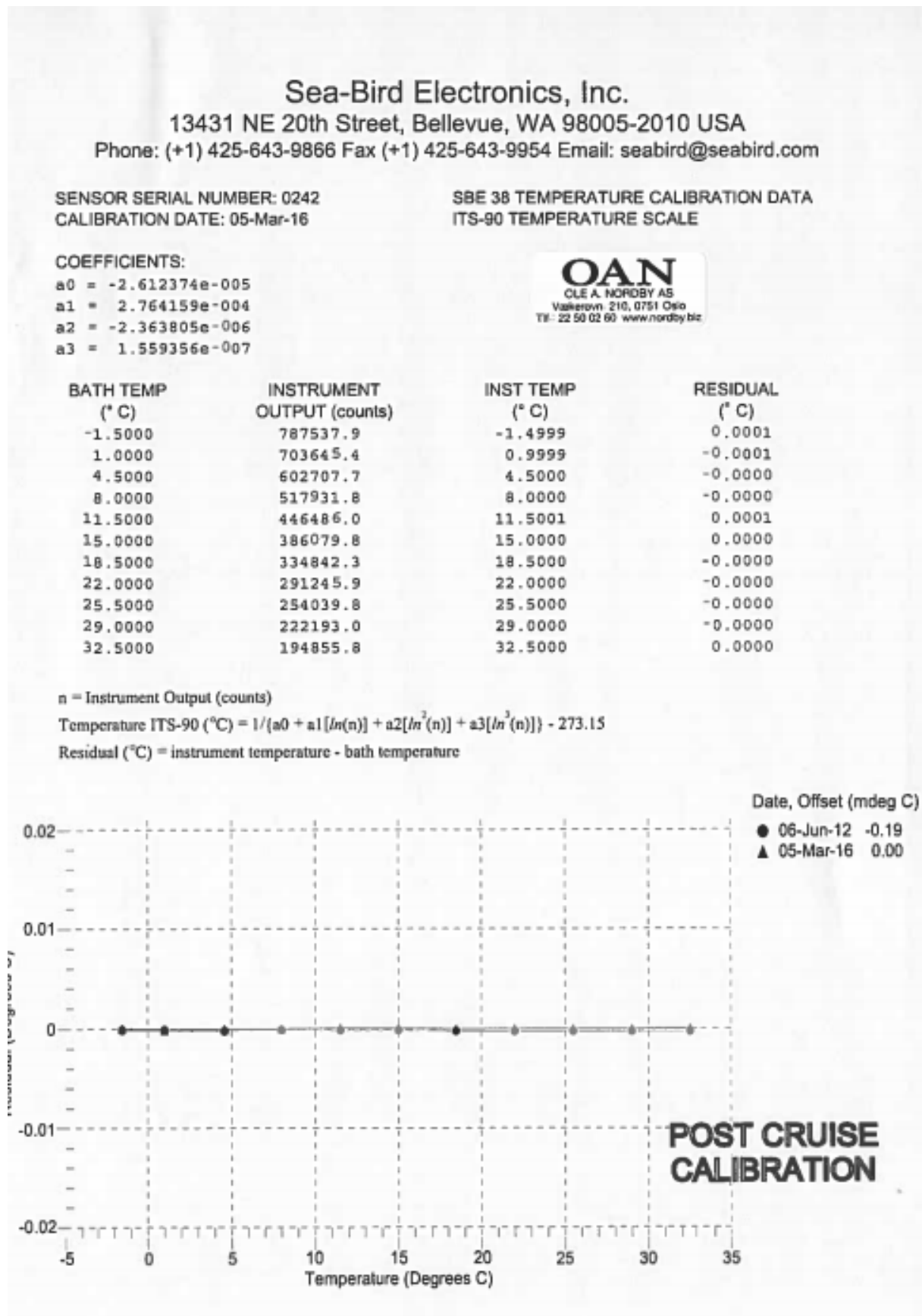
*Temperature sensors are normally calibrated 'as received', without adjustments, allowing a determination sensor drift. If the calibration identifies a problem, then a second calibration is performed after work is completed. The 'as received' calibration is not performed if the sensor is damaged or non-functional, or by customer request.*

*An 'as received' calibration certificate is provided, listing coefficients to convert sensor frequency to temperature. Users must choose whether the 'as received' calibration or the previous calibration better represents the sensor condition during deployment. In SEASOFT enter the chosen coefficients. The coefficient 'offset' allows a small correction for drift between calibrations (consult the SEASOFT manual). Calibration coefficients obtained after a repair apply only to subsequent data.*

'AS RECEIVED CALIBRATION'  Performed  Not Performed  
 Date:  Drift since last cal:  Degrees Celsius/year  
 Comments:

'CALIBRATION AFTER REPAIR'  Performed  Not Performed  
 Date:  Drift since Last cal:  Degrees Celsius/year  
 Comments:

## III. Temperature sensor nr.03







## SEA-BIRD ELECTRONICS, INC.

13431 NE 20th St. Bellevue, Washington 98005 USA

Phone: (425) 643-9866 Fax: (425) 643-9954 www.seabird.com

### Temperature Calibration Report

Customer:	Ole A. Nordby AS		
Job Number:	88673	Date of Report:	3/7/2016
Model Number:	SBE 38	Serial Number:	3839551-0242

*Temperature sensors are normally calibrated 'as received', without adjustments, allowing a determination sensor drift. If the calibration identifies a problem, then a second calibration is performed after work is completed. The 'as received' calibration is not performed if the sensor is damaged or non-functional, or by customer request.*

*An 'as received' calibration certificate is provided, listing coefficients to convert sensor frequency to temperature. Users must choose whether the 'as received' calibration or the previous calibration better represents the sensor condition during deployment. In SEASOFT enter the chosen coefficients. The coefficient 'offset' allows a small correction for drift between calibrations (consult the SEASOFT manual). Calibration coefficients obtained after a repair apply only to subsequent data.*

#### 'AS RECEIVED CALIBRATION'

Performed  Not Performed

Date:

Drift since last cal:  Degrees Celsius/year

Comments:

#### 'CALIBRATION AFTER REPAIR'

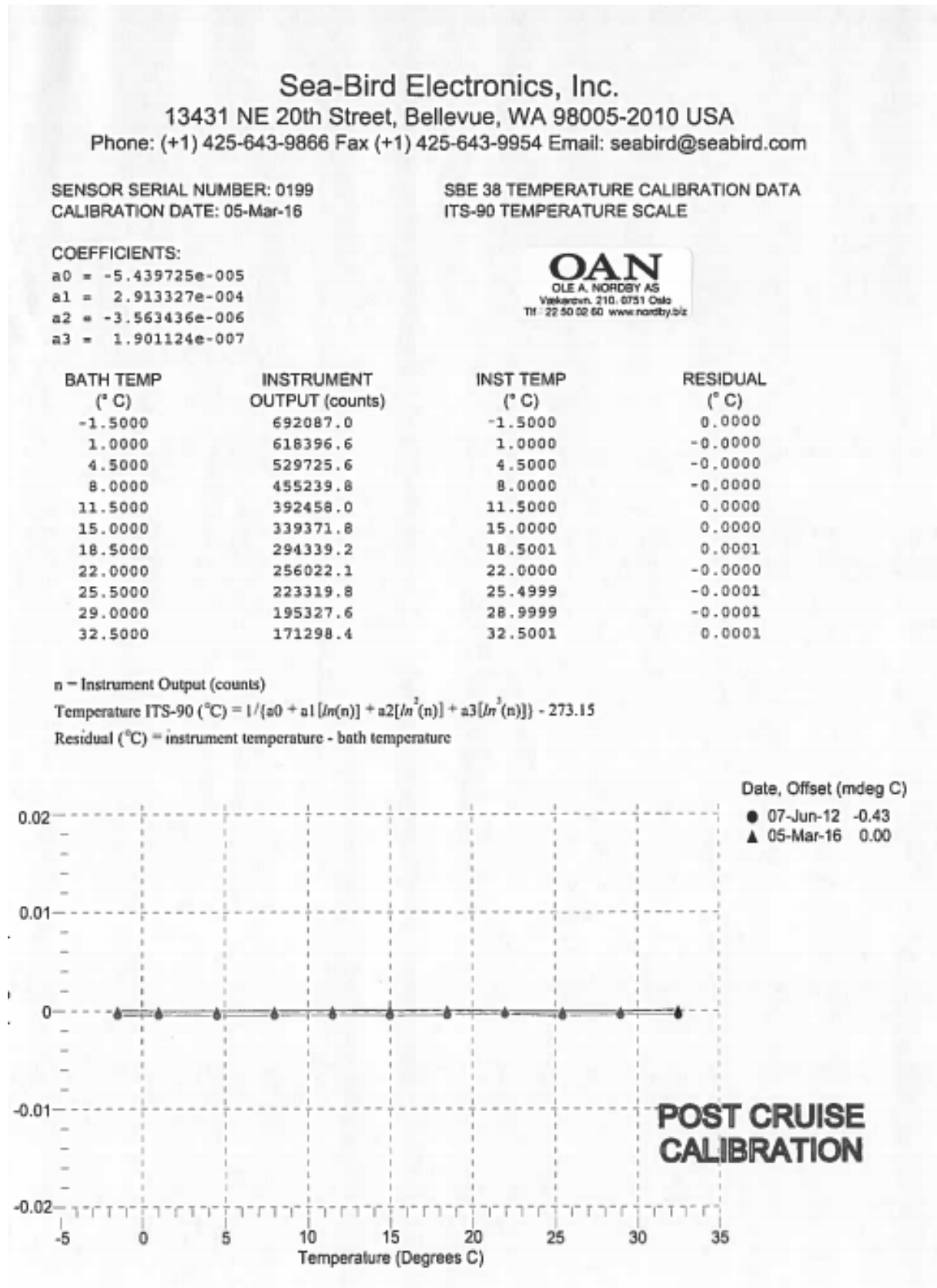
Performed  Not Performed

Date:

Drift since Last cal:  Degrees Celsius/year

Comments:

**IV. Temperature sensor nr.04**





## SEA-BIRD ELECTRONICS, INC.

13431 NE 20th St. Bellevue, Washington 98005 USA

Phone: (425) 643-9866 Fax: (425) 643-9954 www.seabird.com

### Temperature Calibration Report

Customer:	Ole A. Nordby AS		
Job Number:	88673	Date of Report:	3/7/2016
Model Number	SBE 38	Serial Number:	3832689-0199

*Temperature sensors are normally calibrated 'as received', without adjustments, allowing a determination sensor drift. If the calibration identifies a problem, then a second calibration is performed after work is completed. The 'as received' calibration is not performed if the sensor is damaged or non-functional, or by customer request.*

*An 'as received' calibration certificate is provided, listing coefficients to convert sensor frequency to temperature. Users must choose whether the 'as received' calibration or the previous calibration better represents the sensor condition during deployment. In SEASOFT enter the chosen coefficients. The coefficient 'offset' allows a small correction for drift between calibrations (consult the SEASOFT manual). Calibration coefficients obtained after a repair apply only to subsequent data.*

#### 'AS RECEIVED CALIBRATION'

Performed  Not Performed

Date:

Drift since last cal:  Degrees Celsius/year

Comments:

#### 'CALIBRATION AFTER REPAIR'

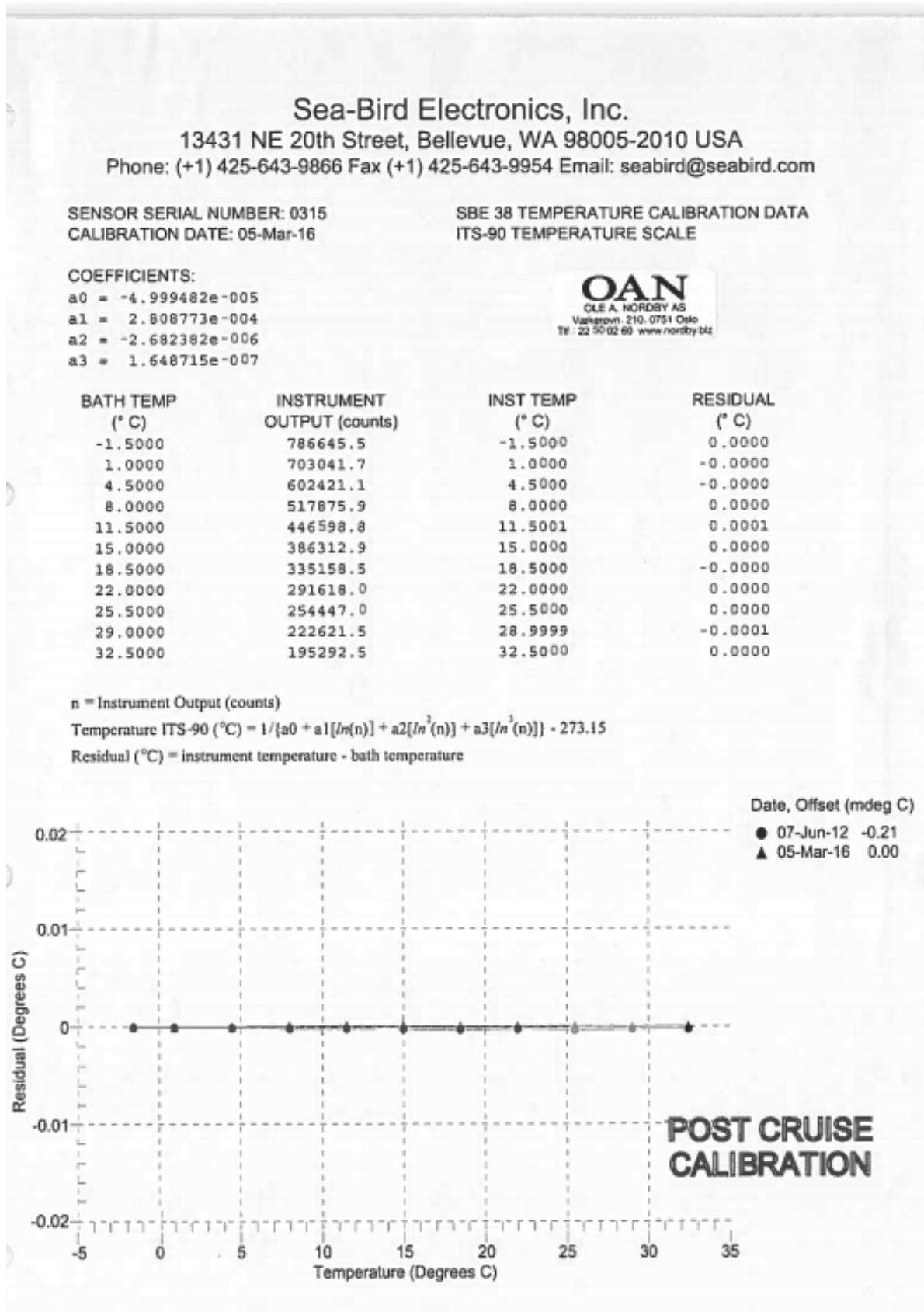
Performed  Not Performed

Date:

Drift since Last cal:  Degrees Celsius/year

Comments:

V. Temperature sensor nr.05



**SBE** SEA-BIRD ELECTRONICS, INC.  
 13431 NE 20th St. Bellevue, Washington 98005 USA  
 Phone: (425) 643-9866 Fax: (425) 643-9954 www.seabird.com

### Temperature Calibration Report

Customer:	Ole A. Nordby AS		
Job Number:	88645	Date of Report:	3/8/2016
Model Number	SBE 38	Serial Number:	3844844-0315

*Temperature sensors are normally calibrated 'as received', without adjustments, allowing a determination sensor drift. If the calibration identifies a problem, then a second calibration is performed after work is completed. The 'as received' calibration is not performed if the sensor is damaged or non-functional, or by customer request.*

*An 'as received' calibration certificate is provided, listing coefficients to convert sensor frequency to temperature. Users must choose whether the 'as received' calibration or the previous calibration better represents the sensor condition during deployment. In SEASOFT enter the chosen coefficients. The coefficient 'offset' allows a small correction for drift between calibrations (consult the SEASOFT manual). Calibration coefficients obtained after a repair apply only to subsequent data.*

'AS RECEIVED CALIBRATION'  Performed  Not Performed

Date:  Drift since last cal:  Degrees Celsius/year

Comments:

'CALIBRATION AFTER REPAIR'  Performed  Not Performed

Date:  Drift since Last cal:  Degrees Celsius/year

Comments:



## Appendix Q Risk Assessment

Template	The Statkraft Way		
Internal	Safe Job Analysis form		

Type jobb: Virkningsgradmåling Leifossene K.V., agg2.	AO-nr: 701414	Ansvarlig for gjennomføring:	Dato/sted: 23.5.2016/Trondheim
---	------------------	------------------------------	-----------------------------------

Beskrivelse av arbeidsoppgavene:

1. Nedtapping og fylling av sugerør. Gjennomføres av vakta. (Noe usikkert på tidsbruk. Viktig å notere denne slik at instruksjer kan oppdateres)
2. Montering av måleutstyr: Måleramme i avløp, trykksensorer i sugerør, temperatursensor innløp nedstrøms hovedventil, temperatursensor på måleramme i avløp, kabling fra sensorer.
3. Måling av termodynamisk virkningsgrad. Under prøvingen vil gjennomsnittlig effekt i timen ligge på ca 11-12MW.
4. Demontering av utstyr. Vi demonterer kun temperatursensor på innløp nedstrøms hovedventil. Resten av utstyret skal stå til vi får testet ut stulken. Det er foreløpig ønske om å få denne montert i uke 24/25 (19/6-22/6)

**OBS!** Viktig at alle klokkeslett blir notert ned slik at vi får oppdatert instruksene med korrekt tidsangivelse for nedtapping, montering og fylling av ramme, fylling etc

#### A) Forenklet SJA – skal gjennomføres for alle jobber som kan innebære fare for helse, sikkerhet og/eller ytre miljø.

Vurder for arbeidsoppgaven:	ja	nei
1. Finnes det dekkende prosedyrer eller instruksjer?	x	
2. Har du/dere avklart at ikke kreves SJA for denne jobben (i for eksempel i lovverk/prosedyrer/instruksjer/ risikovurdering)?		x
3. Har du/dere nødvendig opplæring, kompetanse og erfaring?	x	
4. Er godkjente maskiner, verktøy og/eller verneutstyr på plass?	x	
5. Har du/dere tatt hensyn til parallelle aktiviteter som krever koordinering? (Dersom det er noen)	x	
6. Er du/alle i form til å utføre arbeidsoppgaven sikkert i dag?	x	
7. Har du/dere nok tid og ressurser til å utføre jobben sikkert?	x	

Approver: Kirsti Elsfjordstrand  
Owner: Head of P&A - Controlling & HSE  
Published: 03.12.2012

Rev. no.: 02  
Doc. no.: 12-591  
Doc. id.: H-10/105  
Page: 1 av 3

Template	The Statkraft Way <b>Safe Job Analysis form</b>		
Internal			

**B) SJA - skal gjennomføres dersom det krysses i en av "nei feltene" over**

Deloppgave	Faremoment	Mulig konsekvens	Tiltak	Ansvarlig for tiltak
Tapping og fylling	Håndtering av vann	Oversvømming med skade på utstyr	<ul style="list-style-type: none"> <li>-Følge med nivå på pumpekum.</li> <li>-Varsel blir gitt på høyt nivå.</li> <li>-Justere tappeventil forsiktig til nedtapping og utpumping er synkrone.</li> <li>-Før entring i vannvei, skal all sikring og isolering av energi i vannvei være utført. (Ansvarelig er LFSV)</li> </ul>	Terje Thorsen
Montering av måleramme	Fall / klem og løft	Personskade, skade på utstyr	<ul style="list-style-type: none"> <li>-Fallsikringssele med fallblokk benyttes ved arbeid i høyden.</li> <li>-Ingen personer under hengende last.</li> <li>-Ha med 4-foting.</li> <li>-Bruke nye taustige med brede trinn.</li> <li>-Bruk av personlig verneutstyr med lys og synlighetsbeledning</li> </ul>	Alle / LFSV
Montering av måleramme	Friskluft og lystilgang	Personskade, svimmelhet, framkommelighet	<ul style="list-style-type: none"> <li>-Ha med LED lys og personlig hodelykt</li> <li>-Ha med vifte for tilførsel av luft</li> </ul>	Alle
Montering av måleramme	Snublefeller	Personskade, skade på utstyr	<ul style="list-style-type: none"> <li>-Kabler og utstyr må festes og merkes slik at dette ikke blir til hinder for framkomst eller sårbart i forhold til skade. Bruk gjerne synlighetsstape.</li> <li>-Måleramme skal stå i</li> </ul>	Alle
Montasje av trykksensorer	Arbeid i høyde	Personskade, skade på utstyr	<ul style="list-style-type: none"> <li>-Bruk stige i henhold til Statkraft prosedyrer</li> </ul>	Alle
Demontering av temperatursensor på innløp	Håndtering av vann	Personskade, vann i stasjon	<ul style="list-style-type: none"> <li>-Hovedventil sikres i lås posisjon.</li> <li>-Før demontering av sensor må tromme tappes ned til underkant av flens for sensor. Sensoren har en ventil som kan åpnes for å sjekke om det står vanntrykk i tromme.</li> </ul>	LFSV/Alle

Approver: Kirsti Elisfordstrand  
 Owner: Head of PGA - Controlling & HSE  
 Published: 03.12.2012

Rev. no.: 02  
 Doc. no.: 12-591  
 Doc. id.: H-10/105  
 Page: 2 av 3